Doctoral Thesis

Scale Formation in Tunnel Drainage Systems - Reaction Mechanisms, Countermeasures and Monitoring

by

Stefanie Eichinger

to

achieve the university degree of Natural Sciences

– ***Doctor rerum naturalium*** –

(Dr. rer. nat.)

submitted to

Graz University of Technology

Supervisors

Univ.-Prof. Dr. Martin Dietzel and Priv.-Doz. Dr. Ronny Boch

Graz, September 2022

STATUTORY DECLARATION

I declare that I have authored this thesis independently, that I have not used other than the declared sources/resources, and that I have explicitly indicated all material which has been quoted either literally or by content from the sources used. The text document uploaded to TUGRAZonline is identical to the present doctoral thesis

……. …….

Date Signature

Acknowledgements

First of all, I would like to thank my supervisor Martin Dietzel, for his active and great support during the writing of this thesis. Thank you for this great topic and for your time during all the numerous meetings and questions. It's always a pleasure to work with you.

Another big thank you goes to my co-supervisor Ronny Boch for the many conversations and advice we shared. Thank you for taking me “by the hand” and giving me much more than I thought I could do right from the start.

A big thank you also goes to my colleagues Sylvia Perchthold, Andrea Wolf, Maria Hierz, Judith Jernej, Andre Baldermann and Dorothee Hippler. Thank you for your support and for always having an open ear and coffee for me. Thanks also to Katja, Bettina, Michi, Jean-Michel, Flo and Cyrill for their loving support through the years together. Many thanks also to Albrecht Leis for the great support and that I was allowed to ask you everything at any time.

Furthermore, I would like to thank all my friends. Thank you, Niki, Julia, Luki, Alex, Raffi, Viki, Kathi, Chrisi, Xandi, Eva, Ludwig and Natalie for your support. You are the best evidence that family does not always have to be related by blood.

The biggest thanks go to my family, first and foremost to my grandparents Maria and Josef Eichinger, who support me in all kinds of situations and are always there for me. An especially big thank you goes to my sister Katrin, without whom I would not be able to do all this professionally but also privately. Thank you for your unwavering support and that you are always there for me. You are the best sister I could ever wish for. Thanks also to my brother Michael and his girlfriend Kathi for the loving support and for every open ear during the last years. Thanks also to Marianne and Erich Herzog and Annemarie and Martin Mühlhauser for the loving support and that you always believe in me.

I would like to dedicate this work to my beloved Mami, who unfortunately can no longer witness my title, but is nevertheless always by my side and will always be my greatest idol. She made me the person I am today and supported me in her own special way.

Thank you all so much!

Danksagung

An erster Stelle möchte ich mich bei meinem Betreuter Martin Dietzel für die tatkräftige und großartige Unterstützung beim Verfassen dieser Doktorarbeit bedanken. Danke für dieses großartige Thema und für deine Zeit bei all den zahlreichen Besprechungen und Fragen. Es ist immer ein Vergnügen mit dir zusammen arbeiten zu dürfen.

Ein weiteres großes Dankeschön geht an meinen Co-Betreuer Ronny Boch für die vielen gemeinsamen Gespräche und Ratschläge. Danke, dass du mich „an die Hand genommen“ hast und mir von Anfang an viel mehr als ich selbst zugetraut hast.

Ein herzliches Dankeschön geht natürlich auch an meine Kollegen Sylvia Perchthold, Andrea Wolf, Maria Hierz, Judith Jernej, Andre Baldermann und Dorothee Hippler. Danke für eure Unterstützung und dass ihr immer ein offenes Ohr und Kaffee für mich hattet. Danke auch an Katja, Bettina, Michi, Jean-Michel, Flo und Cyrill für die liebe Unterstützen durch die gemeinsamen Jahre. Vielen lieben Dank auch an Albrecht Leis für die großartige Unterstützung und dass ich dich jederzeit alles Fragen durfte.

Weiters möchte ich mich auch bei allen meinen Freunden bedanken. Danke Niki, Julia, Luki, Alex, Raffi, Viki, Kathi, Chrisi, Xandi, Eva, Ludwig und Natalie für eure Unterstützung. Ihr seid der Beste Beweis, dass Familie nicht immer blutsverwandt sein muss.

Der größte Dank geht natürlich an meine Familie, allen voran meinen Großeltern Maria und Josef Eichinger, die mich in allen möglichen Lebenslagen unterstützen und immer für mich da sind. Ein besonders großes Dankeschön geht an meine Schwester Katrin, ohne die ich beruflich aber auch privat all das nicht schaffen würde. Danke für deine bedingungslose Unterstützung und dass du immer für mich da bist. Du bist die beste Schwester, die man sich nur wünschen kann. Danke auch an meinen Bruder Michael und seine Freundin Kathi für die liebevolle Unterstützung und für jedes offene Ohr während der letzten Jahre. Danke auch an Marianne und Erich Herzog und Annemarie und Martin Mühlhauser für die liebevolle Unterstützung und dass ihr immer an mich glaubt.

Widmen möchte ich diese Doktorarbeit meiner geliebten Mami, die meinen Titel leider nicht mehr miterleben kann, jedoch trotzdem immer an meiner Seite ist und immer mein größtes Vorbild sein wird. Sie hat mich zu dem Menschen gemacht, der ich heute bin und mich auf ihre ganz eigene Art und Weise unterstützt. *Vielen lieben Dank euch allen!*

Abstract

Calcium carbonate and iron/manganese (hydr)oxide formation in aquatic media is widespread in different natural and technical environments. Especially in technical settings such precipitates, so called scale deposits, constitute a serious and challenging issue if deposition and clogging (scaling) affect or limit the continuous water transport in tunnel drainage systems, wells, pipelines or industrial water circuits. In some cases, such unwanted deposits can cause irreparable damage to the drainage systems if mineral formation leads to a dramatic loss in the efficiency of water and/or energy transfers, and in serious cases to a total blockage of fluid flows. Regular inspections as well as services and maintenance are therefore essential. However, maintenance work, including mechanical or chemical removal of such unwanted scale deposits is highly cost and labour intensive and leads to traffic disturbances. All these troubles with detrital and precipitated mineral deposits in drainage systems argue for an enhanced understanding of processes and formation mechanisms, as well as an assessment of the interplay between the evolution of precipitating solutions and the composition, microstructure, material consistency and durability etc. of the geogenic or anthropogenic deposits. Thus, the main focus of this PhD thesis is an advanced and detailed knowledge on relevant formation mechanisms and the site-specific source of scale deposit formation, as well as the dependencies of various and variable environmental influences. Another important factor is to investigate the spatiotemporal occurrence and influences of variable scale material consistency, macroscopic appearances of the scale deposits and chemical-sedimentary dynamics in different tunnels. Microbes can also significantly influence the scaling process. Tunnel drainage systems are therefore a highly complex and partly seasonally dependent environmental system in which the interaction of the hydrosphere, lithosphere, biosphere, atmosphere and also anthroposphere plays a significant role. Thus, natural (geogenic) conditions, such as the geological setting, occurrence of diverse microbes (bacteria), the chemical composition of the local groundwater or the amount of water ingress as well as technical-operative settings, such as the drainage design and associated flow geometries or interaction with cement-bound building materials affect the case-specific formation mechanisms of scale deposits and their specific appearances, compositions and material characteristics. In order to prevent such unwanted mineral deposits and to use suitable prevention strategies an advanced process understanding is fundamental. Sustainable prevention strategies involve the case-specific use of eco-friendly chemical additives (e.g. green inhibitors) and an appropriate drainage design with suitable building materials (e.g. plastics).

Considering all these processes, it is important to mention that each tunnel drainage system must be assessed individually in order to develop appropriate and sustainable prevention strategies.

Kurzfassung

Die Bildung von Kalziumkarbonaten und Eisen-/Mangan(hydr)oxiden in wässrigen Medien ist in verschiedenen natürlichen und technischen Umgebungen weit verbreitet. Insbesondere in technischen Umgebungen stellen solche Ausfällungen, so genannten Versinterungen, ein ernstes Problem dar, wenn derartige minerlischen Ablagerungen und Blockaden (Prozess „Scaling“) den kontinuierlichen Wassertransport, etwa in Tunnelentwässerungssystemen, Bohrlöchern, Pipelines oder industriellen Wasserkreisläufen, beeinträchtigen oder einschränken. In einigen Fällen können solche unerwünschten Ablagerungen irreparable Schäden an Entwässerungssystemen verursachen, wenn die Mineralbildung zu einem drastischen Verlust der Effizienz des Wasser- und/oder Energietransfers und in schwerwiegenden Fällen zu einer vollständigen Blockierung der Flüssigkeitsströme führt. Regelmäßige Inspektionen sowie Wartungs- und Instandhaltungsarbeiten sind daher unerlässlich. Wartungsarbeiten, einschließlich der mechanischen oder chemischen Entfernung solcher unerwünschten Ablagerungen, sind jedoch kosten- und arbeitsintensiv und führen zu begleitenden Verkehrsbeeinträchtigungen. Alle diese Probleme mit häufig wiederholt ausgefällten mineralischen Ablagerungen in Entwässerungssystemen sprechen klar für die Notwendigkeit eines verbesserten Verständnisses der Prozesse und Bildungsmechanismen, sowie für eine systematische Bewertung des Zusammenspiels zwischen der Entwicklung von zur Ausfällung neigenden Wässern und der Zusammensetzung, Mikrostruktur, Materialbeschaffenheit und Porosität der geogen und anthropogen bedingten Ablagerungen. Das Hauptaugenmerk dieser Doktorarbeit liegt daher auf vertieften und detaillierten Kenntnissen der Bildungsmechanismen und der standortspezifischen Herkunft der gebildeten Minerale und Sedimente, sowie der Abhängigkeiten von verschiedenen Umwelteinflüssen. Ein weiterer wichtiger Faktor ist die Untersuchung des Auftretens und der Einflüsse variabler Materialkonsistenzen der Präzipitate, der makroskopischen Erscheinungsformen von mineralischen Ablagerungen und der räumlich-zeitlichen sedimentären Dynamik. Auch Mikroben (v.a. Bakterien) können die Ablagerungsreaktionen erheblich beeinflussen. Tunnelentwässerungssysteme sind folglich ein komplexes und teilweise jahreszeitlich

abhängiges Umweltsystem, in dem das Zusammenspiel von Hydrosphäre, Lithosphäre, Biosphäre, Atmosphäre und auch Anthroposphäre eine wesentliche Rolle spielt. So beeinflussen sowohl natürliche (geogene) Bedingungen, wie die geologische Umgebung, das Vorkommen von spezifischen Mikroben, die chemische Zusammensetzung des lokalen Grundwassers oder die Menge des Wasseraufkommens und damit der Entwässerung, als auch technisch-betriebliche Gegebenheiten, wie die Entwässerungsgestaltung und die damit verbundenen Strömungsgeometrien oder auch die Wechselwirkung mit zementgebundenen Baustoffen, die fallspezifischen Bildungsmechanismen von Ablagerungen und deren Erscheinungsformen, Zusammensetzungen und Materialeigenschaften. Um solche unerwünschten Ausfällungen zu verhindern und geeignete Präventionsstrategien anzuwenden, ist ein vorausgehendes Prozessverständnis dringend erforderlich. Nachhaltige Präventionsstrategien sind der tunnelspezifische Einsatz ökologisch unbedenklicher, chemischer Additive (z.B. Grüne Inhibitoren) und eine geeignete Entwässerungsplanung mit geeigneten Baustoffen (z.B. Kunststoffe). Bei all diesen Prozessen ist es wichtig zu betonen, dass jedes Tunnelentwässerungssystem systematisch und individuell bewertet werden muss, um geeignete Präventionsstrategien entwickeln zu können.

Table of Content

Chapter 1 – Introduction

The overall aim of this PhD thesis is to get an advanced process understanding of the formation mechanisms and reaction kinetics of $CaCO_3$ and accessory mineral precipitates (e.g. Fe-(hydr)oxides) as well as microbial biofilms in tunnel drainage systems to prevent such unwanted scale deposits. The main focus of this thesis is therefore to decipher and assess the causes, mechanisms, influencing factors as well as environmental dependencies that lead to scale deposit formations in individual drainage systems to develop suitable and sustainable prevention strategies. This is done by considering the entire reactive system including the aquatic solution by dissolving and precipitation of solids and exchanging with the atmosphere. Three interfacial phenomena are of particular importance: atmosphere – solution, solution – precipitate and precipitate – substrate (solid surfaces; e.g. drainage pipe). To investigate the above aspects, a multiproxy approach was choosen including a broad range of bulk and high-resolution optical, chemical, mineralogical and isotopic tools. The solid scale samples were additionally analyzed for their microbial content. In some cases, automated and remotely controlled sensors were implemented for in-situ and online monitoring, for instance continuous measurements of pH, temperature, and electric conductivity of the drainage water. Chapter 2 gives a summarized overview of the most significant research data and state of knowledge for scale deposit formation and prevention strategies over the last years, which are discussed in details in the following chapters. In the Chapters 3 and 4 the reaction mechanisms and environmental influences of scale formation are discussed. The use of green inhibitors (ecofriendly and biodegradable chemical additives), as well as a suitable drainage design with adequate building materials (e.g., different plastics) are two strategies for preventing unwanted scale deposits, which are topics of Chapters 5 to 7. Finally, Chapter 8 summarizes future perspectives for further research approaches and possible prevention strategies for the highly variable and complex formation mechanisms of scale deposits in tunnel drainage systems.

This doctoral thesis is composed of the following individual chapters, which are based on research contributions published in international peer-reviewed journals.

Chapter 2 gives a brief overview of the whole doctoral thesis and sums up the state of knowledge as well as current challenges of scale deposit formation in tunnel drainage systems over the last few years. In particular, the process mechanisms of scale deposit formation in terms of typification, controlling parameters of the formation, such as water chemistry, interfacial phenomena, microbial activity, and prevention strategies, such as appropriate

adaptation of construction materials, drainage design, inhibitor use and cleaning procedures. Chapter 2 has been published in the journal "Geomechanics & Tunneling" in 2022:

Dietzel, M.; Eichinger, S. (2022) Scale formation processes – state of knowledge and current challenges. Geomechanics and Tunnelling 15, No. 4, pp. 347–357. https://doi.org/10.1002/geot.202200009.

Chapter 3 deals with the physicochemical driving forces to induce and control the formation processes of scale deposits in tunnel drainage systems, using the Semmering tunnel chain (series of road tunnels) as a case study. In particular, lights are shed on the hydrochemical parameters and mechanisms controlling the formation and fabrics of unwanted carbonate $CaCO_3$ scale deposits, using a multiproxy approach

- to implement data from periodical sampling as well as continuous in-situ monitoring of aqueous carbonate precipitating solution parameters,
- to explain the formation mechanisms of the visually highly divers scale deposits,
- to trace scale formation by stable carbon and oxygen isotopes, and
- to verify the occurrence of distinct bacteria and their influence on scale formation

Chapter 3 has been published in the journal "Science of the Total Environment" (IF:10.7) in 2020:

Eichinger, S., Boch, R., Leis, A., Koraimann, G., Grengg, C., Domberger, G., Nachtnebel, M., Schwab, C., Dietzel, M. (2020). Scale deposits in tunnel drainage systems – A study on fabrics and formation mechanisms. Science of the Total Environment, 718, 137140. https://doi.org/10.1016/j.scitotenv.2020.137140.

Chapter 4 describes the results from the research project of the "Task Force Drainage". In this study 16 railway tunnels were investigated for a systematic compilation, characterization, and evaluation of scale deposits in relation to their formation mechanisms and the influence of variable environmental factors. A classification in four different major types of scale deposits according to their macroscopic appearance and material consistency is developed. Chapter 4 has been published in the international journal "Geomechanics & Tunneling" in 2020:

Eichinger, S., Leis, A., Boch, R., Seywald, C., Dietzel, M. (2020). Assessment and formation mechanisms of scale deposits in tunnels of the ÖBB-Infrastruktur AG – A subproject of the Task Force Drainage. Geomechanics and Tunnelling, 13(3), 273-285. https://doi.org/10.1002/geot.202000006.

Chapter 5 provides new insights into the use of a specific green inhibitor in a tunnel drainage system as a suitable prevention strategy. The eco-friendly and biodegradable inhibitor polyaspartate (PASP) was tested and assessed in order to significantly reduce and modify the (micro)structure, amount, and material consistency of the widespread $CaCO_3$ scale deposits. The application of trace concentrations of PASP causes a significant inhibition of $CaCO_3$ precipitation, as well as a more porous or even loose scale consistency (calcareous mud) of the $CaCO_3$ scale deposits and a shift in $CaCO_3$ mineralogy from predominant calcite to metastable aragonite and vaterite. Even a few mg PASP per litre induced a highly elevated saturation index of calcite of up to ~2, i.e. close to the saturation level of amorphous calcium carbonate (ACC). The use of PASP has to be evaluated case-specifically, since microbial activity may metabolize PASP, i.e. consume it as a nutrient. This study combines promising results with regard to fundamental carbonate research as well as technical applications in the context of tunnel maintenance. Chapter 5 has been published in Water Research (IF: 13.4) in 2022:

Eichinger, S., Boch, R., Leis, A., Baldermann, A., Domberger, G., Schwab, C., & Dietzel, M. (2022). Green inhibitors reduce unwanted calcium carbonate precipitation: Implications for technical settings. Water Research, 208, 117850.

Chapter 6 describes the application of scale inhibitor treatment as an efficient preventive measure. Especially PASP-based products, available as liquid and in the form of depot stones (Polysuccinimid (PSI) - releasing tabs) has been compared and evaluated. Advantages and disadvantages of the respective applications are discussed. In this study a novel compact test (rapid, small space requirement) for determining the effectiveness of green inhibitors on liquid conditioning has been developed, which is suitable for future case studies and current concepts. Chapter 6 has been published in the journal "Geomechanics & Tunnelling" in 2022:
Leis, A.; Wagner, H.; Eichinger, S.; Dombrger, G.; Wedenig, M.; Dietzel, M.; Boch, R. (2022) Use of green inhibitors for hardness stabilisation of tunnel drainage systems. Geomechanics and Tunnelling 15, No. 4, pp. 402–413. https://doi.org/10.1002/geot.202200018.

Chapter 7 summarizes three publications which were developed within the interdisciplinary research project PolyDrain. PolyDrain was funded by the FFG (österreichische Forschungsförderungsgesellschaft) from 2017 to 2020 and involved the cooperation of 9 different research disciplines. The approach of this study is based on developing methods and modifying the polymer matrix of drainage pipes by adding active fillers to reduce the scale deposit formation in tunnel drainage pipes. Seven different compounds, consisting of a polyethylene-based polymer with individual fillers were developed and tested in the laboratory

as well as at field sites in tunnel buildings. The amount and crystal shape of the newly formed $CaCO_3$ precipitates on the polymer surface of these 7 compounds were assessed using chemically and (electron)optical analytical methods. Chapter 7.1 includes a synthesis of two publications from the journal "BHM (Berg- und Hüttenmännische Monatshefte)", Chapter 7.2 has been published in the international journal "Geomechanics & Tunneling" in 2019:

7.1: *Arbeiter, F.; Eichinger, S.; Rieß, G.; Schachinger, T.; Boch, R.; Wenighofer, R.; Galler, R.; Hausberger, A.; Strobl, E.; Stur, M.; Saliger, F.; Steiner, M.; Dietzel, M., Pinter; G. (2019) Optimierte Polymer-Rohrwerkstoffe für effiziente Drainagesysteme in Tunnelbauwerken – Poly-Drain. Berg- u. Hüttenmännische Monatshefte 164, H. 12, S. 545–551. https://doi.org/10.1007/s00501-019-00918-6.*

Arbeiter, F., Eichinger, S., Rieß, G., Schachinger, T., Boch, R., Wenighofer, R.; Galler, R., Hausberger, A.; Strobl, E.; Stur, M.; Saliger, F.; Steiner, M.; Dietzel, M., & Pinter, G. (2020). Optimierte Polymer-Rohrwerkstoffe für effiziente Drainagesysteme in Tunnelbauwerken—PolyDrain Teil II. BHM Berg-und Hüttenmännische Monatshefte, 165(12), 623-630.

7.2: *Schachinger, T., Arbeiter, F. J., Eichinger, S., & Saliger, F. (2019). Research on pipe materials for tunnel drainage by the ÖBB Task Force Drainage. Geomechanics and Tunnelling, 12(5), 467-471.*

Chapter 2 - Scale formation processes – state of knowledge and current challenges

Martin Dietzel[1] & Stefanie Eichinger[1]

[1] Institute of Applied Geosciences, Graz University of Technology & NAWI Graz GeoCenter, Rechbauerstrasse. 12, 8010 Graz, Austria.

2.1 Abstract

Scale formation in water drainage systems occurs in diverse forms. In tunnel drainage systems in particular, calcium carbonate deposition can significantly impair water discharge, resulting in costly maintenance work and tunnel closures. This review paper presents and discusses the state of knowledge as well as the current challenges regarding scale formation in tunnel drainage systems in terms of typification, parameters controlling formation, such as hydrochemistry, interfacial phenomena, microbial activity, and countermeasures, such as appropriate adaptation of construction materials, drainage design, inhibitor use and cleaning. Detailed knowledge of the case-specific scale formation environment and the scaling capacities of the waters provides the basis for the tailored development and evaluation of suitable strategies for successfully reducing maintenance efforts and tunnel closure. For this purpose, time- and site-resolved monitoring of the composition of the solid phases, waters and the tunnel atmosphere during the implementation of the construction project and during the operation of the tunnel is paramount.

2.2 Introduction

The maintenance of the functionality of tunnel drainage systems is essential to ensure the usability and subsequent load-bearing capacity of a tunnel construction. Drainage systems are specifically designed to suit the structural requirements of the tunnel project, the local geology and the prevailing groundwater conditions thus play an essential role in this regard. Unwanted scale deposits in drainage systems which impede or prevent the proper discharge of water from the tunnel to the outfall drain present a major challenge. In recent decades, a multitude of field, laboratory and simulation studies have investigated the possible causes of such scale deposits as well as strategies to prevent or remove them [1–3]. In most cases, calcium carbonate precipitation is the dominant scale formation process in tunnel drainage systems, in addition to iron hydroxide deposits and material entrained in suspension. Driving forces are the amount

and composition of water inflows, the interaction of these inflows with both the building materials used and the tunnel atmosphere as well as the mixing of waters along the tunnel drainage system [4]. Scale formation in tunnel drainage systems tends to intensify in the presence of calcium and carbonate-rich groundwater in combination with exposed building materials that readily mobilise calcium and hydroxides, e.g. calcium silicate hydrate phases (CSH) or Portlandite ($Ca(OH)_2$) from shotcrete and anchor mortar. In almost all scenarios, the predominant overall conversion rates for calcium carbonate ($CaCO_3$) precipitation can illustrated by the following chemical reactions:

$$\mathbf{Ca^{2+} + 2HCO_3^- = CaCO_3 + CO_2 + H_2O} \quad (1)$$

$$\mathbf{Ca(OH)_2 + Ca^{2+} + 2HCO_3^- = 2CaCO_3 + 2H_2O} \quad (2)$$

$$\mathbf{CSH + CO_{2(g)} = CaCO_3 + SiO_2 * nH_2O} \quad (3)$$

whereby the carbonate can come from the groundwater (HCO_3^-) (Equations 1 and 2) and/or the tunnel atmosphere ($CO_{2(g)}$) (Equation 3). It should be noted that $CaCO_3$ formation often does not occur in isolation; instead, it is characterised by interactions with mainly siliciclastic components, e.g. clay minerals, and (hydr)oxidic components, e.g. quartz and iron hydroxides, as well as more complex interactions with organic components – often metabolically catalysed (microbiology) [5]. Thus the occurrence, consistency and variability over time of different scale deposits are complex and must be mapped, documented and assessed on a case-by-case basis for each individual drainage system [5, 6]. Currently successful approaches to prevent such scale deposits thus increasingly focus on the development and use of novel building materials which exhibit significantly reduced calcium leaching behaviour, as well as the use of inhibitors (also referred to as hardness stabilisers) to suppress and thus reduce or prevent $CaCO_3$ precipitation along the tunnel drainage system [7–9]. Furthermore, significant advances have been made in the planning and design of drainage systems in terms of optimising their spatial arrangement and operating conditions, e.g. separate drainage, preventing the mixing of different water sources, reducing water turbulences, reducing water-atmosphere exchange and adapting lining materials [10, 11]. This paper gives an overview of the processes of scale deposition with the focus on typification and the parameters controlling scaling mechanisms, such as hydrochemistry, interfacial phenomena, microbial activity, drainage design, the use of inhibitors and the assessment of scaling capacity. It describes the current state of knowledge

and challenges regarding the formation and prevention of scale deposits in tunnel drainage systems which will be discussed in greater depth in subsequent articles in this edition of Geomechanics and Tunnelling [6, 9, 10].

2.3 Types of scale deposits

Scale deposits forming in tunnel drainage systems consist mainly of the carbonate minerals calcite (trigonal $CaCO_3$) and aragonite (orthorhombic $CaCO_3$), with vaterite (hexagonal $CaCO_3$), brucite ($Mg(OH)_2$), and Fe/MnOOH containing and organically induced precipitates occurring to a lesser degree. In addition to these newly formed deposits from the drainage water, siliciclastic fractions mostly entrained in suspension, such as feldspars, illite and quartz, are also found as solids. Scale deposits are characterised and typified in simple terms by their macro- and microscopic appearance, the individual consistency of the material and the dominance of the $CaCO_3$ minerals [12] (Figure 1). Compact scales take the form of hard, highly compacted material with low porosity. They occur mainly as a result of CO_2 degassing, with clear evidence of microbial activity in some cases. Compact scales are dominated by calcite, whereby the calcite crystals are typically columnar shaped (Figure 1A). Porous scale deposits show high porosity even at macroscopic level. This type of scaling can form as a result of CO_2 degassing or absorption of atmospheric CO_2. These precipitates typically consist of calcite and aragonite in varying amounts, which significantly controls the porous material consistency (Figure 1B). With these types of scale deposit there is increased evidence of microbial activity, which can influence the formation mechanisms and consistency. Shard-like scales include precipitates which mainly extend a few millimetres vertically and have a dense, compact structure with very low porosity (Figure 1C). Potential formation mechanisms for shard-like scales are associated with both CO_2 degassing and CO_2 absorption. These scales consist mainly of well-formed calcite crystals with clear evidence of microbial activity. Unconsolidated-particulate scale deposits are characterised by separate, fine-grained particles which can also form loose aggregates, e.g. lime sludge. This type often consists of calcite and/or aragonite and usually forms due to absorption of atmospheric CO_2 and can be additionally formed as a result of the targeted use of countermeasures, e.g. inhibitors (Figure 1D).

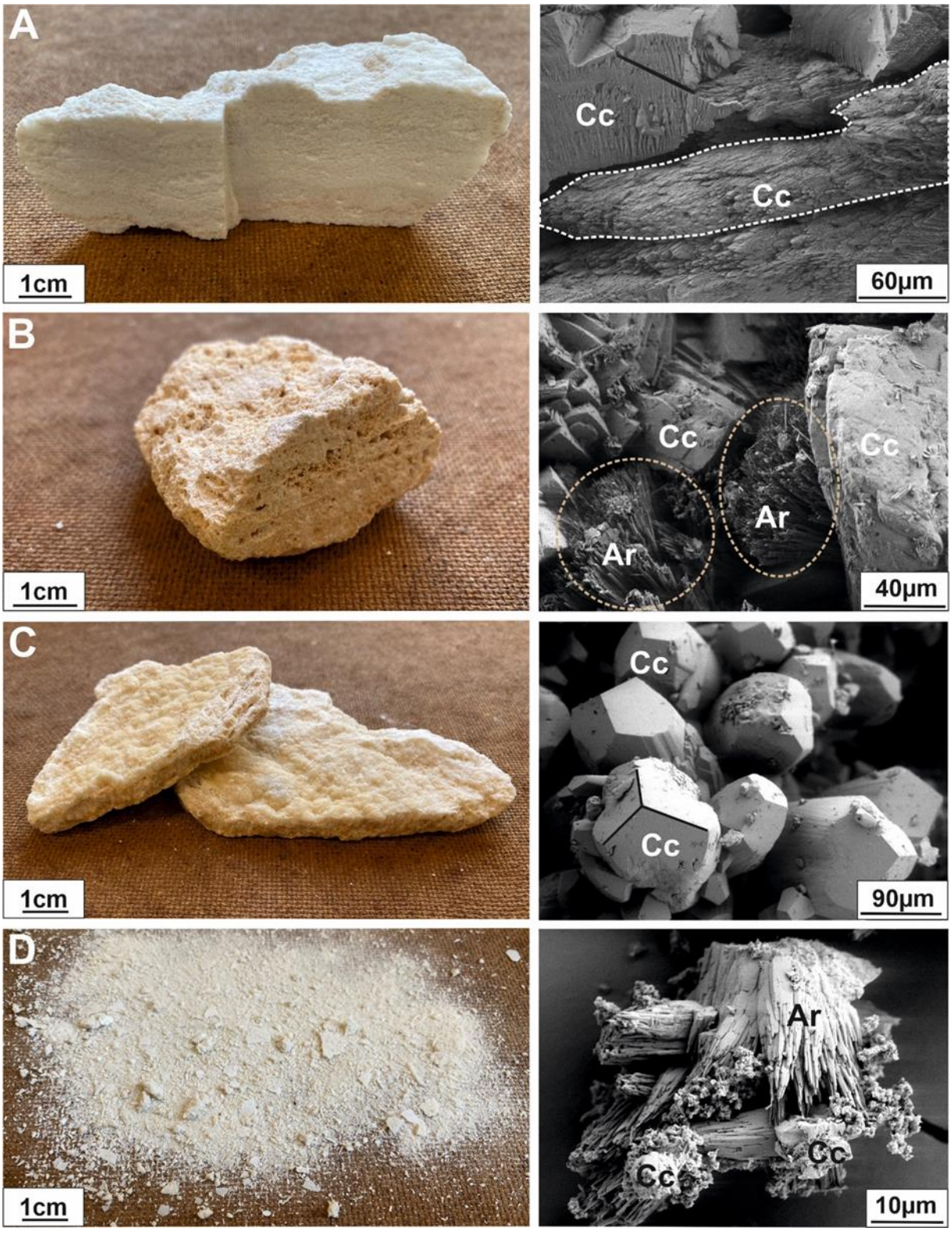

Figure 1: *Macroscopic appearance (left column) and microstructures from scanning electron microscopy (right column) of four major types of Ca-carbonate scale deposits. A: compact scales, showing columnar calcite (Cc) crystals; B: porous scale deposits mainly consists of aragonite (Ar; dotted circles) and calcite; C: shard-like scales contain well-shaped calcite crystals; D: unconsolidated-particulate scale deposits comprise aragonite and calcite.*

2.4 Controlling parameters

Scale formation mechanisms and thus the appearance, composition and consistency of individual scale deposits are determined and controlled by natural (geogenic) boundary conditions, such as groundwater composition and local hydrogeology, as well as technical and operational (anthropogenic) conditions, such as interactions with cement-bound building materials, drainage design and the use of inhibitors [5, 13].

2.4.1 Hydrochemistry and interfacial reactions

The formation of scale deposits in drainage systems is controlled by the chemical composition of the drainage water as well as the temperature and CO_2 partial pressure of the tunnel atmosphere. Reactions at the gas-water phase boundary, i.e. the interface between the tunnel atmosphere and the drainage water, are instrumental to this process. Gases such as CO_2, O_2 and CH_4 can be exchanged at this interface (Figure 2). Degassing of CO_2 from the water to the atmosphere causes the pH level to rise, thereby significantly favouring the formation of $CaCO_3$ scale deposits. CO_2 absorption tends to occur in strongly alkaline waters and can also favour carbonatic scaling at pH levels above 11, although it inhibits scale formation at lower pH levels [14]. High pH levels (e.g. pH > 10) are mostly caused by a strong interaction between the groundwater and the cement-bound building materials, which alters the overall composition of the water (see Figure 2). Another major factor for possible $CaCO_3$ scale formation is the unfavourable mixing of waters of different compositions. The reactions at the solid-water phase boundary, i.e. the interface between a growing calcite crystal and the drainage water, also have a significant influence on $CaCO_3$ precipitation.

2.4.2 Microbial activity

Fine, fiber-like structures indicate microbial activity in some scale deposits (Figure 3B and 3C). These structures are ‘extracellular polymeric substances’ (EPS) which intertwine and envelop individual mineral components like a spider’s web (Figure 3B and 3C). Hollow microtubes and twisted ribbon-like structures associated with the iron-oxidising bacteria *Leptothrix ochracea* and *Gallionella ferruginea* also occur (Figure 3A and 3D). These two bacterial species oxidise FeII to FeIII ions to obtain energy for their metabolism and for biomass production [15]. Microbial activity can thus bring about changes which affect the hydrochemistry of the water, the conditions for scale formation and the composition of scale deposits (e.g. Fe/MnOOH precipitation and EPS networks) [5, 13].

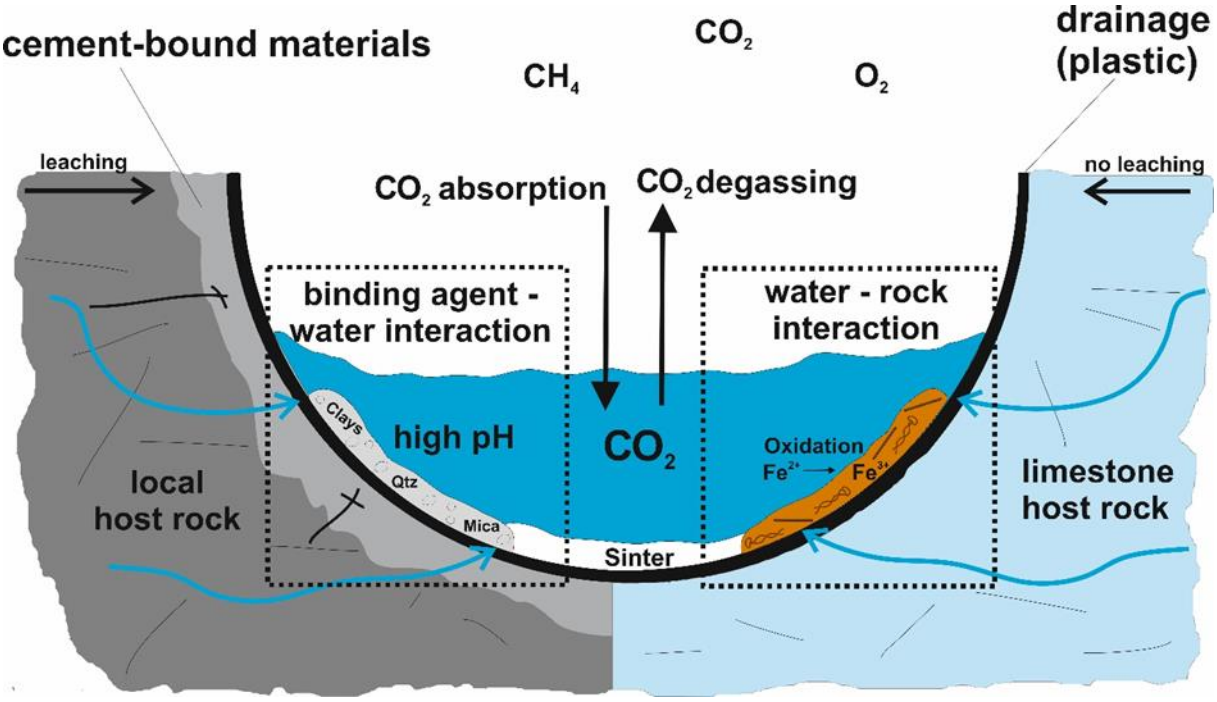

Figure 2: *Schematic illustration of different chemical-sedimentary formation mechanisms of scale deposits. The left side illustrates scale deposit formation caused by binding agent - water interaction (anthropogenic; leaching of cement phases yields high pH), while the right side shows geologically related scale formations (geogenic water – rock interaction). The reactions can be further influenced by gas exchange dynamics between tunnel atmosphere and water (e.g. CO_2 degassing or absorption, O_2 ingress), as well as the formation of Fe/MnOOH and organic components (see Fig.3).*

2.4.3 Drainage design

The design of a drainage system, including the choice of suitable building materials, components and flow geometries, has a significant influence on scale formation, inhibitor use and the removal of scale deposits (maintenance). For instance, turbulence in the drainage water can increase the rate of CO_2 exchange between the gas phase and the water and thus favour scale formation. Furthermore, crystal nucleation and growth can occur at the interface between the drainage system and the drainage water. Adapting the composition and design of plastic drainage pipes can reduce growth on the surface of the pipes and the capacity for scaling. For example, plastics containing polyethylene glycol copolymer and zeolite additives are suitable for reducing scale deposit formation [11].

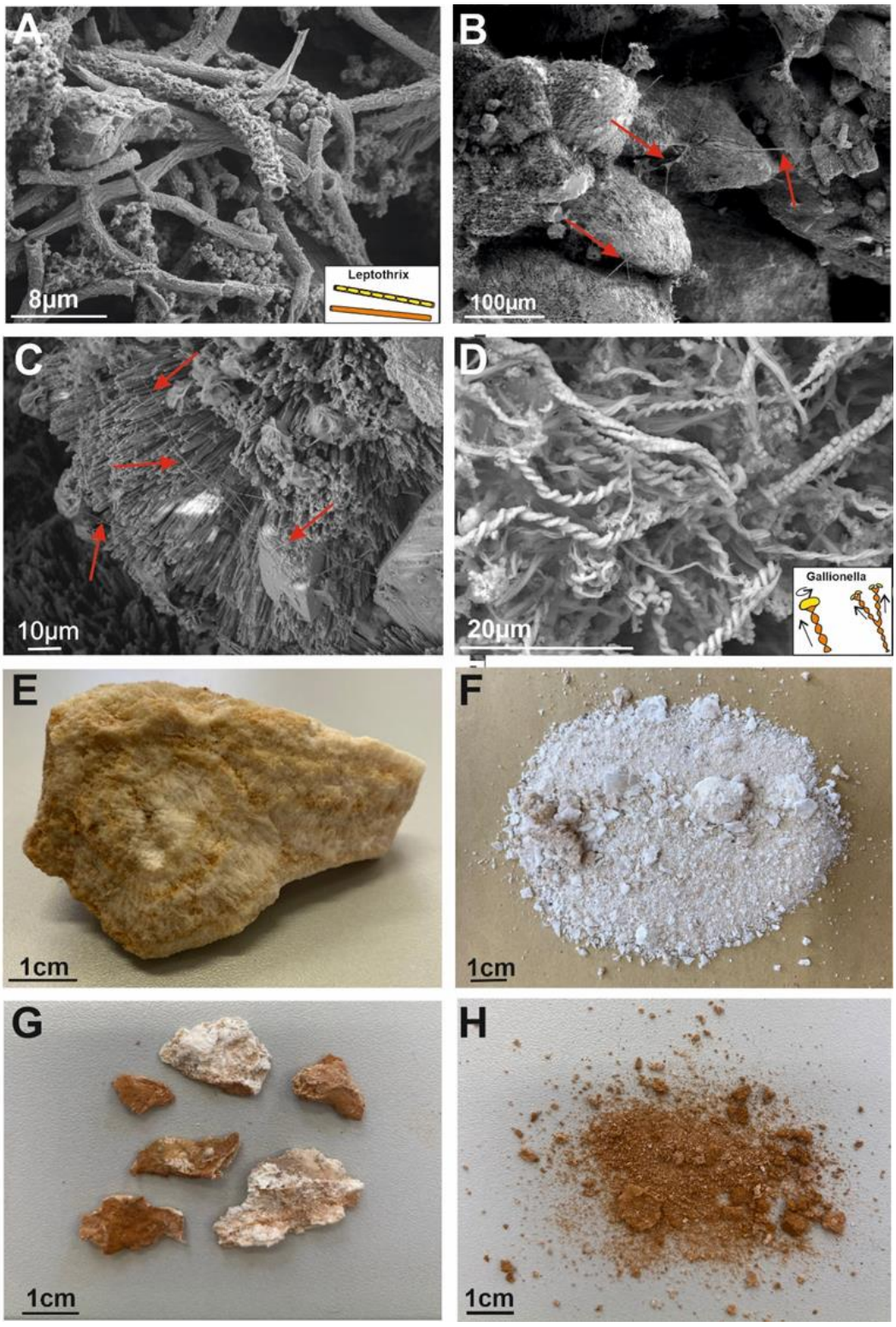

Figure 3: *Effect of bacteria and addition of an inhibitor on formation of scale deposits in tunnel drainage systems. A-D: microbial activities of different bacteria can affect the formation processes. Fe-oxidizing bacteria Leptothrix (sheaths in A) und Gallionella (twisted stalks in D), as well as bacterially undefined EPS structures (red arrows in B and C) mediate occurrences /evidences of microbial activities. Another influencing factor is the use of inhibitors. Pictures E and G show scale deposits before the usage of the inhibitor agent PASP, while F and H indicate the corresponding sinters with influence of the inhibitor PASP in the same drainage water.*

2.4.4 Inhibitor use

The addition of very small quantities of a suitable inhibitor (active substance) can suppress the formation of scale deposits and change their material consistency. The use of substances containing polyaspartic acid (PASP) – also referred to as green inhibitors – has proved particularly effective [8, 13]. Dissolved PASP in concentrations of just a few milligrams per litre of water can very effectively reduce $CaCO_3$ nucleation and deposition rate. Furthermore, in many cases PASP can change the consistency of the developing scale deposits from a hard, compact material to an unconsolidated slurry. For cleaning operations such as high-pressure flushing, this slurry-like consistency is particularly advantageous [13] (Figure 3E to 3H).

2.5 Assessing the scaling capacity

An effective assessment of the expected scale type, consistency, precipitation rate, and amount of potential solid-phase precipitation from a body of water largely depends on the individual physical and chemical conditions and gradients such as pressure, temperature and chemical composition. The concentrations of dissolved constituents and the controlling parameters at the water-gas phase and water-solid interfaces are used to assess the scaling capacity with respect to calcium carbonate formation (Figure 4A). Consequently, to determine the capacity for $CaCO_3$ precipitation it is necessary to sample the drainage water using different sample preparation techniques such as in-situ membrane filtration and on-site analytics (temperature, pH value). The samples obtained in this way are promptly dispatched to the laboratory where the concentrations of dissolved components are quantified using analytical methods such as ion chromatography, alkalinity titration and optical emission spectroscopy. Parameters such as the saturation index for the precipitation of calcite (SI) and the internal CO_2 partial pressure (Pco_2 in atm) are also determined using hydrogeochemical modelling approaches. The SI value is a logarithmic measure in which > 0 indicates possible calcite precipitation, 0.2 to 0.7 an expected moderate precipitation rate and > 0.7 a high overall precipitation rate resulting in increasingly spontaneous calcite formation. The internal Pco_2 value refers to the CO_2 partial pressure that would be found assuming thermodynamic equilibrium with the water, and thus when aligned with the actual CO_2 partial pressure of the tunnel atmosphere ($Pco_{2(g)} = 10^{-3.4}$ for the Earth's atmosphere while $10^{-2.5 \pm 0.5}$ atm is the typical value range for tunnel atmospheres) serves as an indicator of the absorption of CO_2 ($Pco_2 < Pco_{2(g)}$) into the water or the degassing CO_2 ($Pco_2 > Pco_{2(g)}$) from the water to the atmosphere. CO_2 degassing is associated with an increase in the pH value and redistribution of the dissolved carbonate species to the dissolved carbonate ion.

Consequently, it can induce or increase $CaCO_3$ formation. It is important to adjust the threshold of $10^{-2.5}$ atm (Figure 4A) to suit local conditions and CO_2 measurements in the tunnel atmosphere. The model presented in Figure 4 provides the basis for assessing the scaling capacity of drainage water. Scaling capacity is thus determined primarily by the abovementioned parameters (Pco_2 und SI) and the chemical composition of the drainage water. The following reactions and processes are used to assess the chemical composition of the water (i.e. its hydrochemistry:

– pH: $CaCO_3$ precipitation rates and effects of mixing different drainage waters to the abovementioned effect of increased pH

– [Ca], the calcium concentration: Amount of precipitation and mixing effects, e.g. with carbonate-rich waters

– [Mg], the magnesium concentration: pH limit for $Mg(OH)_2$ precipitation as a measure of the evolution of water that has already come into contact with cement-bound materials, e.g. shotcrete and anchor mortar

– [K], the potassium concentration: Indicator of the intensity of contact with cement-bound materials (leaching effect)

– [Sr], the strontium concentration: Measure of the leaching effect and $CaCO_3$ precipitation that has already taken place

– HydroEnv: Assessment of the local hydrochemical environment in terms of potential localised mixing effects, hydrochemical evolution over time and the consistency of observed deposits, where present (default value: 1).

The traffic light assessment system illustrated in Figure 4A is based on the score assigned to the parameters (0, 1 or 2) combined with a weighting index (WI) in accordance with the relationship

$$\mathbf{\Sigma\ (Score_i * WI_i) = Sign} \qquad (4)$$

The traffic light colour coding refers to the numerical value of sign: ≥ 1 indicates high (red); 1 to 0.5 moderate (yellow); and < 0.5 low scaling capacity (green). Waters classified as yellow and red in this traffic light system – based on the chemical composition – must be verified to

ensure that the results correspond to a local hydrological assessment (water ingress). In the Koralm Tunnel, the traffic light system was used to select locations for installing dosage systems for hardness stabilisation on the basis of the temporal and spatial evolution of flow rates and the sign values in the drainage water as well as the local drainage conditions in the tunnel and the properties of the groundwater reservoir. This approach results in an individual assessment for each relevant water inflow in the tunnel.

A

Parameter	Value	Score	WI[#1]	Assessment
pH	9 to 9.8	1	0.2	Moderate precipitation rate and mixing
	>9.8	2	0.2	High precipitation rate and mixing
[Ca]	50 bis 100	1	0.1	Moderate precipitation amount and mixing
[Ca]	>100	2	0.1	High precipitation amount and mixing
[Mg]	<1	2	0.05	Evolution and pH-limit for $Mg(OH)_2$ formation
[K]	>10	2	0.05	Leaching intensity, e.g. of shotcrete
[Sr]	>0.3	2	0.05	Leaching intensity and prior $CaCO_3$ formation
SI[#2]	0.2 to 0.7	1	0.2	Moderate $CaCO_3$ precipitation rate
SI[#2]	>0.7	2	0.2	Spontaneous $CaCO_3$ precipitation
Pco_2[#3]	$>10^{-2.5}$	2	0.1	CO_2 degasing and induced $CaCO_3$ formation
HydroEnv		(1)	0.25	Mixing and water evolution

Sign for water chemistry	$\sum(Score_i * WI_i)$	Sinter capacity	
		≥1	high
		1 to 0.5	moderate
		<0.5	low

[#1] **WI**: weighted index
[#2] **SI**: saturation index in respect to calcite
[#3] **Pco_2**: internal CO_2 partial pressure (atm)
[#4] **HydroEnv**: Hydrochemical Environment
[ ]: concentration (mg L^{-1})

B

Value							Sinter capacity	Score							
pH	[Ca]	[Mg]	[K]	[Sr]	SI[#2]	log(Pco_2[#3])	Sign for water chemistry	pH	[Ca]	[Mg]	[K]	[Sr]	SI[#2]	Pco_2[#3]	HyroEnv[#4]
12.60	212.6	<0.1	238.5	4.60	2.50	-10.0	**1.6**	2	2	2	2	2	2	0	1
11.05	14.8	1.1	49.5	0.32	1.37	-7.2	**1.5**	2	0	0	2	2	2	0	2
10.31	2.4	<0.1	43.4	0.05	0.79	-5.3	**1.3**	2	0	2	2	0	2	0	1
9.65	3.1	<0.1	6.6	0.04	0.27	-5.1	**0.8**	1	0	2	0	0	1	0	1
8.94	24.2	0.6	3.8	0.22	0.52	-4.3	**0.7**	0	0	2	0	0	1	0	1
8.97	25.2	0.8	2.4	0.09	0.54	-4.4	**0.7**	0	0	2	0	0	1	0	1
6.35	24.0	1.1	4.3	0.43	-1.81	-1.5	**0.3**	0	0	0	0	2	0	2	0
8.72	26.0	1.4	2.2	0.20	0.27	-4.0	**0.3**	0	0	0	0	0	1	0	0
9.45	2.7	<0.1	0.8	0.04	-2.68	-7.6	**0.2**	1	0	2	0	0	0	0	0

Figure 4: *The traffic light system for scaling capacity based on water chemistry: (A) Calculation scheme for determining the scaling capacity of drainage water, developed with the specifications in the Koralmtunnel (Austria). (B) Exemplary calculations of the scaling capacities of drainage water from the Koralmtunnel using the traffic light system according to (A).*

2.6 Conclusion and outlook

Scaling processes in tunnel drainage systems are generally well understood in terms of the interactions and reactions, the development of suitable investigative strategies and associated procedures, and the options for reducing scaling. In the past ten years, diverse comprehensive studies based on interdisciplinary approaches have succeeded in identifying the controlling parameters and highlighting concrete solutions [3, 5, 8, 11–14, 16]. To ensure successful and effective drainage of tunnel systems in the long-term, it is essential to comprehensively document and fully understand

– the groundwater in terms of composition, time- and site-resolved inflow rates and contact time with local rock and tunnel materials

– the use and composition of building materials such as shotcrete, concrete, anchor mortar and pea gravel in terms of their chemical and mechanical stability, leaching behaviour, porosity and permeability

– the drainage design requirements, including possible flushing, dosing and monitoring installations, and type, composition, surface texture, mechanical and chemical resistance and flow behaviour of drainage pipes.

Current challenges thus relate primarily to tailoring the above-mentioned requirements and measures to prevent or reduce precipitations in individual drainage systems. This requires a detailed knowledge of all processes connected with the formation of scale deposits. The nature of individual scale deposits must first be analysed, assessed and classified before measures can be taken to reduce or entirely eliminate them. Case-specific knowledge of the conditions favouring scale formation is needed to develop and assess targeted strategies to reduce or prevent scale deposit formations. Tailored time- and site-resolved monitoring of the composition of the deposits, the drainage waters and the tunnel atmosphere during the construction phase as well as during operation of the tunnel is paramount. Specific issues and aspects can be investigated and assessed using methods designed specifically for the project in question, such as test tracks and field trials in the tunnel itself, simulation experiments at laboratory scale or the development and use of computer-based modelling tools. Examples include modifying shotcrete and pipework formulations, efficient inhibitor dosing, drainage design and flushing processes [7, 8, 11, 13, 16].

2.7 Acknowledgements

The authors would like to thank Roman Heissenberger and Hanns Wagner (ÖBB-Infrastruktur AG) for their invaluable support with this paper on scale formation in tunnel drainage systems.

References

[1] Girmscheid, G.; Gamisch, T. (2007) Versinterungsprobleme in Bauwerksentwässerungen. Berlin: Bauwerk.

[2] Rinder, T.; Dietzel, M.; Leis, A. (2013) Calcium carbonate scaling under alkaline conditions – case studies and hydrochemical modelling in Applied Geochemistry 35, pp. 132–141.

[3] Chen, Y.; Cui, Y.; Barrett, A.G.; Chille, F.; Lassalle, S. (2019) Investigation of calcite precipitation in the drainage system of railway tunnels in Tunnelling and Underground Space Technology 84, pp. 45–55.

[4] Kusterle, W.; Pichler, W.; Saxer, A. (2011) Prüfverfahren zur Bestimmung des Versinterungspotenzials von Spritzbeton–Einflussfaktoren in Beton- und Stahlbetonbau, 106, No. 12, pp. 847–852

[5] Eichinger, S.; Boch, R.; Leis, A.; Koraimann, G.; Grengg, C.; Domberger, G.; Nachtnebel, M.; Schwab, C.; Dietzel, M. (2020) Scale deposits in tunnel drainage systems – A study on fabrics and formation mechanisms in Science of the Total Environment 718, 137140.

[6] Pointer, P.; Sellner, S. (2022) Documentation of scale deposits in the Koralm Tunnel – Mapping and Sampling in practice/ Dokumentation von Versinterungen im Koralmtunnel - Kartierung und Beprobung in der Praxis in Geomechanics and Tunnelling 22, no. 4, pp. 392–401. https://doi. org/10.1002/ geot.202200013.

[7] Sakoparnig, M.; Galan, I.; Steindl, F.R.; Kusterle, W.; Juhart, J.; Grengg, C.; Briendl, L.; Saxer, A.; Thumann, M.; Mittermayr, F. (2021) Durability of clinker reduced shotcrete: Ca^{2+} leaching, sintering, carbonation and chloride penetration in Materials and Structures 54, no. 2, pp. 1–23.

[8] Wedenig, M.; Boch, R., Leis, A.; Wagner, H.; Dietzel, M. (2021) Green inhibitor performance against $CaCO_3$ scaling: rate-modeling aided test procedure in Crystal Growth & Design 21, no. 4, pp. 1959–1971.

[9] Leis, A.; Wagner, H.; Eichinger, S.; Domberger, G.; Wedenig, M.; Dietzel, M.; Boch, R. (2022) Application of "Green Inhibitors" for threshold scale inhibitor treatment of tunnel drainage systems / Anwendung von grünen Inhibitoren zur Härtestabilisierung in Tunneldrainagen in Geomechanics and Tunnelling 22, no. 4, pp. 402–413. https://doi.org/10.1002/geot.202200018.

[10] Boch, R.; Pilgersdorfer; Moritz; B. (2022) Reduction of scale formation by optimized drainage conditions – Insights from field testing / Reduzierung von Versinterung durch optimierte Drainagebedingungen – Erkenntnisse eines Feldversuchs in Geomechanics and Tunnelling 22, no. 4, pp. 371–391. https://doi.org/10.1002/geot.202200011.

[11] Arbeiter, F.; Eichinger, S.; Rieß, G.; Schachinger, T.; Boch, R.; Wenighofer, R.; Galler, R.; Hausberger, A.; Strobl, E.; Stur, M.; Salinger, F.; Steiner, M.; Dietzel, M.; Pinter, G. (2020) Optimierte Polymer-Rohrwerkstoffe für effiziente Drainagesysteme in Tunnelbauwerken – PolyDrain Teil II in BHM Berg-und Hüttenmännische Monatshefte 165, no.12, pp. 623–630.

[12] Eichinger, S.; Leis, A.; Boch, R.; Seywald, C.; Dietzel, M. (2020). Assessment and formation mechanisms of scale deposits in tunnels of the ÖBB-Infrastruktur AG – A subproject of the Task Force Drainage / Bewertung von Sinter und deren Bildungsbedingungen in Tunnelbauwerken der ÖBB-Infrastruktur AG – Ein Teilprojekt der Task Force Drainage in Geomechanics and Tunnelling 1, no. 3, pp. 273–285. https://doi.org/10.1002/geot.202000006

[13] Eichinger, S.; Boch, R.; Leis, A.; Baldermann, A.; Domberger, G.; Schwab, C.; Dietzel, M. (2022) Green inhibitors reduce unwanted calcium carbonate precipitation: Implications for technical settings in Water Research 208, 117850.

[14] Dietzel, M.; Purgstaller, B.; Leis, A.; Reichl, P.; Stadler, H.; Niedermayr, A.; Rinder, T.; Wagner, H. (2013) Current challenges for scaling of tunnel drainage systems-modelling approaches, monitoring tools and prevention strategies/Aktuelle Herausforderungen bei der Versinterung von Tunneldränagen- Modellierungsansätze, Monitoringwerkzeuge und Präventionsstrategien in Geomechanics and Tunnelling 6, no. 6, pp. 743–753. https://doi.org/10.1002/geot.201310014

[15] Chan, C.S.; McAllister, S.M.; Leavitt, A.H.; Glazer, B.T.; Krepski, S.T.; Emerson, D. (2016) The architecture of iron microbial mats reflects the adaptation of chemolithotrophic iron oxidation in freshwater and marine environments in Frontiers in Microbiology 7, 796.

[16] Wedenig, M.; Eichinger, S.; Boch, R.; Leis, A.; Wagner, H.; Dietzel, M. (2022) Understanding of Tunnel Drainage Scale Formation by In-Situ Monitoring (under review in Tunnelling and Underground Space Technology).

Chapter 3 - Scale deposits in tunnel drainage systems – A study on fabrics and formation mechanisms

Stefanie Eichinger[1], Ronny Boch[1,6], Albrecht Leis[2], Günther Koraimann[3], Cyrill Grengg[1], Gunnar Domberger[2], Manfred Nachtnebel[4], Christian Schwab[5] & Martin Dietzel[1]

[1] Institute of Applied Geosciences, Graz University of Technology & NAWI Graz GeoCenter, Rechbauerstrasse. 12, 8010 Graz, Austria.

[2] JR-AquaConSol GmbH, Steyrergasse 21, 8010 Graz, Austria.

[3] Institute of Molecular Biosciences, University of Graz, Humboldtstrasse. 50, 8010 Graz, Austria.

[4] Graz Centre for Electron Microscopy (FELMI-ZFE), Steyrergasse 17, 8010 Graz, Austria.

[5] ASFINAG Service GmbH Graz, Fuchsenfeldweg 71, 8074 Graz – Raaba, Austria.

[6] now at: Geoconsult ZT GmbH, Team Geochemistry & Monitoring, Hütteldorfer Str. 85, 1150 Vienna, Austria.

Graphical Abstract

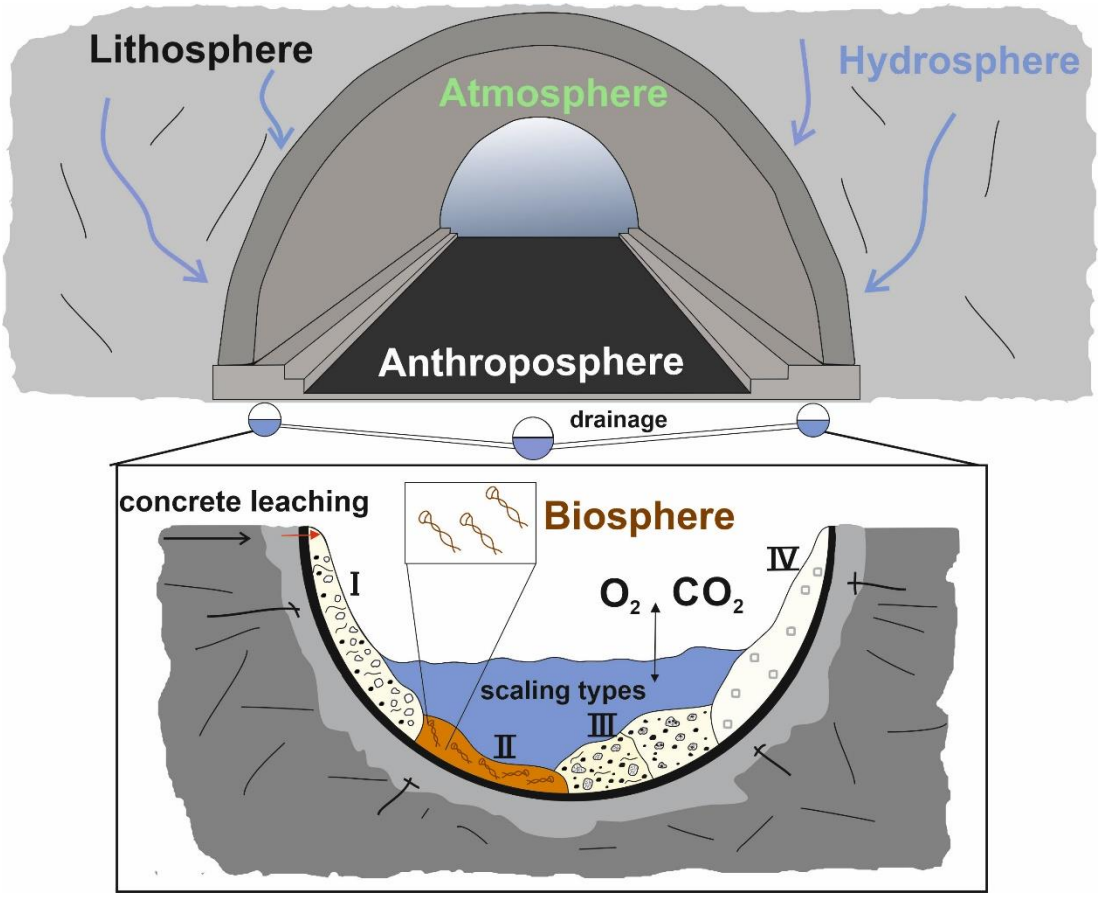

3.1 Abstract

Rapid deposition of chemical sediments, particularly calcium carbonate, is a widespread phenomenon in tunnel constructions, which can significantly disturb water draining. The removal of the scale deposits in the drainage setting is labor and cost intensive. Prediction or prevention of these unwanted scale deposits are challenging and require detailed knowledge on their site-specific source, formation mechanisms and environmental dependencies. This case study combines a mineralogical, (micro)structural, isotopic, microbiological, and hydrochemical approach to understand the formation of scale deposits in an Austrian motorway tunnel. Chemical and isotopic results revealed that all investigated solutions originate from a distinct local aquifer. High pH (11), indicative high alkaline element concentrations (Na 26 mg/l; K 67 mg/l), originated from concrete leaching, and a strong supersaturation in respect to calcite (SI>1) are representative for the environmental setting of scaling type 1. This type is characterized by the formation of calcite, aragonite, and rarely documented dypingite ($Mg_5(CO_3)_4(OH)_2*5H_2O$), and yields in a highly porous material showing minor indications of microbial presence. In contrast, scale deposits of type 2 are strongly microbially influenced, yielding dense and layered mineral deposits, typically consisting of calcite. The corresponding aqueous solution revealed elevated Mg concentration (38 mg/l) and a high molar Mg/Ca ratio (0.8). Scale deposits containing distinct aragonite precipitates next to calcite, mostly growing in pore spaces of the scale fabric, are accounted as type 3. Therein, dypingite is always growing on top of aragonite needles, indicative for prior $CaCO_3$ precipitation. The composition of corresponding solutions shows the highest Mg/Ca ratio (1.1). Scale type 4 is characterized as a compact deposit consisting entirely of calcite. Its corresponding solution exhibits a molar Mg/Ca ratio of 0.6. From the obtained data sets a conceptual model was developed describing the distinct operative and (micro)environmental conditions responsible for the distinct diversity of scale deposits.

3.2 Introduction

The local precipitation and transport related deposition of unwanted minerals constitute a serious problem encountered in numerous industrial processes and geotechnical environments such as highway and railway tunnel drainage systems or other man-made water circuits, such as artificial channels, pipelines and wells (scaling processes manifested in scale deposits; e.g. Hasson et al., 1968; Dietzel et al., 2013). These scale deposits can lead to a dramatic loss in the efficiency of water and/or energy transfers, and in serious cases to a total blockage of fluid

flows (e.g. Dietzel et al., 2008a; Boch et al., 2017). Thereby, unwanted scale deposits depend on geogenic (natural), as well as man-made (technical) environmental conditions. Similar carbonate dominated mineral deposits were reported from water streams in concrete beds (Boch et al., 2015), in historic Roman aqueducts (Sürmelihindi et al., 2013; Passchier et al., 2016) and in wells and related technical components (pump, filter, heat exchanger) exploiting oil/gas and deep geothermal reservoirs (Ma et al., 2013; Boch et al., 2017; Kumar et al., 2018).

In the case of tunnel drainage systems, the formation of calcium carbonate minerals such as calcite ($CaCO_3$) constitutes a severe issue if ongoing deposition and clogging affect water transport in the tunnel water channels and pipe systems (Chen et al., 2019). Tunnel drainage systems facing strongly variable scale deposits have to be continuously monitored and cleaned periodically in order to provide an undisturbed water discharge out of the tunnel. A considerable part of the maintenance costs is associated with the work intensive inspections and mechanical or chemical cleaning of the tunnel drainage systems. In railway tunnels, 15-20% of the entire maintenance work is related to an efficient draining. In highway tunnels ≥ 10,000 € per kilometer and year have to be typically invested for drainage system maintenance (Harer, 2017; Chen et al., 2019). In addition to these direct costs, the service associated tunnel closures or traffic disturbances generate additional indirect costs (Harer, 2017). This clearly argues for a more advanced process understanding and problem-solving strategies with regard to distinct scale formation conditions, i.e. investigating the spatiotemporal reaction mechanisms and pathways and their variable geogenic as well as anthropogenic environmental constraints (Dietzel et al., 2008a). Amongst the major determining geogenic factors involved in unwanted mineral formation in tunnel drainage channels are the local geology and atmospheric/climate conditions, variable water recharge/discharge, flow conditions (turbulent/stagnant) and the site-specific hydrochemistry. Man-made conditions include the constructional design and materials of the tunnel infrastructure (e.g. concrete, steel and plastics), flow geometries, technical ventilation and maintenance strategies (Girmscheid et al., 2003; Dietzel et al., 2008a). Considering the dominant physicochemical mechanisms for rapid $CaCO_3$ precipitation, fluid-solid interaction involving highly soluble concrete components (e.g. portlandite), enhanced exchange of CO_2 between the drainage solution and tunnel atmosphere, potential evaporation, or mixing of solutions are of widespread relevance for scale formation (Rinder et al., 2013; Boch et al., 2015). For example, Chen et al. (2019) investigated several tunnels in France and reported that all tunnels showing major calcium carbonate precipitation in their drainage systems are located in sedimentary rocks. The nature of lining materials and the geometry of tunnels play an important role, as well as the $CaCO_3$ content of the surrounding geology. They

established a database including all principal influencing factors such as the surrounding soil cover, lining materials, cleaning intervals, and others in order to systematically analyze the calcite precipitation problem in the drainage system of railway tunnels and to create an empirical index for quantifying the calcification level. Correlations of this calcification level with different parameters - hydraulic conductivity measurements in surrounding host rocks and soils, pH values, concentrations of Ca^{2+} and HCO_3^-, water temperature - indicate significant effects of surrounding rocks, the hydraulic conductivity and the tunnel length for function and processes in the drainage system. As a potential mitigation solution, removable geotextiles on the surface of gutters are proposed (Chen at al., 2019). Another study by Dietzel et al. (2008b) examined mineral deposition in the Austrian Koralmtunnel showing that individual mechanisms of Ca-carbonate precipitation could be deciphered by hydrochemical modelling in combination with mineralogical, chemical and isotopic analyses. Different scale deposits as well as related aqueous solutions were characterized by laboratory based analytical methods (e.g. X-ray diffraction, FT-IR, ICP-OES, CF-IRMS). The results revealed that the carbonate in the dominantly calcitic scale deposits is either originated from the widespread calcareous groundwater or from the enhanced absorption of atmospheric CO_2 at higher pH conditions promoted by water interacting with soluble concrete constituents (e.g. portlandite). Additional in-situ experiments were used to support the promising application of Ca-carbonate inhibitors, as well as tailored construction materials in order to reduce scale deposit formation.

The above previous studies reveal the importance of an advanced understanding regarding the formation processes of scale deposits. However, none of these investigations have demonstrated or even considered, the impact of microbial activities for the formation of scale deposits in tunnel drainage systems. In the present manuscript, the occurrence of distinct bacteria and their influence on scale formation were clearly verified. Another essential innovation herein is to implement data from continuous in-situ monitoring of aqueous carbonate precipitating solution parameters, in order to uncover effects causing changes in seasonal environmental precipitation conditions. Evaluating our extensive multiproxy based data sets yields in a conceptual model, which is developed to (i) explain the formation mechanisms of the highly divers scale deposits in the investigated tunnel drainage and (ii) address techniques in order to reduce or prevent their occurrence. The highway tunnel Spital am Semmering (Austria) was selected as a case study for a site-specific assessment of common scale material diversities. Scale deposits and related aqueous solutions were collected from different tunnel sections and were analyzed using a broad range of bulk and high-resolution optical, chemical and isotopic tools of mineralogical, petrographic, stable isotope, and hydrochemical analysis (e.g. XRD, transmitted-light,

epifluorescence and electron based microscopy, EPMA, CF-IRMS). An automated and remotely controlled sensor system was implemented as scale guard for in-situ and online monitoring of the ongoing carbonate scaling process in different sections of the drainage system, including continuous measurements of pH, temperature, and electric conductivity.

3.3 Study site and environmental setting

The study area is located in the northeastern part of the Austrian province of Styria hosting the major mountain pass “Semmering” towards the province of Lower Austria and Vienna. The investigated highway tunnel Spital is located near the village Spital am Semmering and is part of the so-called Semmering tunnel chain, which consists of the major (>1 km length) consecutive tunnels Spital (~2500m), Steinhaus and Semmering, as well as some short and unnamed tunnel segments. It is composed of two separate tunnel tubes accommodating unidirectional traffic (northern and southern tube).

The tunnel Spital traverses unconsolidated sediments and solid rocks of variable but limited thickness (10–125m), which are covered by meadows and temperate mixed forests. The major part penetrates through weak metamorphic host rock zones, consisting of graphite- and calcite/sericite phyllites of the Upper Triassic Keuper formation. These strongly foliated phyllites possess distinct intercalations with dolomite and calcite containing rauhwacke (central-alpine sediments), recurrent intercalations of quartzite sequences and occasional lime-/dolostone marbles (Cornelius, 1952; TBBG-Dr.Heim, 2001). The major water discharges (>1 l/s) in the tunnel are mainly located in the carbonate bearing rocks (marble and calcareous rauhwacke; Fig.1).

The tunnel Spital was selected for this study based on its major scaling issues in the tunnel drainage channels, the intermediate length and limited overburden and its diverse geology supporting a dynamic behaviour with regard to changing environmental and scale formation conditions. Former observations revealed that the carbonate dominated scale deposits and accessory minerals are different in their visual appearance and material consistency, even within nearby sections and over time, since hard scale deposits are generally more difficult to remove both mechanically and chemically. In this tunnel, no scale inhibitors (chemical agents suppressing mineral precipitation) are added (neither constantly nor episodically), and the material of the drainage channels is made of polyvinylchloride (PVC) entirely.

The analyzed scale deposits and associated aqueous solutions were collected during a regular maintenance interval in the year 2016 in the northern tube of the tunnel Spital. One of the scale deposits (RAB 4) lacks in the collection of a locally related water sample. RAB 4, 6 and 9 were derived from the major water collecting central-drainage underneath the driving lane, while RAB 17, 18, 23, 24 and 25 formed in the smaller diameter (250mm) lateral-drainage ("Ulmen" drainage) located in the southern tunnel wall (Fig.1).

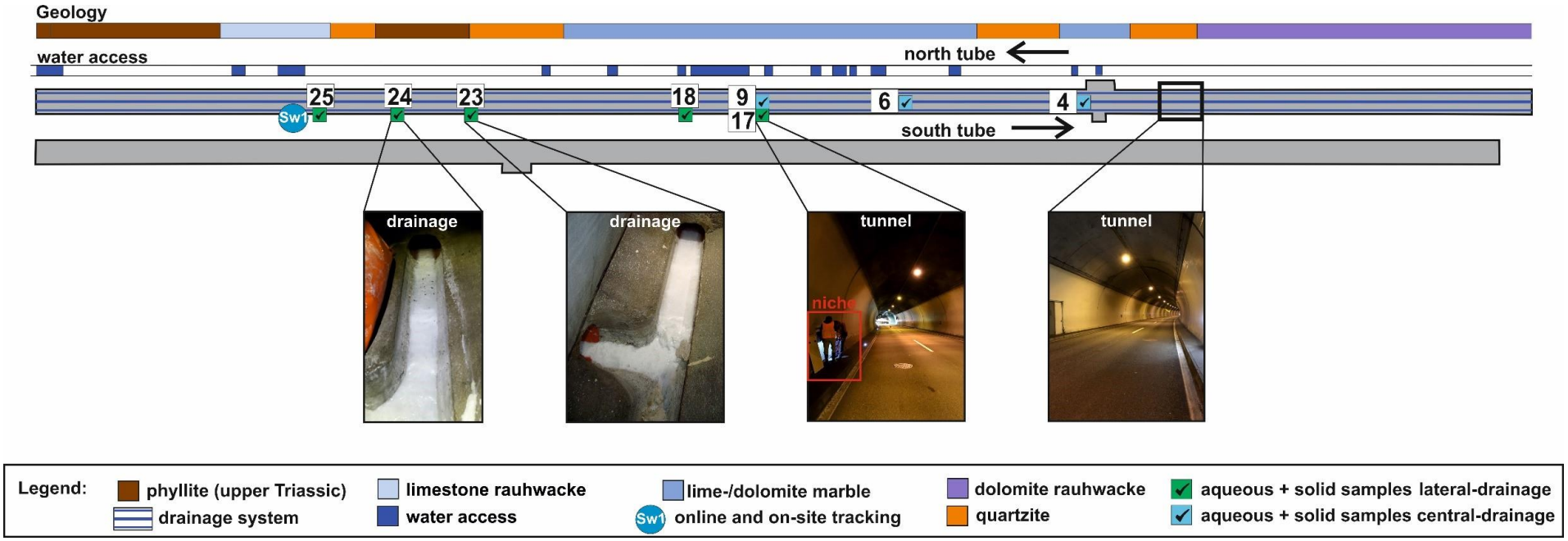

Figure 1: *Overview of the tunnel Spital am Semmering. Surrounding geology of the tunnel and positions of the aqueous solutions and related scale deposits collected from maintenance niches are indicated. SW1: Position of the automated and remotely controlled scale guard sensor system. The two images of the drainage system show severe clogging of the southern lateral-drainage. The arrows denote the direction of traffic in the individual pipes.*

3.4 Analytical methods

3.4.1 Precipitates

The mineral precipitates (scale deposits) were sampled from the drainage channels at the same positions as the aqueous solutions. Each of the two tubes of the tunnel Spital includes southern and northern lateral-drainage channels as well as a larger central-drainage channel. Samples were gathered in the central and southern channels; the northern channel was dry during the time of sampling. Partly red-brownish colored scale deposits (RAB 4, 6 and 9; Figs. 2 & 3) were recovered from the central-drainage of the tunnel, while others (RAB 17, 18, 23, 24 and 25; Figs. 2 & 3) are rather whitish colored and derive from the southern channel.

Mineralogical analyses of the scales were carried out by powder X-ray diffraction (XRD) using a PANalytical X`Pert Pro diffractometer equipped with a Co-Kα-radiation source (40 mA, 40 kV) applied at a 2θ range from 4° to 85°. The mineral phases were quantified by Rietveld refinement using the PANalytical X`Pert HighScore Plus software (version 3.0.4 with the PDF-4 database). The phase compositions of RAB 6 and RAB 9 were further determined by acid digestion with 10 M HCl and the residual solids were then analyzed via powder X-ray diffraction (XRD). The chemical compositions of the acid leachable part of the scale deposits were measured using ICP-OES (Perkin Elmer Optima 8300) with an analytical uncertainty of ±5 % after grinding and acid digestion using 6% suprapure HNO_3. Petrographic studies were conducted on thin sections (30-50 µm) made from cross-sections of the scale deposits using transmitted and reflected light microscopic techniques. Small pieces cut from the scale deposits were gold/palladium-coated and subsequently imaged at high spatial resolution (>2 µm) using a Zeiss DSM 982 Gemini scanning electron microscope (SEM) operating at 2 kV accelerating voltage. Selected samples were also investigated utilizing a Zeiss Sigma 300 VP Environmental Scanning Electron Microscope (ESEM; Schmidt et al., 2019) operating at ~40 Pa pressure and 7 kV voltage in order to avoid the necessity of a conductive coating and to examine the samples by energy-dispersive X-ray spectroscopy (EDX), backscattered electrons (BSE) and Raman spectroscopic analyses. Additionally, qualitative high-resolution elemental distribution images of Al, Ca, Si, K and S, together with backscattered electron images (BSE) of the same areas were recorded by electron probe microanalysis (EPMA) using a JEOL JXA8530F Plus Hyper Probe equipped with a field emission gun. For the measurements the wavelength-dispersive analytical mode with 15 kV acceleration voltage, a beam current of 10 nA and a pixel size of 3 x 3 microns was chosen.

The solid samples were analyzed for their possible microbial content. For this purpose, the scale deposits were cut into hand pieces (6 x 4 cm) and examined using nucleic acid specific fluorescent dyes in combination with a fluorescence detection system. The epifluorescence images were directly obtained from the stained surface of the individual samples using a ChemiDoc MP (BioRad) fluorescence imager as described in (Grengg et al., 2017). Staining of the material was performed using SYTO9 and propidium iodide (PI) from the LIVE/DEAD BacLight bacterial viability kit (Molecular Probes). The dye SYTO9 can enter living and dead cells, while PI only penetrates into dead cells, i.e. when no membrane potential is maintained. When both dyes enter a cell or can bind to free nucleic acids, PI is preferentially bound to DNA or RNA. Only dye molecules interacting with nucleic acids produce a detectable fluorescence signal (Stocks, 2004). 1.5µl of each dye was diluted in 5 ml PBS buffer. The surface of each specimen was covered with the dye solution and kept in the dark for one hour. Subsequently, the surface was carefully rinsed with distilled water and dried for approximately 24h before detecting fluorescent signals. For each sample, three images with three different imager settings (blue or green excitation LEDs together with fluorescein or rhodamine filter sets; white light without filter) were obtained. Exposure times were 0.036, 0.428 or 0.081 seconds for fluorescein (SYTO9), rhodamine (PI), or white light, respectively. Images were also taken before staining using identical settings ("no stain"), allowing for background fluorescence detection. Multichannel, false color images were created by overlay and further processed using Image Lab 4.0 software (BioRad). Identical image parameters were used for all color channels and exported in jpg-format. Final figures were composed using CorelDraw software.

The spatial distribution and related temporal evolution of stable C and O isotopes of the $CaCO_3$ precipitates were sampled pointwise across transects using a hand-held drill and tungsten-carbide drill bits and were measured by a fully automated peripheral continuous-flow gas preparation device (Gasbench II), which is connected to a Finnigan DELTA^{plus}XP isotope ratio mass spectrometer (Thermo Fisher Scientific). Five to twelve spot-samples ("n" in table 3) per scale deposit were extracted across approximately linear transects for evaluating the spatiotemporal distribution in relation to the progressive growth dynamics of the mineral precipitates (Fig. 3). Respective $\delta^{13}C$ and $\delta^{18}O$ values are given in ‰ relative to the VPDB (Vienna Pee Dee Belemnite) reference, with a typical analytical uncertainty (2σ) of ±0.1 and ±0.08 ‰, respectively (cf. Dietzel et al., 2015).

3.4.2 Drainage solutions

Immediately after sampling, the aqueous drainage solutions were filtered through 0.45 µm cellulose acetate filters in the tunnel. The solutions were filled in gas-tight borosilicate glass vessels (0.25 l) for titration (alkalinity) and major anion analyses, as well as in PE vessels (0.05 l) preloaded with 1 ml supra-pure HNO_3 (69%) for major cation, and minor and trace element analyses. On site measurements included pH and specific conductivity (SpC: µS/cm), expressed at a reference temperature of 25° and water temperature (°C), using a handheld WTW pH/Con 3320 instrument connected to a TetraCon 325 probe and for pH a WTW SenTix 41 probe was used. Standard buffer solutions of pH 4, 7 and 10 (Merck) were applied for pH calibration yielding an uncertainty of ± 0.05 pH units.

Alkalinity (given as HCO_3^-) was measured in the laboratory on the same day with a Schott TitroLine alpha plus titrator using a 0.02 M HCl solution resulting in an analytical uncertainty of ±2 %. Concentrations of major cations (Na^+, K^+, Mg^{2+}, Ca^{2+}) and anions (Cl^-, NO_3^- and SO_4^{2-}) were determined by ion chromatography (Dionex ICS-3000 with a KOH eluent generator module) with an analytical uncertainty of ±3 %. SiO_2, ∑Al, Ba^{2+}, Sr^{2+} and ∑Fe were measured applying a Perkin Elmer Optima 8300 DV ICP-OES with a typical analytical uncertainty of ±5 % relative to NIST 1640a standard. Dissolved organic carbon (DOC) was determined using a Shimadzu TOC-V-CPH Total Organic Carbon Analyzer with an analytical uncertainty of ±0.1 mg/l of C.

The computer code PhreeqC (version 3.1.7.9213; Parkhurst & Appelo, 2013) and the integrated aqueous speciation database phreeqc.dat were used to calculate ion charge balances, ionic strengths, activities and DIC values. Accordingly, thermodynamic mineral saturation indices ($SI=\log(IAP/K_{sp}$; where IAP= ion activity product and K_{sp}= solubility product) with respect to calcite ($SI_{calcite}$), aragonite ($SI_{aragonite}$), brucite ($SI_{brucite}$), dypingite ($SI_{dypingite}$; solubility constant from Harrison et al., 2019), strontianite ($SI_{strontianite}$), barite (SI_{barite}), ferrihydrite ($SI_{ferrihydrite}$; solubility constant from mineteq.v4.dat) and the internal partial pressure of CO_2 (P_{CO2} in atm) were calculated.

Stable isotope analyses of the aqueous solutions comprised the hydrogen (δ^2H_{H2O}) and oxygen ($\delta^{18}O_{H2O}$) isotopic compositions of water, as well as the carbon isotopes of dissolved inorganic carbon ($\delta^{13}C_{DIC}$). The δ^2H_{H20} and $\delta^{18}O_{H20}$ of water were analyzed by wavelength-scanned cavity ring-down spectroscopy (WS-CRDS) using a L2120-I system (Picarro). Measurements were done in the high precision mode at the isotope laboratory of JR-AquaConSol in Graz. Results of isotopic measurements are given in per mil (‰) with respect to Vienna Mean Ocean Water

(VSMOW), using the standard delta notation. The analytical uncertainties for stable isotope measurements in water are ±0.8 ‰ and ±0.08 ‰ for δ^2H and $\delta^{18}O$, respectively (cf. Boch et al., 2019). The $\delta^{13}C_{DIC}$ values were analyzed with a continuous-flow mass spectrometer (Finnigan DeltaplusXP; Thermo Fisher Scientific) coupled to a Gasbench II device (Thermo Fisher Scientific). The $\delta^{13}C_{DIC}$ values were determined following the sampling procedure and measurement protocol reported in Spötl (2005). The carbon stable isotope ratios are referred to Vienna Pee Dee Belemnite (VPDB); the analytical uncertainty is ±0.1 ‰.

In addition, an automated and remotely controlled scale guard sensor system was installed in 2017 in the lateral-drainage of the same drainage system, which recorded the temperature, SpC and pH value continuously in intervals of 15 minutes throughout the year 2018 (the selected stationary point of measurement is close to the solution of RAB 25; Fig.1). The robust sensors (SpC and pH electrodes) allow for an online and on-site tracking of these in-situ parameters based on a WTW TetraCon 325 electrode for the electric conductivity and a PHEHT sensor of Aqualabo/Ponsel for pH measurements. This data logging system was implemented for in-situ environmental monitoring of the ongoing scaling process in a selected section of the tunnel drainage system.

3.5 Results

3.5.1 Scale deposits

3.5.1.1 Morphology, mineralogy and chemistry

In Fig. 2 and 3 the macroscopic morphologies and cross sections of the scale deposits are shown. All of the collected scale deposits indicate some individual appearance with respect to coloring, material consistency, layering and texture, although being recovered from the same tunnel. The scale deposits RAB 17, 23, 24 and 25 are visually characterized by a snow-white to creme-whitish color, whereas RAB 9 is prominently red-brownish colored (Fig.2C and 3C). RAB 4 and RAB 6 consist of prominent white and brown layers in different proportions, while RAB 18 shows variations of beige and white colors (Figs. 2A, B, E and 3A, B, E). Interestingly, the white colored scale deposits typically formed in the southern lateral-drainage channel, while the red-brownish precipitates deposited in the larger diameter central-drainage channel. In addition, the morphology, surface topography and interior fabrics of the scale deposits differ significantly. RAB 6, 17, 18 and 25 appear highly porous in major parts, while RAB 23 and 24 microstructures are relatively compact and dense regarding their growth fabric (Figs. 2F, G and

3F, G). Especially, scale deposit RAB 17 represents a highly porous precipitate (Figs. 2D and 3D). In some parts, RAB 18 shows macroscopically visible plane structures (Figs. 2E and 3E). RAB 9 is relatively thin with a constant thickness of ~1 cm and distinct ripple structures on its growth surface. This scale deposit is also relatively compact and thus hard and further exhibits some distinct mm-range layering, while RAB 25 exhibits some strongly curved and curtain-like structures (Figs. 2C, H and 3C, H). Notably, the scale deposits RAB 6, 18 and 25 display a prominently curved and floating surface topography and a high overall porosity fabric compared to RAB 4, 9, 17, 23 and 24, which are characterized by smoother and less sculptured growth surfaces.

The dominant mineralogical component of all collected scale deposits is low-Mg calcite (<4 mol.% of $MgCO_3$; table 1). In most of the scale deposits studied, except for RAB 9, 23 and 24, the $CaCO_3$ polymorph aragonite was also detected. RAB 4, 6 and 17 display an elevated aragonite content (8, 10 and 14 wt.%, respectively; see table 1 and Figs. A.1-6 and B.1-2; Appendix), but solely in RAB 18 the aragonite content (49 wt.%) is about equal than the calcite content (50 wt.%). In two scale deposits (RAB 6 and 18), the mineral brucite ($Mg(OH)_2$) was found as a trace component (~1 wt.%, table 1; Figs. A.3 and B.1; Appendix). Mineralogy obtained from residual solids after hydrochloric acid (10M HCl) digestion of colored carbonate subsamples revealed the (detrital) occurrence of quartz, rutile, muscovite, clinochlore and kaolinite (see Figs.B.1-2; Appendix).

Table 1: *Mineralogical composition (in wt.%) of the investigated deposits according to XRD analyses and Rietveld refinement. $MgCO_3$ in mol% means $MgCO_3$ percentage in calcite. All scale deposits are $CaCO_3$ dominated, accessory minerals comprising quartz, feldspar and dypingite are <1 wt.% and not included in the given calculations.*

Sample ID	Calcite	Aragonite	Brucite	$MgCO_3$
	wt.%	wt.%	wt.%	mol%
RAB 4	92	8	-	1.0
RAB 6	89	10	1	0.1
RAB 9	100	-	-	1.8
RAB 17	86	14	-	1.6
RAB 18	50	49	1	2.0
RAB 23	100	-	-	0.0
RAB 24	100	-	-	0.0
RAB 25	99	1	-	0.3

Based on chemical analyses after acid digestion of the carbonate scale deposits, the measured calcium contents in the carbonate scales vary between 33.9 and 39.3 wt.%. The red-colored and prominently compact scale deposit RAB 9 contains the lowest calcium content (33.9 wt.%),

while scale deposits hosting a calcium concentration of ~40 wt.% consist of more or less pure calcite (e.g. RAB 23; table 2). For magnesium, the concentrations determined in the solids are in the range of 0.1 – 1.8 wt.%. Strontium and barium contents are also highly variable and show concentrations between 223 and 6052 mg/kg and 155 to 567 mg/kg, respectively. The iron contents are highly different for the individual scales and yield values between 10 and 2526 mg/kg (table 2). The four scale deposits (RAB 4, 6, 9 and 18) possessing some distinct coloring show iron and manganese values between 939 and 2526 mg/kg and 36 to 110 mg/kg, respectively (table 2).

Table 2: *Chemical composition of the scale deposits collected from the drainage channels of the tunnel Spital.*

Sample ID	Ca^{2+}	Mg^{2+}	K^{+}	Na^{+}	Sr^{2+}	Ba^{2+}	∑Fe	∑Mn	∑Al	SiO_2
	wt.%	wt.%	mg/kg	mg/kg	mg/kg	mg/kg	mg/kg	mg/kg	mg/kg	mg/kg
RAB4	36.2	0.8	163	791	4656	319	939	41	145	881
RAB6	37.4	1.8	270	506	4735	155	973	36	110	1933
RAB9	33.9	0.3	23	278	2491	157	2526	110	74	549
RAB17	39.3	0.5	291	581	6052	288	30	4	79	450
RAB18	35.9	1.1	92	482	1271	453	1313	49	174	1287
RAB23	39.3	0.1	130	290	223	183	14	<1	128	310
RAB24	37.3	0.1	82	267	267	241	17	<1	73	261
RAB25	38.6	0.6	215	378	888	567	10	<1	202	640

***Figure 2**: Macroscopic appearance of the scale deposits collected from the motorway tunnel Spital am Semmering (Austria). Specimens RAB 4, 6 and 9 (A, B and C) were sampled from the central drainage channel and display prominent areas of red-brownish coloring, where RAB 9 is rather thin layered and brownish stained (C). Sample RAB 9 is more compact (dense), while RAB 4 and 6 are more porous (A and B). The white colored samples originate from the southern lateral-drainage channel. Precipitates RAB 17, 18 and 25 are highly porous (D, E and H), while the specimens RAB 23 and 24 are more compact (F and G).*

3.5.1.2 Petrography and microstructure

Petrographic characterization was conducted using transmitted and reflected light microscopy. The thin-section based microscopic evaluation supports the highly variable macroscopic appearance of the individual solid specimens. Scale deposit RAB 4 is characterized by columnar shaped calcite and recurrent micritic particle layers. Small crystallites (~15 µm) often act as a nucleation substrate for the development of subsequent columnar and competitive crystal growth (Fig.4A). The aragonite is mostly fascicular and spherically shaped and is mainly localized inside and near the widespread pore spaces. In some areas of the thin-section studied, aragonite is partially converted to calcite. RAB 9 represents a relatively thin (~1 cm), compact and well-layered (mm-range) scale deposit exhibiting low porosity and two main zones can be distinguished based on the layers and coloring (zonation). Areas of more or less continuous crystal growth can be distinguished from areas characterized by allochthonous (detrital) material introduced (Fig.4C and D). The calcite crystals are frequently fan-shaped owing to the competitive growth evolution with some minor contributions of detrital particles in pore spaces. The individual layers of RAB 9 are characterized by a dominant red-brownish coloring, although of different color intensity, and constitute a repeated but variable growth succession based on the thin-section analysis. Scale deposit RAB 17 shows an overall porous growth fabric and is composed of porous and rounded rhombohedral calcite crystals and more spherical and fascicular aragonite bundles. The fascicular shaped aragonite crystals have obviously grown heterogeneously on a previous calcite substrate, while the spherical aragonite crystals are mostly localized within the frequent pore spaces of the mineral precipitate (Fig.4E and F). The calcite crystals in scale deposit RAB 23 show non-oriented (c-axis) and rounded crystal shapes (Fig.4G). Scale deposit RAB 24 consists of typically smaller (~30 µm) and some lager (~150 µm) calcite crystals. In this scale deposit, recurrent growth interruptions occur, which are characterized by micritic and randomly agglomerated calcite crystals (Fig.4H). Finally, scale deposit RAB 25 contains calcite as the main and aragonite as a minor mineral component. The aragonite crystals are again characterized by a spherical and fascicular fabric. The calcite layers typically consist of feather-like columnar to dendritic and competitively growing (well-oriented) crystals (Fig.4B). In general, most of the investigated scale deposits are characterized by a strongly directed columnar and competitive crystal growth and by some intra-crystalline growth interruptions indicated by thin micritic layers. These growth interruptions often act as an attractive nucleation substrate for subsequent vivid crystal growth. Scale deposits containing aragonite typically appear more porous partially owing to the fascicular crystal fabric and related intercrystalline voids.

The ESEM analyses of selected solid scale deposits and micrometer-range areas largely confirm the mineralogical results inferred from XRD. Some scale deposits show distinct remnants of microbial presence associated with the $CaCO_3$ crystals. In one of the scale deposits (RAB 9), the microbial influence can be associated with small spherical crystallite aggregates of high specific surface area, which contain Fe according to EDX analyses and thus most likely represent an iron-(hydr)oxide solid, e.g. the mineral ferrihydrite ($Fe_{10}O_{14}(OH)_2$); Fig.5B). RAB 9 further revealed microbial structures that were previously assigned to the bacterial genus and species *Gallionella ferruginea* (Hallberg & Ferris, 2004; Suzuki et al., 2011; Heim et al., 2015; Fig.5A and E). According to distinct EDX spot analyses, the typically twisted stalks of these microorganisms primarily consist of the elements Fe, Ca, O, C and Si (Fig.5A). These twisted filaments are distributed over the entire scale deposit RAB 9. RAB 17 also shows evidence of microbial activity in the form of extracellular polymeric substances (EPS) related to mineral deposition in the tunnel drainages. Described EPS structures were found to be distributed over the entire deposit RAB 17, resembling a spider web (Fig.5C, red arrows). In scale deposit RAB 17, however, it was not possible to relate the observed microbially-induced structures to a particular genus or even species.

The main component of all investigated scale deposits based on ESEM is calcite, whereby aragonite was found in some of it. In the scale deposits (RAB 4, 6, 17, 18 and 25) consisting of both calcite and aragonite, the aragonite crystals typically exhibit acicular to fascicular crystal shapes and are further mostly restricted to the widespread pore spaces (Fig.5F). A few scale deposits (RAB 6, 17 and 25) occasionally show (hemi)spherical and prominently rosette-shaped crystal forms of 10 to 50 µm in size. Based on Raman spectroscopy, they are attributed to the rarely documented hydrous magnesium hydroxide carbonate mineral dypingite ($Mg_5(CO_3)_4(OH)_2*5H_20$; Fig.5D). Dypingite exhibits a distinct peak at ~3600 cm^{-1} assigned to the MgOH stretching vibration of dypingite (Frost et al., 2009; Fig.12). To the knowledge of the authors, this is the first time that dypingite was found in scale deposits of a tunnel (drainage) setting. The other distinct peaks in the measured Raman pattern belong to the mineral aragonite (Fig.12), since dypingite is closely associated with aragonite and typically grows on the top of locally widespread acicular aragonite bundles (Fig.5D).

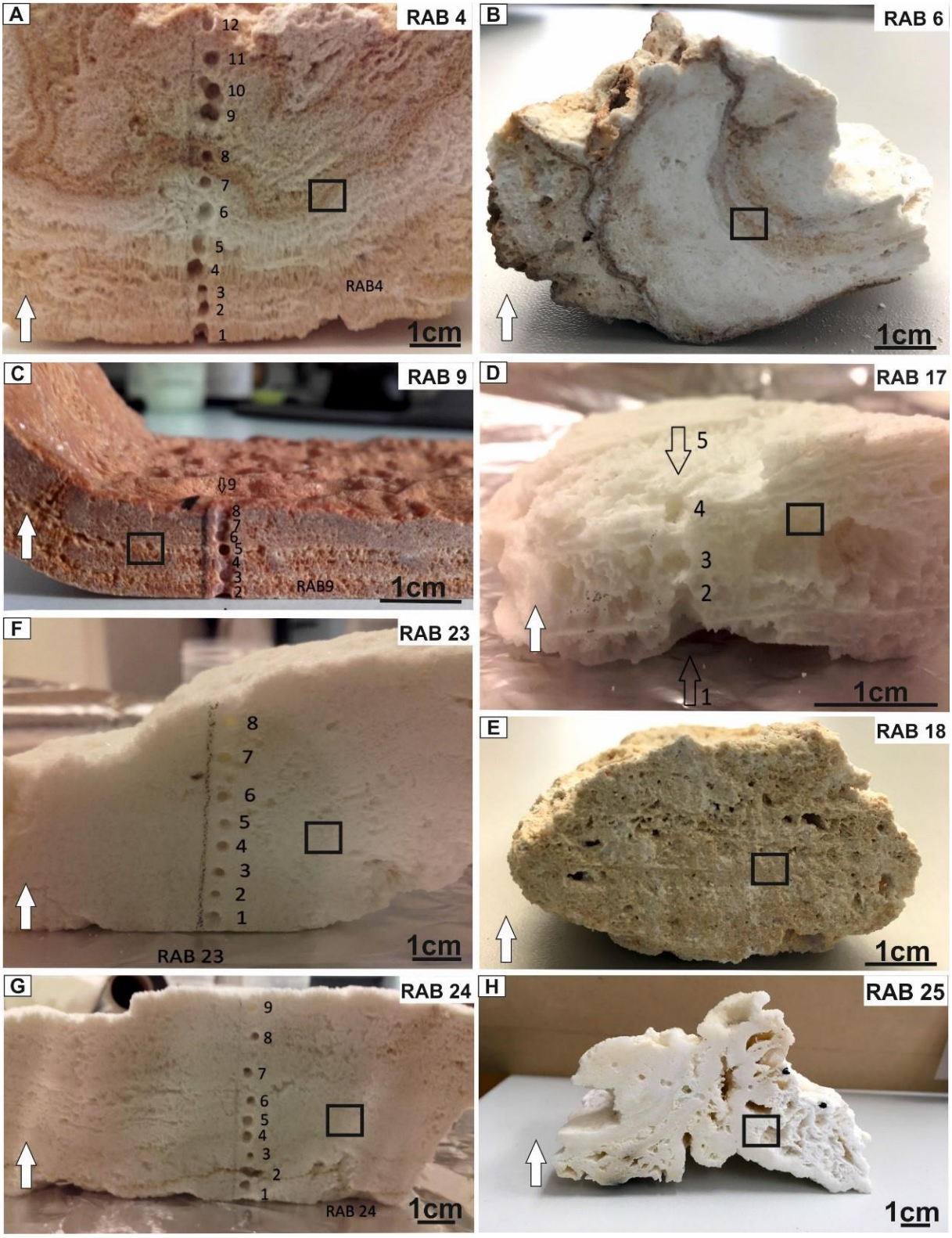

***Figure 3**: Cross-sections of the investigated scale deposits. The white arrows indicate growth direction (bottom to top), while the black squares show areas for micro structure analysis in Fig. 4. Numbers point to drillings for stable C and O isotope analysis.*

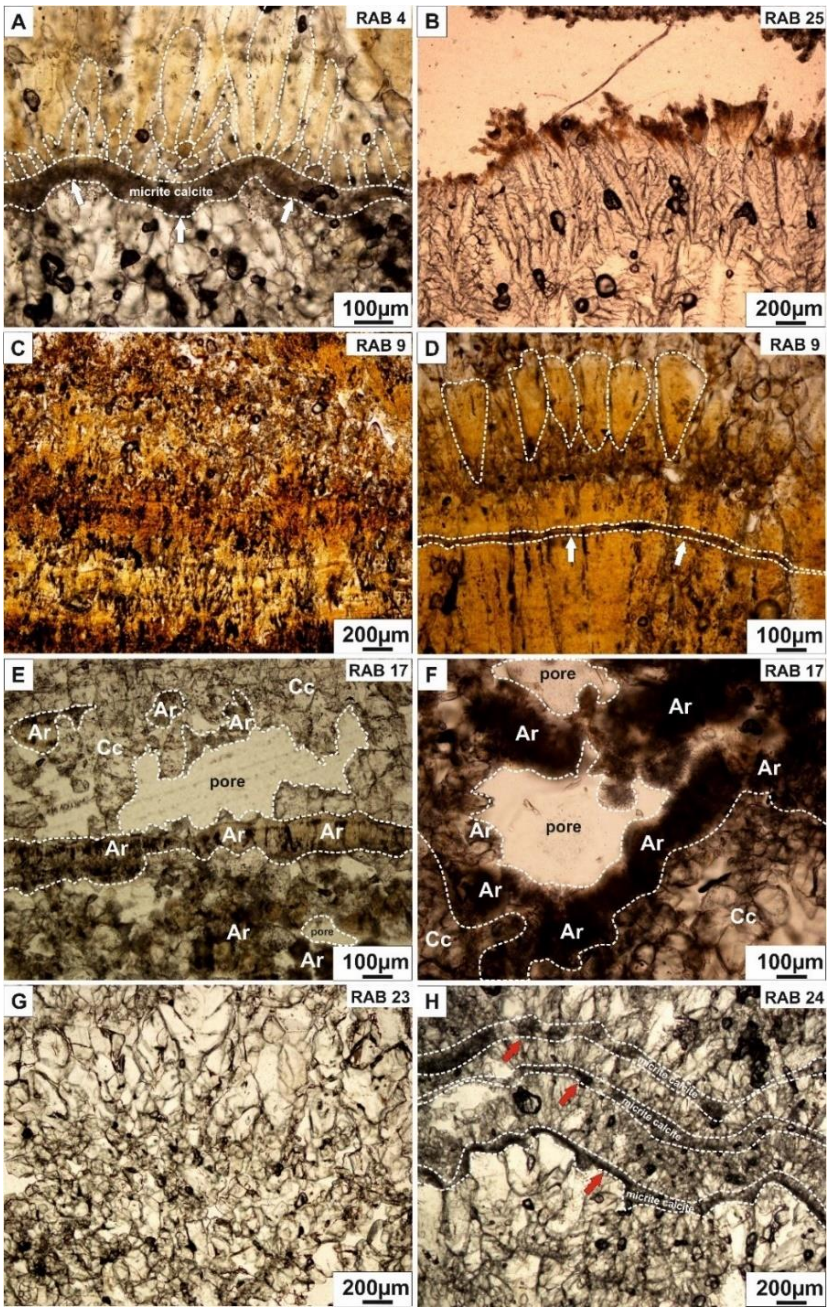

***Figure 4**: Microscopic characterization of the scale deposits shown in Fig. 3 using thin section transmitted-light imaging. A) Precipitate RAB 4 indicates a distinct growth interruption with micritic calcite (white arrows) and subsequent re-nucleation of competitively growing columnar shaped and well-oriented calcite fabric. B) RAB 25 exhibits feather-like dendritic calcite crystals. C and D) RAB 9 reveals fan-shaped, reddish colored calcite crystals with fine intra-crystalline detritus layers (white arrows). E and F) Occurrence of interrelated aragonite (Ar) and calcite (Cc) crystals in precipitate RAB 17. Note the prominent localization of aragonite in and near major pores of the dominantly calcitic precipitate. The large growth pores, which are filled with secondary aragonite, tend to indicate the presence of relatively porous biofilms often relevant for the deposition of such scale deposits in tunnel drainages. G) Calcite crystals of RAB 23 appear non-orientated with almost rounded shapes, suggesting suspended particle transport and subsequent agglomeration associated with later stage cementation. H) RAB 24 shows intervals of repeatedly interrupted growth indicated by micritic calcite crystals (red arrows).*

3.5.1.3 Distribution of elements

The elemental distribution maps of cross sections of scale deposit RAB 4 clearly reflect the variable strontium and magnesium concentrations to be closely related to the occurrence of the different $CaCO_3$ polymorphs calcite and aragonite (Fig.6A). Calcite crystals are indicated by elevated magnesium contents, while the aragonite crystals are characterized by elevated Sr contents (see also Böttcher and Dietzel, 2010). Moreover, the Sr concentration is typically higher in the exterior parts of the spherulitic-fascicular aragonite crystals compared to their interior sections of individual crystals (Fig.6, RAB 4, Sr). RAB 9 entirely consists of calcite and is further characterized by an increased iron content, typically located close to local pore spaces within the otherwise compact scale deposit (Fig.6, RAB 9). The Fe concentrations, and to a lesser extent also Mg, vary with regard to the pronounced layering which can be observed both micro- and macroscopically showing a close relationship between the variable chemical composition and petrography (e.g. more Fe corresponds to a more porous texture). Scale deposit RAB 25 shows elevated Mg concentrations in some of the carbonate matrix and detrital components. Around some distinct pore spaces, the Mg concentration is higher, most likely due to the restricted occurrence of dypingite (Fig.6, RAB 25, Mg). Sr and Fe contents do neither reveal high concentrations nor distinct spatial variations in the scale deposit RAB 25.

3.5.1.4 Microbial activity

Epifluorescence imaging of the stained scale deposit surfaces using specific DNA and RNA sensitive dyes revealed some general microbial presence by distinct clusters of enhanced fluorescence (Fig.7). In RAB 17 the chemical treatment and subsequent optical evaluation revealed clear evidence of both dead as well as living cells being present in the scale deposit; while RAB 18 only supports the occurrence of remnants of some indistinct former microbial presence (Fig.7). Both, RAB 17 and 18, indicate relatively strong preexisting (auto-)fluorescence despite of some clear additional microbially induced fluorescence, while RAB 9 reveals no significant (auto)fluorescence. All of the other scale deposits investigated (RAB 4, 6, 23, 24 and 25) show no striking evidence of microbial activity according to the epifluorescence analysis.

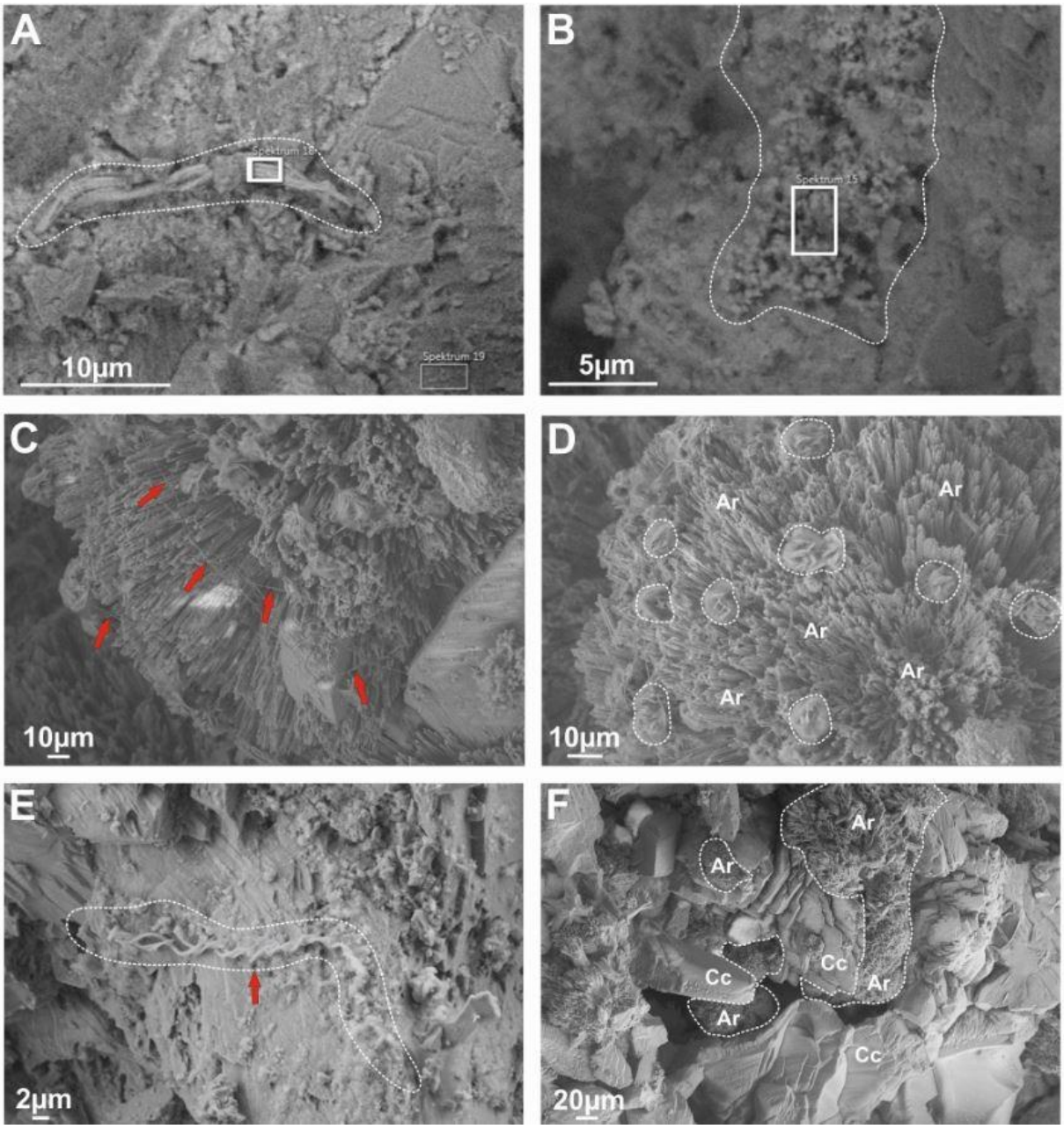

Figure 5*: High-resolution environmental scanning electron microscope (ESEM) images of selected surface and interstitial sections from scale deposits introduced in Figs.2 and 3. A) RAB 9 clearly exhibits remnants of the bacteria Gallionella ferruginea. The typically twisted stalks mainly consist of the elements Fe, O, C, Ca and Si according to its EDX spectrum (white rectangle; see Fig. D.1, Appendix). B) The bacterial influence of Gallionella is often associated with nano-sized spherical particles, which can be assigned to the mineral ferrihydrite ($Fe^{III}_{10}O_{14}(OH)_2$, white delimited area)). The white square shows the area of an EDX measurement reported in Fig. D.2, Appendix. C and D) RAB 17 mainly consists of calcite and aragonite (Ar); Ar shows a common occurrence together with dypingite ($(Mg_5(CO_3)_4(OH)_2*5H_2O)$; dotted circles in D). RAB 17 displays some microbial activity in the form of EPS strands (red arrows in C). E) Twisted stalk of the bacterium Gallionella ferruginea in RAB 9. F). Ar is mostly located in interstitial pore spaces of the calcite (Cc) dominated matrix in RAB 17.*

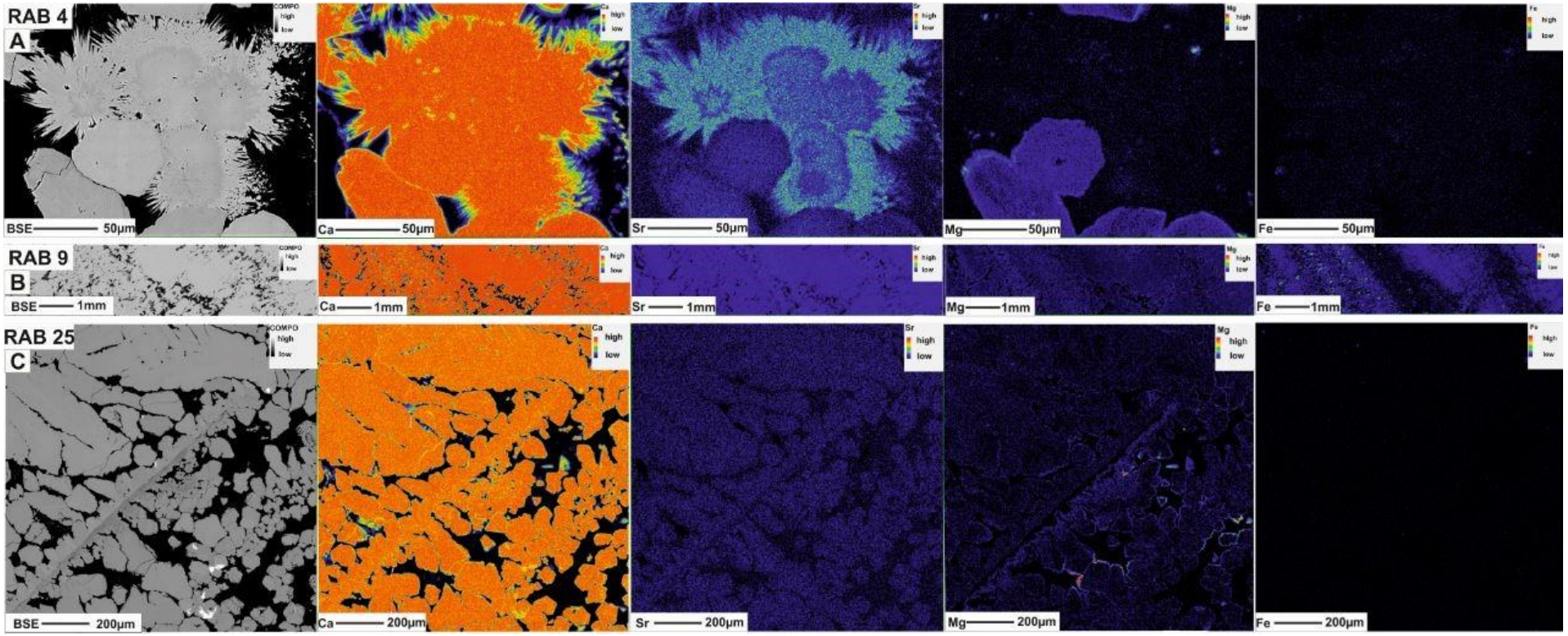

***Figure 6**: Characteristic BSE and elemental images of the calcium, strontium, magnesium and iron concentration distribution of the precipitates RAB 4, 9 and 25 being indicative for variable mineral formation conditions (see text). A) RAB 4 contains significant amounts of aragonite besides calcite (see table 2; Appendix 1A) also indicated by BSE analysis (left-hand image). The strontium content is higher at the rim consisting of aragonite needles compared to its denser central part. This is indicative of the successive transformation from pristine aragonite to calcite. B) RAB 9 contains calcite as dominant precipitate related to some bacterial influence (see Fig. 4). Element mapping indicates distinct areas and layers in the sample where high Fe contents are visible (ferrihydrite). These correspond to sections of increased pore space in the scale deposit. In contrast, in precipitates RAB 4 and 25 no significant iron enrichment could be detected. C) In RAB 25, the high magnesium content is most likely related to the Mg-carbonate mineral dypingite. Thus, RAB 25 consists of aragonite and dypingite next to the prevailing calcite domains. The Mg concentration is partly conspicuous on the grain boundaries or in the pore spaces of the porous carbonate matrix. This indicates the significance of variable and hydrochemically evolved interstitial solutions circulating in the pore spaces of the matrix. For instance, a Mg (versus Ca) enriched interstitial solution can lead to the precipitation of aragonite and/or dypingite.*

3.5.1.5 Stable isotopes

In order to decipher the origin and formation conditions of the carbonate component (CO_3^{2-}), stable C and O isotopic compositions of the selected scale deposits RAB 4, 9, 17, 23, 24 and 25 were analyzed. The measured $\delta^{13}C_{prec}$ values range from -12.2 to -9.4 ‰ (mean: -10.9 ± 1.1 ‰ VPDB) considering all of the investigated solids (table 3). RAB 9 shows the highest $\delta^{13}C_{prec}$ from -9.6 to -9.3 ‰ (mean: -9.4 ‰), while scale deposit RAB 23 displays the lowest $\delta^{13}C_{prec}$ (-12.4 to -12.0 ‰; mean: -12.2 ‰; table A.1; Appendix). The analyzed $\delta^{18}O_{prec}$ values of the scale deposits vary between -10.4 and -7.3 ‰ (mean: -9.1 ± 0.6 ‰; table 3), i.e. a similar amplitude of ~3 ‰ compared to $\delta^{13}C_{prec}$. RAB 17 shows the highest $\delta^{18}O_{prec}$ values of -9.6 to -7.3 ‰ (mean: -8.2 ± 0.9 ‰), while scale deposit RAB 24 displays the overall lowest $\delta^{18}O_{prec}$ values (-10.4 to -9.1 ‰; mean: -9.7 ± 0.6 ‰; table A.1; Appendix).

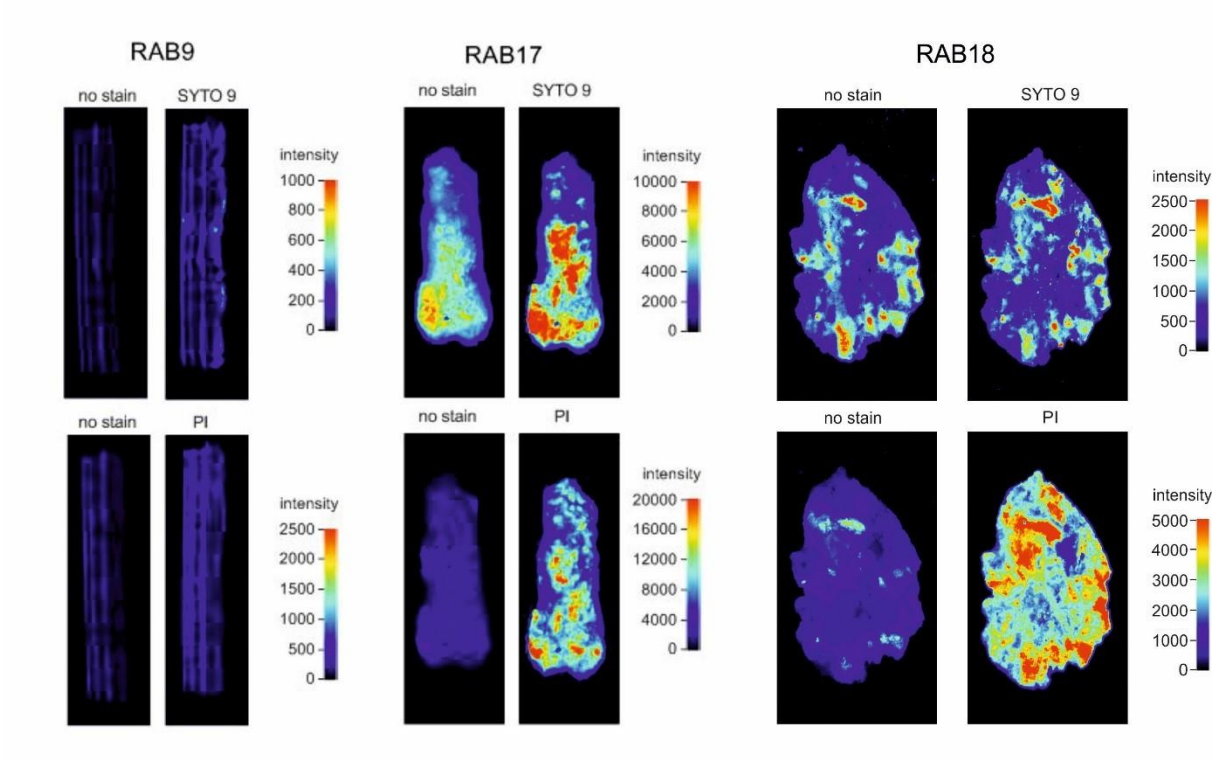

Figure 7: *Epifluorescence images of selected scale deposits. RAB 17 and 18 clearly revealed distinct evidence of microbial presence, while specimen RAB 9 revealed no clear indication of bacterial DNA/RNA in the carbonate precipitate. RAB 17 indicates the possibility of alive (based on SYTO 9 stain), as well as dead bacterial organic matter (PI stain), while RAB 18 contains dead bacterial cells primarily (PI stain). No stain does not exclude other (organic) sources of fluorescence in the sample (e.g. humic and fulvic acids).*

3.5.2 Composition of drainage solutions

Hydrochemical characteristics of the investigated drainage solutions (n=7) are highly variable regarding pH, alkalinity and the dominant ion concentrations such as Ca^{2+}, Mg^{2+}, SO_4^{2-}, Na^+, and K^+ (table 4). The measured pH values range from 7.7 to 11.2 and show a broad range for this small number of samples. Electric conductivity (SpC) was analyzed to be between 313 and 784 µS/cm, which mirrors the change in ion concentrations briefly presented in the following: Ca^{2+} (54 - 77 mg/l); Mg^{2+} (6.7 - 38.3 mg/l); SO_4^{2-} (13 - 152 mg/l); Alkalinity (as HCO_3^-: 90 - 328 mg/l); DIC (0.5 – 5.5 mmol/l); NO_3^- (<0.1 – 7.4 mg/l) and Cl^- (1 - 9 mg/l). Potassium and sodium concentrations are low to intermediate in most of the drainage solutions (2 – 14 mg/l and 2 – 8 mg/l), except solution RAB 17 showing higher values (67 and 26 mg/l, respectively). Minor and trace components in solution are aluminum (34 to 63 µg/l), barium (40 to 163 µg/l) and strontium (0.1 – 2 mg/l), as well as iron (up to 10 µg/l; see table 4). DOC values range from 0.5 to 2 mg/l of carbon.

Calculated ionic balance (Percent error: 100*[(Cat-An)/(Cat+An)]; Cat and An refer to total positive and negative charges induced by dissolved cations and anions, respectively) of the drainage solutions is below <5 %. As an exception the ionic balance of solution RAB 17 shows a deviation of 12 % (table 4). The latter high value can be explained by an elevated analytical error caused by very low H^+ activities at high pH (11.2) of this solution. Calculated saturation indices for calcite range from 0.2 to 1.4, i.e. from slight to strong supersaturation. Other calcium carbonate phases such as aragonite show slightly lower $SI_{aragonite}$ values from 0.01 to 1.2 due to the different (higher) solubility constant. Thus, all solutions are characterized as being (super)saturated with respect to calcite and aragonite. Most of the drainage solutions are also supersaturated with respect to barite ($BaSO_4$; SI_{barite} = 0.2 – 0.7). Brucite ($Mg(OH)_2$), supersaturation is only reached in solution RAB 17 ($SI_{brucite}$ = 0.9), while the other drainage solutions are undersaturated. Solutions RAB 9 and RAB 17 approach saturation of strontianite (SI_{SrCO3}= 0.02 - 0.1). All solutions are undersaturated with respect to dypingite ($SI_{dypingite}$= -4.4 to -15.9). The internal partial pressure of CO_2 (P_{CO2} in atm) ranges from $10^{-2.4}$ to $10^{-8.0}$ atm.

Combining the field, laboratory and calculated hydrochemical parameters of the fluids, some distinct relationships can be identified. Na^+ and K^+ concentrations covary positively and increase with pH (elevated Na^+ and K^+ at higher pH). Mg^{2+} and Ca^{2+} concentrations show a negative correlation with pH (lower concentrations at higher pH; Fig.8B). Consequently, Mg^{2+} and Ca^{2+} contents display a positive relationship. The drainage solutions further exhibit variable

molar Mg^{2+}/Ca^{2+} ratios from 0.2 up to 1.0. A strong negative covariation is valid for pH versus $logP_{CO2}$ (Fig.8A).

Monitoring of selected physicochemical parameters in the drainage system from January to December 2018 based on automated sensors (scale guard monitoring tool) 2000m inside from the west portal of the tunnel revealed variable water temperatures from 5.1 to 12.1 °C (Figs.1 & 8). The contemporaneous seasonal variations in air temperature were gained from a nearby weather station (Fröschnitztal near Spital am Semmering; January – December 2018; 990m a.s.l. ÖBB-Infrastruktur AG). During the summer months, the air temperature measured outside the tunnel is rather similar to the water temperature of the drainage solution (12 vs. 10 °C, i.e. on average 2 °C difference), while in winter (ca. November until March) it differed significantly from the water temperature (-1 vs. 6 °C, i.e. ~8 °C difference). The pH values also revealed some relevant seasonal variation. Within the winter months, the pH was overall higher, at around 8.3 ± 0.1, while being significantly lower during the summer months (7.9 ± 0.1; April until October). The electric conductivity measurements ranged from 480 to 662 µS/cm during a year of observation and were typically ~100 µS/cm higher during the winter months (Fig.8C and D). The stable isotopic compositions of the investigated drainage solutions (n=7) based on one sampling campaign vary between different sampling points within a relatively narrow range from -73.6 to -75.4 ‰ (VSMOW) for the H isotopes (δ^2H_{H2O}) and from -10.6 to -10.8 ‰ (VSMOW) for the stable O isotopes ($\delta^{18}O_{H2O}$). The $\delta^{13}C_{DIC}$ values range from -9.7 to -11.9 ‰ VPDB (table 3). RAB 17 (-11.9 ‰) is significantly depleted in $^{13}C/^{12}C$ compared to the other drainage solutions (-9.7 to -10.8 ‰; mean: -10.5 ‰ VPDB).

***Table 3**: Stable isotopic composition of the water (δ^2H, $\delta^{18}O$) and of the DIC ($\delta^{13}C_{DIC}$) and $\Delta^{13}C_{prec\text{-}DIC}$ as well as mean $\delta^{13}C_{prec}$ and $\delta^{18}O_{prec}$ values (n=5-12) of the carbonate precipitates. Calculated calcite formation temperatures after Coplen (2007) and Kim & O `Neil (1997) are mean values (n=5-12). Temp (meas.) is the temperature measured in the precipitating drainage solution (see also Tab. 3).*

Sample ID	δ^2H ‰, VSMOW	$\delta^{18}O$ ‰, VSMOW	$\delta^{13}C_{DIC}$ ‰, VPDB	$\delta^{13}C_{prec}$ ‰, VPDB	$\delta^{18}O_{prec}$ ‰, VPDB	n	$\Delta^{13}C_{prec\text{-}DIC}$	Temp (°C) (after Coplen, 2007)	Temp (°C) (after Kim& O`Neil,1997)	Temp (°C) (meas.)
RAB 4	–	–	–	-10.5	-9.0	12	–	–	–	–
RAB 6	-73.6	-10.7	-9.9	–	–	–	–	–	–	–
RAB 9	-74.4	-10.7	-9.7	-9.4	-9.3	9	0.3	14.3	7.1	8.1
RAB 17	-75.4	-10.8	-11.9	-10.1	-8.2	5	1.8	9.1	2.2	9.0
RAB 18	-73.9	-10.6	-10.8	–	–	–	–	–	–	–
RAB 23	-75.0	-10.7	-11.3	-12.2	-9.6	8	-0.9	15.7	8.3	8.2
RAB 24	-74.3	-10.8	-10.8	-11.8	-9.8	9	-1.0	16.7	9.2	8.8
RAB 25	-74.5	-10.7	-10.8	-11.2	-8.6	8	-0.4	11.2	4.2	8.7

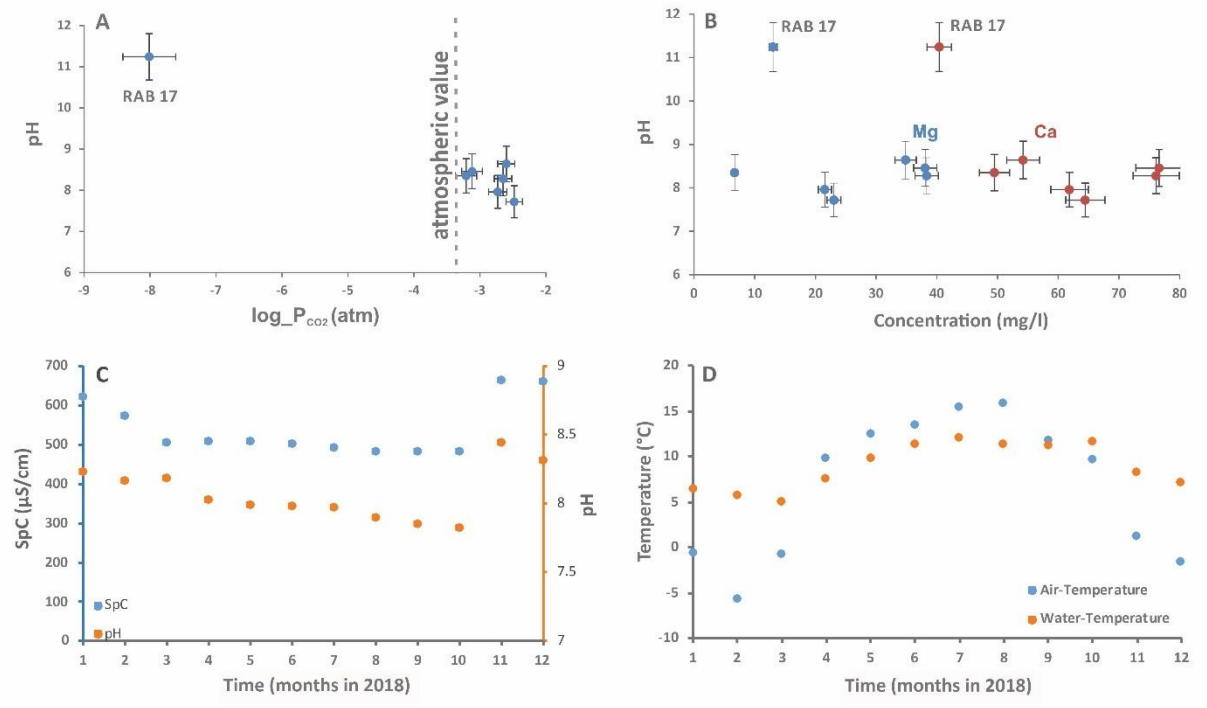

***Figure 8**: Hydrochemical and temperature data. A) pH vs. internal carbon dioxide partial pressure of the aqueous solutions showing a clear inverse relationship. Lower P_{CO2} (< $10^{-3.4}$ atm; dashed line) causes CO_2 absorption from the Earth`s atmosphere into the solution. B) pH vs. calcium and magnesium concentrations reflecting a trend of lower Ca^{2+} and Mg^{2+} concentration at elevated pH (RAB 17) (see Tab.3). In-situ and online "scale guard" monitoring: C) Temporal evolution of the specific electric conductivity (SpC) and pH of the investigated drainage solution measured at a stationary location of the drainage system close to the solution RAB 9 during one year of observation, and D) Temperature evolution of the drainage solution measured in-situ and of the Earth`s atmosphere from a nearby meteorological station (Fröschnitztal) during the year 2018 indicates distinct and corresponding seasonal trends. The points in figures C and D were calculated and plotted using the average of each month.*

3.6 Discussion

3.6.1 Variable spatial and temporal conditions for scale formation

3.6.1.1 Evolution of drainage solutions

The formation of scale deposits is usually induced by the chemical evolution of the drainage solution towards precipitation of solid phases, like minerals. Accordingly, main reaction mechanisms for scale formation are related to the local geology and pore/ground water specification, leaching of cement phases (e.g. portlandite $Ca(OH)_2$), mixing of solutions,

evaporation, gas absorption or degassing , microbial activity, temperature changes, and others (e.g. Rinder et al., 2013). In the tunnel Spital studied herein, the surrounding rocks indicate a high geogenic level of Mg^{2+} and Ca^{2+} concentration in the locally occurring ground water due to dissolution of dolomite and Mg-calcite from the rauhwacke and marble within the aquifer. The site-specific hydrochemical composition of the tunnel drainage solutions collected reveals only a few distinct spatial differences, indicating an almost constant ground water composition as an initial solution for all of the investigated drainage solutions. The varieties are mostly caused by spatiotemporally variable interactions with the concrete, ongoing scale formation, and interaction with the variable tunnel atmosphere (table 4). In the present case study only the aqueous solution RAB 17 differs significantly from the others in pH, Na^+, K^+, Mg^{2+} and SO_4^{2-} concentration, as well as in its DOC content. The strongly elevated pH of 11.2 is caused by pronounced leaching of Ca^{2+} and alkali elements (Na^+, K^+) out of the concrete yielding a higher alkaline solution (see also Boch et al., 2015). Elevated K^+ and Na^+ concentrations (67 mg/l and 26 mg/l, respectively) were analyzed in the solution, whereas a low Ca^{2+} concentration is probably caused by prior $CaCO_3$ precipitation due to prevailing supersaturation in respect to calcite in this strong alkaline setting (table 4). In contrast, the aqueous Mg^{2+} concentration measured in solution RAB 17 is relatively low at 13 mg/l corresponding to the negative covariation with pH (Fig.8B) and the associated indication for brucite precipitation (Dietzel et al., 2008b; Mittermayr et al., 2017). Brucite, however, could not be detected in scale deposit RAB 17 by XRD and microscopic investigations, although strongly supported by hydrochemical calculations ($SI_{brucite} > 0$; table 4). Instead, there is clear evidence for the occurrence of the Mg-bearing carbonate mineral dypingite, even though the SI values display undersaturation. The solution RAB 17 also shows a high SO_4^{2-} content (153 mg/l) and a low HCO_3^- content (91 mg/l, table 4). All other investigated drainage solutions reveal lower SO_4^{2-} and typically higher Mg^{2+} concentrations compared to RAB 17. The elevated sulfate content originates either from the dissolution of the surrounding host rock (e.g. rauhwacke), or from enhanced concrete interaction. According to the calculated SI values, barite could also be formed in small amounts, but has no quantitative relevance regarding the sulfate concentrations. The variations between Mg^{2+} concentrations could be best explained by distinct mineral formation (e.g. dypingite), as well as variable prior $CaCO_3$ (calcite or aragonite) precipitation during hydrochemical evolution along the flow path (drainage channels), well known to alter Mg/Ca ratios in aqueous solutions and precipitates (Fairchild et al., 2000; Boch et al., 2019).

The aluminum and silica contents (up to 64 µg/l and 4 mg/l, respectively) of the drainage solutions most likely result from dissolution of feldspar, mica and/or quartz in the host rocks

and not from water-concrete interaction as solution RAB 17 (strong interaction with concrete: high pH and alkali concentrations) contain limited aluminum (34 µg/l, table 4). Furthermore, solution RAB 17 reveals the lowest Ca^{2+} concentration compared to the other solutions, since a high supersaturation with respect to $CaCO_3$ fosters its precipitation and consequently lowers dissolved Ca^{2+} (shown in Fig.8B). In contrast, the more conservative K^+ and Na^+ ions remain in solution tracing concrete leaching (Rinder et al., 2013). A simple explanation for this particular drainage solution being most affected by water-concrete interaction is its migration through leachable concrete/shotcrete for a rather long time. Locally differentiated (e.g. weakened) spots in the concrete or some inhomogeneous concrete processing (e.g. composition and microstructure of the concrete: cf. Boch et al., 2015) may stimulate strength of water-concrete interaction.

Extended periodical monitoring of the temperature of the drainage solution indicates that during the summer months the temperature was only a few degrees lower than the monthly-averaged outside air temperature, while in winter the mean air temperature differed significantly (up to 10 °C) from the measured water temperature (Fig.8D). The seasonal temperature differences can be explained by the high heat and therefore buffering capacity of the water. The temperature of drainage solutions needs time to be adjusted to the air temperature. Moreover, the tunnel atmosphere is thermally buffered from the surrounding host rock (geothermal gradient and thermal assimilation; e.g. Luetscher et al., 2008). The tunnel water temperature variations of up to 7 °C recorded within one year of monitoring, however, clearly indicate a significant influence of the seasonally changing intensity of air exchange (ventilation) (Fig.8D). Such variable air exchange is well known from multi-annual monitoring of various cave systems, i.e. some natural analogue to technical passages through mountain sections (Mattey et al., 2008; Boch et al., 2011). In particular, the changing air ventilation partly controls various tunnel atmospheric (e.g. temperature, humidity, air composition), and consequently drainage solution parameters (temperature, hydrochemical composition). A strongly dynamic tunnel atmosphere intimately coupled to the hydrochemistry has also an effect on variable growth of carbonate precipitates. Importantly, the seasonal and operational (e.g. technical ventilation, traffic, maintenance intervals) dynamics exert a relevant effect on seasonally or episodically variable air versus drainage solution gradients (e.g. temperature, P_{CO2}, humidity), influencing processes of fluid-solid interaction such as CO_2 outgassing. The monitored electric conductivity was higher during the winter months (Fig.8C). Corresponding higher degree of mineralization of the drainage solutions in winter could be explained by an enhanced air exchange (higher interior vs. exterior air temperature), thus inducing a progressive desiccation during the meteorologically overall

drier winter months (reduced precipitation, snow cover, less recharge). Considering the annual pH evolution of the selected aqueous solutions, the prevailing values are significantly higher during the cold season (up to ~8.5 in winter vs. ~8.0 during the warm season; Fig. 8C). This could be indicative of seasonally enhanced CO_2 outgassing during the cold season.

***Table 4**: Hydrochemical in-situ parameters (pH, Temp: temperature, SpC: specific electric conductivity), Alkalinity is given as HCO_3^-, concentration of dissolved components, SiO_2 present in solution as $Si(OH)_4$, dissolved organic carbon (DOC), dissolved inorganic carbon (DIC), ionic balance Error in percentage %, mineral saturation indices for calcite, aragonite, barite, brucite, dypingite, strontianite and the internal partial pressure of CO_2 (P_{CO2}).*

Sample ID	Temp	SpC	pH	HCO_3^-	Ca^{2+}	Mg^{2+}	K^+	Na^+	SiO_2
	°C	µS/cm		mg/l	mg/l	mg/l	mg/l	mg/l	mg/l
RAB 6	8.0	652	8.28	302.1	76.1	38.3	3.4	7.3	4.4
RAB 9	8.1	665	8.46	304.5	76.6	38.1	4.5	7.8	4.4
RAB 17	9.0	784	11.24	90.9	40.4	13.0	67.4	26.4	2.3
RAB 18	8.8	560	8.64	328.3	54.2	34.9	14.0	7.2	3.7
RAB 23	8.2	313	8.35	178.2	49.5	6.7	5.6	3.1	2.7
RAB 24	8.8	468	7.72	226.4	64.4	23.1	2.0	2.3	2.9
RAB 25	8.7	469	7.96	222.7	61.9	21.6	2.7	2.5	2.9
Sample ID	**∑Al**	**Ba^{2+}**	**Sr^{2+}**	**∑Fe**	**SO_4^{2-}**	**Cl^-**	**NO_3^-**	**DOC**	**Mg^{2+}/Ca^{2+}**
	µg/l	µg/l	µg/l	µg/l	mg/l	mg/l	mg/l	mg/l	(molar)
RAB 6	62	51	2010	4	102.2	9.3	<0.1	0.45	0.83
RAB 9	63	52	2065	3	102.2	9.1	<0.1	0.50	0.82
RAB 17	34	40	564	2	152.5	2.3	1.7	2.05	0.53
RAB 18	64	69	250	10	44.0	2.1	0.5	0.70	1.06
RAB 23	46	59	148	4	12.6	1.4	7.4	0.73	0.22
RAB 24	54	163	476	1	66.8	2.0	7.4	0.49	0.59
RAB 25	51	157	444	<1	62.2	1.8	7.3	0.50	0.57
Sample ID	**DIC**	**Error**	**$SI_{calcite}$**	**$SI_{aragonite}$**	**SI_{barite}**	**$SI_{brucite}$**	**$SI_{dypingite}$**	**$SI_{strontianite}$**	**$logP_{CO2}$**
	mmol/l	%							atm.
RAB 6	5.0	0.5	0.6	0.4	0.4	-5.1	-12.9	-0.4	-2.7
RAB 9	4.9	0.7	1.0	0.9	0.4	-4.2	-10.2	0.0	-3.1
RAB 17	0.5	12.1	1.4	1.2	0.4	0.9	-4.4	0.1	-8.0
RAB 18	5.5	-1.4	0.5	0.4	0.2	-5.1	-12.9	-1.3	-2.6
RAB 23	2.9	-6.4	0.6	0.5	-0.3	-5.1	-15.1	-1.4	-3.2
RAB 24	3.9	-3.9	0.2	0.0	0.7	-5.3	-15.9	-1.4	-2.5
RAB 25	3.7	-4.6	0.4	0.2	0.7	-5.4	-14.6	-1.2	-2.7

3.6.1.2 Mechanisms and types of scale deposit

Petrographic observations reveal layering in almost all scale deposits, i.e. the occurrence of distinct interfaces at which the continuous mineral growth is interrupted, renewed nucleation and/or mineral accumulation (e.g. detrital) takes place and new (younger) growth layers formed successively (see Fig.4). The repeated growth interruptions in nearly pure carbonate scale

deposits usually appear as visually darker layers in the thin sections, where light is strongly scattered due to the small crystal sizes. The latter mineral deposits were most likely accumulated in the scale deposit after particulate transport in the (turbulent) water, forming micritic $CaCO_3$ as a common sedimentary feature (Frisia, 2014; see Fig.4A, D and H). In the scale deposit RAB 9 intercalated micritic $CaCO_3$ layers occur within larger idiomorphic calcite crystals, where crystal growth is not necessarily interrupted. Re-nucleation of small initial crystallites might not occur and the columnar competitive crystal growth continues more or less undisturbed (cf. Fig. 4D). However, delicate (fine) layers are repeatedly intercalated based on an altered chemical composition or as micritic and/or fluid inclusions. These repeated and typically microcrystalline growth interruptions of the dominant and ongoing $CaCO_3$ deposition and mineralogical/chemical variations support significant changes in the prevailing environmental conditions (e.g. variable water discharge, temporary desiccation, increased chemical gradients) in the tunnel drainage system. A potentially pronounced hydrological, hydrochemical and atmospheric variability is further supported by the relatively low overburden (tens to max. 125m) and short overall length (2500 m) of this tunnel. Scale deposit RAB 4, for example, suggests a distinct change in the carbonate forming processes over time. Both, aragonite and calcite, occur closely related to each other and some pristine aragonite is partially replaced by calcite at a later stage (diagenetic origin). Reasons therefore are either a significant change in the hydrochemistry (e.g. $CaCO_3$ supersaturation, Mg concentration and Mg/Ca ratio), causing changes in the crystal growth dynamics and precipitation rates, and/or the beginning diagenetic transformation (dissolution and re-precipitation ripening) of aragonite to calcite (Fig.6, RAB 4). In general, these petrographic observations correspond well to the observed seasonal and/or episodic environmental changes affecting the aqueous solution chemistry as discussed above.

3.6.2 Tracing scale formation by stable isotopes

In order to decipher the dominant mechanisms of $CaCO_3$ precipitation, the signature and distribution of stable C and O isotopes in the carbonate of the scale deposits and associated solutions (water and DIC) are evaluated. The O isotope distribution of the water clearly reflects its meteoric origin, whereas isotopic enrichment from evaporation can be excluded as a significant influencing parameter ($\delta^{18}O_{H2O}$ versus $\delta^{2}H_{H2O}$ values in Fig. C.1; Appendix). The small range of isotope distribution in all solutions (see table 3) is characteristic for one single aquifer. The $\delta^{18}O_{H2O}$ and $\delta^{2}H_{H2O}$ values, however, are significantly higher compared to those

reported for the Austrian Meteoric Water Line (AMWL), as well as the Global Meteoric Water Line (GMWL; Craig, 1961; Hager & Foelsche, 2015; Fig.C.1; Appendix). Calculated deuterium excesses (D-excess = $\delta D - 8 * \delta^{18}O$, as defined by Dansgaard (1964)) vary from 10.9 to 11.6 ‰ (average = 11.3 ‰ ± 0.4). The dominant sources of meteoric precipitation in Austria are the Atlantic Ocean in the (North)West and the Adriatic Sea in the South, whereby the regions south of the Alps are less affected by the Atlantic climate and more influenced by Mediterranean air masses (Auer et al., 2007; Liebminger at al., 2007). Variable evaporation of the Mediterranean versus Atlantic moisture sources (surface water) affects the Austrian deuterium excess values (Hager & Foelsche, 2015). Therefore, the enriched D-excess of the drainage solutions most likely reflect some distinct contribution of isotopically enriched Mediterranean moisture in its infiltration area (Fig.C.1; Appendix). In addition, the isotopic composition measured at the location Nasswald close to the investigated tunnel amounts to -10.5 ‰ (VSMOW) for $\delta^{18}O$ and -75.0 ‰ (VSMOW) for $\delta^{2}H$ (weighted mean values for the period 1973 to 2002; Hager & Foelsche, 2015). This fits well with the $\delta^{18}O$ and $\delta^{2}H$ values of the investigated drainage solutions (average (n=7) -10.7 ‰ for $\delta^{18}O$ and -74.4 ‰ for $\delta^{2}H$; cf. table 3).

Considering $\delta^{18}O$ values of the precipitated carbonate and aqueous precipitating solution the temperatures during carbonate mineral formation, in the present case mostly calcite, can be estimated using the equations

$$\mathbf{1000 \ln \alpha_{calcite\text{-}H2O} = 17.4(10^3 T^{-1}) - 28.6} \quad \text{(Eq.1)}$$

and

$$\mathbf{1000 \ln \alpha_{calcite\text{-}H2O} = 18.03(10^3 T^{-1}) - 32.42} \quad \text{(Eq.2)}$$

reported by Coplen (2007) and Kim & O`Neil (1997) for slow and more rapid precipitation rates, respectively ($\alpha_{calcite\text{-}H2O}$ is the isotope fractionation factor for oxygen isotopes between calcite and the water molecules; T is the temperature in Kelvin). In principle, Eqs (1) and (2) can only be used for calcite, since e.g. aragonite follows a slightly different fractionation equation. However, the analyzed scale deposits show a dominance of calcite, which allows to use these equations for T approximation during carbonate scale deposit formation. The obtained scale formation temperatures by oxygen isotope data using Eq (2) fit best with the measured

temperatures based on in-situ and online monitoring of the drainage system (mean: 9 °C, min: 5°C, max: 12 °C). As exceptions scale deposits RAB 17 and 25 show measured T values to be in accordance with scale formation T by oxygen isotope data using Eq (1) (Fig.9, table 3).

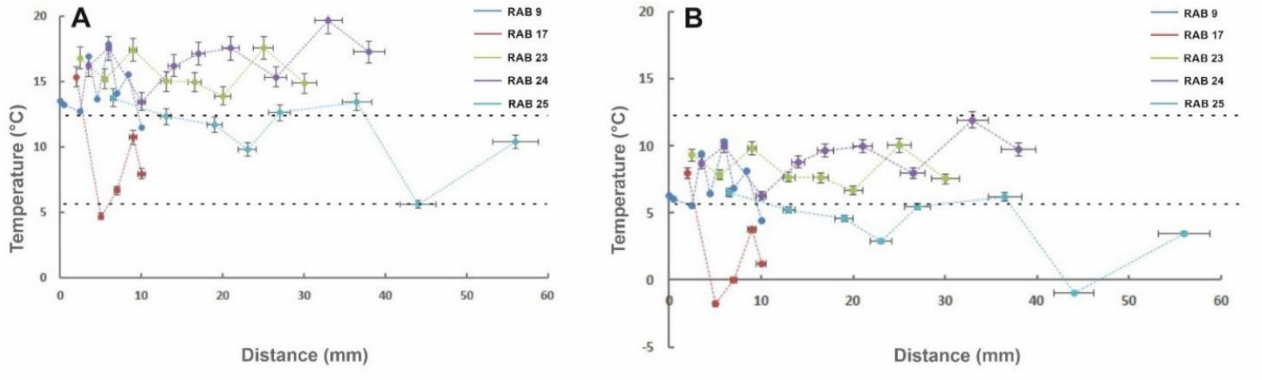

Figure 9: *Calculated temperatures during calcite precipitation from analyzed oxygen isotope distribution (see drillings in Fig.2) after Coplen (2007; Daeron et al., 2019; diagram A) and Kim & O`Neil (1997; diagram B) compared to the minimum and maximum water temperatures (dashed lines) measured in the drainage system using the in-situ and online "scale guard" monitoring tool (Fig.8D).*

Accordingly, RAB 17 and 25 reveal a different (kinetic) fractionation behaviour compared to the other scale deposits: Both carbonate scales have probably grown slower than the others e.g. during a desiccation interval in the drainage and ongoing $CaCO_3$ precipitation to reach very low supersaturation degrees with respect to calcite. Prior $CaCO_3$ precipitation induces elevated Mg^{2+}/Ca^{2+} ratios in the solutions, which can finally yield in dypingite formation as documented in the pore spaces of these scale deposits. The relatively low calculated formation temperatures of the scale deposits RAB 17 and 25 (<5 °C) support their precipitation/formation during winter season and associated temporary desiccation in the drainage system indicative by dypingite occurrence in both scale deposits. However, assessing absolute temperatures during calcite formation seems to be challenging due to kinetic effects during precipitation in the tunnel drainage setting. These kinetic effects can comprise locally turbulent flow conditions, pronounced CO_2 degassing, intermittent low water levels or even desiccation, calcite growth inhibition due to elevated Mg/Ca ratio, or the artificial templates by drainage substrate favoring crystallization. Variations of several °C are indicative, in particular as the water isotopic composition is rather constant (Fig.9). Scale deposits RAB 9, 23 and 25 confirm this assumption based on their $\delta^{13}C_{prec}$ versus $\delta^{18}O_{prec}$ isotope values. All three scale deposits reveal almost constant $\delta^{13}C_{CaCO3}$ values, generally reflecting the isotopic composition of the DIC, but

extensive variation in their $\delta^{18}O_{CaCO3}$ compositions, which corresponds to rather constant precipitation conditions, except change of temperature (Fig.10A). Scale deposits RAB 17 and 24 show some distinct variation in both, C and O isotopes, which are explained by changes in respective DIC values and temperature (Fig.10B). Note, that the temperature variability of 7 °C from O isotopes fits well with that measured in-situ with the scale guard sensor system (table 3, Fig. 9).

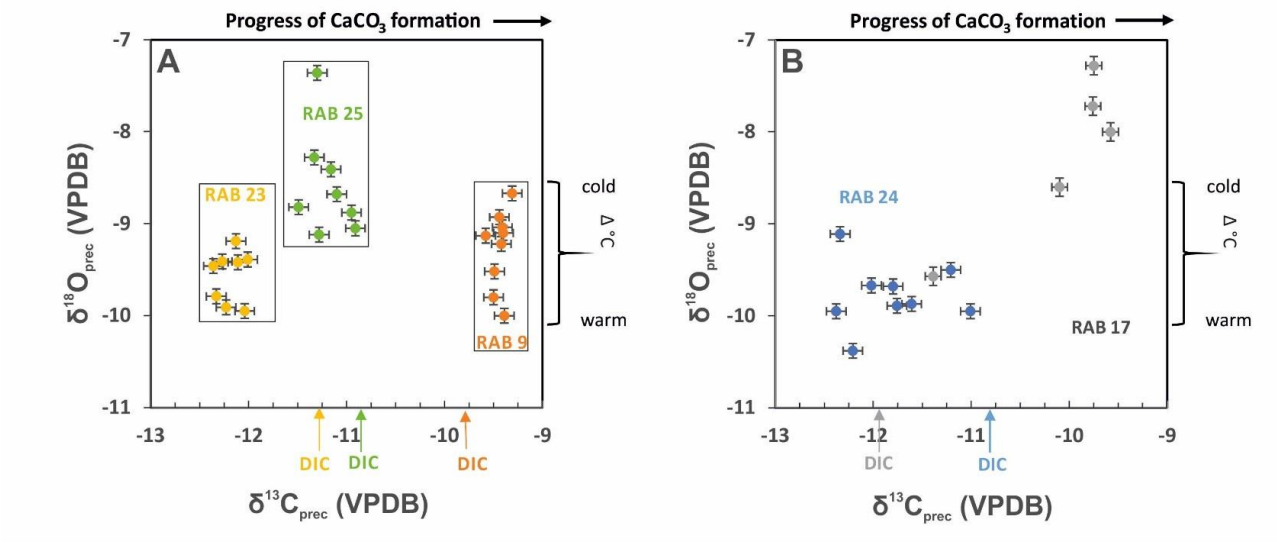

Figure 10: *Stable isotopic composition $\delta^{13}C_{prec}$ and $\delta^{18}O_{prec}$ of the investigated scale deposits (RAB 9, 17, 23, 24 and 25; see drillings in Fig.2). Figure A suggests, that carbonate precipitation conditions (e.g. rate of $CaCO_3$ formation; carbon source) are relatively constant over time for individual scale deposits (almost constant $\delta^{13}C_{prec}$ values captured in RAB 9, 23 and 25). In contrast, variability of $\delta^{18}O_{prec}$ values indicates prominent temperature changes during carbonate deposition, which are within the Δ°C range for seasonal temperature monitored in the drainage solutions of the tunnel building (Fig.7D). For scale deposits RAB 17 and 24 (B), variability of both, $\delta^{13}C_{prec}$ and $\delta^{18}O_{prec}$ values, traces $CaCO_3$ formation conditions both being significantly variable in space and/or time.*

Although, the $\delta^{13}C_{prec}$ are generally reflecting the isotopic composition of the DIC (see Fig. 10), the C isotopes can be influenced by a large number of parameters: e.g. CO_2 degassing, uptake of CO_2 and microbes, precipitation rate and ongoing calcite formation. Except for RAB 17 (high pH, low P_{CO2}, Fig.8A), degassing of CO_2 is considered as a major driving mechanism of concomitant $CaCO_3$ precipitation. Since the internal partial pressure of CO_2 (P_{CO2} in atm) ranged from $10^{-2.4}$ to $10^{-8.0}$ atm, values being either significantly higher or much lower compared to the mean Earth`s atmospheric CO_2 level (~$10^{-3.4}$ atm). This is further reflected in the intermediate $\delta^{13}C$ values of the $CaCO_3$ precipitates as these values range between -12.2 and -9.4 ‰ VPDB (table 3), i.e. values significantly higher compared to typical (strongly depleted)

CO_2 absorption-based Ca-carbonate signatures (Kosednar-Legenstein et al., 2008; Rinder et al., 2013). Both, the elevated pH and the according CO_2 partial pressure of the solution RAB 17 (10^{-8} atm, table 4) have been suspected to involve some major contribution from CO_2 absorption as the dominant CO_3^{2-} source for subsequent carbonate precipitation. However, based on the measured $\delta^{13}C_{DIC}$ values of the appropriate drainage solutions neither pronounced CO_2 absorption nor degassing of CO_2 represent the determining carbonate formation and isotope fractionation mechanism since the $\delta^{13}C_{DIC}$ values became even lower (lighter) instead of the expected increased (heavier) isotopic composition during CO_2 degassing inducing carbonate precipitation (Dietzel, 1995; Hoefs, 2015; table 3). In this regard, figure 11 is displaying the stable C isotope composition of the DIC as a function of the decrease of aqueous Ca concentration (reflecting progressing $CaCO_3$ formation). Thus, the assumed predominance of CO_2 degassing for most of the samples does not dominantly influence the $\delta^{13}C_{DIC}$ values of the investigated water samples. Alternatively, the ongoing calcite formation might be the cause for $\delta^{13}C$ scattering in Fig.11. Assuming stable C isotope fractionation between precipitating calcite and DIC ($\alpha_{calcite–DIC}$) at near equilibrium conditions, a Rayleigh fractionation effect according to the equation

$$\delta^{13}C_{(DIC)i} = (\delta^{13}C_{(DIC)0} + 10^3) * f^{\alpha(calcite\text{-}DIC)\,-1} - 10^3 \qquad \text{(Eq.3)}$$

can be calculated and followed, considering relative aqueous Ca concentration to trace $CaCO_3$ formation ($\alpha_{calcite\text{-}DIC}$ = 1.00355 at 8±1 °C and pH= 8±1; f: $[Ca]/[Ca]_0$; see Dietzel & Kirchhof (2002); $\delta^{13}C_{(DIC)0}$= -9.74 ‰; isotope value for solution with highest Ca content in table 4 representing initial Ca concentration). According to this Rayleigh isotope fractionation approach for ongoing calcite formation and its excellent fit with the measured data of the present study shown in Fig.11, the degassing or absorption of CO_2 is not the dominant process for DIC isotopic evolution, but ongoing $CaCO_3$ precipitation accompanied with stable C isotope fractionation. Thus, stable carbon isotope composition of the DIC can be used to trace the ongoing calcite precipitation from the drainage solution and in the present case confirms a single initial solution to be reasonably assumed for all drainage solutions in respect to the source and concentration of inorganic carbon (Fig.11). CO_2 exchange between solution and atmosphere as well as microbial activities may also control specific precipitation mechanisms as discussed above, but are not changing $\delta^{13}C_{DIC}$ values.

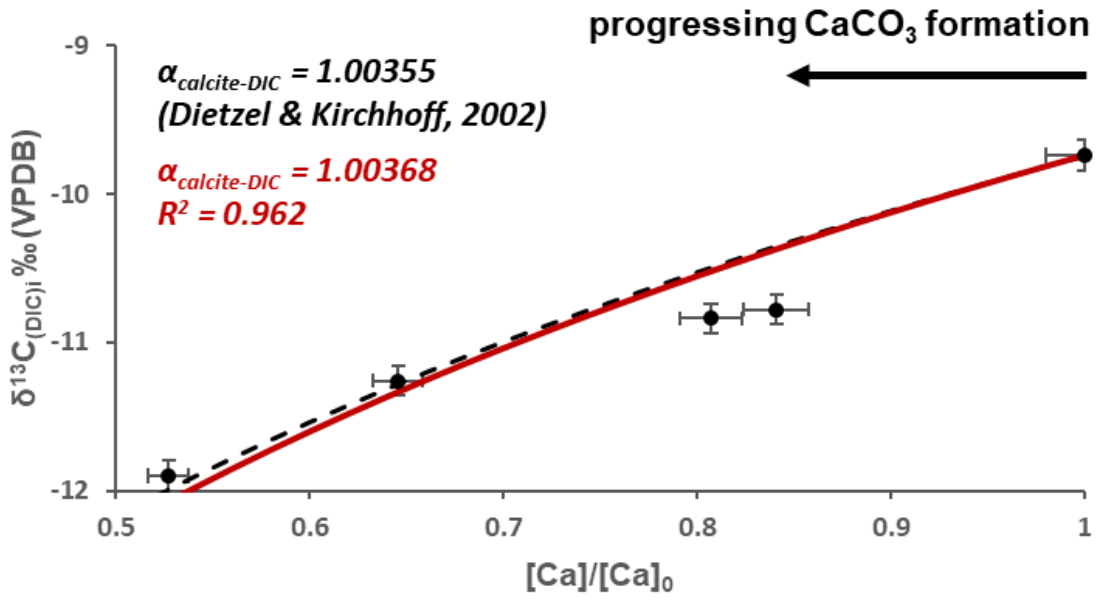

***Figure 11**: The analyzed stable carbon isotope composition of the dissolved inorganic carbon (DIC) as a function of progressing $CaCO_3$ precipitation assuming the highest calcium concentration of the drainage solutions ($[Ca]_o$ = 76.6 mg/l; solution RAB 9; Tab.3) to be the initial value. Plotted values are referred exclusively to calcite dominated deposits. [Ca] denotes the individual, but lower, calcium concentrations ($[Ca] < [Ca]_o$) measured in the other drainage solutions. Dashed black line: Modelled carbon isotope fractionation according to the Rayleigh fractionation approach for ongoing calcite formation considering the isotope fractionation coefficient at isotopic equilibrium between calcite and DIC to be $\alpha_{CaCO3\text{-}DIC}$ = 1.00355 (see Eq. 3; Dietzel & Kirchhoff, 2002). The red line shows the regression line for the analyzed values, resulting in $\alpha_{CaCO3\text{-}DIC}$ = 1.00368 (R^2 = 0.962). The latter α value correlates well with above value from the literature (see dashed black vs. red solid line). Thus, the analyzed stable carbon isotope composition of the DIC clearly indicates all solution to be originated - in the scope of Ca and DIC evolution from a single initial solution (e.g. local groundwater) by considering close to isotope equilibrium condition during calcite formation. Kinetically driven carbon isotope fractionation - e.g. caused by enhanced degassing and/or uptake of atmospheric CO_2 - does not significantly affecting the carbon isotope composition of DIC of the present drainage solutions.*

3.6.3 Controls on carbonate mineralogy and scale microstructures

Trigonal-rhombohedral low-Mg calcite is the main component in all scale deposits in this study, whereby in some a variable amount of the orthorhombic aragonite is additionally present. The aragonite content varies between 1 and 49 wt.% in RAB 4, 6, 17, 18 and 25 (table 1; Figs. A.1-6 and B.1-2; Appendix). Interestingly, aragonite containing scale deposits appear more porous or even highly porous in major parts of the fabric (Fig.3A, B, D, E and H). The aragonite crystals typically occur in the variably sized pore spaces or grow well-orientated inside the voids of the scale deposits, e.g. some isopachous ingrowth and successive cementation (Fig.4E and F). Dypingite is growing on the aragonite crystals located in the widespread pore spaces (RAB 6,

17 and 25; Figs. 5D & 12). Although all initial solutions reveal undersaturation with respect to dypingite, the spatiotemporally relevant observation of dypingite on the top of aragonite needles could be explained by temporary desiccation of the drainage in combination with prior $CaCO_3$ precipitation (PCP); Fairchild et al., 2000; Boch et al., 2019). According to the observation of a desiccated northern lateral-drainage during the sampling campaign, the limited overburden of the tunnel Spital associated with an increased influence of variable environmental conditions (e.g. recharge and discharge) and the distinct occurrence of dypingite, a temporary desiccation in the drainage system can be reasonably suggested for the past. PCP induces aqueous Mg^{2+}/Ca^{2+} ratio to be rising (Huang & Fairchild, 2001; Riechelmann et al., 2014). Importantly, during reduced discharge, water flow and desiccation, the carbonate precipitating aqueous solutions partially remain in the pore spaces of the scale deposits (residual pore solutions). The aqueous Mg^{2+}/Ca^{2+} ratios evolving during ongoing $CaCO_3$ (low-Mg calcite initially) precipitation are increasing until the precipitation of aragonite or even dypingite occurs. Elevated magnesium concentrations are well known to promote aragonite instead of calcite nucleation in low-temperature aqueous settings (Riechelmann et al., 2014; Rossi & Lozano, 2016; Purgstaller et al., 2017; Boch et al., 2019). Essentially, the continuously increasing Mg content inhibits further calcite nucleation from the supersaturated solution and aragonite formation is preferred, when the molar Mg^{2+}/Ca^{2+} ratio increases above some critical limit (Rodriguez-Navarro & Benning, 2013; Casella et al., 2017; Boch et al., 2019). Different studies considering aragonite versus calcite precipitation revealed values between 1 and 3 for molar Mg^{2+}/Ca^{2+}ratios as thresholds for aragonite replacing calcite formation at ambient surface temperature (Frisia et al., 2002; Dietzel et al., 2004). The investigated Mg^{2+}/Ca^{2+} ratios range between 0.2 and 1 (table 4). Aqueous solutions with molar Mg^{2+}/Ca^{2+} values of >0.8 contain aragonite, except of RAB 17 (Mg^{2+}/Ca^{2+}: ~0.5). This specimen, however, contains the Mg-bearing mineral dypingite and therefore a lower Mg concentration in the corresponding solution. Consequently, the lower molar Mg^{2+}/Ca^{2+} ratio could be explained from this mineral occurrence. The solution forming aragonitic scales (RAB 6, 17, 18, 25) exhibit lower Sr and Ba concentrations, as the latter elements are preferably incorporated into aragonite in contrast to Mg (Böttcher & Dietzel, 2010). The aragonite and dypingite bearing scale deposits are typically more porous in their fabric compared to the specimens made out of ~100 wt.% calcite (RAB 9, 23 and 24). This could be explained by temporary desiccation forming an irregular water film on the solid surfaces causing porous fabric developed by capillary forces and ion diffusion as assumed for curled speleothem formation (helictite; Onuk et al., 2014). Accordingly, the mineral dypingite is found (i) even when the bulk solution is undersaturated with respect to

dypingite (table 4) and (ii) in limited pores of the scale indicating temporary and/or partial desiccation. Thus, the evolving Mg^{2+}/Ca^{2+} ratio throughout carbonate mineral precipitation dynamics can be correlated to porosities and fabric characteristics of the scale. The initial Mg^{2+}/Ca^{2+} ratio in the drainage solutions (groundwater) appears to be controlled by the local geology (dolomite marble, rauhwacke), providing relatively high Mg contents of the percolating waters. Furthermore, increased Mg concentrations in the tunnel drainage and pore solutions could also be provided from some dissolution of the preexisting Mg-hydroxide mineral brucite ($Mg(OH)_2$), either because of a decrease in formerly alkaline pH or from a major drop in air- and water-temperature, which would increase the solubility of brucite. Seasonal water temperature variations were recorded (Fig. 8) and are indicative of changing tunnel atmospheric conditions in this relatively short tunnel, i.e. relying on variable air pressure and air exchange (e.g. ingress) and leading to cooling of the tunnel atmosphere in winter (cf. Flueckiger & Reinke, 2013). The efficient dissolution of preexisting brucite would further support the necessary high Mg^{2+} and OH^- ion concentrations for the restricted formation of dypingite in the drainage scale deposits. For example, this mechanism might be the case in RAB 17, which is composed of calcite, aragonite and dypingite, but lacks brucite, although expected based on the higher alkaline aqueous solution composition. In contrast, RAB 18 contains aragonite but no dypingite, together with brucite, while RAB 6 contains both, dypingite as well as brucite. Based on these mineralogical relationships and the observed amounts of brucite, the dissolution of brucite might play a minor role for the prominently increased Mg contents and the formation of aragonite and dypingite in the voids of the scales. This conceptual approach for dypingite formation is supported in the literature, mentioning that dypingite may form under high CO_2 partial pressures by reaction of CO_2 with magnesium minerals such as brucite. This is further similar in composition and appearance to hydromagnesite ($Mg_5(CO_3)_4(OH)_2*H_2O$), i.e. forming rosette-shaped crystal morphologies (Canterford & Tsambourakis, 1984; Frost et al., 2009). Furthermore, dypingite is readily formed during reaction of Mg-rich minerals with CO_2 at ambient temperatures and favored under atmospheric pCO_2 (400ppm) and microbially mediated conditions (Mavromatis et al., 2012; Harrison et al., 2012; Harrison et al., 2019). Dypingite is also known to be either an alteration product of serpentine, or to be biologically induced, e.g. in microbial mats hosting photosynthesis conducting cyanobacteria (Raade, 1970; Power et al., 2007). Under such biomediated formation conditions dypingite typically shows a flakey texture. Hydroxyl ions, e.g. produced during photosynthesis, can promote the precipitation of dypingite (Thompson & Ferris, 1990). Due to prevailing high alkaline conditions of the drainage solution caused by OH^- leaching from concrete, dypingite formation

can be best explained by abiotic formation conditions as no distinct evidence of byproducts from cyanobacterial photosynthesis is manifested.

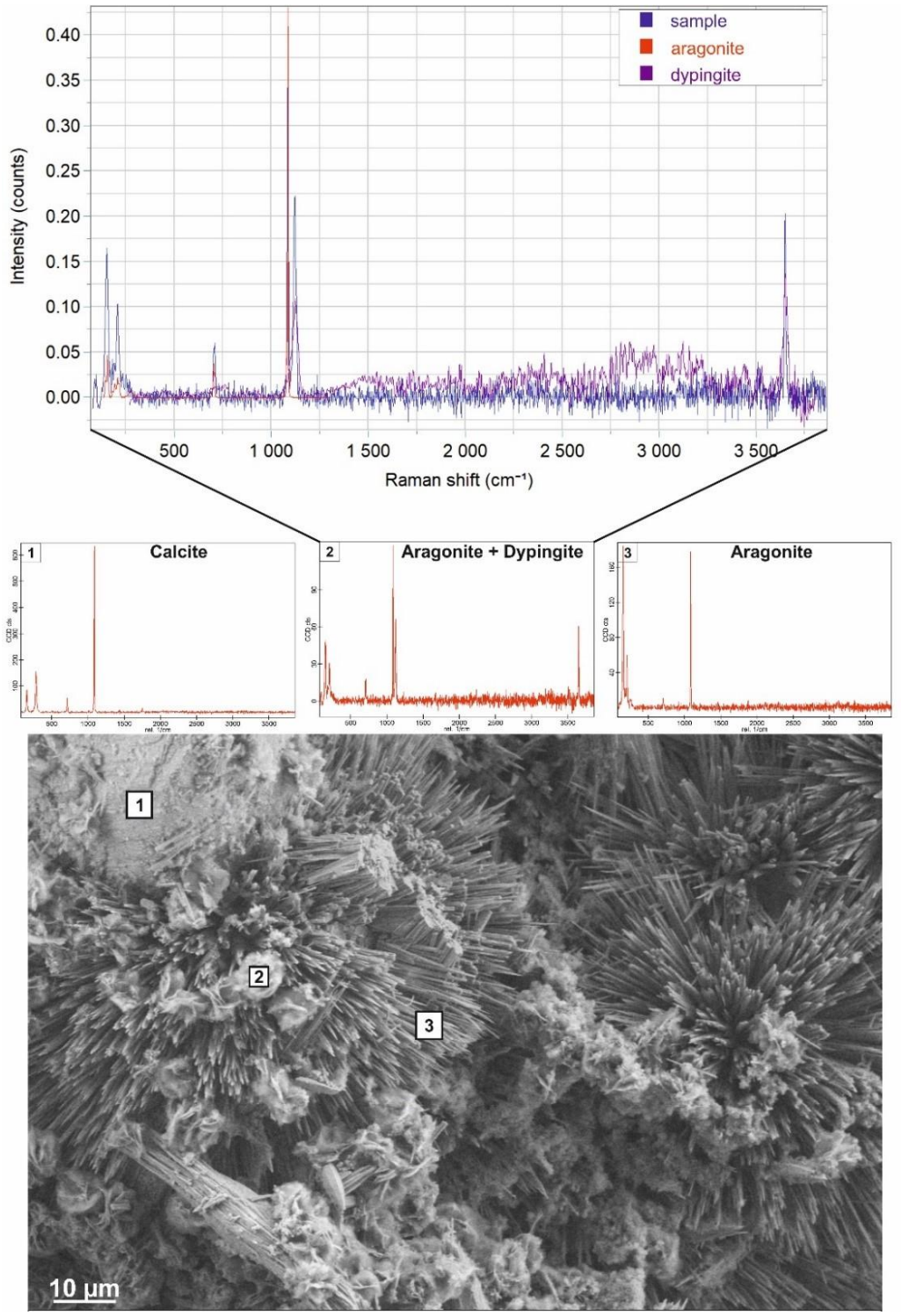

Figure 12: *SEM image and Raman spectra of sample RAB 17 consisting of calcite (1), aragonite (3) and dypingite (2). The selected pattern supports the occurrence of aragonite closely related with dypingite and caused by progressive prior calcium carbonate precipitation. Prior $CaCO_3$ formation is most likely associated with variable water flow conditions and/or temporary desiccation of the tunnel drainage channels. 1) Calcite according to Raman spectrum. 2) Raman spectrum exhibits dypingite and aragonite, where dypingite is typically growing onto the top of the aragonite needles. 3) Raman spectrum supporting aragonite only.*

3.6.4 Microbial influence on scale formation

Several of the tunnel scale deposits investigated (RAB 9, 17 and 18) show evidence of microbial presence in the form of prominent remains of filamentous structures as well as indicative minerals. This is an essential observation since microorganisms can have a significant impact on carbonate mineral precipitation rate and crystal fabrics (Andrews et al., 1997; Shiraishi et al., 2019).

According to the epifluorescence analysis and high-resolution visual results (Figs. 5 & 7; small filamentous structures in the micrometer range), the scale deposits RAB 17 and 18 clearly indicate bacterial influences, while RAB 9 reveals remnants of microbial activity based on the SEM images, although not be seen within the epifluorescence staining images (Fig.7). In the latter case, the bacteria might be well dispersed in the scale deposit and thus not be detected by the screening epifluorescence analysis. The bacteria in RAB 9 can be classified based on their typical size, shape and structural features. Accordingly, they were characterized as *Gallionella ferruginea* (Ehrenberg, 1836, Chan et al., 2016). *Gallionella ferruginea* belongs to the iron-oxidizing group of bacteria (FeOB), which produce extracellular polymeric substances (EPS) in the form of a spirally twisted filamentous stalks on which the oxidized iron ($Fe^{2+} \rightarrow Fe^{3+}$) is precipitating and encrusting (Vatter & Wolfe, 1956). This kind of widespread redox-sensitive bacteria is an auto- and mixotrophic microaerophilic FeOB using Fe(II) as the electron donor and CO_2 or carbohydrates as a carbon source (Hallbeck & Peterson, 1991; Hallbeck et al., 1993). Growth conditions require circum-neutral pH conditions and temperatures ranging between ~5 and 25°C (Heim et al., 2015). The metabolically associated iron precipitates on the organic tissue (substrate) are often referred to as poorly crystallized iron-(hydr)oxides such as ferrihydrite ($Fe_{10}O_{14}(OH)_2$) or amorphous ferric hydroxide ($Fe(OH)_3$; Ghiorse, 1984; Tuhela et al., 1997). Ferrihydrite is known to be a biomineralization product of iron-oxidizing environments and microorganisms (Banfield & Welch, 2013). Figure 5B shows indications of ferrihydrite (tiny-sized spherical components), most likely of bacterial origin, explaining the prominent red-brownish color of scale deposit RAB 9. These rapidly formed and poorly crystallized (limited degree of ionic ordering) minerals are known to successively transform into higher crystalline forms of Fe-(hydr)oxides, e.g. goethite (FeOOH; Banfield et al. 2000; Hallberg & Ferris, 2004) over time. However, our investigations revealed that the twisted filaments mainly consist of Fe, O, Ca, C and Si (Fig.5A; Figs.D.1, D.2; Appendix). Over time, the initially smooth and pristine stalk surfaces of the bacterial tissue become increasingly coated with iron-(hydr)oxides (Chan et al., 2011). This is causing a gradual reduction of the exposed EPS-surfaces, which leads to a successive reduction of the passive (but attractive)

mineralization substrate provided by the biofilms (Heim et al., 2015). The oxidation of water-soluble Fe (II) to the less soluble form of Fe (III) results in the formation of iron-(hydr)oxides such as ferrihydrite in the case of RAB 9 (Fig.5B). This redox- as well as pH-sensitive formation processes leads to a decrease in the pH according to equation 4, i.e. an H^+ (H_3O^+) ion is released and OH^- is partially fixed in the solid iron phase. The overall reaction for iron precipitates induced by microbial influences of iron-oxidizing bacteria is reported by Banfield & Welch (2013):

$$\mathbf{2Fe^{2+}_{(aq)} + ½\ O_{2\,(g)} + 3H_2O \rightarrow 2FeOOH_{(s)} + 4H^+_{(aq)}} \qquad \text{(Eq.4)}$$

More specifically, the pH value decreases in conjunction with more Fe being removed from the aqueous solution and being incorporated into the solid iron phase. Ferrous (Fe (II)) and ferric (Fe (III)) ions are further known to inhibit calcite growth (Katz et al., 1993; Takasaki et al., 1994). Fe (III) inhibits calcite crystal growth even better at lower pH values probably by absorption of ferric ions or small colloidal ferric hydroxide particles onto the calcite growth surface (Katz et al., 1993). As the overall iron ion concentration increases in the solution, the growth of calcite is increasingly inhibited (Takasaki et al., 1994). Laboratory experiments revealed that the oxidation process of Fe (II) to Fe (III) leads to a strong increase in growth inhibition and is even better than adding the same amount of Fe (III) directly (Katz et al., 1993). In the case of scale deposit RAB 9, the bacteria detected are well known to oxidize Fe (II) to Fe (III) and could thus significantly increase the inhibition of calcite growth from the Ca-carbonate supersaturated drainage solutions. Electron microprobe studies showed that the increased iron content in RAB 9 is spatially related to the tiny but widely occurring micro-pores (ev. remnants of bacterial filaments), as the iron-oxidizing bacteria were mostly found in these micro-pores (Fig.6, RAB 9). All of these processes discussed support some of the characteristics of scale deposit RAB 9, being prominently red-brownish (iron staining) colored, more condensed (thinner) and compact (hard) compared to the other scale deposits.

Two of the scale deposits (RAB 17 and RAB 18) show distinct autofluorescence and clear evidence of some microbial presence according to the epifluorescence tracing method (Fig.7). In RAB 17, bacterial presence could be detected employing high-resolution SEM images, whereas in RAB 18 no distinct microbial activity could be observed by SEM. Moreover, RAB 18 exhibits some major pore spaces (Fig.3E). Pristine growth imperfections like major pore

spaces of different size in the carbonate precipitates have been recognized to occur in relation to crystals grown on EPS and on braided surfaces of microbial biofilms (Pedley, 2014). Furthermore, RAB 17 - the most porous and softest scale deposit of the investigated scales - hosts a significant and eventually microbial-mediated aragonite content and shows the highest DOC content (2.1 mg/l). These observations agree well with the epifluorescence analysis suggesting widespread microbial activity in scale RAB 17. The tunnel scale deposits with some obvious bacterial presence are partially comparable to microbial communities of environmental settings such as hot springs and ambient-temperature streams influencing travertine and calcareous tufa formation (Ford & Pedley, 1996; Chafetz and Guidry, 1999; Fouke, 2011). From such travertine focused studies, it is well known that variable flow velocities, temperatures, aqueous ion speciation and microbial compositions cause indicative differences in mineralogy and fabrics (Shiraishi et al., 2019). In this context, the biomediated carbonate precipitation could have been resulted in the repeatedly observed micritic fabrics. In particular, the biofilm hosting in-situ formed microscopic (calcite) crystallites dies off (e.g. vanishes during stagnant flow conditions), and the micrite crystals remain in the local sample or are flushed away later (Ford & Pedley, 1996; Pedley, 2014; Shiraishi et al., 2019). Some scales, however, contain micritic fabrics without any distinct evidence of earlier microbial presence. Consequently, the micritic Ca-carbonate crystals could also have precipitated entirely from temporary high Ca-carbonate supersaturation and crystallization and transport in suspension, indicating some pronounced environmental and related tunnel drainage solution changes (e.g. RAB 4).

3.7 Conceptual model for scale deposits in tunnel drainage settings

According to the data and arguments presented above, the investigated scale deposits in the drainage can be differentiated into four distinct types regarding their material characteristics and environment of formation (summarized in figure 13). Carbonate scales of type 1 (represented by scale deposit RAB 17) are mainly characterized by a highly porous and relatively soft material consistency, a very high pH, prominently high Na^+ and K^+ concentrations (26 mg/l and 67 mg/l, respectively), and very high SI values of calcite (>1) of the corresponding aqueous solution caused by intense concrete/shotcrete interaction. The composition of the solution shows low Ca^{2+}, Mg^{2+} and HCO_3^- concentrations (40 mg/l, 38 mg/l, and 91 mg/l; see table 4). Furthermore, the association of aragonite with dypingite in pore spaces - caused by prior $CaCO_3$ precipitation - as well as the microbial presence documented

by EPS-structures are indicative for type 1. Scale deposit of type 2 is represented by the red-brownish colored, typically thin, well-layered and compact (hard) scale deposit RAB 9. Accordingly, type 2 is involving some distinct influence of iron-oxidizing bacteria such as *Gallionella ferruginea* facilitating ferrihydrite and/or goethite formation. The corresponding aqueous solution revealed the highest Ca^{2+} and Mg^{2+} concentrations of all investigated drainage solutions (76 mg/l and 38 mg/l, respectively), a high molar Mg/Ca ratio (~0.8) as well as high SI values for calcite (up to 1.2). Type 2 typically consists of strongly consolidated and spatiotemporally evolved (e.g. layered) scale deposits with a pronounced durability dominated by calcite and favored by high flow rates (ripple structures). The red-brownish staining of the scale deposits of the central-drainage can be explained by bacterial influence of *Gallionella ferruginea*. This type of bacteria seems to occur in particular in the central-drainage of the investigated tunnel. This is reflected by up to 10 times higher flow rates, continuously providing aqueous Fe^{2+}, in individual drainages: the central-drainage flow rate, compared to the southern and northern lateral-drainages (assessed from visual rating). An additional strong indication of a high flow rate in the central-drainage is provided by the ripple structures characterizing the surface topography (growth surface) of the respective scale deposits (e.g. Figs. 2C and 3C). Such streaming and turbulence related features are particularly prominent for RAB 4, 6, and 9. A constantly available water flow and high flow rate is an advantage for a steady microbial presence, since bacteria develop best in areas of active turbulent flow and aeration, favoring gas exchanges and nutrients (e.g. Fe^{2+}; Pedley, 2014; Chan et al., 2016).

Considering the variable contribution of the northern drainage channel to the central-drainage and the variable coloring and layering (zonation) in some of the central-drainage scale deposits (RAB 4, 6 & 9; Figs. 2A-C & 3A-C), changing Fe concentrations - related to the ground- and subsequent drainage water coming from the northern drainage - can be reasonably assumed. In this regard, a relatively Fe-rich, but episodic water supply would facilitate variable nutrient input (e.g. Fe^{2+}) and consequently a more unsteady microbial activity. A complete vanishing of the microbial presence seems to be likely during complete desiccation of the northern and/or central-drainage. The major relevance of the spatiotemporally variable flow conditions in the drainages is further supported by observed variations in the carbonate content (coloring, and structure) as well as accessory mineralogy. The drainage deposits of type 3 are characterized by a porous scale fabric, a high aragonite content (up to 49 wt.%) and the occurrence of the rarely documented minerals dypingite and/or brucite (RAB 6, 18, and 25). In particular, a variable degree of prior $CaCO_3$ precipitation in association with variable Mg/Ca content in the drainage solution explains this complex carbonate/hydroxide mineral association. The spatial

mineral arrangement, e.g. dypingite on top of aragonite needles, hints on variable hydrochemical and flow conditions, including temporary desiccation. The slightly alkaline pH of the related aqueous solution of scale deposit type 3 ranges from 7.9 to 8.6 with a molar Mg/Ca ratio up to 1.1. Type 4, including RAB 23 and 24, comprises scale deposits dominantly consisting of calcite with a compact and dense (low porosity) fabric and whitish colored appearance, i.e. a low iron and accessory mineral content. The type 4 related solutions show molar Mg/Ca ratios <0.6 and relatively low, but still supersaturated solutions in respect to calcite (SI <0.6; RAB 23 and 24; Fig.13).

An advanced understanding on the reaction mechanisms and influencing factors for scale deposit formation from the tunnel Spital can be applied to other tunnel systems: Air/gas exchange between the drainage solution and the atmosphere and variable flow rates are essential for all drainage systems. In most cases, microorganisms have a significant impact in the formation and fabrics of scale deposits and thus have to be considered in tunnel drainage systems. In particular, in tunnels with little rock overburden, temporary desiccation of drainages may occur affecting microbial communities and related mineral deposits.

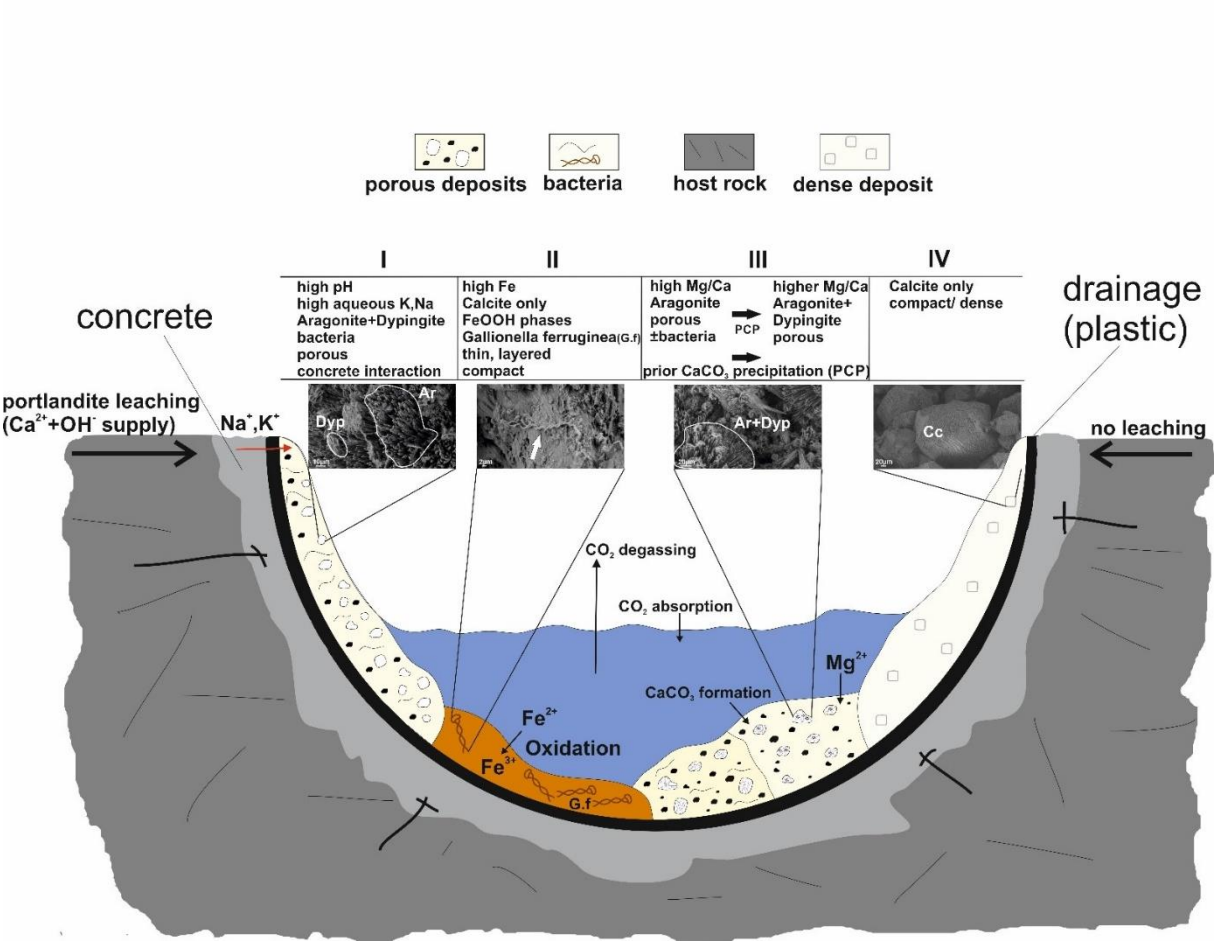

Figure 13: *Schematic illustration of different chemical-sedimentary reaction mechanisms occurring in the drainage system of the Tunnel Spital as a case study for scale deposits in drainage pipes. Scales of type 1, represented by RAB 17, are characterized by porous, white precipitates precipiated from a solution with high pH at elevated* Na^+ *and* K^+ *concentrations due to enhanced shotcrete/concrete interaction of the locally percolatingground water and/or interstitial solutions entering the tunnel. Type 2 is represented by reddish, thin layered and prominently compact sample RAB 9 involving the iron-oxidizing bacteria Gallionella ferruginea (white arrow) and a solution with a moderate pH and higher* HCO_3^-, Ca^{2+} *and* Mg^{2+} *concentration than the solution of type 1. Type 3 is reflected by the carbonate deposits RAB 6, 18, and 25. All of these precipitates revealed high aqueous molar Mg/Ca ratios, the occurrence of significant amounts of aragonite (Ar) and dypingyte (Dy) mainly located in the scale pore spaces, as well as overall porous and relatively soft material consistencies. One of the samples in this group (RAB 18) indicates microbial activities. The corresponding solutions exhibit a moderate pH value and higher* HCO_3^-, Mg^{2+} *and* Ca^{2+} *concentrations than the solution of type 1. Type 4 stands for the scale deposits RAB 23 and 24, which comprise of almost pure calcite (Cc) and a compact/dense fabric. The chemical composition of type 4 solutions is comparable to those of types 2 and 3.*

3.8 Conclusions and outlook

The present contribution on unwanted scale deposits in a tunnel drainage system gained an increased understanding of the scale formation dynamics and their variable environmental dependencies:

- All investigated aqueous solutions show a relatively similar chemical composition, only the water related to scale deposit RAB 17 exhibited a different composition due to strong fluid-solid interaction with the concrete. In the related scale deposits, recurrent growth interruptions, partial replacement of aragonite by calcite, evidence of temporary water flow reduction and even complete desiccation support the critical role of variable flow rates and the influence of a (seasonally) variable air exchange (dynamic tunnel atmosphere).
- Almost constant $\delta^{2}H_{H2O}$ and $\delta^{18}O_{H2O}$ values indicate a distinct and homogeneous local aquifer discharging regional meteoric water into the tunnel. A hydrochemical evolution occurs mainly across the flow paths in the tunnel drainage system. Aqueous $\delta^{13}C_{DIC}$ values and the calculated Rayleigh fractionation process indicate near stable carbon isotope equilibrium fractionation during calcium carbonate formation instead of pronounced degassing of CO_2 or dominant CO_2 absorption to be traced. $\delta^{18}O_{prec}$ measurements across scale profiles indicate changes in the temperature of the tunnel water tracing seasonal temperature changes of the tunnel atmosphere.
- The rarely documented mineral dypingite was detected in the scale deposits, indicating drainage solution evolution based on prior $CaCO_3$ precipitation. Dypingite on top of aragonite needles hint on temporary desiccation.
- Microbial activity (e.g. *Gallionella ferruginea*) has been detected in some of the scale deposits (RAB 9, 17 and 18). The microbes appear to significantly influence the variable scaling process and in particular its mineralogy (e.g. ferrihydrite formation), fabric (e.g. enhanced porosity) and overall scale material consistency.

In conclusion, natural (geogenic) as well as operative (anthropogenic) physicochemical conditions control the chemical evolution of the drainage solutions and the related formation of variable scale deposits. Based on an advanced understanding on scale formation mechanisms and fabrics, the environmental conditions determining the scale deposits could be adapted and controlled by optimized operative versus natural conditions (e.g. prevailing physicochemical gradients, tunnel air ventilation, flow rate, drainage geometries and selected materials) to reduce and/or prevent unwanted scaling. More specifically, a suitable choice of the materials in contact

with the scale precipitating and/or transporting (detrital components) ground- and tunnel waters (e.g. pipes and concrete/shotcrete) is essential to reduce and/or prevent unwanted scale deposits or material alteration. In this context, a high durability concrete could be used and/or drainage pipe material avoiding crystal growth on its surface (e.g. PE instead of PVC plastics). A promising intervening technique may include adding of small dosages (ppm range) of tailored "green" inhibitors to the drainage solution in order to reduce or delay the unwanted nucleation and precipitation of calcium carbonate, i.e. long enough to drain the carbonate supersaturated solution out of the tunnel. Another strategy for reducing the evolution of scale deposits is to keep the CO_2 and H_2O gas/air exchange rates between the drainage solution and the tunnel atmosphere as low as possible, e.g. by adapting drainage construction designs. In tunnels with little overburden water draining concepts at the Earth 's surface could limit seasonally variable water draining into the tunnel. Thus, effective strategies to reduce or prevent the formation of scale deposits and related processes should be developed for the individual case.

In future studies, seasonal and episodic (temporary) variations of the temperatures in the tunnel atmosphere and aqueous solutions, air pressure variations inside and outside the tunnel partially controlling air exchange, critical gradients (pCO_2, humidity) of the water versus the tunnel atmosphere and the drainage water flow conditions (recharge vs. discharge, mixing) should be monitored at high spatial and temporal resolution, e.g. applying data loggers in critical sections to assess the changing environmental conditions for scale formation.

3.9 Acknowledgements

The study was financially supported by the "Autobahnen und Schnellstraßen Finanzierungs-Aktiengesellschaft" (ASFINAG). Judith Jernej, Maria Hierz and Andrea Wolf are acknowledged for their dedicated work at the TU Graz laboratories. We would also like to thank Hermann Stadler, the initiator of the project as well as Sabine Lindbichler and Barbara Zirngast from AquaConSol for their work related to stable isotope analysis. Chemical and mineralogical analyses were conducted in the NAWI Graz Central Lab for Water, Minerals and Rocks.

3.10 Supplementary material

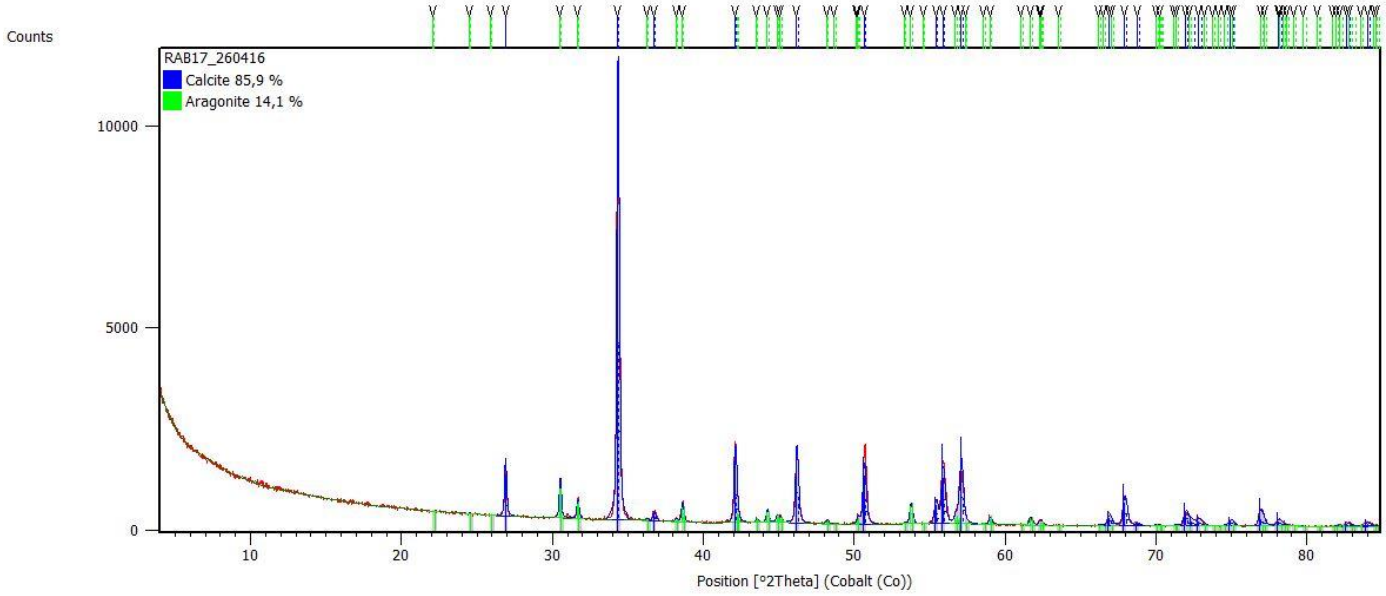

Figure A.1: *XRD-pattern of sample RAB 4.*

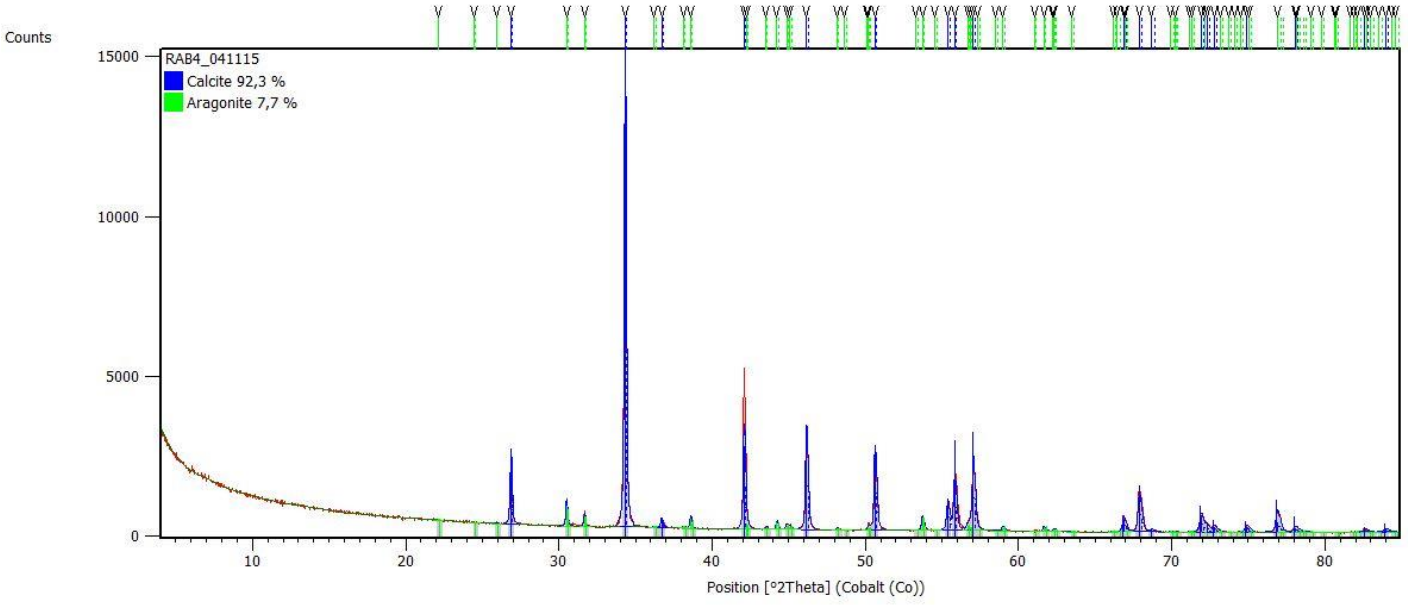

Figure A.2: *XRD-pattern of sample RAB 17.*

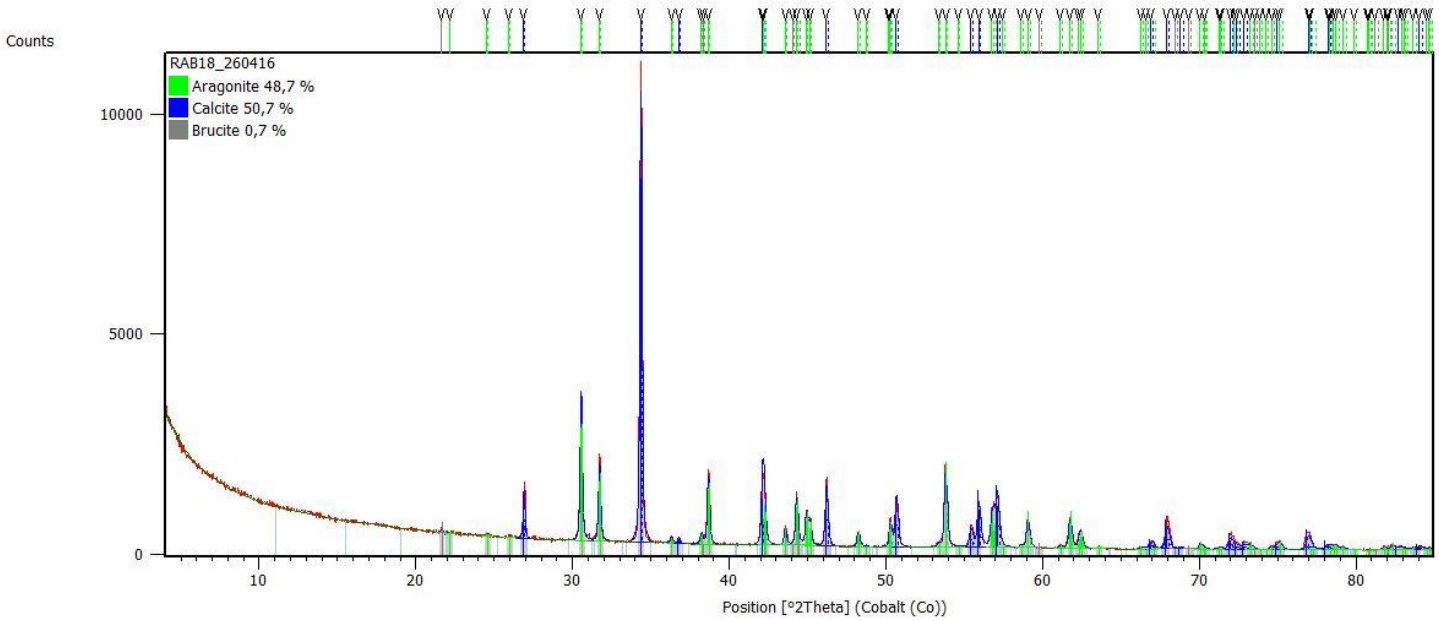

Figure A.3: *XRD-pattern of sample RAB 18.*

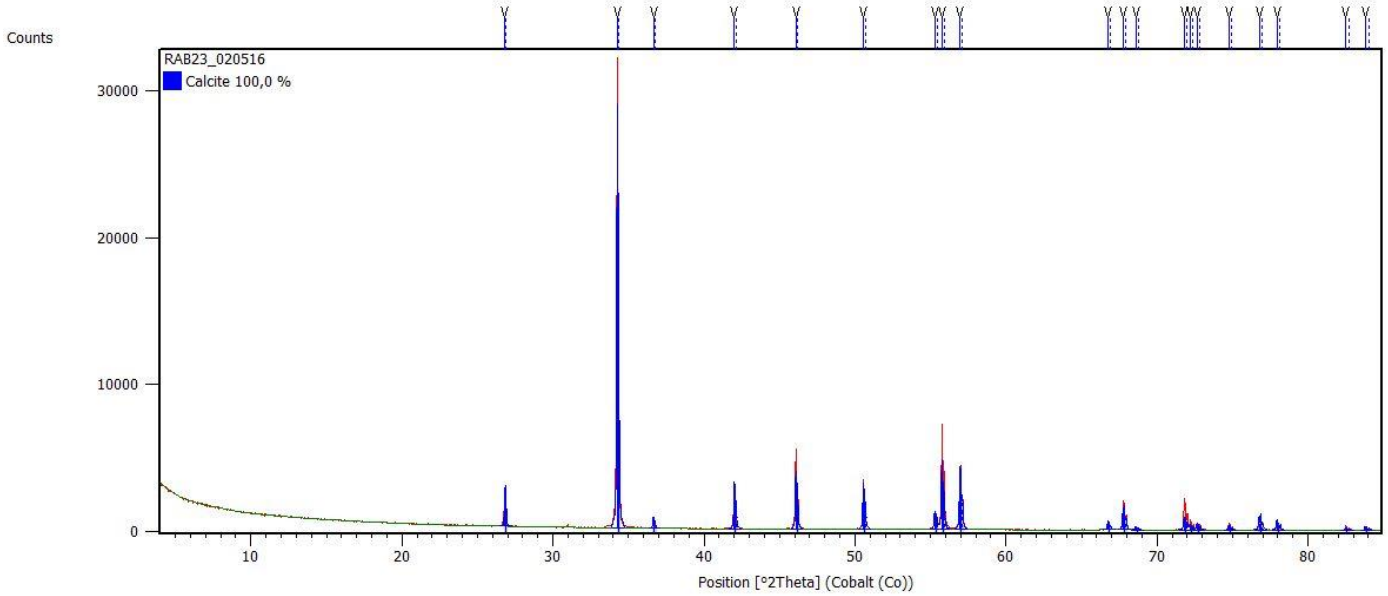

Figure A.4: *XRD-pattern of sample RAB 23.*

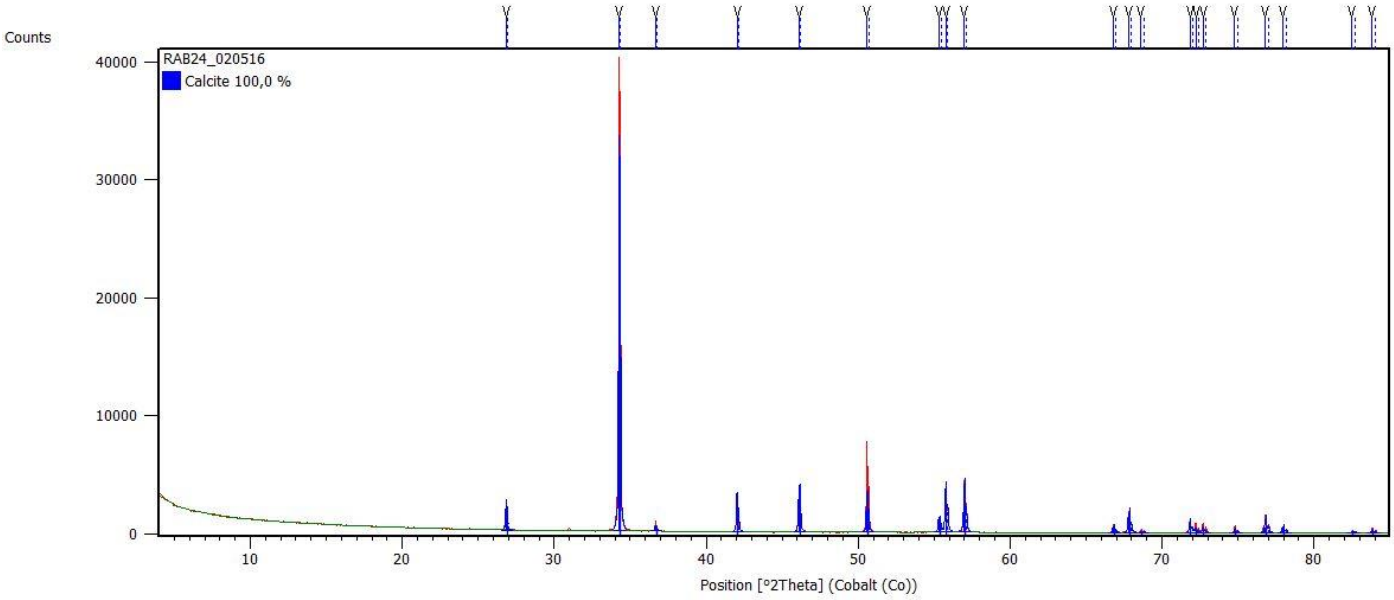

Figure A.5: *XRD-pattern of sample RAB 24.*

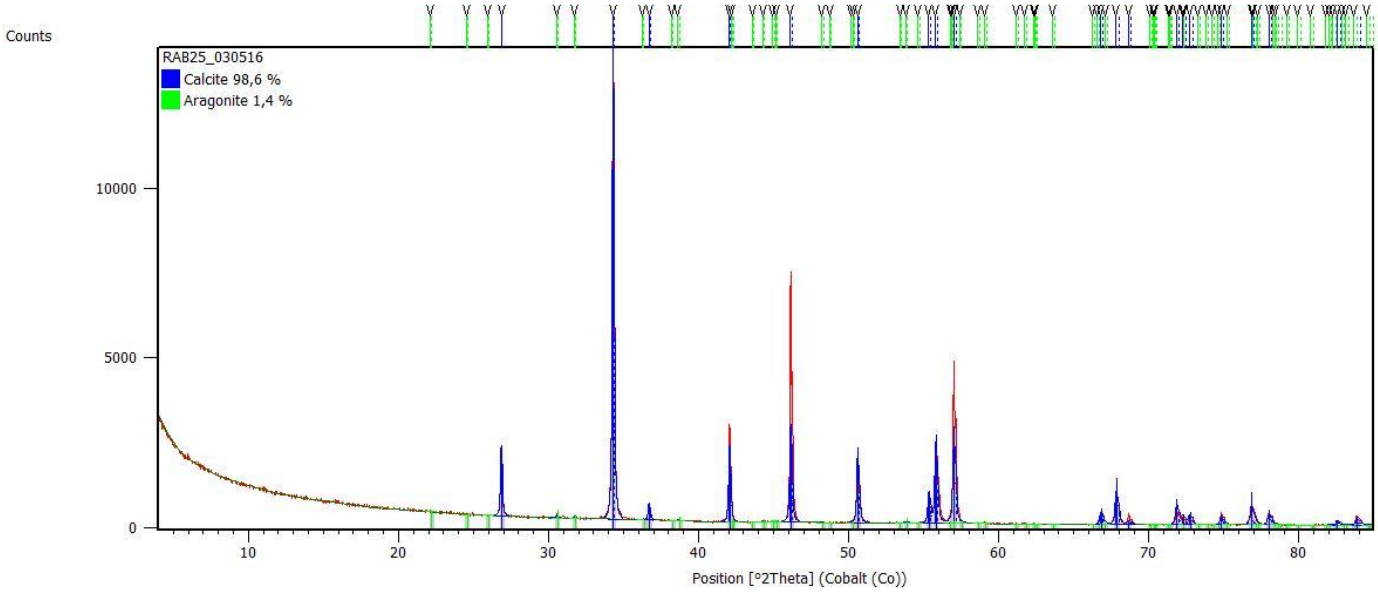

Figur A.6: *XRD-pattern of sample RAB 25.*

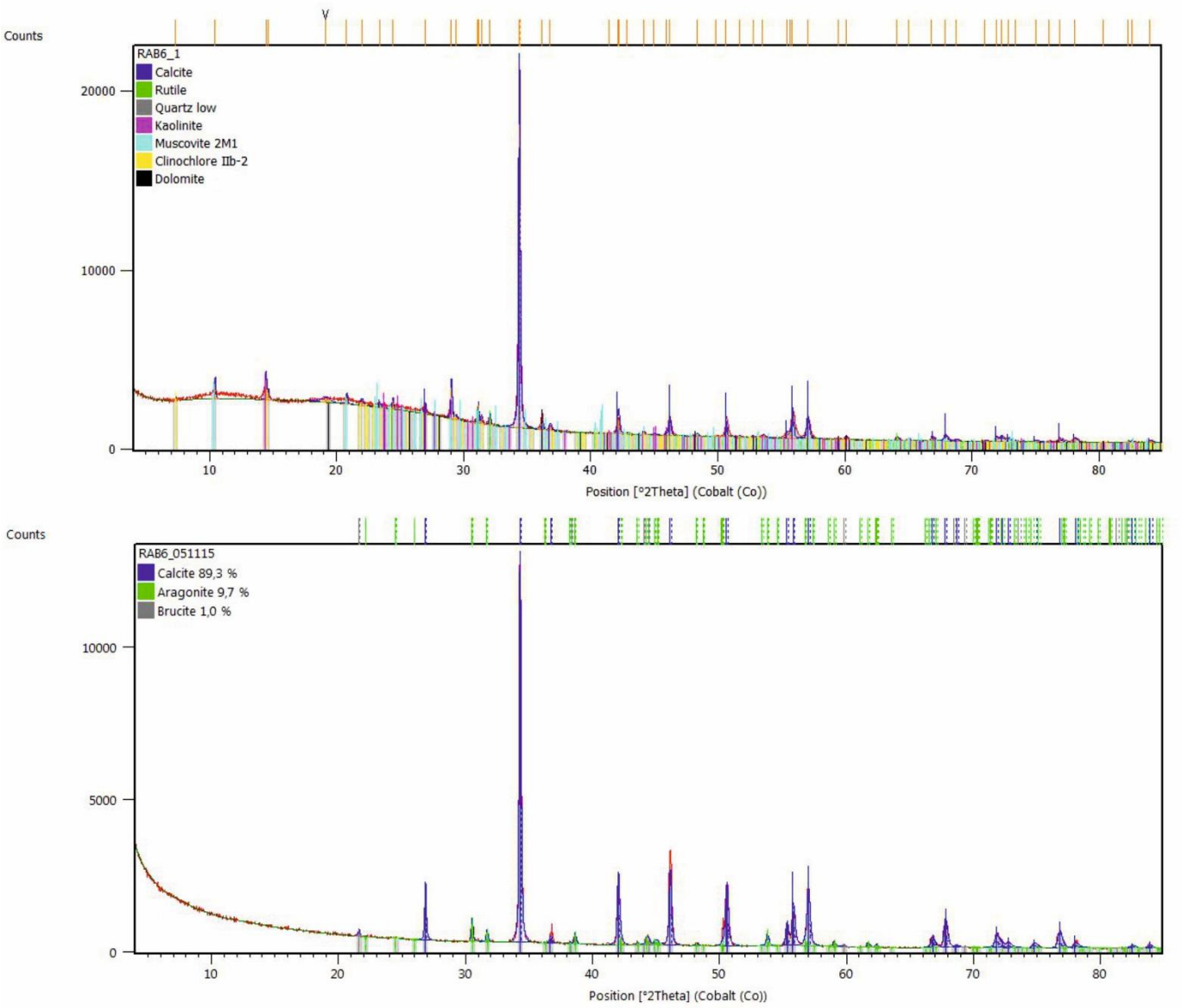

Figure B.1: *XRD-pattern of sample RAB 6. The top diffractogram shows the composition of the solid residuum after nitric acid digestion of the carbonate matrix. The lower diagram reveals the bulk composition of sample RAB 6.*

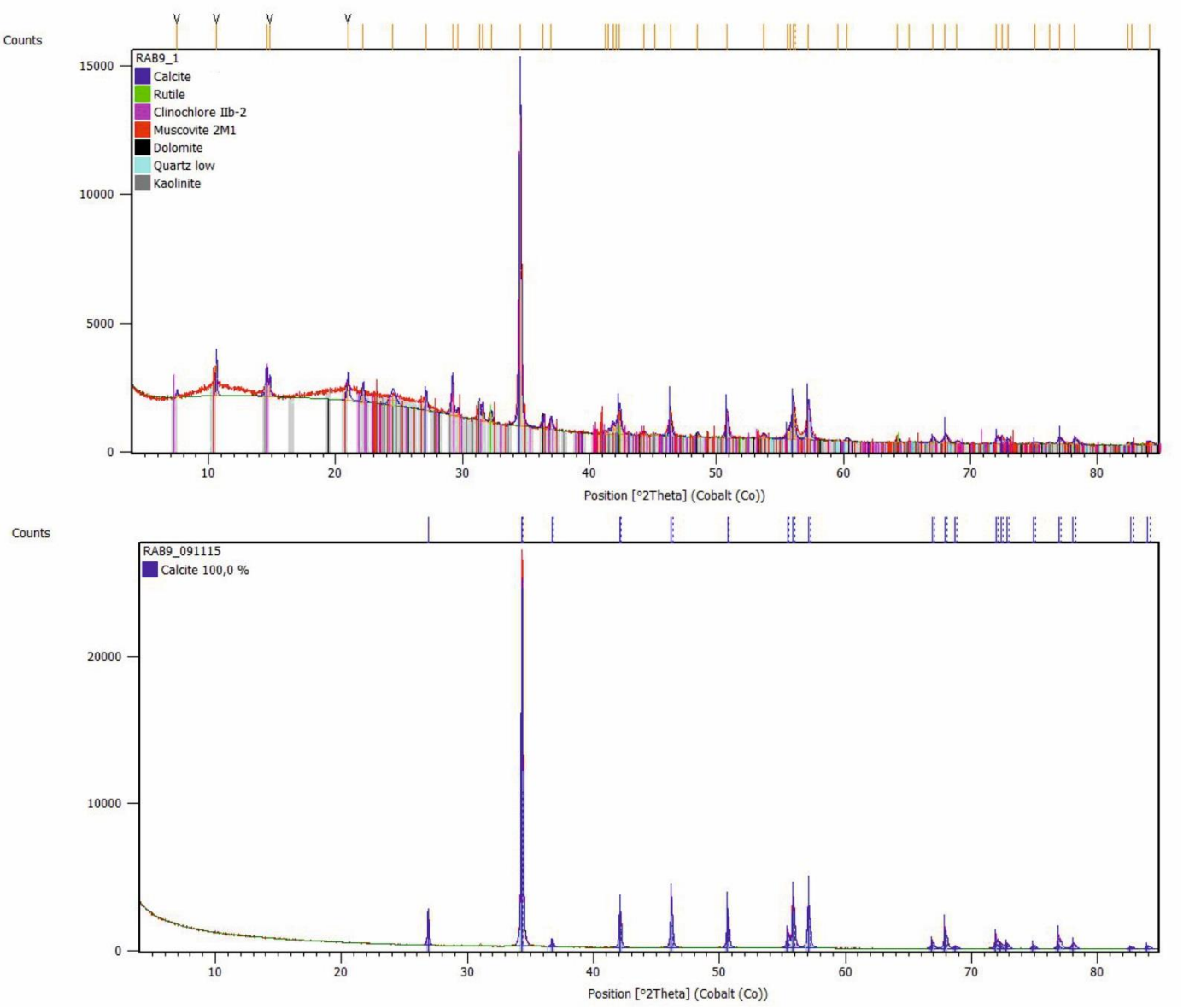

Figure B.2*: XRD-pattern of sample RAB 9. The top diffractogram shows the composition of the solid residuum after acid digestion of the carbonate matrix. The lower image reveals the bulk composition of sample RAB 9.*

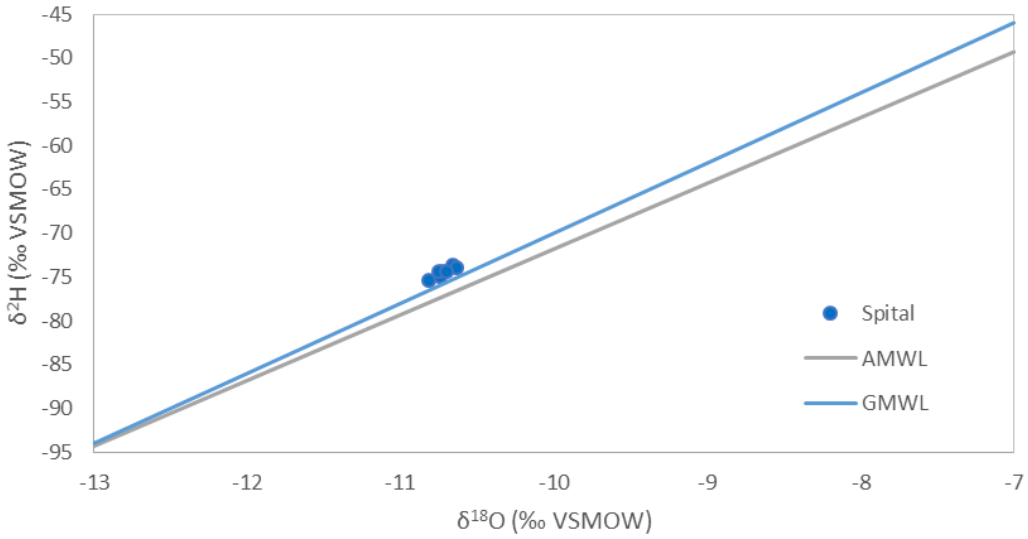

Figure C.1: *δ^2H and $\delta^{18}O$ isotopic compositions of the investigated tunnel drainage solutions (tunnel Spital am Semmering) compared to the Global Meteoric Water Line (GMWL) according to Craig (1961) and the Austrian Meteoric Water Line (AMWL) according to Hager & Fölsche (2015). The investigated aqueous solutions show enriched stable isotope values (increased Deuterium-excess) compared to the GMWL and AMWL.*

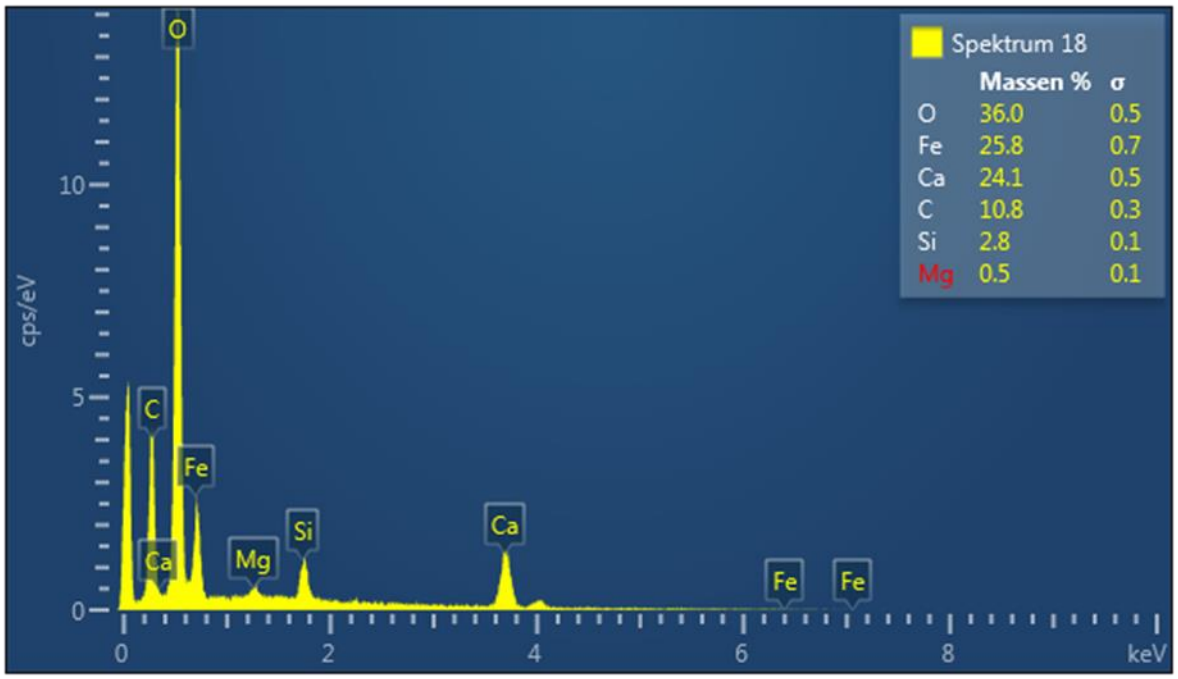

Figure D.1*: EDX spectrum of twisted stalks in sample RAB 9 which exhibits the occurrence of the iron oxidizing bacteria Gallionella ferruginea.*

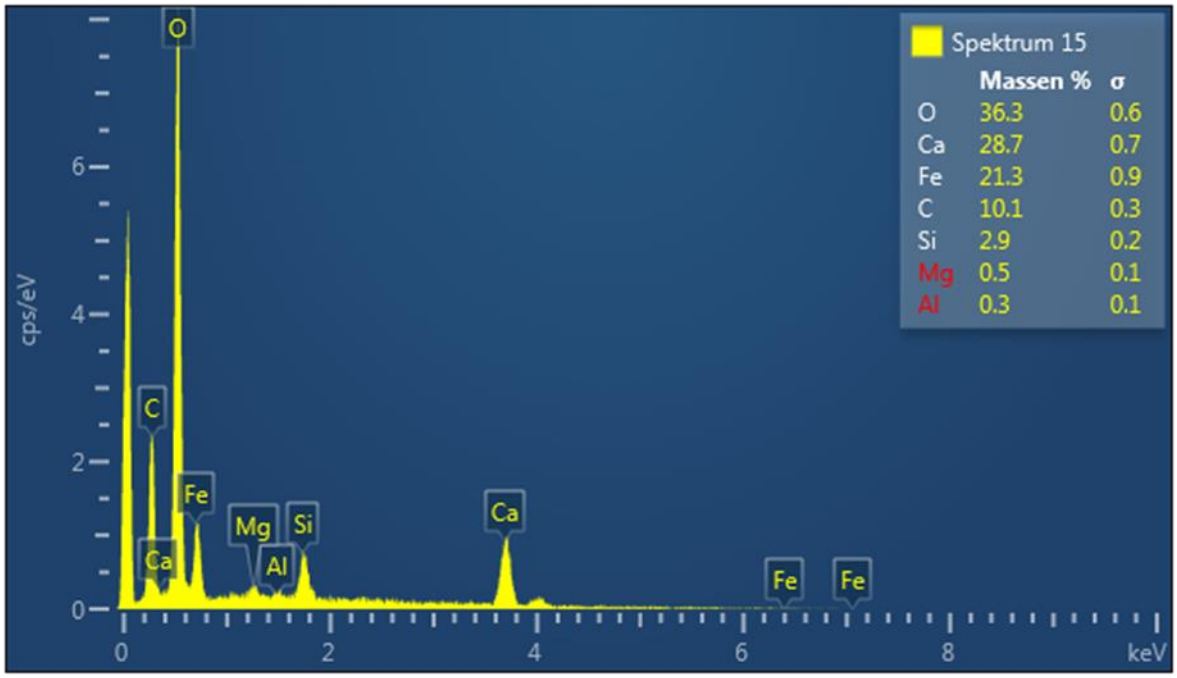

***Figure D.2**: EDX spectrum of the sample RAB 9 indicating the mineral ferrihydrite.*

***Table A.1**: Stable isotopic composition $\delta^{13}C$ and $\delta^{18}O$ of the analyzed carbonate precipitates (RAB 4, 9, 17, 23, 24 and 25) based on selected (pointwise using handheld drill) sampling across transects.*

Sample	$\delta^{13}C$ ‰, VPDB	$\delta^{18}O$ ‰, VPDB	Sample	$\delta^{13}C$ ‰, VPDB	$\delta^{18}O$ ‰, VPDB	Sample	$\delta^{13}C$ ‰, VPDB	$\delta^{18}O$ ‰, VPDB	Sample	$\delta^{13}C$ ‰, VPDB	$\delta^{18}O$ ‰, VPDB	Sample	$\delta^{13}C$ ‰, VPDB	$\delta^{18}O$ ‰, VPDB	Sample	$\delta^{13}C$ ‰, VPDB	$\delta^{18}O$ ‰, VPDB
RAB4-1	-10.4	-8.5	RAB9-1	-9.4	-9.1	RAB17-1	-11.4	-9.6	RAB23-1	-12.3	-9.8	RAB24-1	-12.0	-9.7	RAB25-1	-11.3	-9.1
RAB4-2	-10.5	-9.3	RAB9-2	-9.4	-9.0	RAB17-2	-9.8	-7.3	RAB23-2	-12.4	-9.5	RAB24-2	-12.4	-10.0	RAB25-2	-11.5	-8.8
RAB4-3	-10.8	-9.1	RAB9-3	-9.4	-8.9	RAB17-3	-9.8	-7.7	RAB23-3	-12.2	-9.9	RAB24-3	-12.3	-9.1	RAB25-3	-11.1	-8.7
RAB4-4	-10.8	-9.7	RAB9-4	-9.5	-9.8	RAB17-4	-10.1	-8.6	RAB23-4	-12.1	-9.4	RAB24-4	-11.8	-9.7	RAB25-4	-11.3	-8.3
RAB4-5	-11.3	-9.4	RAB9-5	-9.6	-9.1	RAB17-5	-9.6	-8.0	RAB23-5	-12.3	-9.4	RAB24-5	-11.6	-9.9	RAB25-5	-11.0	-8.9
RAB4-6	-10.6	-8.6	RAB9-6	-9.4	-10.0				RAB23-6	-12.1	-9.2	RAB24-6	-11.0	-10.0	RAB25-6	-10.9	-9.1
RAB4-7	-10.5	-9.5	RAB9-7	-9.4	-9.2				RAB23-7	-12.0	-10.0	RAB24-7	-11.2	-9.5	RAB25-7	-11.3	-7.4
RAB4-8	-10.3	-9.7	RAB9-8	-9.5	-9.5				RAB23-8	-12.0	-9.4	RAB24-8	-12.2	-10.4	RAB25-8	-11.2	-8.4
RAB4-9	-10.3	-9.1	RAB9-9	-9.3	-8.7							RAB24-9	-11.8	-9.9			
RAB4-10	-10.1	-8.5															
RAB4-11	-10.1	-8.5															
RAB4-12	-10.2	-8.3															

References

Andrews, J. E., Riding, R., & Dennis, P. F., 1997. The stable isotope record of environmental and climatic signals in modern terrestrial microbial carbonates from Europe. Palaeogeography, Palaeoclimatology, Palaeoecology, 129(1-2), 171-189.

Auer, I., Böhm, R., Jurkovic, A., Lipa, W., Orlik, A., Potzmann, R., Schöner, W., Ungersböck, M., Matulla, C., Briffa, K., Jones, P., Efthymiadis, D., Brunetti, M., Nanni, T., Maugeri, M., Mercalli, L., Mestre, O., Moisselin, J; Bergert, M., Müller-Westermeier, G., Kveton,V., Bochnicek, O., Stastny, P., Lapin, M., Szalai, S., Szentimrey, T., Cegnar, T., Dolinar, M., Gajic-Capka, M., Zaninovic, K., Majstorovic, Z., & Nieplova, E., 2007. HISTALP—historical instrumental climatological surface time series of the Greater Alpine Region. International Journal of Climatology: A Journal of the Royal Meteorological Society, 27(1), 17-46.

Banfield, J. F., Welch, S. A., Zhang, H., Ebert, T. T., & Penn, R. L., 2000. Aggregation-based crystal growth and microstructure development in natural iron oxyhydroxide biomineralization products. Science, 289(5480), 751-754.

Banfield, J. F., & Welch, S. A., 2013. Microbial controls on the mineralogy of the environment. Environmental Mineralogy. EMU (European Mineralogical Union) Notes Mineral, 2, 173-196.

Boch, R., Spötl, C., & Frisia, S., 2011. Origin and palaeoenvironmental significance of lamination in stalagmites from Katerloch Cave, Austria. Sedimentology, 58(2), 508-531.

Boch, R., Dietzel, M., Reichl, P., Leis, A., Baldermann, A., Mittermayr, F., & Pölt, P., 2015. Rapid ikaite ($CaCO_3 \cdot 6H_2O$) crystallization in a man-made river bed: hydrogeochemical monitoring of a rarely documented mineral formation. Applied geochemistry, 63, 366-379.

Boch, R., Leis, A., Haslinger, E., Goldbrunner, J. E., Mittermayr, F., Fröschl, H., Hippler, D., & Dietzel, M., 2017. Scale-fragment formation impairing geothermal energy production: interacting H2S corrosion and $CaCO_3$ crystal growth. Geothermal Energy, 5(1), 4.

Boch, R., Wang, X., Kluge, T., Leis, A., Lin, K., Pluch, H., Mittermayr, F., Baldermann, A., Böttcher, M.E., & Dietzel, M., 2019. Aragonite–calcite veins of the 'Erzberg' iron ore deposit (Austria): Environmental implications from young fractures. Sedimentology, 66(2), 604-635.

Böttcher, M. E., & Dietzel, M., 2010. Metal-ion partitioning during low-temperature precipitation and dissolution of anhydrous carbonates and sulphates. European Mineralogical Union Notes in Mineralogy, 10(1), 139-187.

Chafetz, H. S., & Guidry, S. A., 1999. Bacterial shrubs, crystal shrubs, and ray-crystal shrubs: bacterial vs. abiotic precipitation. Sedimentary Geology, 126(1-4), 57-74.

Canterford JH, Tsambourakis G., 1984. Some observations on the properties of dypingite, Mg5(CO3)4(OH)2 ·5H2O, and related minerals. Mineral Mag 1984, 48:437-442.

Casella, L. A., Griesshaber, E., Yin, X., Ziegler, A., Mavromatis, V., Müller, D., Ritter, A., Hippler, D., Harper, E., Dietzel, M., Immenhauser, A., Schöne, B., Angiolini, L., Schmahl, W., 2017. Experimental diagenesis: insights into aragonite to calcite transformation of Arctica islandica shells by hydrothermal treatment. Biogeosciences, 14(6), 1461-1492.

Chan, C.S., Fakra, S.C., Emerson, D., Fleming, E.J., and Edwards, K.J., 2011. Lithotrophic iron-oxidizing bacteria produce organic stalks to control iron mineral growth: implications for biosignature formation. ISME J. 5, 717–727.doi:10.1038/ismej.2010.173

Chan, C.S., McAllister, S.M., Leavitt, A.H., Glazer, B.T., Krepski, S.T., Emerson, D., 2016. The Architecture of Iron Microbial Mats Reflects the Adaptation of Chemolithotrophic Iron Oxidation in Freshwater and Marine Environments. Frontiers in Microbiology 7, 796.

Chen, Y., Cui, Y., Barrett, A. G., Chille, F., & Lassalle, S., 2019. Investigation of calcite precipitation in the drainage system of railway tunnels. Tunnelling and Underground Space Technology, 84, 45-55.

Coplen, T. B., 2007. Calibration of the calcite–water oxygen-isotope geothermometer at Devils Hole, Nevada, a natural laboratory. Geochimica et Cosmochimica Acta, 71(16), 3948-3957.

Cornelius, H. P., 1952. Die Geologie des Mürztalgebietes – Jahrbuch der Geologischen Bundesanstalt, Sonderbände-04:1-94.

Craig, H., 1961. Isotopic Variations in Meteoric Waters. In: Science (New York, N.Y.) 133 (3465), S. 1702–1703.

Daëron, M., Drysdale, R. N., Peral, M., Huyghe, D., Blamart, D., Coplen, T. B., Lartaud, F., & Zanchetta, G., 2019. Most Earth-surface calcites precipitate out of isotopic equilibrium. Nature communications, 10(1), 1-7.

Dansgaard, W., 1964. Stable isotopes in precipitation. Tellus, 16(4), 436-468.

Dietzel, M., 1995. 13C/12C-und 18O16O-Signaturen von Calcit-Abscheidungen in Drainagesystemen. Acta hydrochimica et hydrobiologica, 23(4), 180-184.

Dietzel, M., & Kirchhoff, T., 2002. Stable isotope ratios and the evolution of acidulous ground water. Aquatic geochemistry, 8(4), 229-254.

Dietzel, M., Gussone, N., & Eisenhauer, A., 2004. Co-precipitation of Sr2+ and Ba2+ with aragonite by membrane diffusion of CO_2 between 10 and 50 C. Chemical Geology, 203(1-2), 139-151.

Dietzel, M., Rinder, T., Niedermayr, A., Mittermayr, F., Leis, A., Klammer, D., Köhler, S., Reichl, P., 2008a. Mechanisms of sinter formation in drainage systems. BHM Berg- und Hüttenmännische Monatshefte 153, 369–372.

Dietzel, M., Rinder, T., Leis, A., Reichl, P., Sellner, P., Draschitz, C., Plank, G., Klammer, D., & Schöfer, H., 2008b. Koralm tunnel as a case study for sinter formation in drainage systems–precipitation mechanisms and retaliatory action. Geomechanik und Tunnelbau: Geomechanik und Tunnelbau, 1(4), 271-278.

Dietzel, M., Purgstaller, B., Leis, A., Reichl, P., Stadler, H., Niedermayr, A., Rinder, T. & Wagner, H., 2013. Current challenges for scaling of tunnel drainage systems - Modelling approaches, monitoring tools and prevention strategies / Aktuelle Herausforderungen bei der Versinterung von Tunneldränagen - Modellie-rungsansätze, Monitoringwerkzeuge und Präventionsst. In: Geomechanik Tunnelbau 6 (6), S. 743–753.

Dietzel, M., Schön, F., Heinrichs, J., Deditius, A.P. and Leis, A. 2015. Tracing formation and durability of calcite in a Punic-Roman cistern mortar (PantelleriaIsland, Italy). Isotopes Environ. Health Stud.,52, 112–127.

Ehrenberg, C. G., 1836. Vorläufige Mitteilungen über das wirkliche Vorkommen fossiler Infusorien und ihre große Verbreitung. Poggendorff Ann, 38, 213-227.

Fairchild, I.J., Borsato, A., Tooth, A.F., Frisia, S., Hawkesworth, C.J., Huang, Y., McDermott, F., Spiro, B., 2000. Controls on trace element (Sr-Mg) compositions of carbonate cave waters: implications for speleothem climatic records. Chemical Geology 166, 255-269.

Flueckiger, M., Reinke, P., 2013. Aerodynamics, climate and ventilation in long rail tunnels considering an Andean base tunnel between Argentina and Chile.Geomechanics and Tunnelling 6, 312-326.

Ford, T. D., & Pedley, H. M., 1996. A review of tufa and travertine deposits of the world. Earth-Science Reviews, 41(3-4), 117-175.

Fouke, B. W., 2011. Hot-spring Systems Geobiology: abiotic and biotic influences on travertine formation at Mammoth Hot Springs, Yellowstone National Park, USA. Sedimentology, 58(1), 170-219.

Frost, R. L., Bahfenne, S., & Graham, J., 2009. Raman spectroscopic study of the magnesium-carbonate minerals—artinite and dypingite. Journal of Raman Spectroscopy: An International Journal for Original Work in all Aspects of Raman Spectroscopy, Including Higher Order Processes, and also Brillouin and Rayleigh Scattering, 40(8), 855-860.

Frisia, S., Borsato, A., Fairchild, I. J., McDermott, F., & Selmo, E. M., 2002. Aragonite-calcite relationships in speleothems (Grotte de Clamouse, France): environment, fabrics, and carbonate geochemistry. Journal of Sedimentary Research, 72(5), 687-699.

Frisia, S., 2014. Microstratigraphic logging of calcite fabrics in speleothems as tool for palaeoclimate studies. International Journal of Speleology, 44(1), 1.

Ghiorse, W. C., 1984. Biology of iron-and manganese-depositing bacteria. Annual review of microbiology, 38(1), 515-550.

Girmscheid, G., Gamisch, T., Klein, T., & Meinlschmidt, A., 2003. Versinterung von Tunneldrainagen-Mechanismen der Versinterungsentstehung. Bauingenieur, 292-300.

Grengg, C., Mittermayr, F., Koraimann, G., Konrad, F., Szabó, M., Demeny, A., & Dietzel, M., 2017. The decisive role of acidophilic bacteria in concrete sewer networks: A new model for fast progressing microbial concrete corrosion. Cement and Concrete Research, 101, 93-101.

Hager, B., & Foelsche, U., 2015. Stable isotope composition of precipitation in Austria. Austrian Journal of Earth Sciences, 108(2).

Hallbeck, L., & Pedersen, K., 1991. Autotrophic and mixotrophic growth of Gallionella ferruginea. Microbiology, 137(11), 2657-2661.

Hallbeck, L., Ståhl, F., & Pedersen, K., 1993. Phytogeny and phenotypic characterization of the stalk-forming and iron-oxidizing bacterium Gallionella ferruginea. Microbiology, 139(7), 1531-1535.

Hallberg, R., & Ferris, F. G., 2004. Biomineralization by Gallionella. Geomicrobiology Journal, 21(5), 325-330.

Harer, G., 2017. Measures for the reduction of sinter formations in tunnels. In IOP Conference Series: Materials Science and Engineering (Vol. 236, No. 1, p. 012071). IOP Publishing.

Harrison, A. L., Power, I. M., & Dipple, G. M., 2012. Accelerated carbonation of brucite in mine tailings for carbon sequestration. Environmental science & technology, 47(1), 126-134.

Harrison, A. L., Mavromatis, V., Oelkers, E. H., & Bénézeth, P., 2019. Solubility of the hydrated Mg-carbonates nesquehonite and dypingite from 5 to 35° C: Implications for CO_2 storage and the relative stability of Mg-carbonates. Chemical Geology, 504, 123-135.

Hasson, D., Avriel, M., Resnick, W., Rozenman, T., & Windreich, S., 1968. Calcium carbonate scale deposition on heat transfer surfaces. Desalination, 5(1), 107-119.

Heim, C., Simon, K., Ionescu, D., Reimer, A., De Beer, D., Quéric, N. V., Reitner, J., & Thiel, V., 2015. Assessing the utility of trace and rare earth elements as biosignatures in microbial iron oxyhydroxides. Frontiers in Earth Science, 3, 6.

Hoefs, J., 2015. Theoretical and experimental principles. In Stable isotope geochemistry (pp. 1-46). Springer, Cham.

Huang, Y., & Fairchild, I. J., 2001. Partitioning of Sr2+ and Mg2+ into calcite under karst-analogue experimental conditions. Geochimica et Cosmochimica Acta, 65(1), 47-62.

Katz, J. L., Reick, M. R., Herzog, R. E., & Parsiegla, K. I., 1993. Calcite growth inhibition by iron. Langmuir, 9(5), 1423-1430.

Kim, S. T., & O'Neil, J. R., 1997. Equilibrium and nonequilibrium oxygen isotope effects in synthetic carbonates. Geochimica et cosmochimica acta, 61(16), 3461-3475.

Kosednar-Legenstein, B., Dietzel, M., Leis, A., & Stingl, K., 2008. Stable carbon and oxygen isotope investigation in historical lime mortar and plaster–Results from field and experimental study. Applied Geochemistry, 23(8), 2425-2437.

Kumar, B., Kumar, M., Patil, A. K., & Jain, S., 2018. Effect of V cut in perforated twisted tape insert on heat transfer and fluid flow behaviour of tube flow: An experimental study. Experimental Heat Transfer, 1-21.

Liebminger, A., Papesch, W., Haberhauer, G., & Varmuza, K., 2007. Multivariate models for the concentration of oxygen-18 in precipitation based on meteorological and geographical features. Chemometrics and Intelligent Laboratory Systems, 89(1), 1-8.

Luetscher, M., Lismonde, B., & Jeannin, P. Y., 2008. Heat exchanges in the heterothermic zone of a karst system: Monlesi cave, Swiss Jura Mountains. Journal of Geophysical Research: Earth Surface, 113(F2).

Ma, Z., Yan, H., Zhou, X., Hou, C., 2013. Impact of carbonate scaling on the efficiency of used geothermal water reinjection from low-middle temperature geothermal fluid in xianyang porous geothermal field, NW China, Advanced Materials Research, pp. 307-310.

Mattey, D., Lowry, D., Duffet, J., Fisher, R., Hodge, E., & Frisia, S., 2008. A 53 year seasonally resolved oxygen and carbon isotope record from a modern Gibraltar speleothem: reconstructed drip water and relationship to local precipitation. Earth and Planetary Science Letters, 269(1-2), 80-95.

Mavromatis, V., Pearce, C. R., Shirokova, L. S., Bundeleva, I. A., Pokrovsky, O. S., Benezeth, P., & Oelkers, E. H., 2012. Magnesium isotope fractionation during hydrous magnesium carbonate precipitation with and without cyanobacteria. Geochimica et Cosmochimica Acta, 76, 161-174.

Mittermayr, F., Baldermann, A., Baldermann, C., Grathoff, G. H., Klammer, D., Köhler, S. J., Leis, A., Warr, L., & Dietzel, M., 2017. Environmental controls and reaction pathways of coupled de-dolomitization and thaumasite formation. Cement and concrete research, 95, 282-293.

Onuk, P., Dietzel, M., & Hauzenberger, C. A., 2014. Formation of helictite in the cave Dragon Belly (Sardinia, Italy)—Microstructure and incorporation of Mg, Sr, and Ba. Chemie der Erde-Geochemistry, 74(3), 443-452.

ÖBB-Infrastruktur AG; Semmering-Basistunnel Projekt; accessed: 24.01.2019.

Parkhurst, D. L., & Appelo, C. A. J., 2013. Description of input and examples for PHREEQC version 3: a computer program for speciation, batch-reaction, one-dimensional transport, and inverse geochemical calculations (No. 6-A43). US Geological Survey.

Passchier, C., Sürmelihindi, G., Spötl, C., Mertz-Kraus, R., & Scholz, D., 2016. Carbonate deposits from the ancient aqueduct of Béziers, France—A high-resolution palaeoenvironmental archive for the Roman Empire. Palaeogeography, Palaeoclimatology, Palaeoecology, 461, 328-340.

Pedley, M., 2014. The morphology and function of thrombolitic calcite precipitating biofilms: A universal model derived from freshwater mesocosm experiments. Sedimentology, 61(1), 22-40.

Power, I. M., Wilson, S. A., Thom, J. M., Dipple, G. M., & Southam, G., 2007. Biologically induced mineralization of dypingite by cyanobacteria from an alkaline wetland near Atlin, British Columbia, Canada. Geochemical Transactions, 8(1), 13.

Purgstaller, B., Dietzel, M., Baldermann, A., & Mavromatis, V., 2017. Control of temperature and aqueous Mg2+/Ca2+ ratio on the (trans-) formation of ikaite. Geochimica et cosmochimica acta, 217, 128-143.

Raade, G., 1970. Dypingite, a new hydrous basic carbonate of magnesium, from Norway. American Mineralogist: Journal of Earth and Planetary Materials, 55(9-10), 1457-1465.

Riechelmann, S., Schröder-Ritzrau, A., Wassenburg, J.A., Schreuer, J., Richter, D.K., Riechelmann, D.F.C., Terente, M., Constantin, S., Mangini, A. and Immenhauser, A., 2014. Physicochemical characteristics of drip waters: influence on mineralogy and crystal morphology of recent cave carbonate precipitates. Geochim. Cosmochim. Acta, 145, 13–29

Rinder, T., Dietzel, M., & Leis, A., 2013. Calcium carbonate scaling under alkaline conditions–case studies and hydrochemical modelling. Applied geochemistry, 35, 132-141.

Rodriguez-Navarro, C., & Benning, L. G., 2013. Control of crystal nucleation and growth by additives. Elements, 9(3), 203-209.

Rossi, C., & Lozano, R. P., 2016. Hydrochemical controls on aragonite versus calcite precipitation in cave dripwaters. Geochimica et Cosmochimica Acta, 192, 70-96.

Schmidt, R., Fitzek, H., Nachtnebel, M., Mayrhofer, C., Schroettner, H., & Zankel, A., 2019. The Combination of Electron Microscopy, Raman Microscopy and Energy Dispersive X-Ray Spectroscopy for the Investigation of Polymeric Materials. In Macromolecular symposia (Vol. 384, No. 1, p. 1800237).

Shiraishi, F., Eno, Y., Nakamura, Y., Hanzawa, Y., Asada, J., & Bahniuk, A. M., 2019. Relative influence of biotic and abiotic processes on travertine fabrics, Satono-yu hot spring, Japan. Sedimentology, 66(2), 459-479.

Spötl, C., 2005. A robust and fast method of sampling and analysis ofd13C of dissolved inorganic carbon in groundwaters. Isotopes Environ. Health Stud., 41, 217–221.

Suzuki, T., Hashimoto, H., Matsumoto, N., Furutani, M., Kunoh, H., & Takada, J., 2011. Nanometer-scale visualization and structural analysis of the inorganic/organic hybrid structure of Gallionella ferruginea twisted stalks. Appl. Environ. Microbiol., 77(9), 2877-2881.

Stocks, S. M., 2004. Mechanism and use of the commercially available viability stain, BacLight. Cytometry Part A: The Journal of the International Society for Analytical Cytology, 61(2), 189-195.

Sürmelihindi, G., Passchier, C. W., Spötl, C., Kessener, P., Bestmann, M., Jacob, D. E., & Baykan, O. N., 2013. Laminated carbonate deposits in Roman aqueducts: Origin, processes and implications. Sedimentology, 60(4), 961-982.

Takasaki, S., Parsiegla, K. I., & Katz, J. L., 1994. Calcite growth and the inhibiting effect of iron (III). Journal of Crystal Growth, 143(3-4), 261-268.

TBGG-Dr.Heim, 2001: S6 Semmering Schnellstraße; Tunnel Spital-Schlussbericht der baugeologischen Dokumentation; ink. Beilage und Plandarstellung; 2001.

Thompson, J. B., & Ferris, F. G., 1990. Cyanobacterial precipitation of gypsum, calcite, and magnesite from natural alkaline lake water. Geology, 18(10), 995-998.

Tuhela, L., Carlson, L., & Tuovinen, O. H., 1997. Biogeochemical transformations of Fe and Mn in oxic groundwater and well water environments. Journal of Environmental Science & Health Part A, 32(2), 407-426.

Vatter, A. E., & Wolfe, R. S., 1956. Electron microscopy of Gallionella ferruginea. Journal of bacteriology, 72(2), 248.

Chapter 4 - Assessment and formation mechanisms of scale deposits in tunnels of the ÖBB-Infrastruktur AG – A subproject of the Task Force Drainage

Stefanie Eichinger[1], Albrecht Leis[2], Ronny Boch[1,3], Christian Seywald[4], Martin Dietzel[1]

[1] Institute of Applied Geosciences, Graz University of Technology & NAWI Graz GeoCenter, Rechbauerstrasse 12, 8010 Graz, Austria.

[2] JR-AquaConSol GmbH, Steyrergasse 21, 8010 Graz, Austria.

[3]Geoconsult ZT GmbH, Team Geochemie & Monitoring, Urstein Süd 13, 5412 Puch bei Hallein, Austria.

[4]ÖBB-Infrastruktur AG Fachbereich Bautechnik-Tunnelbau, Weiserstraße 7, 5020 Salzburg, Austria.

4.1 Abstract

Scale deposit formation in drainage systems of railway tunnels represents a major challenge for their functionality and maintenance. The removal of these scale deposits causes high costs and restrictions of system availability. Effective measures to reduce scale deposit formation range from specification of the composition and structure of building materials to the application of tailored prevention and cleaning strategies. This requires advanced knowledge of the origin and type of scale deposits. The aim of this study is a systematic compilation, characterization, classification, and evaluation of scale deposits in relation to their formation mechanisms and the influence of variable environmental factors. The scale deposits from the 16 investigated tunnels mainly consist of the minerals calcite, aragonite, brucite as well as iron (hydr)oxides and detrital components. Four major types of scale deposits are distinguished: (i) unconsolidated-particulate, (ii) shard-like, (iii) porous, and (iv) compact scales. Types ii to iv show clear indications of microbial activity affecting the formation and appearance of individual deposits by various metabolic processes. The determining factors for the formation of scales – in addition to the geogenic composition of the aqueous solutions in the drainage system (groundwater / surface water) – are the variable interaction of these waters with the binding agents of the building materials used and the tunnel atmosphere. Geogenic conditions and technical-operational specifications of a tunnel determine the type and character of scale deposits, which can be actively influenced based on the case-specific reaction mechanisms by individual adaptations of environmental conditions.

4.2 Introduction

Scale deposits are formed in the drainage systems of many tunnels managed by the Austrian railway operator ÖBB-Infrastruktur AG, and usually have to be laboriously removed in the course of maintenance services for retaining their functionality [1-3]. The material consistency, mineralogical and chemical compositions, as well as the formation rates of scale deposits are highly variable in space and time. The removal of scale deposits and the sustainability of drainage systems thus represent an essential part of the overall maintenance demand [4, 5]. With the aim of long-term optimisation of maintenance activities, the "Task Force Drainage" project has undertaken extensive testing of water and scale deposit compositions in the drainage systems of 16 tunnels managed by the ÖBB Infrastruktur AG in order to gain insights into the causes and specific formation mechanisms of the scale deposits and their formation potentials. For this purpose, tunnel structures with different construction characteristics and drainage systems and with distinct scaling potentials were selected. The aim of this work is to characterise and identify types of scale deposits and to clarify their formation conditions in order to derive practical strategies for prevention of scale deposit formation and to develop straightforward strategies for maintenance and cleaning of drainage systems.

4.3 Methodology

The selection of the sampling locations for scale deposits and drainage solutions in contact with each other was carried out due to frequent problems with scale deposit formation and where sufficient scale material and aqueous solution volume were available in the appropriate sections of the individual tunnels. Therefore, scale deposits were studied (2 to 7 per tunnel), where associated drainage solution could also be taken for analysis. The number of water samples exceeds that of the scale deposits as solids could not be taken for several sampled solutions in the drainage system due to the lack of scale deposits, recent cleaning works or inadequate spatial access. Consequently, in the Pottenbrunner, Kaponig, Zammerer, New Semmering, Lainzer Tunnels and the east section of the Wienerwald Tunnel solely drainage solutions were sampled. The investigated tunnels are designed for water pressure relief by a closed construction and side drainages. A special case, however, applies to the Pottenbrunner Tunnel and the St. Marx Tunnel. The Pottenbrunner Tunnel drains surface water from the carriageway, while the St. Marx Tunnel drains groundwater and surface water near an inner-city built-up area.

The analysis of the drainage solution comprises on-site parameters (pH-value, electrical conductivity and temperature), as well as the chemical composition using ion chromatography,

potentiometric titration and optical emission spectrometry. Hydrochemical modelling was performed using the computer code PhreeqC [6]. The solids were mineralogically and petrographically characterised by X-ray diffraction and scanning electron microscopy.

4.4 Characterisation of the scale deposits

4.4.1. Mineralogical composition

Most of the investigated scale deposits consist of the mineral calcite (trigonal $CaCO_3$), whereas aragonite (orthorhombic $CaCO_3$) is dominating in a few samples (Table 1). Minerals like brucite ($Mg(OH)_2$), iron oxide/hydroxide (e.g. goethite (FeOOH) and hematite (Fe_2O_3)) and detrital minerals (e.g. silicate minerals) occur as accessory components (< 10 % by weight). The individual scale deposits can be categorised into the following four types depending on their macroscopic appearance and microstructures (cf. Table 1).

Table 1: *Characterization of the analyzed scale deposits based on their material characteristics and the related drainage solutions. Data on microbial activity, pH, application of carbonate scale inhibitor and mineralogy. The blue/cursive numbers represent average and standard deviation of pH-values, except for drainage solutions of sinter type i, where the pH-range is given. n.a: not analyzed.*

Texture	Tunnel	Sample	Microbial activity	pH	Inhibitor	Mineralogy
(i) unconsolidated particulate	Hengsberg	H81R	-	11.53	tabs	calcite+aragonite
unverfestigt-partikulär	Hengsberg	H89R	-	11.36	tabs	calcite+aragonite
(Figure 1)	Hengsberg	H13	-	10.49	tabs	calcite
	Hengsberg	H58	-	10.86	tabs	calcite
	Hengsberg	H89	-	10.55	tabs	calcite+aragonite
	Birgl	B21	-	8.46	tabs	calcite+detritus
	Münsterer	B29075	n.a	8.63	-	calcite+detritus
	Wienerwald Abschnitt LT26	WW9/66	n.a	7.75	-	calcite
	Wienerwald Abschnitt LT26	WW7/66	n.a	10.2	tabs	calcite
	Wienerwald Abschnitt LT26	WW9/50	n.a	8.48	-	calcite
	Wienerwald Abschnitt LT26	WW7/94	n.a	7.88	tabs	calcite
	Wienerwald Abschnitt LT26	WW7/140	n.a	8.03	tabs	calcite
	Birgl	B25	n.a	8.54	tabs	calcite+detritus
				7.7-11.5		
(ii) shard-like	Inntal	B724	x	8.41	-	calcite
scherbenartig	Inntal	B715	x	8.53	-	calcite
(Figure 2)	Inntal	B760	x	8.31	-	calcite
	Birgl	B69a	-	-	-	calcite
	Birgl	B29	-	8.47	-	calcite
	Münsterer	B29033	x	8.21	-	calcite
	St. Marxer	M8.6_1	x	8.29	-	calcite
	Sittenberg	S3/250	n.a	8.37	-	calcite
	Sonnstein	STS1108d	n.a	8.38	-	calcite
	Inntal	B736	n.a	8.45	-	calcite
				8.4±0.2		
(iii) porous	Münsterer	B29063	-	7.95	-	calcite
porös	Münsterer	B29007	x	8.26	-	calcite+aragonite
(Figure 3)	Münsterer	B29063a	x	8.09	-	calcite
	Sonnstein	STQ1	-	8.04	-	calcite
	St. Marxer	M7.8	x	7.89	-	calcite
	St. Marxer	M7.13	x	8	-	calcite
	Sieberg	SB323	x	7.92	liquid	calcite
	Sieberg	SB461	x	8.1	-	calcite
	Sieberg	SB208	x	7.86	liquid	calcite
	Sieberg	SB224	x	7.94	liquid	calcite
	Johannesberg	B19	n.a	8.68	-	calcite+aragonite
	Johannesberg	B32	n.a	8.56	-	calcite+aragonite
	Johannesberg	B44	n.a	8.65	-	calcite+aragonite
	Johannesberg	B59	n.a	8.74	-	calcite+aragonite
	Wienerwald Abschnitt LT26	WW9/140	n.a	8.18	-	calcite
	Wienerwald Abschnitt LT26	WW7/153	n.a	7.95	tabs	calcite
	Münsterer	B31009	n.a	8.05	-	calcite
	Sittenberg	S3/332	n.a	8.11	-	calcite
				8.2±0.3		
(iv) compact	Münsterer	B29063b	x	8.77	-	calcite
kompakt	Birgl	B57	-	8.41	-	calcite
(Figure 4)	Inntal	B748	-	8.48	-	calcite
	Sonnstein	ST122R	n.a	8.64	-	calcite+detritus
				8.6±0.2		

4.4.2. Macro- and microstructural types

4.4.2.1 Unconsolidated-particulate scale deposits

This type of scale deposit often occurs as a fine-grained, unconsolidated particulate material (e.g. lime sludge), which can also form clumps in places. Its material consistency is significantly influenced by high pH-values and/or addition of inhibitors, in the present case polysuccinimide/polyaspartic acid (cf. Table 1). These substances can influence the formation of aragonite instead of calcite as well as the microstructure and material consistency of the precipitates. The addition of proper inhibitors into the drainage solutions with already compactly formed scale deposits can cause a change in material consistency to the unconsolidated-particulate scale deposit type. The use of inhibitors, also known as hardness stabilisers, can significantly delay $CaCO_3$ precipitation from drainage solutions [7]. The microstructures show fine-grained calcite crystals (micrite) with a size of 0.04 to 0.2 mm and mostly well-formed rhombohedral crystal surfaces. Some scale deposits contain associations of acicular and fascicular aragonites. The aragonites are often covered with a thin coating of brucite, the appearance of which reflects a high pH-value (Figure 1; cf. Table 1). The unconsolidated-particulate type of scale deposit shows no specific pH range for its formation, although it is promoted by high pH (elevated supersaturation and rapid precipitation of $CaCO_3$). No influence of microbial activity could be detected in this type of scale deposit (cf. Table 1). Thus, the direct precipitation of tiny crystals out of the aqueous solution and its suspensive transport followed by sedimentation in the drainage system, e.g. at obstructions or at low flow rates, is the dominant process for the formation of the unconsolidated-particulate scale deposit type.

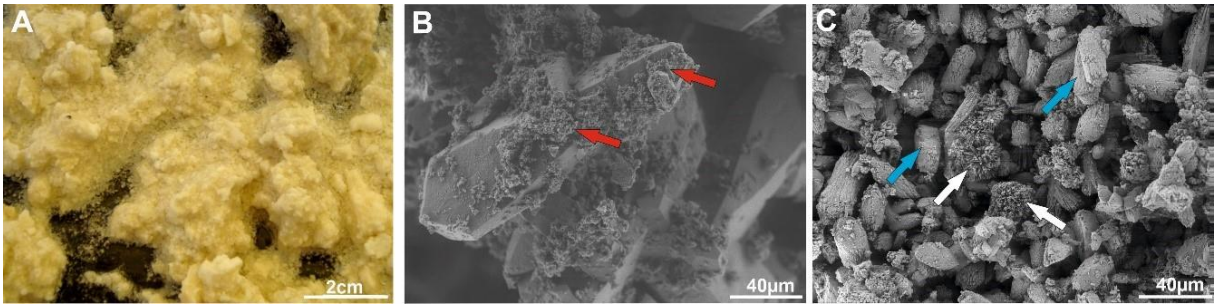

Figure 1: *Macroscopic appearance (A) and microstructures from scanning electron microscopy (B, C) of the unconsolidated-particulate scale deposits. The red arrows show thin coatings of brucite on calcite, while the white arrows indicate acicular and fascicular aragonite. The blue arrows point to rhombohedral calcite crystals.*

4.4.2.2 Shard-like scale deposits

Shard-like scale deposits consist of a mostly flat and compact base frequently covered by small rounded (spherical) structures on its surface (Figure 2). This type of scale deposit is formed at pH of about 8.4 ± 0.2. The microstructure of shard-like scale deposits show in most cases calcite crystals with - referring to the internal crystal structure - non-ideal external appearance (e.g. rounded edges), wherein the crystal size can vary significantly from 0.01 to 1 mm in the individual scale deposits. In a few scale deposits a clear indication of microbial activity is given by thin, fibrous components (likely EPS: extracellular polymeric substances), which interlink the individual particles within the scale material (cf. Figure 2). Typically, these scale deposits exhibit spherical surface structures, while shard-like scale deposits without indications of microbial activity do not show this surface structure. The latter scales are characterised by well defined (idiomorphic) calcite crystals and consequently rough surfaces in contact with the aqueous medium.

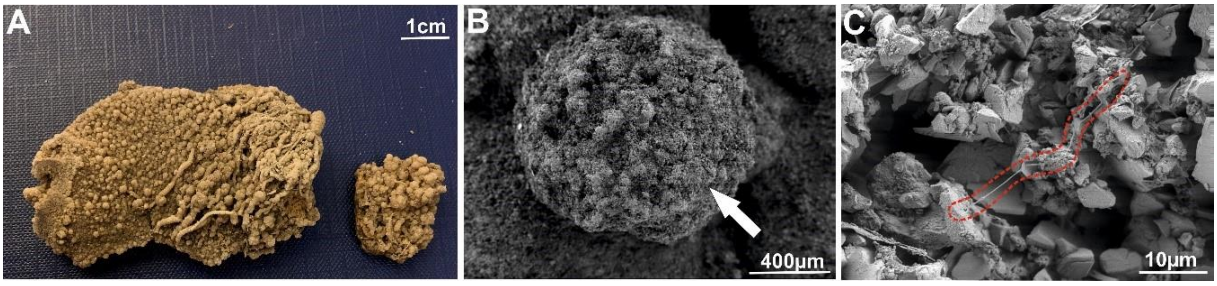

Figure 2: *Macroscopic appearance (A) and microstructures of the shard-like scale deposits by scanning electron microscopy (B, C). B shows spherical surface structures, while the red area in C encircles a fiber-like EPS-structure indicative of microbial activity.*

4.4.2.3 Porous scale deposits

This type of scale deposit is characterised by an overall porous material consistency, especially at its interface toward the draining water (Figure 3). It mostly occurs in the pH range from 7.9 to 8.7 (8.2 ± 0.3; cf. Table 1). The mineralogical composition mainly comprises calcite, wherein occasionally also high aragonite contents are present, which influence the microstructural formation and material consistency of the precipitates. Most of these scale deposits show indications of microbial activity obvious by fibrous components (EPS structures) within the carbonate matrix. The microstructures show columnar shaped and competitively growing calcite crystals (cf. Figure 3). In contrast, some of the scale deposits are characterised by branched growth structures (dendritic), rounded surfaces of the calcite crystals or an association of several different crystal forms. Aragonite occurs by forming acicular and fascicular crystals,

mainly in the pore spaces. This indicates a temporary desiccation of the present scale deposit structures in the tunnel drainage system and precipitation of aragonite from the remaining solution. Thus, a change of environmental conditions can strongly influence the formation of the porous scale deposit type [8].

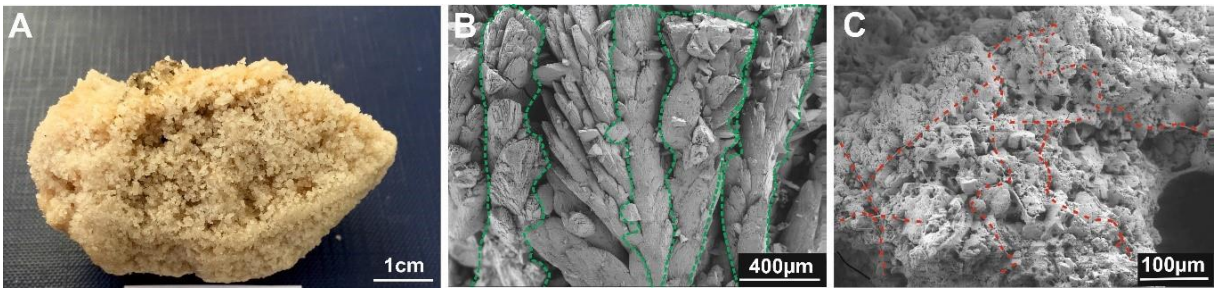

Figure 3: *Macroscopic appearance (A) and microstructures of the porous scale deposits using scanning electron microscopy (B, C). Green marked areas outline adjacent columnar shaped and competitively growing calcite crystals, while the red marked areas in C point to fiber-like EPS structures.*

4.4.2.4 Compact scale deposits

Compact scale deposits occur as heavily consolidated material, i.e. dense and compact with a low porosity. Such scale deposit is predominantly found at a pH of about 8.6 ± 0.2. Calcite is the dominant newly formed mineral, with detrital minerals being of less significance. Compact scale deposits indeed show a uniform macroscopic material consistency but differ clearly from each other in respect to their microstructures (Figure 4). Several scale deposits of this type have well-formed, rhombohedral calcite crystals and most likely indicate microbial activity due to the occurrence of fibrous structures (EPS). The microscopic appearance of some compact scale deposits shows partial secondary dissolution features on the calcite crystal surface, which can be caused by weathering processes in the form of subsequent hydrochemical alteration (overprinting by highly diverse waters or from condensation of air moisture).

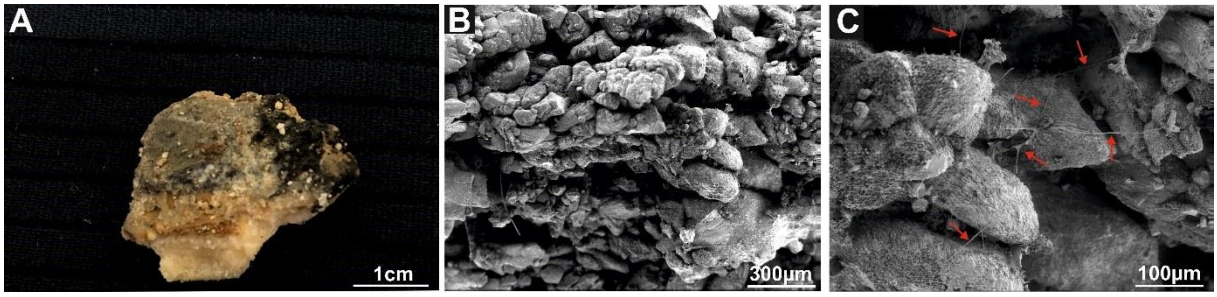

Figure 4: *Macroscopic appearance (A) and microstructures of the compact scale deposits shown by scanning electron microscopy (B, C). B shows densely packed idiomorphic calcite crystals. Red arrows: EPS structures as strong evidence of microbial activity.*

4.5 Characterisation of the drainage solutions

Illustrating the solution composition in the Piper diagram shows the drainage solutions to be highly differentiated [9, 10] (Figure 5). These differences are essentially caused by local (hydro)geological, meteorological and climatic conditions (geogenic conditions) in the area of a tunnel, as well as by technical and operative factors (e.g. binding agent vs. water interaction). Pronounced interaction by leaching of alkaline constituents, e.g. from shotcrete and/or anchor mortar, leads to an increase of the Na+ and K+ concentrations. Such water samples are typical e.g. for the Hengsberg and Johannesberg Tunnels (cf. Figure 5, areas d, f and g). The Johannesberg Tunnel (built in the 1960s) is an excellent example to confirm binding agents-water interaction lasting for several decades. However, most of the investigated drainage solutions are less affected by this interaction (a). In a few of the earth alkali-sulphate (c) and the earth alkali-alkali-sulphate waters (e), both geogenic factors, such as migration through sulphate-containing geological units, and the interaction with cement-bound construction materials have to be considered (cf. Figure 5).

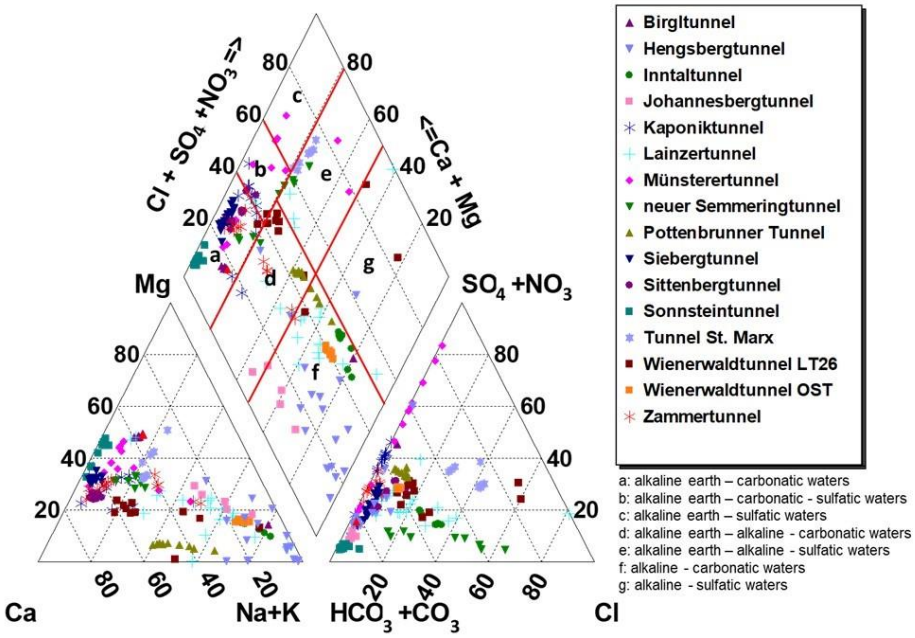

Figure 5: *Classification of drainage solutions within a modified Piper diagram*.

Elevated values of the electric conductivity (measure of the total concentration of dissolved ions) and a pH in the highly alkaline range is a first indication of anthropogenically influenced solutions (e.g. Hengsberg and Johannesberg Tunnels). Also in the Birgl, Kaponig, Lainzer

Tunnels and section LT26 of the Wienerwald Tunnel, there are indications of strong interaction of individual solutions with the construction materials mentioned above, as the pH-values of individual measurement points are significantly above 9, confirming the hydrochemical classification of the solutions (Figure 5 and 6). pH values of drainage solutions from other tunnels range between 7 and 9, which is typical for most common groundwaters. Comparing the electric conductivity of the drainage solutions of the distinct tunnels shows highest electric conductivities to occur in younger tunnel constructions, like the St. Marx Tunnel, the east section and section LT26 of the Wienerwald Tunnel, the New Semmering Tunnel and the Lainzer Tunnel. In some cases, also the drainage waters of the Hengsberg Tunnel reach high electric conductivities. In contrast, the electric conductivities of the solutions from most other tunnels are below 1000 µS/cm (cf. Figure 6).

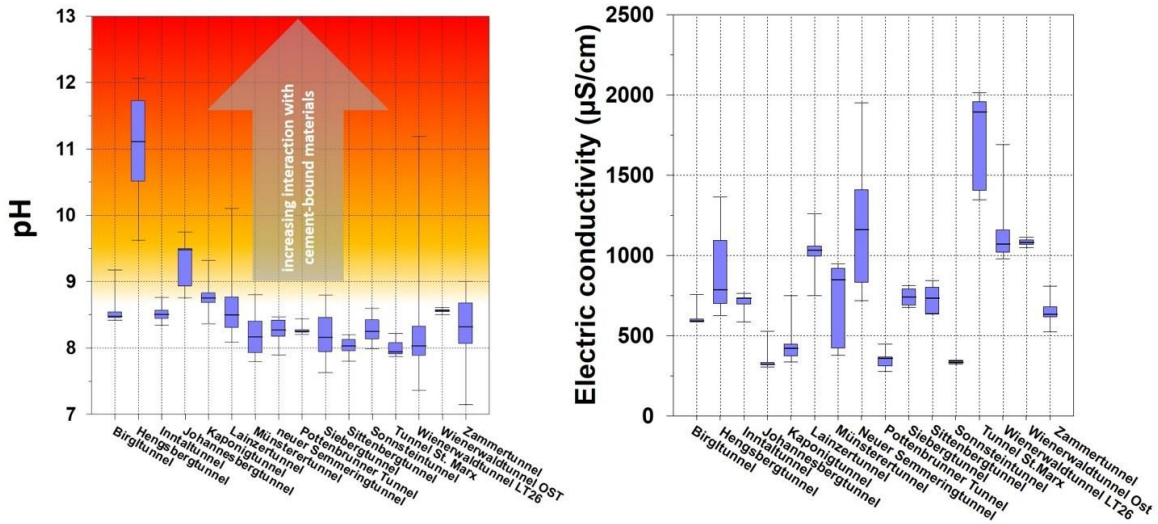

Figure 6: *Diagram to the left: pH ranges of drainage solutions. Diagram to the right: range of electric conductivities of drainage solutions.*

A further indicator of an intensive interaction with cement-bound construction materials is the magnesium concentration of the drainage solution in comparison with the geogenic groundwater. In particular, the drainage solutions of the Hengsberg and the Pottenbrunner Tunnel show very low magnesium concentrations. Very low magnesium concentrations are also measured in several solutions from the Birgl, Kaponig, Lainzer, Johannesberg Tunnels and section LT26 of the Wienerwald Tunnel. Plotting the magnesium concentration of the investigated solutions as a function of the pH indicates all solutions, with the exception of the Pottenbrunner Tunnel, to be low in magnesium concentration at elevated pH (Figure 7). This behaviour can be reasonably explained by the precipitation of magnesium - originated from the

groundwater - as magnesium hydroxide (brucite). In contrast, the low magnesium concentration of the drainage solutions from the Pottenbrunner Tunnel is not justified to be caused by the interaction with cement-bound construction materials. In this tunnel, the drainage solutions are generated by surface water / rainwater from the carriageway. Consequently, in these solutions the natural content of Mg is most likely very low as Mg ions are not received by leaching of local rocks.

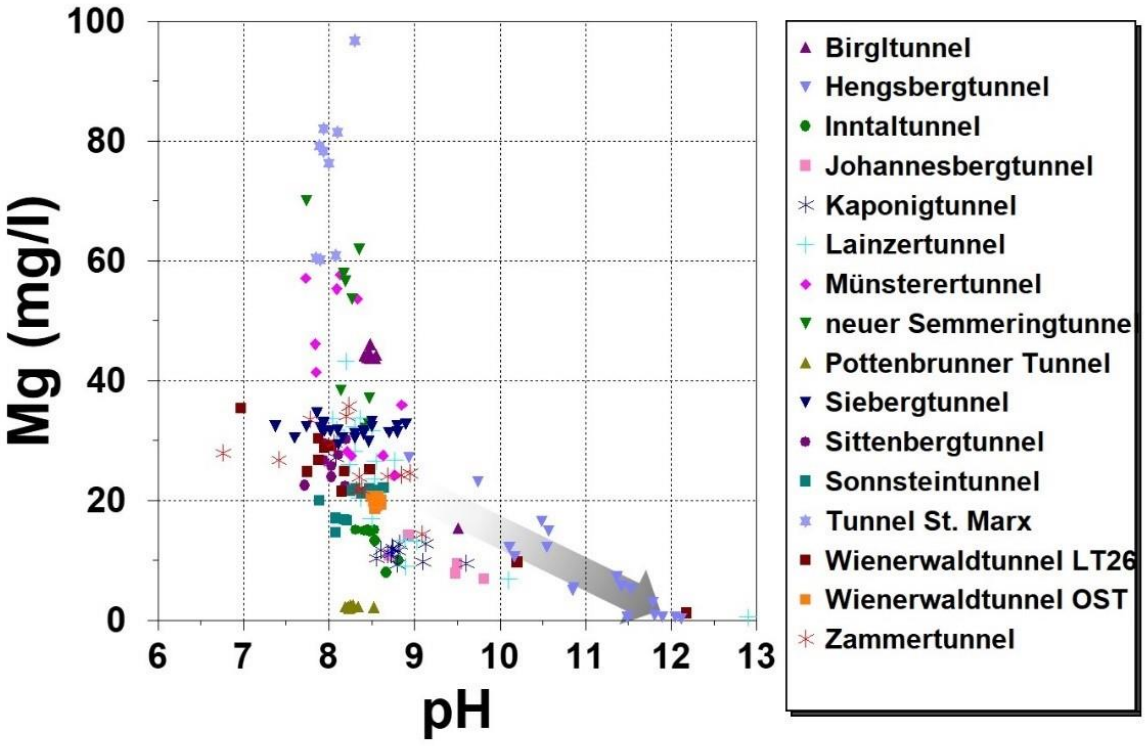

Figure 7: *Magnesium content of the drainage solutions as a function of pH. The grey arrow illustrates the general trend of decreasing magnesium concentrations caused by precipitation of the mineral brucite ($Mg[OH]_2$).*

In addition to the dissolved ions mentioned above, the internal CO_2 partial pressure (pCO_2) of the drainage solutions, determined by hydrochemical modelling, represents a significant parameter for scaling processes. If the pCO_2 of a solution decreases due to degassing of CO_2, the consequent distribution shift within the carbonate-CO_2 equilibrium can trigger the precipitation of calcium carbonate. The CO_2 concentrations of the tunnel atmosphere are close to the CO_2 concentration of the Earth`s atmosphere (log pCO_2 = – 3.4 atm, about 400 ppmv) when considering sufficient ventilation. Moreover, at adequate aeration (e.g. due to piston effect during the tunnel passage of a train) the atmosphere in the drainage system is most likely corresponding to the CO_2 partial pressure of the tunnel atmosphere. In the investigated drainage

solutions, the median values of the internal CO_2 partial pressure for most tunnels are considerably higher than those of the Earth`s atmosphere. Accordingly, for these drainage solutions the degassing of CO_2 represents the dominant hydrochemical process to increase the scaling potential regarding calcium carbonate precipitation (Figure 8).

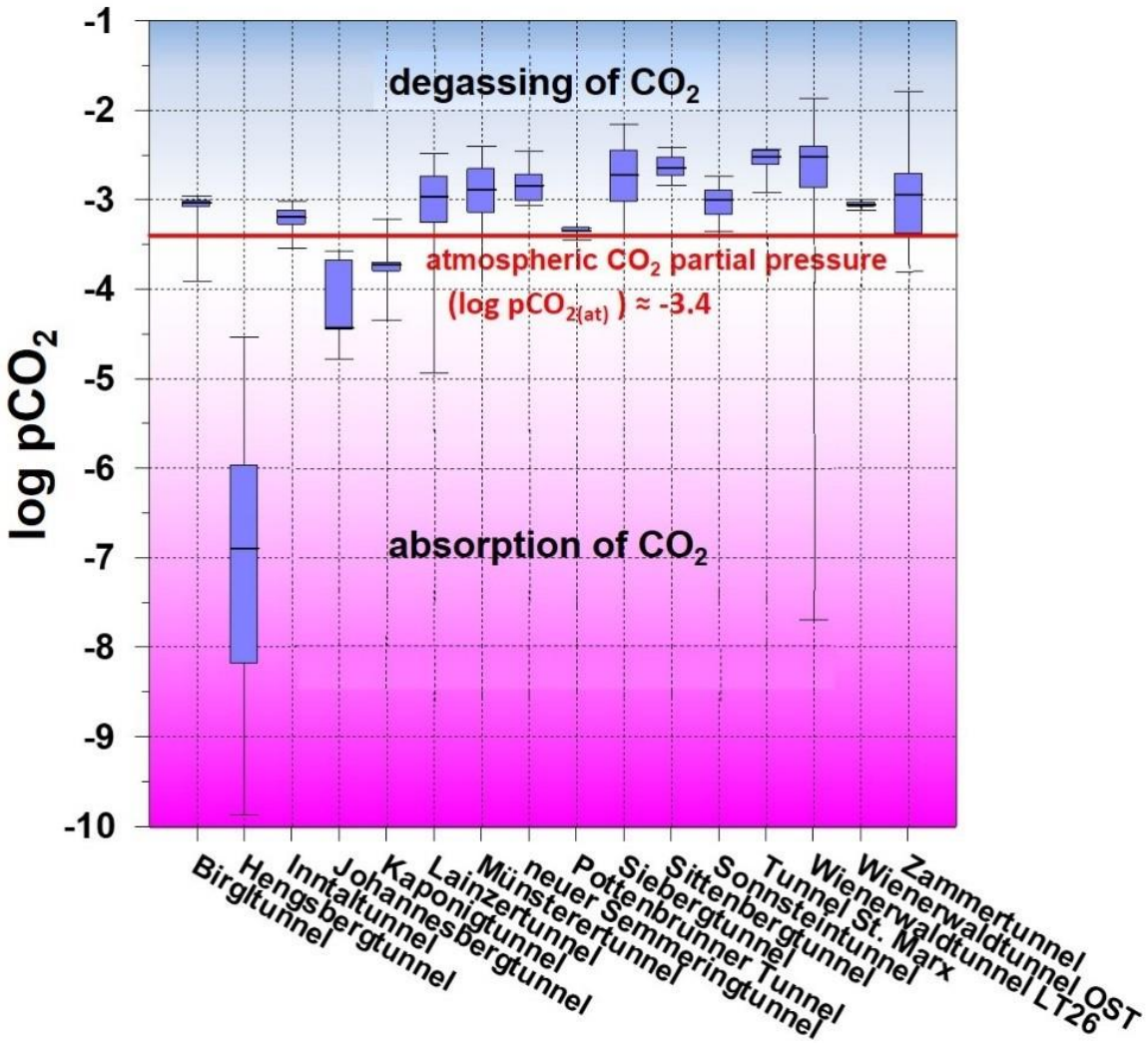

Figure 8: *The internal CO_2-partial pressures (log pCO_2 in atm) of the drainage solutions.*

In drainage solutions whose internal CO_2 partial pressure is in the range of the atmospheric CO_2 partial pressure, such as the Pottenbrunner Tunnel, hardly any significant degassing of dissolved CO_2 is possible and thus the scaling potential is not increasing. Drainage solutions whose internal CO_2 partial pressure is lowered by the interaction with cement-bound construction materials far below the atmospheric CO_2 partial pressure, can absorb CO_2 from the tunnel atmosphere until the internal value reaches the atmospheric CO_2 partial pressure. In practice,

however, a significant CO_2 uptake is only occurring at pH > 9.5. From the drainage solutions, the median values of the Hengsberg, Johannesberg and Kaponig Tunnels are below the atmospheric CO_2 partial pressure. Occasionally, internal CO_2 partial pressures significantly below the atmospheric CO_2 partial pressure can also be found in drainage solutions from the Birgl, Inntal, and Lainzer Tunnels and section LT 26 of the Wienerwald Tunnel. This observation confirms the drainage solutions from the Hengsberg and Johannesberg Tunnels as well as from some sections of the Birgl, Kaponig, Lainzer Tunnels and section LT 26 of the Wienerwald Tunnel to be strongly affected by binding agent vs. water interaction. In analogy to the scale deposit types described above, the drainage solutions show a systematic classification according to their chemical composition, although not inevitably reflecting the specific type of the scale deposits. At a given chemical composition of a drainage solution indeed various types of scale deposits can be induced. Here, both the spatial and temporal evolution of the drainage solutions, e.g. caused by the formation of scale deposits along a flow path as well as the technical-operational conditions can play a decisive role [8].

4.6 Summary and conclusions

Drainage solutions with high pH and low magnesium concentrations indicate an intensive interaction of local groundwaters with cement-bound construction materials. These drainage solutions have internal CO_2 partial pressures below the atmospheric CO_2 partial pressure, i.e. tending to absorb CO_2 from the tunnel atmosphere, frequently associated with instantaneous $CaCO_3$ precipitation. Most of scale deposits precipitating from these drainage solutions correspond to the unconsolidated-particulate type, favouring a high porosity of the scale deposits (rapid precipitation and scale deposit formation). However, most of the investigated tunnel solutions are hardly affected by construction materials. In the latter case, the dominant hydrochemical process of scaling potential to increase is the degassing of CO_2 from the drainage solution into the atmosphere.

The investigated scale deposits are essentially formed by mineral precipitation from the drainage solutions described above and can be classified into four types: (i) unconsolidated-particulate, (ii) shard-like, (iii) porous, (iv) compact scale deposit. By comparison of the types of scale deposits and the respective drainage solutions, it is obvious that different types of scale deposits regarding mineralogy, microstructure and material consistency can form from similar compositions of drainage solutions. The formation of a certain type of scale deposit is mainly determined by the geogenic conditions (e.g. geological conditions, composition and flow

behaviour of local groundwater and surface water), the technical-operational conditions (e.g. binding agent vs. water interaction; drainage design; flow rate; air supply to the drainage), as well as the spatial and temporal evolution of the solution composition during its flowing through the drainage and in the course of progressive mineral precipitation (see also [3, 8]). Such spatial and temporal changes arise mainly due to different flow rates, mixing of solutions, individual degassing behaviour of CO_2, microbial activity, leaching and precipitation sequences, as well as individual reaction rates. Highly distinct carbonate precipitation occurs depending on the respective and often variable environmental conditions. Therefore, it has to be highlighted that in a drainage system of a tunnel quite different types of scale deposits can be formed and an individual investigation and evaluation of a tunnel structure is necessary for the characterisation of scale deposits and the assessment of their formation. The parameters and characteristics mentioned above must be evaluated interactively in order to obtain reliable statements about past precipitation processes and current chemical reactions for scale deposit formation and to predict scale deposit formation and to develop guidelines for reducing or even preventing scale deposit formation. Based on the assessment of various types of scale deposit and the associated drainage solutions, targeted strategies for preventing/reducing of scale deposit formation can be developed for each individual tunnel building. Strategies comprise of, e.g. tailored additions of a proper inhibitor into a drainage solution, adaptation of the drainage design to minimise gas/air exchange between drainage solution and atmosphere, as well as using drainage materials with a surface structure inhibiting precipitation (see [8, 11] for detailed explanations).

4.7 Acknowledgement

The study was performed in cooperation with the ÖBB-Infrastruktur AG. Special thanks are given to our colleagues Lukas Sperger (ÖBB-Infrastruktur AG), Peter Brugger and Samir Susic (Ingenieurbüro Laabmayr & Partner ZT GmbH) for planning and supporting the sampling, as well as the entire team of the "Task Force Drainage" of the ÖBB-Infrastruktur AG.

References

[1] Chen, Y.; Cui, Y.; Barrett, A.G.; Chille, F.; Lassalle, S.: (2019) Investigation of calcite precipitation in the drain system of railway tunnels: In Tunnelling and Underground Space Technology 84, pp. 45–55.

[2] Dietzel, M.; Kieffer, S.; Schubert, W.; Schweiger, H.F.; Semprich, S. (2008) (eds.): Drainagesysteme im Tunnelbau: Design, Versinterung und Instandhaltung. Mitteilungshefte Gruppe Geotechnik Graz 34.

[3] Gamisch, T.; Girmscheid, G. (2007): Versinterungsprobleme in Bauwerksentwässerungen. Berlin: Bauwerk.

[4] Harer, G. (2009): Planerische Vorkehrungen zur Erzielung eines erhaltungsarmen Entwässerungssystems beim Koralmtunnel. In Dietzel, Kieffer, Schubert, Schweiger, Semprich (eds.): Drainagesysteme im Tunnelbau: Design, Versinterung und Instandhaltung, pp. 1–14. Mitteilungshefte Gruppe Geotechnik Graz 34

[5] Saxer, A.; Draschitz, C. (2006): Versinterungsproblematik der Tunneldrainagen – Einfluss zementgebundener Tunnelbaustoffe. In: Spritzbeton-Technologie 1, pp. 87–103.

[6] Parkhurst, D.L.; Appelo, C.A.J. (2013): Description of input and examples for PHREEQC version 3: a computer program for speciation, batch-reaction, one-dimensional transport, and inverse geochemical calculations. No. 6-A43. US Geological Survey.

[7] Niedermayr, A.; Köhler, S.J.; Dietzel, M. (2013): Impacts of aqueous carbonate accumulation rate, magnesium and polyaspartic acid on calcium carbonate formation (6–40 C). In: Chemical Geology 340, pp. 105–120.

[8] Eichinger, S. et al. (2020): Scale deposits in tunnel drain systems – A study on fabrics and formation mechanisms. In: Science of the Total Environment, 137140.

[9] Furtak, H.; Langguth, H.R. (1967): Zur hydrochemischen Kennzeichnung von Grundwässern und Grundwassertypen mittels Kennzahlen. Mem. IAH-Congress 1965, pp. 86–96.

[10] Piper, A.M. (1944): A graphic procedure in the geochemical interpretation of water analysis. In: Trans. Amer. Geophys. Union 25, pp. 914–928.

[11] Schachinger, T.; Arbeiter, F.J.; Eichinger, S.; Saliger, F. (2019): Research on pipe materials for tunnel drainage by the ÖBB Task Force Drainage / Forschung der ÖBB-Task Force Drainage zu Rohrmaterialien der Tunnelentwässerung. In: Geomechanics and Tunnelling 12, No. 5, pp. 467–471. doi:10.1002/geot.201900022

Chapter 5 - Green inhibitors reduce unwanted calcium carbonate precipitation: Implications for technical settings

Stefanie Eichinger[1*], Ronny Boch[1,2], Albrecht Leis[3], Andre Baldermann[1], Gunnar Domberger[3], Christian Schwab[4] & Martin Dietzel[1]

[1] Institute of Applied Geosciences, Graz University of Technology & NAWI Graz GeoCenter, Rechbauerstr. 12, 8010 Graz, Austria.

[2] Geoconsult ZT GmbH, Wissenspark Salzburg Urstein, Urstein Süd 13, 5412 Puch bei Hallein, Austria.

[3] JR-AquaConSol GmbH, Steyrergasse 21, 8010 Graz, Austria.

[4] ASFINAG Service GmbH Graz, Fuchsenfeldweg 71, 8074 Graz – Raaba, Austria.

Graphical Abstract

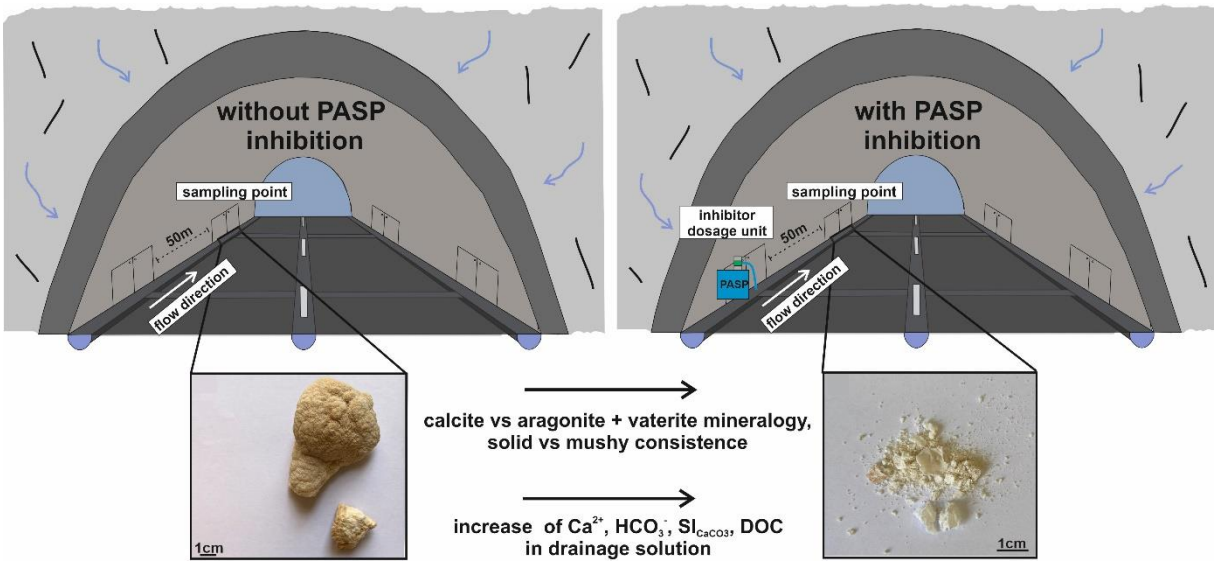

5.1 Abstract

Mineral scale deposits in water drainage and supply systems are a common and challenging issue, especially by clogging the water flow. The removal of such unwanted deposits is cost intensive arguing for case-specific and sustainable prevention strategies. In the present study, a novel on-site approach to prevent calcium carbonate ($CaCO_3$) scale formation was assessed in two road tunnel drainages: Application of the eco-friendly green inhibitor polyaspartate (PASP) caused (i) a significant inhibition of $CaCO_3$ precipitation, (ii) a more porous or even unconsolidated consistence of the deposits, and (iii) a shift from calcite to the metastable aragonite and vaterite polymorphs. Even relatively low PASP concentrations (1-33 mg/l) can

significantly decrease $CaCO_3$ scale deposition, removing up to ~7 t $CaCO_3$/year at an efficiency up to 84 %. Application of PASP for water conditioning should also consider case-specific microbial activity effects, where consumption of PASP, e.g. by *Leptothrix ochracea,* can limit inhibition effects.

5.2 Introduction

Green inhibitors are increasingly used in water treatment applications, as well as in industrial and man-made environments, to prevent the technical infrastructure from unwanted scale formation (i.e., mineral precipitation) owning to their high performance and economic and ecological benefits (Abdel-Aal and Sawada, 2003; Li et al., 2006; Quan et al., 2008; Liu et al., 2012; Chhim et al., 2020). For example, Liu et al. (2012) have investigated the effects of polyepoxysuccinic acid (PESA) and polyaspartic acid (PASP) dosage, Ca^{2+} concentration and temperature on scale inhibition using static- and rapid-controlled precipitation experiments and concluded that PASP performed better than PESA in terms of $CaSO_4 \cdot 2H_2O$ (gypsum) and $BaSO_4$ (barite) scale inhibition, whereas PESA performed superior in $CaCO_3$ scale inhibition. Later, Peronno et al. (2015) showed that poly(acrylic acid-co-maleic acid) and PASP can exhibit a high inhibition efficiency for $CaCO_3$ scales even at low concentration (4 mg/l) using a fast controlled precipitation (FCP) method and provided experimental evidence for a significant alteration of the $CaCO_3$ crystal morphology upon inhibitor addition. More recently, Chhim et al. (2020) tested the performance of PESA and PASP against a homopolymer of acrylic acid (HA) in a controlled laboratory set-up reproducing industrial cooling circuits and reported that the adsorption of the polymer molecules on a growing $CaCO_3$ crystal surface (i) suppresses the $CaCO_3$ growth rate and (ii) shifts the precipitation mode from thermodynamically stable phases towards a metastable phase with PASP (i.e., vaterite). Wedenig et al. (2021) tested the performance of four PASP agents/products from different manufacturers, in addition to maleic and acrylic acid copolymers (MA-AA) and a hydrolyzed polymaleic anhydride agent (HPMA), on $CaCO_3$ scale inhibition in the concentration range from 0.5 to 10 mg/l using a compact experimental test procedure coupled to a computer-based thermodynamic modeling approach. The authors concluded that PASP-based inhibitors performed superior among all inhibitors tested (efficiency: ~70-100 %; retardation times: several hours to days), which provides a solid basis for potential application at distinct field sites (e.g. tunnel, wells). However, to the best of our knowledge, the performance of PASP in large-scale (geo)technical settings has not been investigated, yet. In this contribution, we fill

this knowledge gap by demonstrating the inhibition effect of PASP on $CaCO_3$ scale deposits in two road tunnel drainage systems.

Scale deposit formation ("scaling") of especially $CaCO_3$ minerals (calcite, aragonite or vaterite) in (geo)technical settings is a serious and challenging issue, e.g., affecting water supply or draining by reducing the inner diameter of water pipes, causing water to overflow driving lanes or railway tracks, or by reducing heat, energy and fluid transfer efficiencies in geothermal wells (e.g., Girmscheid et al., 2003; Ketrane et al., 2009; Hasson et al., 2011; Boch et al., 2017; Shen et al., 2017; Jamero et al., 2018; Chen et al., 2019; Eichinger et al., 2020a). These problems apply to road and railway tunnels (e.g., Eichinger et al., 2020b) and have been noticed around the world, i.e. in China, Korea, France and North America (Kukreja and Moran, 2004; Zhengshi, 2012; Jung et al., 2013; Jia et al., 2016; Chen et al., 2019). Maintenance efforts related to drainage systems, such as recurrent cleaning activities and associated tunnel closures, as well as traffic diversions can reach up to 20 % of the costs of the entire inspection and maintenance works. In highway tunnels, costs for maintenance works in drainage systems have been estimated to be ≥10,000 € per kilometer and year (Harer, 2017).

A steadily increasing number of publications have appeared in recent years dealing with widespread $CaCO_3$ scale deposit formation in tunnel drainage systems (e.g., Rinder et al., 2013; Jia et al., 2016; Xin et al., 2018; Chen et al., 2019; Eichinger et al., 2020a; Eichinger et al., 2020b). Most of the scale deposits are dominated by calcite with less aragonite and/or vaterite. $CaCO_3$ formation is often initiated by (i) the exchange of CO_2 between the tunnel (or drainage system) atmosphere and the drained aqueous solution, (ii) mixing of solutions different in composition, (iii) microbial activity, and/or (iv) site-specific fluid-solid interactions (e.g., dissolution of carbonate host rocks and/or cementitious components, such as portlandite ($Ca(OH)_2$; e.g., Rinder et al., 2013; Boch et al., 2015; Eichinger et al., 2020a). The geometry of a tunnel and the aqueous Ca^{2+} and CO_3^{2-} concentration of the interacting groundwater or interstitial solution frequently determine the intensity of $CaCO_3$ scale formation (Chen et al., 2019; Eichinger et al. 2020a). Mechanisms for scale deposit formation can be assessed and quantified by hydrochemical modeling considering environmental aspects, operative conditions, anthropogenic influences etc. (Eichinger et al., 2020a). However, strategies to prevent from unwanted $CaCO_3$ deposits using eco-friendly green scale inhibitors, such as PASP, have never been tested before in tunnel drainages.

In the present study, the use of PASP is investigated by an on-site test track to inhibit $CaCO_3$ scale deposit formation in a tunnel drainage environment. PASP has so far been used in the oil

and gas production industry (e.g. Kumar et al., 2018), in the course of (sea)water desalination (Pervov and Andrianov, 2017), in heat-exchange and cooling systems (e.g. Nayunigari et al., 2014; Guo et al., 2020). Compared to conventional inhibitors applied in different geotechnical sectors (e.g. phosph(on)ates; Spinthaki et al., 2021), PASP is eco-friendly, non-toxic, and easily biodegradable in natural aquatic environments, since it consists of polymers including specific functional chemical groups (e.g. carboxy group – COOH, amino group – NH_2; Wu and Grant, 2002; Gao et al., 2010; Hasson et al., 2011; Liu et al., 2011; Kumar, 2012; Chaussemier et al., 2015). In the present study, the performance of PASP to suppress and/or alter the consistence of $CaCO_3$ scale deposits in a tunnel drainage environment is evaluated; i.e. its function as a Ca-carbonate scale inhibitor and/or modificator.

5.3 Setting and sampling

The effect of PASP as a $CaCO_3$ scale inhibitor in tunnel drainage systems was investigated in drainage pipelines made of plastic in the road tunnels Spital and Steinhaus (2500 m and 1800 m length, respectively). Both tunnels are located in the northeastern area of Styria (Austria). The tunnels were constructed between 1998 and 2001 and consist of an unidirectional northern and southern tunnel tube. Both tunnels traverse metamorphic rocks (greenschist facies), like graphite horizons and marble/mica phyllites of the Keuper formation, as well as central-alpine sediments (dolomite and calcite rauhwacke; Cornelius, 1952; Dissauer et al., 2002).

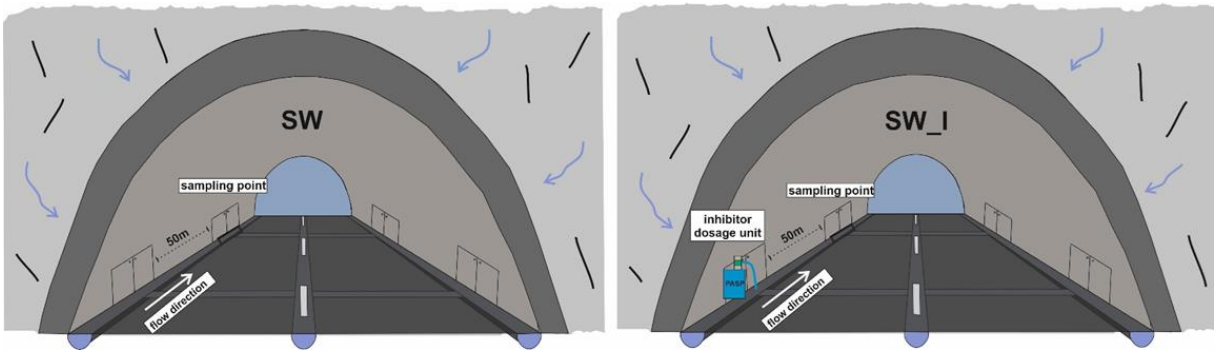

Figure 1: *Schematic setup of on-site rating of polyaspartate (PASP) solution to inhibit $CaCO_3$ scale deposit formation in the drainages of tunnel Steinhaus and tunnel Spital, Austria, including the positioning of the dosage unit and the sampling point without (left: SW) and with addition of the inhibitor agent PASP (right: SW_I). The inhibitor dosage unit was installed in a niche ~50 m before the sampling point in flow direction. The tunnel construction, experimental set-up and in-situ monitoring was identical at the two localities.*

Both tunnel drainages suffer from severe scaling problems (Fig. A.1; Appendix). The inhibition of unwanted mineral precipitates was studied in the right lateral-drainage of the southern tunnel tube. The liquid PASP product Baypure DS 100/40 % (Kurt Obermeier GmbH) was added directly into the drainage solutions. The inhibitor dosage ranged from 3 to 12 ml/h (Table 3), representing low to high dosages in order to account for the different flow rates observed in the two drainages of 0.03 to 0.5 l/s, respectively (i.e., to keep the PASP concentration in solution equal at the two localities). The scale deposits and corresponding solutions were sampled for analyses from different tunnel sections of the drainage channels (250 mm in diameter; diameter filled with drainage solution: ~16-18 cm; water height in pipe: ~1 cm) during two separate sampling campaigns. The first campaign took place in December 2019, where scale deposits and associated solutions (SW1 to SW5) were taken without inhibitor. The second sampling campaign was carried out in October 2020 with the addition of PASP for about 10 months (SW1_I to SW5_I). The inhibitor dosing units, consisting of a storage tank, a pump and a power supply, were installed ~50 m ahead of the sampling positions (Fig. 1). The sampling sites for solutions and precipitates were chosen according to the highest visual degree of scale formation. Two inhibitor units were located in the tunnel Spital (SW1_I and SW2_I) and three in the tunnel Steinhaus (SW3_I, SW4_I and SW5_I). Cleaning activities of the drainage systems were not conducted before or during the PASP addition.

5.4 Analytics

5.4.1 Scale deposits

The scale deposits were photographed to document their macroscopic appearance (Fig. 2). Parts of the precipitates were dried and grinded for powder X-ray diffraction analysis (XRD) in order to determine their mineralogical composition using a PANalytical X`Pert Pro diffractometer equipped with a Co-Kα-radiation source (40 mA, 40 kV) applied at a 2θ range from 4° to 85°. Diffraction patterns were quantitatively evaluated by Rietveld refinement (PANalytical X`Pert HighScore Plus Software version 3.0.4 with PDF-4 database). Petrographic analyses were performed on gold/palladium coated subsamples using a Zeiss DSM 982 Gemini scanning electron microscope (SEM) operated at 2 kV. Aliquots of the solid samples were chemically digested in 6 % HNO_3 solution, and the concentration of the dissolved components measured by ICP-OES (PerkinElmer Optima 8300) with an analytical uncertainty of < 5%.

5.4.2 Drainage solutions

On-site measurements of the drainage solutions comprised pH, specific conductivity (SpC: µS/cm), expressed at a reference temperature of 25°C, and water temperature (°C) using a handheld WTW pH/Con 3320 instrument connected to a TetraCon 325 probe and a WTW SenTix 41 pH probe. Standard buffer solutions of pH 4, 7 and 10 (Merck) were applied for pH calibration yielding an uncertainty of ±0.05 pH units. The aqueous solutions sampled from the drainages were filtered through 0.45 µm cellulose acetate filters. Subsamples for major cations (Na^+, K^+, Mg^{2+}, Ca^{2+}) and anions (Cl^-, NO_3^-, and SO_4^{2-}) analysis by ion chromatography (Dionex ICS-3000) were filled in gas-tight borosilicate vessels (analytical uncertainty of ±3 %). Samples for alkalinity were stored in gas-tight borosilicate vessels and measured in the laboratory at the day of sampling with a Schott TitroLine alpha plus titrator using a 0.01M HCl stock solution with an analytical uncertainty of ±2 %. Samples for minor and trace elements (SiO_2, ΣAl, Ba^{2+}, Sr^{2+} and ΣFe) analysis were filled in PE vessels (50 ml) preloaded with 1 ml suprapure HNO_3 (69 %) and measured with a PerkinElmer Optima 8300 DV ICP-OES calibrated by NIST 1640a standards (analytical error ±5 %). Dissolved organic carbon (DOC) concentrations were determined using a Shimadzu TOC-V-CPH Total Organic Carbon Analyzer with an analytical uncertainty of ±0.1 mg/l of C. Hydrochemical modelling was performed using the computer code PHREEQC (version 3.1.7.9213; Parkhurst and Appelo, 2013) with the database phreeqc.dat for calculating ion activities and specification, saturation indices for calcite ($SI_{calcite}$), vaterite ($SI_{vaterite}$; solubility constant from Plummer and Busenberg, 1982), aragonite ($SI_{aragonite}$), amorphous $CaCO_3$ (SI_{ACC}; solubility constant from Brečević and Nielsen, 1989), ikaite (SI_{ikaite}; solubility constant from Bischoff et al., 1993) and strontianite ($SI_{strontianite}$; SI= log(IAP/K); where IAP = ion activity product for Ca^{2+} or Sr^{2+} and CO_3^{2-}, and K = solubility product), ion charge balance and the internal partial pressure of CO_2 (pCO_2 in atm.). Measured concentrations and on-site water temperature (cf. Table 3) were used as model input parameters. The phreeqc.dat code was used to obtain the aforementioned hydrochemical parameters, as this database adequately accounts for the generally low-mineralized drainage solutions (i.e., ionic strength, I = 0.001-0.01 mol/kgw; Parkhurst and Appelo, 2013). Analyses of PASP were performed in filtered subsamples by a Jasco FP-6500 fluorescence spectrophotometer using a standard quartz cell. All fluorescence measurements were conducted with the synchronous scan technique reported in Behrens (1971) and Lloyd (1971) in constant-wavelength mode using a wavelength offset of 100 nm between light excitation and emission. Under these measurement conditions the indicative PASP peak appeared approximately at 409 nm in the obtained synchronous fluorescence spectrum. Measurements of additional aqueous standard solutions of the PASP inhibitor were prepared and used to transform the measured

fluorescence intensity into concentration values. In the investigated concentration range (1.1 - 32.8 mg/l) a linear relationship was obtained between fluorescence intensity and PASP concentration. The analytical uncertainty (1σ) is about ±0.25 mg/l of PASP. The flow regime in the tunnel drainages and related transport mechanism at the atmosphere-solution interface were characterized further by means of the Reynolds number (Re) using documented pipe geometries (d; 16-18 cm), measured water temperatures (T; 5-11 °C) and fluid velocities (u; 0.001 up to 0.02 m/s), as well as corresponding fluid densities (ρ; 999-1000 kg/m^3) and dynamic fluid viscosities (μ; 1.5-1.8 cP), according to the expression: $Re = \rho ud/\mu$ (Liu et al., 2020). The efficiency (ε in %) of the PASP inhibitor was calculated by the equation: $\varepsilon = (\Delta Ca/Ca_{inh})\cdot 100$ (adapted after Wedenig et al., 2021), where ΔCa is the difference between the Ca concentration in the drainage solution with PASP addition (Ca_{inh}) and without PASP addition.

5.5 Results

5.5.1 Scale deposits

5.5.1.1 Morphology, mineralogy and chemical composition

The scale deposits differed significantly in their morphology, texture, coloration, and consistence (Fig. 2). The PASP-untreated scale deposits (SW1, SW3 and SW5) and their counterparts (SW1_I, SW3_I and SW5_I) are visually characterized by white to beige colors, while the scale deposits SW2 and SW2_I are white-brownish and reddish-brown in color, respectively. As an exception, the scale deposit SW4 is brown, while SW4_I is white. All scale deposits without influence of PASP appear more compact, while deposits affected by PASP - except of scale deposit SW3_I - are rather porous and appear as powdery sand or mud with mushy consistence. Mineralogical investigations revealed low-Mg calcite (<4 mol% of $MgCO_3$; Table 1) as the main component of all analyzed scale deposits in both tunnels, but SW2, SW4 and SW5 exhibit additional aragonite (12 to 20 wt.%; Table 1). Scale deposits in the presence of PASP typically exhibit a smaller amount of calcite and a higher aragonite content (except for SW3_I) compared to PASP-untreated deposits. Samples SW2_I, SW4_I and SW5_I reveal elevated aragonite contents of 27, 49 and 52 wt.%, respectively (see Table 1), the latter two having about equal calcite contents (50 wt.%). Scale deposit SW1_I consists of small amounts of vaterite (3 wt.%) and SW4_I shows minor dolomite (4 wt.%). Note that the detected small amounts of quartz (SiO_2) and dolomite ($CaMg(CO_3)_2$) are considered as detrital components (Figs. B.1 to 5; Appendix).

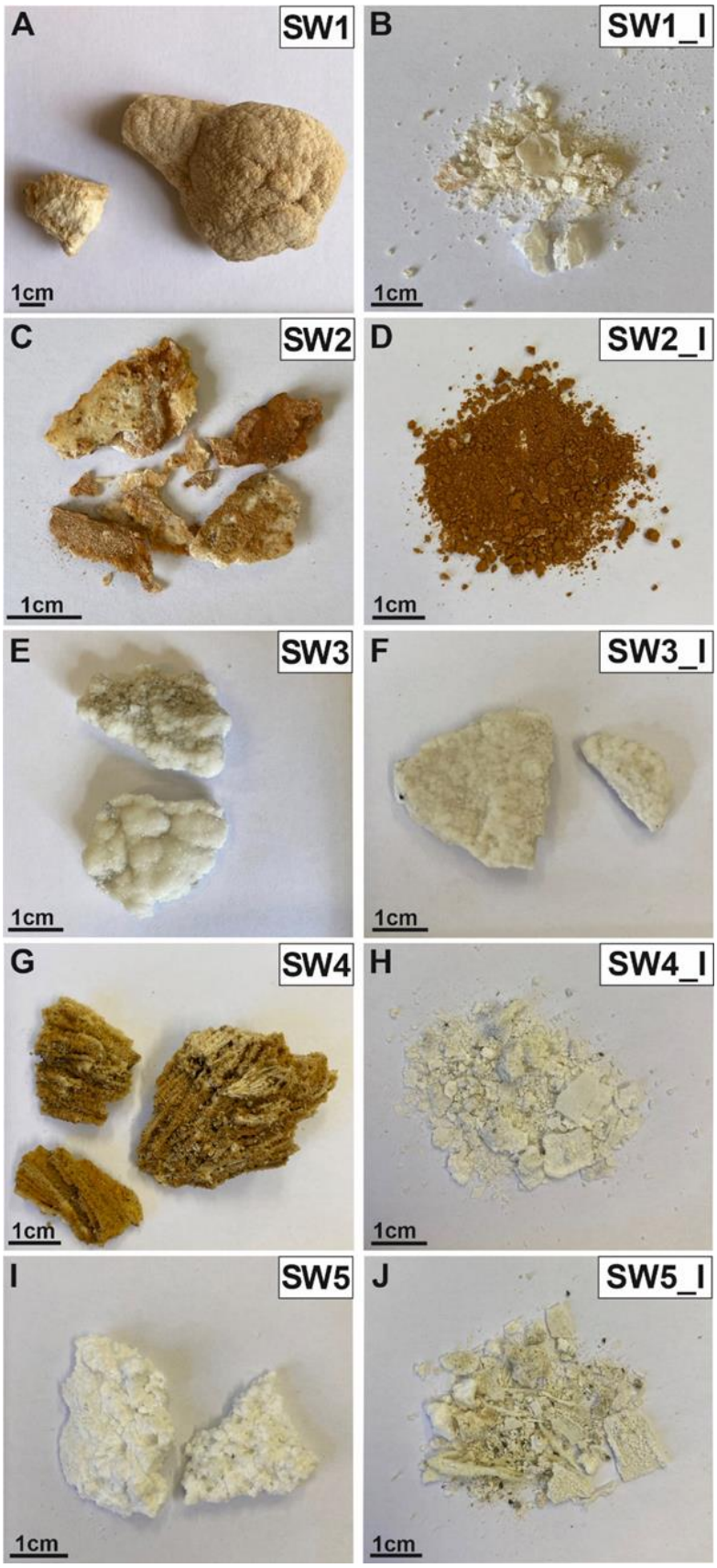

Figure 2: *Macroscopic appearance of the scale deposits collected from tunnel Spital (SW1-2) and tunnel Steinhaus (SW3-5) without (left column) and with (right column) influence of the inhibitor agent PASP. PASP addition changes the consistency of the scale deposits from compact and dense (solid appearance) to soft and loose (mushy appearance).*

Table 1: *Mineralogical composition of the scale deposits from tunnel Spital (SW1-2) and tunnel Steinhaus (SW3-5) according to XRD analyses. The $MgCO_3$ content in calcite was determined to be < 4 mol% for all samples. Accessory minerals are quartz and dolomite. Samples indicated with "I" are influenced by the inhibitor agent PASP.*

Sample ID	Calcite	Aragonite	Vaterite	Accessory
	wt.%	wt.%	wt.%	wt.%
SW1	99	–	–	1
SW1_I	94	2	3	1
SW2	87	12	–	1
SW2_I	72	27	–	1
SW3	100	–	–	–
SW3_I	100	–	–	–
SW4	85	14	–	1
SW4_I	41	49	–	10
SW5	79	20	–	1
SW5_I	47	52	–	1

Chemical analyses of the $CaCO_3$ dominated precipitates reveal no significant differences between scale deposits SW1-SW5 and SW1_I-SW5_I (Table 2). The measured Ca contents in the scales vary between 29.2 and 39.3 wt.%, corresponding to $CaCO_3$ contents between 72.9 and 98.2 wt.%. The prominently red colored sample SW2_I contains the lowest $CaCO_3$ content (72.9 wt.%) and SW3 shows the highest $CaCO_3$ content (98.2 wt.%), consistent with the almost pure calcite mineralogy. The concentrations of K and Na range from <50 to 503 mg/kg and 107 to 1140 mg/kg. The concentrations of Sr and Ba lay between 810 and 3343 mg/kg and 153 to 684 mg/kg for the analyzed scale deposits. The Al and Si concentrations are highly variable in the range from 385 to 16240 mg/kg and 62 to 6814 mg/kg, respectively. The Fe content differs strongly in the individual scale deposits, from 18 to 67726 mg/kg (up to ~10 wt.% Fe_2O_3). The reddish-brown and white-brownish colored scale deposits SW2, SW2_I and SW4 reveal the highest Fe and Mn contents, reflecting a calcite mineralogy with admixtures of Fe-Mn(hydr)oxides.

Table 2: *Chemical composition of the scale deposits from tunnel Spital (SW1-2) and tunnel Steinhaus (SW3-5) determined by ICP-OES analysis. "I" indicates samples influenced by the inhibitor agent PASP.*

Sample ID	Ca^{2+}	Mg^{2+}	K^{+}	Na^{+}	Sr^{2+}	Ba^{2+}	∑Fe	∑Mn	∑Al	SiO_2
	wt.%	wt.%	mg/kg	mg/kg	mg/kg	mg/kg	mg/kg	mg/kg	mg/kg	mg/kg
SW1	37.1	0.5	137	325	1945	280	642	18	1960	320
SW1_I	36.3	0.8	252	261	2313	281	357	< 10	385	446
SW2	35.3	1.9	503	715	3343	369	5515	64	503	1182
SW2_I	29.2	1.3	621	1140	3144	364	67726	830	4541	6814
SW3	39.3	0.4	< 50	107	766	157	18	< 10	373	62
SW3_I	38.3	0.4	80	140	810	153	53	11	502	138
SW4	37.0	0.7	163	406	1464	282	3339	245	614	1048
SW4_I	35.8	1.6	181	676	3095	493	153	32	1795	3304
SW5	38.7	0.8	204	599	2253	684	29	13	1281	161
SW5_I	35.1	0.5	178	733	2182	647	404	35	16240	2989

5.5.1.2 Microstructural characterization

Scanning electron microscopy imaging of the scale deposits confirms calcite to be the main component in both tunnels. Scale deposits without PASP are dominated by idiomorphic trigonal-rhombohedral calcite crystals (50 to 300 µm in size). Scale deposit SW1 reveals compact and columnar shaped calcite crystals (~300 µm; cf. Fig. 3A, B). Orthorhombic aragonite typically exhibits bundles of acicular to fascicular crystal shapes (70 to 120 µm size). In the presence of PASP smaller crystal sizes of calcite (1 to 10 µm) and aragonite (~20 µm) occur compared to the scale deposits without PASP (e.g. Figs. 3 to 7). The calcite formed in the presence of PASP typically shows skeletal shaped crystals often consisting of small stacked crystallites (Figs. 3 and 5). According to SEM images, the aragonite content increases in scale deposits influenced by PASP, which corroborates the mineralogical observations. Nearly all scale deposits, except of SW3 and SW3_I, show evidence of microbial activity, i.e. extracellular polymeric substances (EPS; red arrows in Figures 3D, 6 and 7) are interconnecting crystals. EPS are distributed over the entire scale deposits SW1, SW1_I, SW4, SW4_I, SW5 and SW5_I, but could not be attributed to a specific microbial species. Only scale deposits SW2 and SW2_I exhibit twisted stalks and hollow microtubes, which are characteristic for the Fe-oxidizing bacterial species *Gallionella ferruginea* and *Leptothrix ochracea* (e.g. Ehrenberg, 1836; Hallberg and Ferris, 2004; Chan et al 2016; Fig. 4). Nanometer-sized aggregates frequently intergrown with the bacteria and their remnants are most likely referred to Fe-(hydr)oxide

precipitates, e.g. ferrihydrite ($Fe_{10}O_{14}(OH)_2$), which are difficult to detect by XRD due to low crystallinity degree (see Eichinger et al., 2020a).

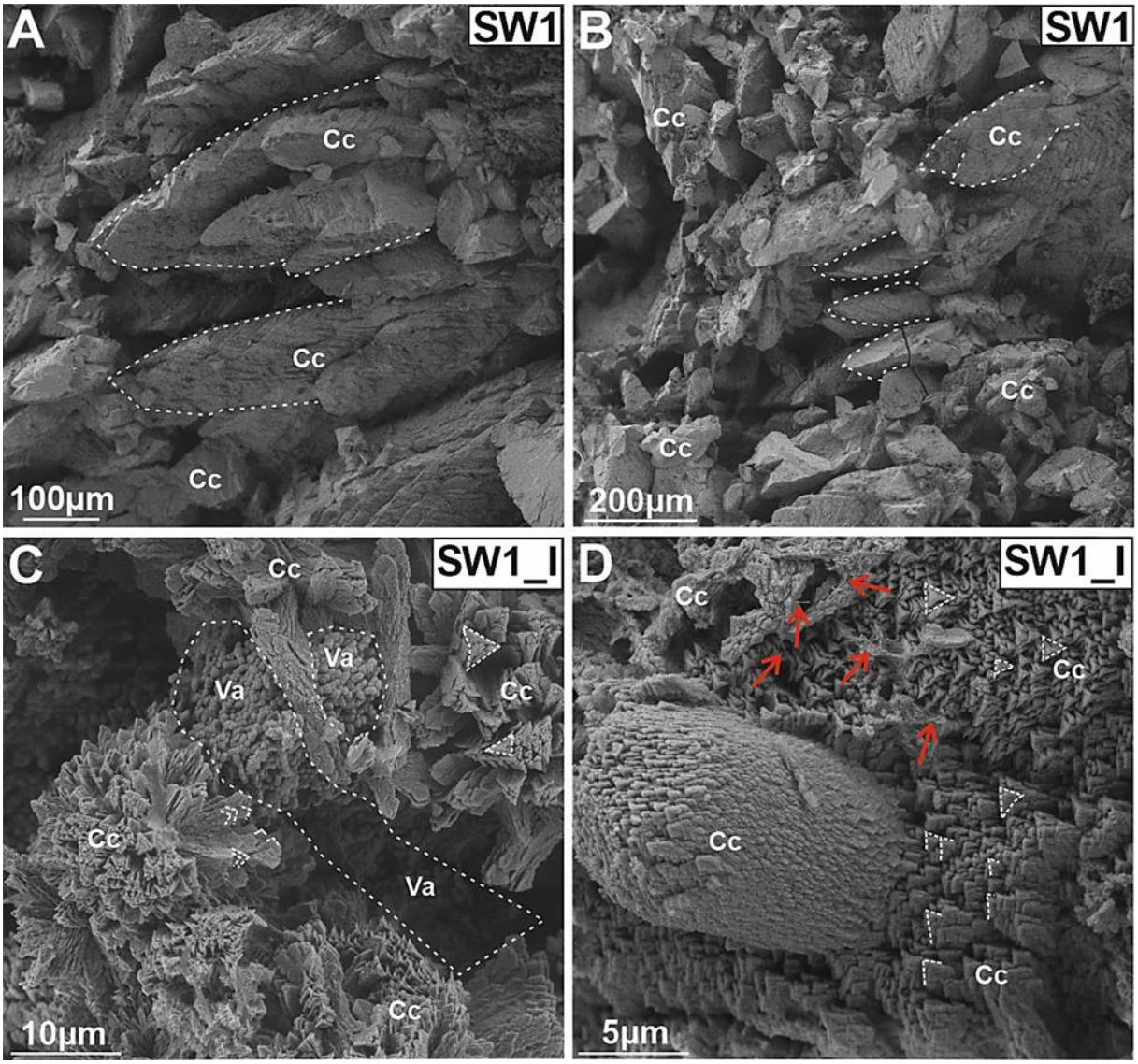

Figure 3: *SEM images of scale deposit SW1 (without PASP; A and B) showing compact and columnar calcite (Cc) crystals, whereas scale deposit SW1_I (with PASP; C and D) reveals small skeletal and stacked calcite crystals (marked with white triangles and dotted lines) as well as fine discus-shaped vaterite (Va) particle aggregates. The red arrows indicate evidence of microbial activity (EPS structures).*

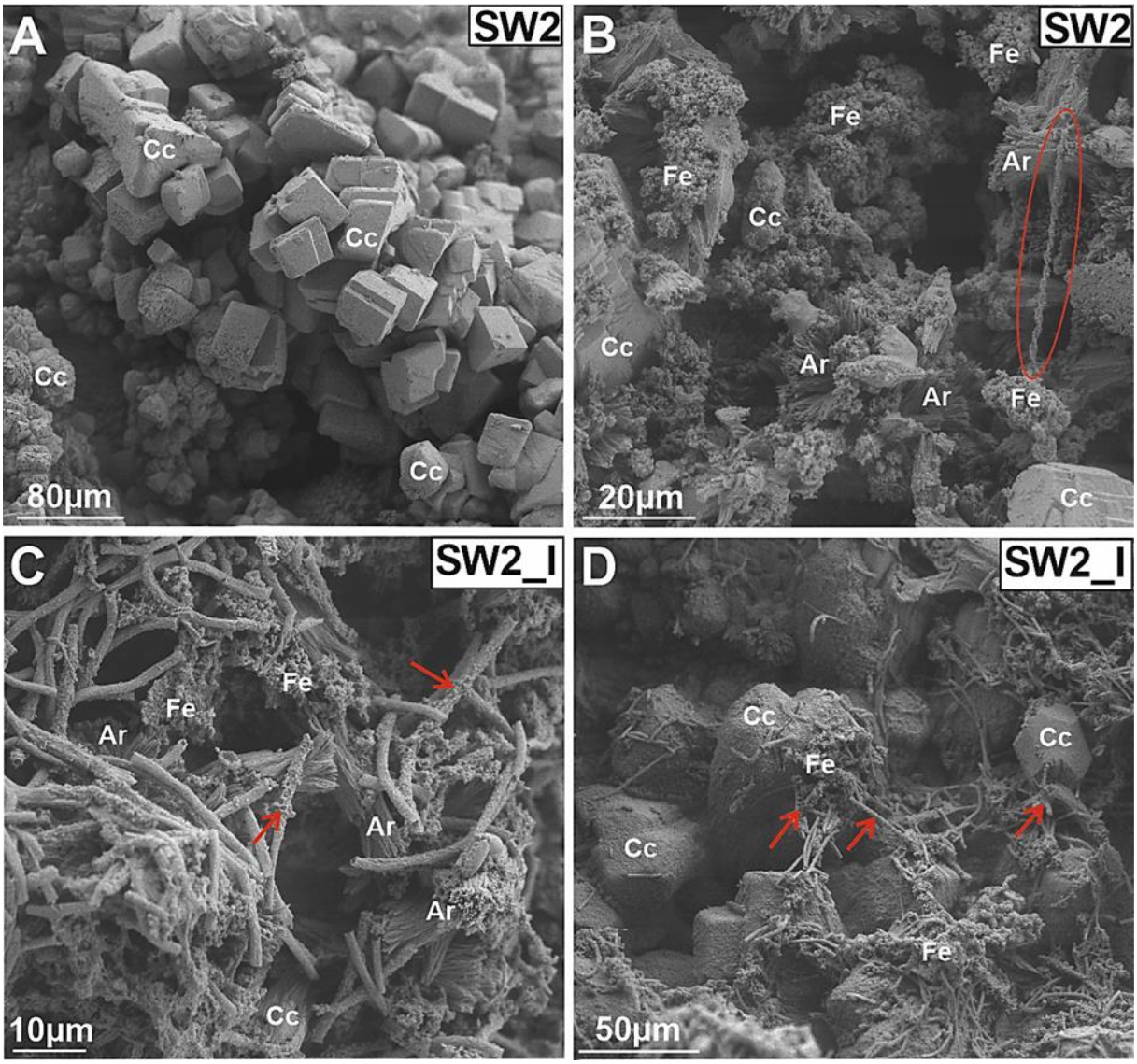

Figure 4: *SEM images of scale deposit SW2 (without PASP) showing rhombohedral calcite crystals (Cc; A), fascicular shaped aragonite (Ar; B) as well as widespread, nanometer-sized spherical particle aggregates (Fe; likely represented by the Fe-(hydr)oxide mineral ferrihydrite), which are often associated with twisted stalks of the Fe-oxidizing bacteria Gallionella ferruginea (red ellipse in B). Scale deposit SW2_I (with PASP) shows hollow microtubes of the Fe-oxidizing bacteria Leptothrix ochracea, which are partly coated with fine Fe-(hydr)oxides (red arrows in C and D).*

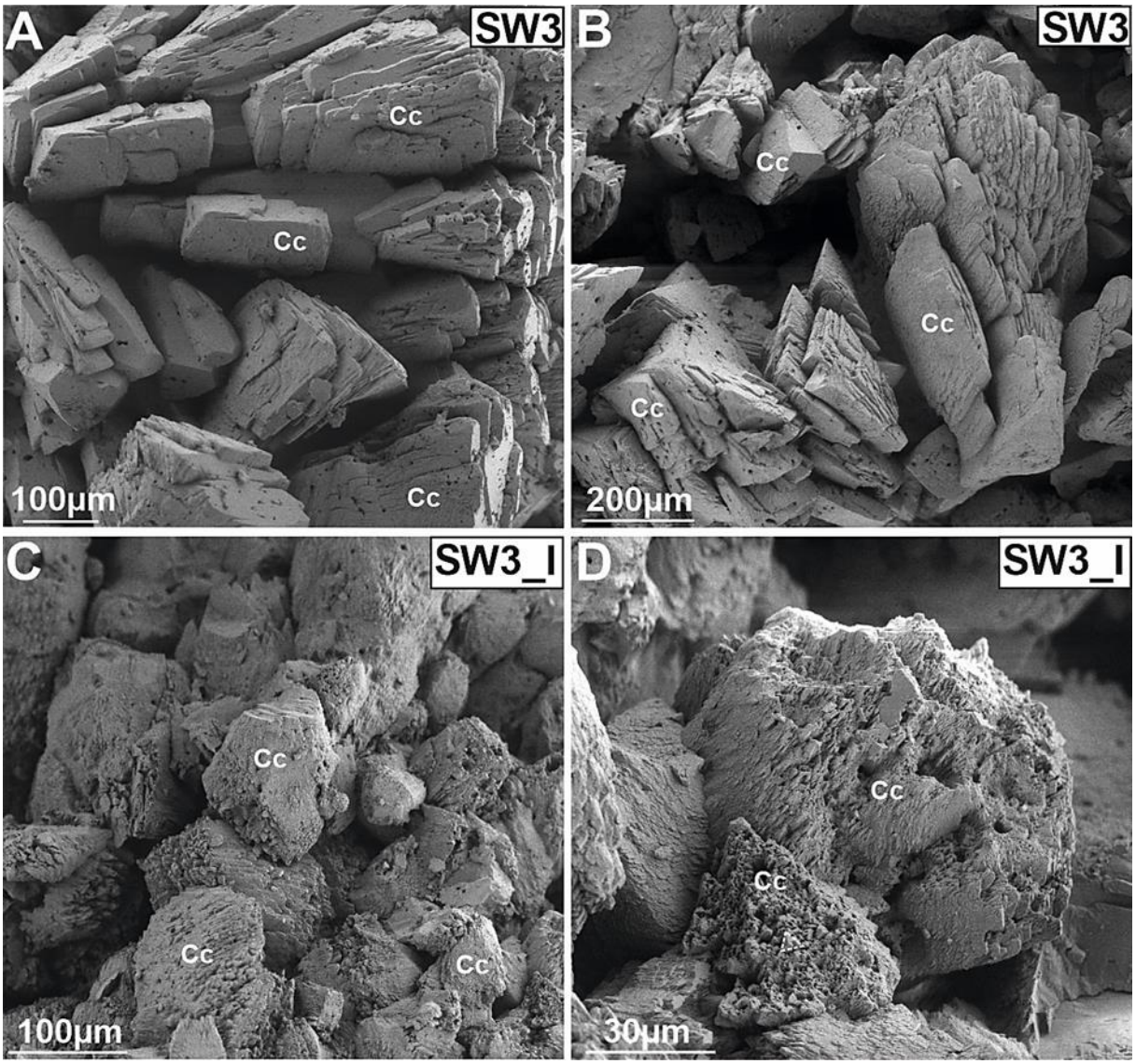

Figure 5: *SEM images of scale deposit SW3 (without PASP) shows relatively large, compact and rhombohedral calcite crystals (Cc in A and B), whereas scale deposit SW3_I (with PASP) shows dominantly smaller and more porous calcite crystals (Cc in C and D) along with skeletal shaped and stacked crystals (marked with white triangle in D).*

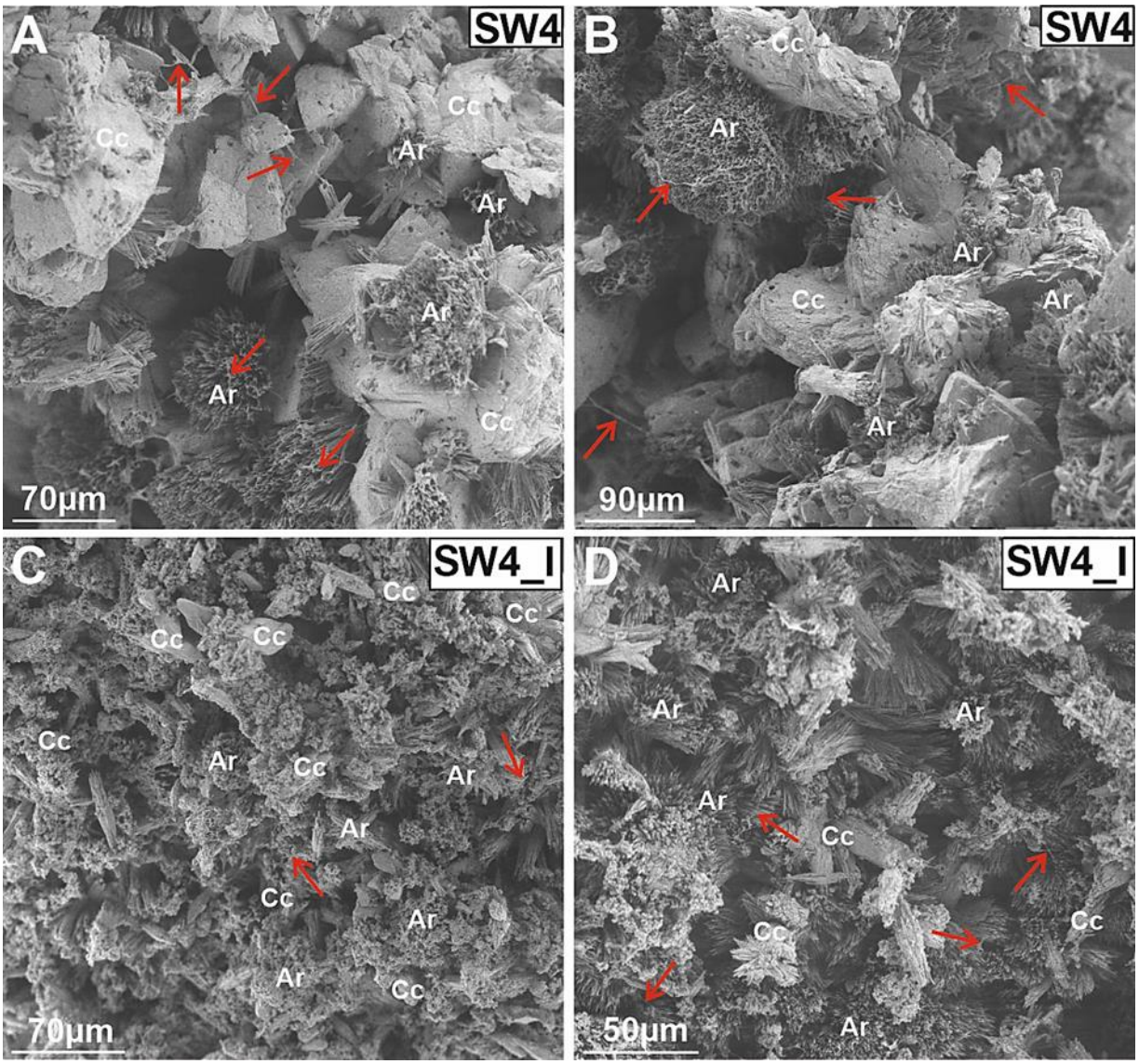

Figure 6: *SEM images of scale deposit SW4 (without PASP; A and B) showing aggregates of relatively large and compact calcite crystals (Cc), fascicular aragonite crystals (Ar) of variable size and evidence of microbial activity in the form of abundant EPS strands (red arrows). Scale deposit SW4_I (with PASP; C and D) exhibits much smaller and porous calcite (Cc) and aragonite (Ar) crystals, which are evenly distributed in microbial biofilm (red arrows).*

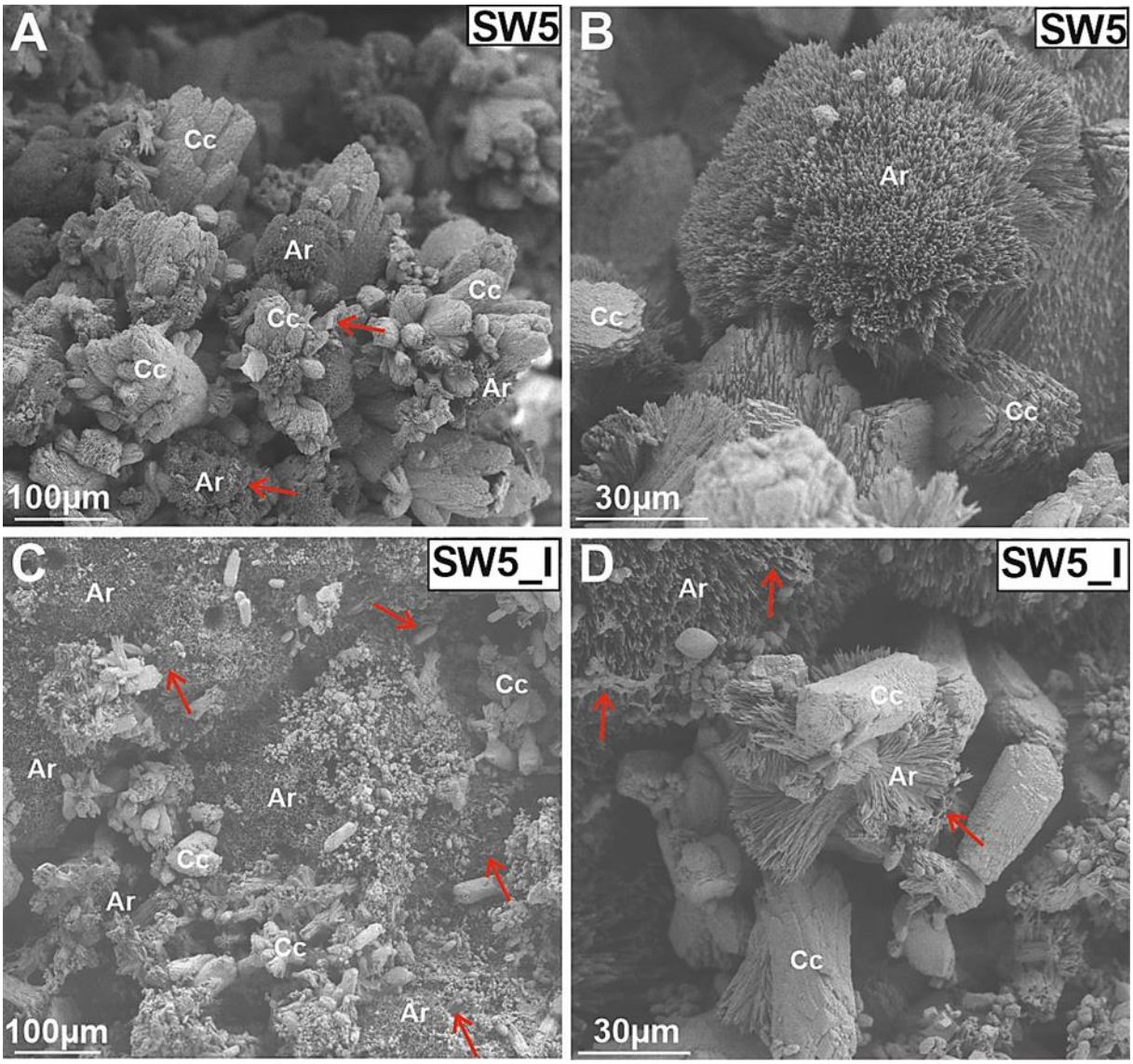

Figure 7: *SEM images of scale deposit SW5 (without PASP; A and B) showing rhombohedral calcite (Cc) and fascicular aragonite (Ar) along with remnants of microbial activity, such as EPS strands interconnecting crystals (red arrows). Scale deposit SW5_I (with PASP; C and D) is characterized by fine-grained calcite and abundant aragonite crystals (about equal to calcite content).*

5.5.2 Chemical composition and flow regime of drainage solutions

All drainage solutions reveal pH values from 7.90 to 9.95, which are typical for local groundwater interacting with concrete (Boch et al., 2015). The SpC values range from 626 to 835 µS/cm. In aqueous solutions without PASP the Ca^{2+} concentrations vary from 15 to 92 mg/l and alkalinity ranges from 161 to 395 mg/l (reported as HCO_3^-). In samples with PASP the Ca^{2+} (69 to 94 mg/l) and HCO_3^- concentrations (370 to 505 mg/l) are significantly higher. The difference in the Ca^{2+} concentration between the original drainage solution without PASP and after PASP treatment varies from 14 up to 77 mg/l (i.e., an increase of 119-613 %),

demonstrating the efficiency of PASP addition (ε = 16 up to 84 % for SW1 and SW3-5; ε =2 % for SW2). Accordingly, ionic strength of the drainage solutions increased upon PASP addition, however, it remained relatively low (I ≤ 0.01 mol/kgw), so that an inhibition effect on PASP performance is unlikely. The Mg^{2+} contents vary from 12 to 50 mg/l. The drainage solutions exhibit molar Mg^{2+}/Ca^{2+} ratios from 0.6 to 3.2, with the lower ratios seen in solutions with PASP. K^+ and Na^+ concentrations range from 5 to 42 mg/l and 4 to 34 mg/l. SO_4^{2-}, NO_3^- and Cl^- contents are strongly variable ranging from 8 to 117 mg/l, <0.1 to 10 mg/l, 3 to 54 mg/l, respectively. The Si concentrations are between 3 and 6 mg/l (given as SiO_2). Minor and trace elements ΣAl, Ba^{2+}, Sr^{2+} and ΣFe are highly variable, but inconspicuous among the different sampling sites (Table 3). The DOC concentrations increase by the addition of PASP (range: 0.8 to 11.0 mg/l of C) and correlate well ($R^2 = 0.99$) with the measured PASP concentrations (range: 1.1 to 32.8 mg/l; Table 3; Fig. C.1; Appendix).

Calculated charge balance errors (CBE; 100*[(Cat-An)/(Cat+An)]) are consistently <5 %. Saturation indices (SI) in respect to calcite, aragonite and vaterite reveal supersaturation of any $CaCO_3$ polymorph in all solutions, for example, $SI_{calcite}$ values range from 0.7 to 1.9. Ikaite ($CaCO_3 * 6H_2O$) and strontianite ($SrCO_3$) are under- or supersaturated, while amorphous $CaCO_3$ (ACC) is undersaturated or close to saturation in all solutions ($SI_{ACC} \leq -0.2$). The calculated internal partial pressure of CO_2 (pCO_2 in atm; Table 3) lay between $10^{-4.95}$ and $10^{-2.43}$ atm. The Re for the two drainages was calculated to be 89 up to 2000, which is indicative of prevailing laminar flow conditions throughout (Liu et al., 2020).

Table 3: *Hydrochemical in-situ parameters (pH, Temp: temperature, SpC: specific electric conductivity), alkalinity (reported as HCO_3^-), concentrations of solutes ($Si(OH)_4$ is reported as SiO_2), and dissolved organic carbon (DOC), charge balance error (CBE), mineral saturation indices (SI) for calcite, aragonite, vaterite, amorphous $CaCO_3$ (ACC), ikaite, strontianite, internal partial pressure of CO_2 (P_{CO2}), PASP dosage and concentration and flow rate (Q) at each sampling point. SW is the collected drainage solution without influence of the scale inhibitor PASP, while "I" indicates a solution affected by PASP. Note that the seasonally induced temperature increase in "I" by ~5 °C has virtually no effect on the system`s behaviour, i.e. SpC and trace elements are randomly distributed between sampling sites.*

Sample ID	Temp	SpC	pH	HCO_3^-	Ca^{2+}	Mg^{2+}	K^+	Na^+	SiO_2
	°C	µS/cm		mg/l	mg/l	mg/l	mg/l	mg/l	mg/l
SW1	6.0	626	8.93	263	50	39	12	11	4
SW1_I	10.3	638	9.42	384	87	31	23	15	3
SW2	7.8	805	8.04	395	92	50	6	4	4
SW2_I	10.0	794	7.90	391	94	50	7	5	4
SW3	5.1	641	8.23	350	72	38	5	5	4
SW3_I	9.5	679	8.17	370	86	33	10	12	4
SW4	5.8	681	9.01	161	31	12	15	9	6
SW4_I	10.5	708	9.30	373	69	30	29	29	4
SW5	5.7	671	9.95	268	15	29	42	34	3
SW5_I	10.7	835	9.02	505	92	41	24	24	4

Sample ID	∑Al	Ba^{2+}	Sr^{2+}	∑Fe	SO_4^{2-}	Cl^-	NO_3^-	Mg^{2+}/Ca^{2+}	DOC	CBE
	µg/l	µg/l	µg/l	µg/l	mg/l	mg/l	mg/l	(molar)	mg/l	%
SW1	68	102	1203	26	84	10	1	1.3	1.1	0.9
SW1_I	89	148	1003	6	73	6	3	0.6	0.8	0.0
SW2	86	53	1582	302	108	3	0	0.9	0.9	1.5
SW2_I	39	34	1460	63	117	3	1	0.9	0.8	2.0
SW3	53	76	677	9	51	5	4	0.9	0.9	-0.7
SW3_I	80	65	541	13	48	10	7	0.7	3.7	-0.5
SW4	53	93	314	13	22	8	<0.1	0.7	1.0	0.3
SW4_I	140	79	620	6	27	54	0	0.7	11.0	-1.9
SW5	96	86	314	181	8	27	7	3.2	3.0	-0.9
SW5_I	76	154	515	20	10	22	10	0.7	6.8	-1.3

Sample ID	$SI_{calcite}$	$SI_{aragonite}$	$SI_{vaterite}$	SI_{ACC}	SI_{ikaite}	$SI_{strontianite}$	$logP_{CO2}$	dosage	PASP	Q
							atm.	(ml/h)	(mg/l)	l/sec
SW1	1.2	1.0	0.6	-1.0	-0.2	0.2	-3.69	–	–	0.25
SW1_I	1.9	1.8	1.4	-0.2	0.4	0.6	-4.13	10	1.4	
SW2	0.8	0.6	0.2	-1.3	-0.6	-0.4	-2.58	–	–	0.5
SW2_I	0.7	0.5	0.1	-1.4	-0.8	-0.6	-2.43	12	1.1	
SW3	0.8	0.7	0.2	-1.3	-0.5	-0.6	-2.82	–	–	0.1-0.05
SW3_I	0.9	0.8	0.3	-1.2	-0.5	-0.7	-2.73	8	10.4	
SW4	0.9	0.8	0.4	-1.2	-0.4	-0.5	-3.96	–	–	0.03
SW4_I	1.8	1.6	1.2	-0.3	0.3	0.3	-3.97	4	32.8	
SW5	1.4	1.2	0.8	-0.8	-0.0	0.4	-4.95	–	–	0.05
SW5_I	1.8	1.7	1.2	-0.3	0.3	0.1	-3.52	3	20.2	

5.6 Discussion

5.6.1 Mechanisms of scale deposit formation

$CaCO_3$ formation in drainage systems is frequently caused by site-specific fluid-solid interactions being impacted by the dissolution of host rocks and local building materials, mixing of solutions different in composition along the water flow path, and/or by CO_2 exchange between the drainage solution and the tunnel atmosphere. The mechanisms and rate-limiting factors causing $CaCO_3$ formation in the tunnels Spital and Steinhaus are detailed in Eichinger et al. (2020a). Briefly, in the tunnel Spital, $CaCO_3$ scale formation is strongly related to the local geology, since the calcareous host rocks provide high Ca^{2+} and Mg^{2+} concentrations to the drained solutions (cf. Eichinger et al., 2020a). Contrary, in the tunnel Steinhaus, higher pCO_2 values ($10^{-2.73}$ atm) than the Earth´s average atmosphere (~$10^{-3.45}$ atm) and water mixing at high flow rates (0.1 – 0.05 l/s) suggest that CO_2 degassing promoted scale deposit formation. However, we note that the flow regime is characterized by laminar flow, as indicated by Re < 2000, which should prevent from extremely fast and excessive CO_2 outgassing from solution into the tunnel atmosphere and associated disruptions of gas-liquid-solid interface processes within the drainage system (Eichinger et al., 2020a). In some cases (SW4 and SW5), elevated K^+ and Na^+ concentrations and pH values up to 10 indicate significant leaching of concrete (Table 3) has stimulated $CaCO_3$ formation by shifting DIC towards CO_3^{2-} species and adding Ca^{2+} ions to the reactive solution (Baldermann et al., 2019). Evidence for intensified water-concrete interaction is given by very low flow rates (0.03 to 0.05 l/s) at tunnel Steinhaus. The scale growth rate in the two tunnels is approximately 0.5 to 1.0 cm over a 6 months period, however, we note that the $CaCO_3$ growth kinetics remain undetermined as the water flow is not continuous between regular cleaning works from summer 2019 until PASP addition in January 2020.

Two types of primary scale deposits precipitated at the bottom of the drainage pipes. Deposits SW1 and SW3 (type 1) display calcite mineralogy forming compact and dense fabrics (Table 2; Fig. 8). Deposits SW2, SW4 and SW5 (type 2) contain aragonite admixtures (Fig. 4B; Fig. 6A, B and Fig. 7A, B) and they also show evidence of microbial activity and appear more porous (Fig. 2). The occurrence of aragonite in such scale deposits is explained by prior $CaCO_3$ precipitation (PCP), which is favored at low flow rates (0.05 l/s or less; Boch, 2019; Fairchild et al., 2000). PCP rises the aqueous Mg^{2+}/Ca^{2+} ratio of the drainage solution by ongoing $CaCO_3$ removal, which progressively poisons calcite precipitation and promotes aragonite formation (molar $Mg^{2+}/Ca^{2+} > 1$; Huang and Fairchild, 2001; Riechelmann et al., 2014; Baldermann et al., 2020). At site SW2, which is characterized by a high flow rate (~0.5 l/s), the higher

concentration ratio of Mg^{2+} and SO_4^{2-} vs. Ca^{2+} (Table 3) inhibited calcite and promoted aragonite formation (Busenberg and Plummer, 1985; Riechelmann et al., 2014; Götschl et al., 2019). In both cases, aragonite formation yields in more porous microfabrics, which explains the observed overall increase of less dense scale material consistence.

5.6.2 Effect of PASP on drainage solution composition

The scale deposits with PASP (SW1_I to SW5_I) possess analogous formation mechanisms, since tunnel sections and fluid-rock interaction remained the same in the considered timeframe. However, the atmospheric conditions (e.g. T, humidity, CO_2 content) in the tunnel are variable to a certain degree due to the specific timing of the sampling campaigns, which express in a seasonal variability of the elemental concentrations (Table 3). Apart from this, increased Ca^{2+}, HCO_3^- and DOC concentrations of solutions SW1_I to SW5_I document that PASP chemically modifies the groundwater and inhibits $CaCO_3$ formation (Fig. 8; Path 1). Inhibition is caused by PASP covering the $CaCO_3$ nuclei and crystallites, as well as chelate (complexation) with Ca^{2+} ions (Wierzbicki et al., 1994; Wada et al., 2001; Wu and Grant, 2002; Martinod et al., 2009; Kirboga and Öner, 2012; Shen et al., 2017), which result in prominently high $SI_{calcite}$ values up to 1.9, that is close to saturation with respect to ACC (Wedenig et al., 2021; see Table 3). Liu et al. (2012) have experimentally shown that the effect of scaling inhibition decreases with increasing temperature, which could affect the PASP performance at distinct tunnel sites. However, at the present study sites the annual variation in temperature amounts only to ~5 °C, which is too low to have an anticipated effect on reducing the total $CaCO_3$ nuclei and crystallites coverage or Ca^{2+} complexation by PASP. Moreover, Liu et al. (2012) and Chhim et al. (2020) have demonstrated that the efficiencies of PASP and polyepoxysuccinic acid (PESA) strongly depend on the Ca^{2+} concentration in solution, i.e., a decrease is seen at higher Ca^{2+}-to-inhibitor concentration ratios. As for the present tunnel sites, where seasonal variations in the Ca^{2+} concentration at constant PASP dosage in the drainage solution are observable (Table 3), changes in the Ca^{2+}-to-inhibitor concentration ratios could result in a temporal increase (i.e., scale deposits formation is reduced) or decrease (i.e., scale deposits formation is favored) of the PASP efficiency. Nevertheless, the observed increase in the Ca^{2+} concentration, the change in the consistence of the $CaCO_3$ scale deposits and the significant reduction of the $CaCO_3$ scale mass after PASP treatment demonstrate the high efficiency of PASP application (up to 84 %) in this dynamic system, which corroborates findings of Liu et al. (2012) and Quan et al. (2008)

who proposed a high efficiency (> 80%) of PASP at comparable dosage concentrations up to 12 and 15 mg/l, respectively.

Inhibitor dosage can be followed and adjusted by PASP and DOC analyses of the local groundwater to achieve a PASP concentration for optimal inhibitor performance. Solutions SW1_I and SW2_I indicate the highest flow rates and the lowest inhibitor concentrations, while SW4_I and SW5_I show lowest flow rates and higher PASP concentrations (1.1 versus 32.8 mg/l of PASP; Table 3), explaining the systematically higher $SI_{calcite}$ values of the latter solutions (see Table 3). Notwithstanding documented (seasonal) variations in the hydrochemical conditions within the drainages, the flow regime was always characterized by laminar flow at the two localities. Even though we cannot completely exclude minor temporal changes in water flow dynamics due to the restricted number of sampling campaigns we argue that fast CO_2 degassing has had no anticipated impact on the gas-liquid-solid interface processes. Moreover, Wedenig et al. (2021) provided experimental evidence that the rates of CO_2 degassing and $CaCO_3$ precipitation are independent from the PASP performance, corroborating the changes in scale deposit mineralogy and material consistence described below. However, SW2_I and SW3_I behave different as the Ca^{2+} and HCO_3^- concentrations remain nearly at the same level compared to the initial solutions without PASP (Table 3). In the case of SW3_I the selected inhibitor dosage of 8 ml/h was too low to significantly tune the inhibition performance (Fig. 2E, F), i.e., the height of the scale deposits was reduced only by ~half. The measured concentrations of PASP in SW3_I and SW5_I were 10.4 and 20.2 mg/l at similar flow rates (Table 3). In the case of SW2_I, occurrences of small hollow microtubes indicate that bacterial activity has influenced the petrography of the scale deposit and the chemical composition of the solution (Fig. 4). This is supported by the lower Fe content and $SI_{calcite}$ in SW2_I (cf. SW2 and SW2_I in Table 3), which is attributed to microbial activity of *Leptothrix ochracea* (cf. Hashimoto et al., 2007; Chan et al., 2016). An elevated Fe content in the scale deposit, a red coloration, and a modified consistence of SW2_I argue for the strong influence of Fe-oxidizing bacteria (Fig. 4), which is expressed by poorly crystallized Fe-(hydr)oxides (Tuhela et al., 1997; Hashimoto et al., 2007).

5.6.3 Influence of PASP on mineralogy, crystal morphology and material consistence

The addition of PASP can either suppress ongoing $CaCO_3$ crystal growth or even change the material`s consistence via the type of $CaCO_3$ polymorph forming the scale deposits. This is expressed by a strong decrease in volume of the tunnel scale deposits by ~50 vol% up to ~90

vol%, where the primary calcite deposits were almost quantitatively removed after exposure to PASP-containing drainage water for 10 months (cf. Fig. 2A, B, E, F), which demonstrates the high efficiency of PASP application. Aragonite containing precipitates are typically more porous and even loose compared to dense and compact calcite scale deposits (Fig. 2; Kirboga and Öner, 2012; Kumar et al., 2012; Shen et al., 2017; Eichinger et al., 2020a). Chemical analyses reveal that scale deposits without PASP barely differ in the elemental composition compared to scale deposits affected by PASP (Table 2). Only SW2_I reveals much higher Fe and Mn concentrations and a lower Ca content compared to SW2, which is related to increased activity of Fe-oxidizing bacteria. The almost constant chemical composition is explained by PASP affecting the mineralogy of $CaCO_3$ precipitates, such as calcite vs. aragonite and vaterite (Yang et al., 2001; Martinod et al., 2009; Niedermayr et al., 2013). Vaterite is the thermodynamically least stable anhydrous $CaCO_3$ polymorph and recrystallizes rapidly toward thermodynamically stable calcite, which explains the scarcity of vaterite in the scale deposits (Kitamura, 2009; Rodriguez-Navarro and Benning, 2013; Jones, 2017; Konopacka-Łyskawa, 2019). In solutions at low temperature (< 10°C), vaterite has a prolonged metastability (>20 h; Andreassen, 2005). The occurrence of PASP results in an effective retardation of calcite crystal growth giving rise to the formation of aragonite and vaterite nuclei at high supersaturation state and further inhibits the transformation of vaterite to calcite (e.g. Han et al., 2006; Njegić-Džakula et al., 2010; Konopacka-Łyskawa, 2019). The suppression of calcite crystal growth and the competitive formation of the other $CaCO_3$ polymorphs is documented by the change in consistence and volume (cf. Fig. 2C, D, G, H, I, J) and the high abundance of aragonite at sampling sites SW2, SW4 and SW5 (up to 12-52 wt.%; Table 1). Thus, the aragonite and vaterite contents increase upon PASP addition, which corresponds well to the high SI values of the drainage solutions, e.g. SW1_I (cf. Table 3; Yang et al., 2001). A lower Mg^{2+}/Ca^{2+} ratio and high PASP concentration induce vaterite instead of calcite formation (Niedermayr et al. 2013). This matches our observations on scale deposit SW1_I, where the lowest Mg^{2+}/Ca^{2+} ratio (0.6), a high dosage of PASP (10 ml/h) and the highest SI values (up to 2) of all three $CaCO_3$ polymorphs (Table 3) favored vaterite to form. Despite the above, we cannot fully exclude temporal ikaite precipitation (cf. Boch et al., 2015) from solutions SW1_I, SW4_I and SW5_I (SI_{ikaite} 0.3 to 0.4), but its lower metastability compared to vaterite and aragonite as well as experimental evidence (Niedermayr et al., 2013) argue against the formation of this mineral phase.

Importantly, the presence of PASP also leads to a modification of $CaCO_3$ crystallization, which significantly affects the morphologies and microfabric of the precipitates: PASP typically yields

in smaller calcite crystallites with smooth surfaces, truncated edges, skeletal and stacked shaped morphologies or rarely irregular shapes (cf. Fig. 8; Path 2). Aragonite crystals mostly retain fibrous crystal shapes, but with consistently reduced average particle sizes, whereas vaterite shows spherical crystal shapes (Fig. 3C). Such crystal morphologies indicate precipitation at high rates, which fits well with high SI values of e.g. SW1_I (Table 3; Jones et al., 2005; Jones, 2017; Yang et al., 2011). In supersaturated solutions, PASP is preferentially sorbed towards the active crystal growth direction, inhibiting or retarding the further crystal growth, thereby modifying the $CaCO_3$ scale mineralogy, crystal morphology and consistence (Liu et al., 2012). The latter may deteriorate the initial compact and dense microfabric of $CaCO_3$ scale deposit towards more porous aragonite microfabrics or even unconsolidated (mushy) material consistence (Fig. 2).

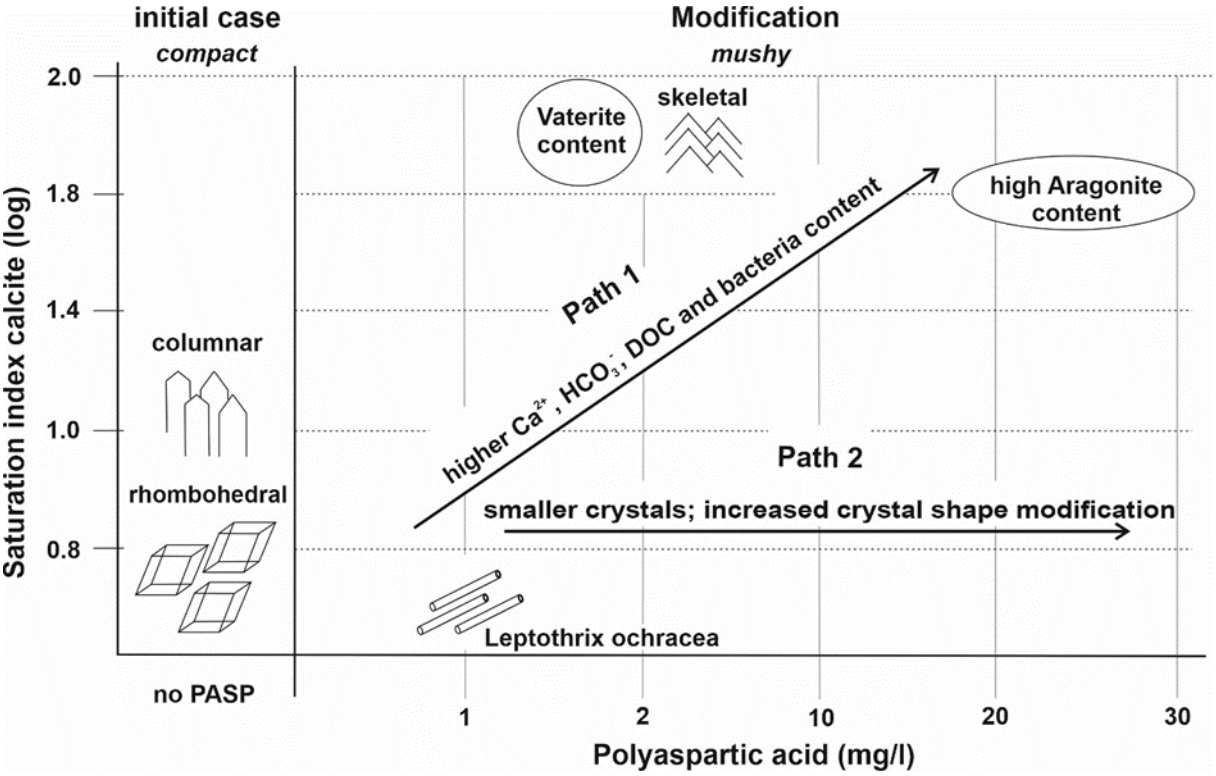

Figure 8: *Schematic reaction model of the scale deposits and related aqueous solutions from tunnel Spital and tunnel Steinhaus. The addition of PASP rise Ca^{2+}, HCO_3^- as well as DOC concentrations in the related solutions (Path 1), changes mineralogy and modifies crystal shapes resulting in a modification of material consistence from compact to mushy $CaCO_3$ scale deposits (Path 2).*

It is beyond the scope of the present paper to elucidate the apparent dissolution or transformation rates of primary calcite scale deposits upon PASP addition, because of poor

resolution in time and limited number of sampling sites in the two tunnel drainages. However, as a first-order approximation, we can calculate $CaCO_3$ removal rates for two contrasting scenarios, reflecting the dominant calcite (type 1) vs. calcite-aragonite (type 2) mineralogy of the scale deposits after PASP addition. Using an estimated volume of the primary calcite scale deposit in the two drainage systems of 1225 ± 672 cm³ (height: 0.5-1.0 cm, coverage in pipe: 15-17 cm in width), a scale density of 2.7 g/cm³ and a volume decrease of 50-90 % over a 10 months period for type 1, the $CaCO_3$ removal rate is 3.3 to 13.6 g $CaCO_3$/day, averaging 7.6 ± 3.1 g $CaCO_3$/day (or 2.8 ± 1.1 kg $CaCO_3$/year). As for type 2, calcite scale reduction amounts to ~60-85 %, which is equivalent to a $CaCO_3$ removal rate of 4.0 to 12.8 g $CaCO_3$/day, averaging 7.9 ± 1.9 g $CaCO_3$/day (or 2.9 ± 0.7 kg $CaCO_3$/year). Upscaling of $CaCO_3$ scale reduction to the total tunnel lengths (2500 vs. 1800 m) yields a total $CaCO_3$ loss of ~7.2 ± 1.8 t $CaCO_3$/year and ~5.2 ± 1.3 t $CaCO_3$/year for Spital and Steinhaus, respectively.

5.6.4 Microbial effects on PASP and scale deposits

The investigated scale deposits show clear evidence of microbial activity in the form of remnants of filamentous EPS structures (cf. Pedley, 2014; Jones, 2017). It is not possible to relate EPS to a species and to evaluate how this microbial activity could have been affected the scale deposits. But it is well known that various microorganisms can have a significant influence of the developing mineralogy, crystal shapes and precipitation rates (Pedley, 2014; Shiraishi et al., 2019; Westphal et al., 2019). In scale deposits SW2 and SW2_I extracellular twisted ribbon-like stalks (Fig. 4B) as well as prominent hollow microtubes (Fig. 4C and D) are indicative of neutrophilic Fe-oxidizing bacterial communities (FeOB), which are represented by *Gallionella ferruginea* and *Leptothrix ochracea* (Ehrenberg, 1836; Hallberg and Ferris, 2004; Chan et al., 2011; Chan et al., 2016; Fleming et al., 2018). In the scale deposit SW2 (without PASP) *Gallionella ferruginea* is detected, whereas scale deposit SW2_I mainly contains *Leptothrix ochracea*. Both FeOBs have different habitat requirements with respect to their metabolism: *Gallionella ferruginea* oxidizes Fe(II) and precipitates Fe(III)(hydr)oxides in environments poor in DOC by using DIC via chemolithoautotrophic processes, while *Leptothrix ochracea* is abundant in DOC-rich solutions assimilating DOC in combination with DIC by mixotrophic processes (Hallbeck and Pedersen, 1991; Fleming et al., 2014; Fleming et al., 2018). Thus, DOC from PASP addition leads to the dominance of *Leptothrix ochracea* over *Gallionella ferruginea* (Fleming et al., 2014; Fleming et al., 2018) as evidenced in the scale deposit SW2_I (Fig. 4B vs. Fig. 4C and D). It is known that the stalks (*Gallionella*) and sheaths

(*Leptothrix*) of such FeOBs are Fe(III)-rich, which is consistent with intergrowths and coatings of Fe-(hydr)oxides (Chan et al., 2011; Hashimoto et al., 2007; Eichinger et al., 2020a).

For solutions SW2 and SW2_I sufficient amounts of dissolved bioavailable Fe are constantly delivered to maintain FeOBs metabolism, which in turn influences the water chemistry and results in the co-precipitation of Fe-(hydr)oxides and $CaCO_3$ phases. This explains the red-brownish coloration of the scale deposits and the high Fe and low Ca contents upon addition of PASP (Table 2). However, *Leptothrix ochracea* may reduce the inhibitor effect of PASP by consuming DOC as inferred from solution SW2_I, which contained the highest PASP content (12 ml/h), but the lowest concentration of PASP (1.1 mg/l) and DOC (0.8 mg/l). This observation is supported by PASP analyses pattern (Fig. D.1; Appendix), where the main peak of the red spectral curve of solution SW2_I is shifted towards lower wavelengths compared to solution SW1_I and the PASP standard. This shift most likely arises from the bacterial degradation of the long-chained PASP polymers in solution SW2_I (Stedmon and Markager, 2005; Jalalvandi and Shavandi, 2018) as *Leptothrix ochracea* progressively consumes DOC provided by PASP. Accordingly, almost constant Ca^{2+} and HCO_3^- concentrations of solutions SW2 and SW2_I indicate a less efficient inhibition effect, while in all other solutions the Ca^{2+} and HCO_3^- concentrations increase significantly; indicative of a highly efficient inhibition effect supressing the precipitation of $CaCO_3$. The above relationships demonstrate that the understanding of site-specific conditions for scale deposit formation is required to identify advanced prevention strategies at the field site and to optimize the applicability of inhibitors for water conditioning. Future studies can make use of the herein presented inhibition effects induced by PASP addition on $CaCO_3$ scale formation in dynamic (i.e., underground) drainage systems. Ongoing research is required to evaluate the impact of specific on-site conditions, inhibitor type and dosage on the magnitude and rate of $CaCO_3$ scale inhibition and green inhibitor efficiency.

5.7 Summary and Conclusions

The application of the green inhibitor polyaspartate (PASP) to reduce $CaCO_3$ scale deposition and to alter the composition and (micro)structure of the unwanted precipitates was rated on-site in two tunnel drainages. Main conclusions are that the addition of PASP (i) results in elevated Ca^{2+}, HCO_3^- and DOC concentrations in solution and in $SI_{calcite}$ values close to saturation with ACC, (ii) effectively retards $CaCO_3$ nucleation even at low PASP concentrations, (iii) favours the formation of metastable vaterite and aragonite over calcite, (iv) changes the $CaCO_3$ scale

consistence from compact to mushy material and (v) modifies bacterial dominance, which may limit PASP scaling inhibition effects. An advanced understanding of the formation mechanisms of unwanted $CaCO_3$ scale deposits is required for an optimized use of proactive prevention strategies, such as the application of the green inhibitor PASP. An appropriate dosage can constitute a comparatively cost-effective measure to prevent scale deposit formation in a given drainage system.

5.8 Acknowledgements

The study was financially supported by the Austrian Motorway and Expressway Network Operator (ASFINAG). Judith Jernej, Maria Hierz and Andrea Wolf are acknowledged for their dedicated work at the TU Graz laboratories. We would like to thank Sabine Lindbichler from JR-AquaConSol GmbH for her work related to Fluorometer and DOC analysis, as well as Clara Chan for her helpful comments on Fe-oxidizing bacteria. Chemical and mineralogical analyses were conducted in the NAWI Graz Central Lab for Water, Minerals and Rocks.

5.9 Supplementary material

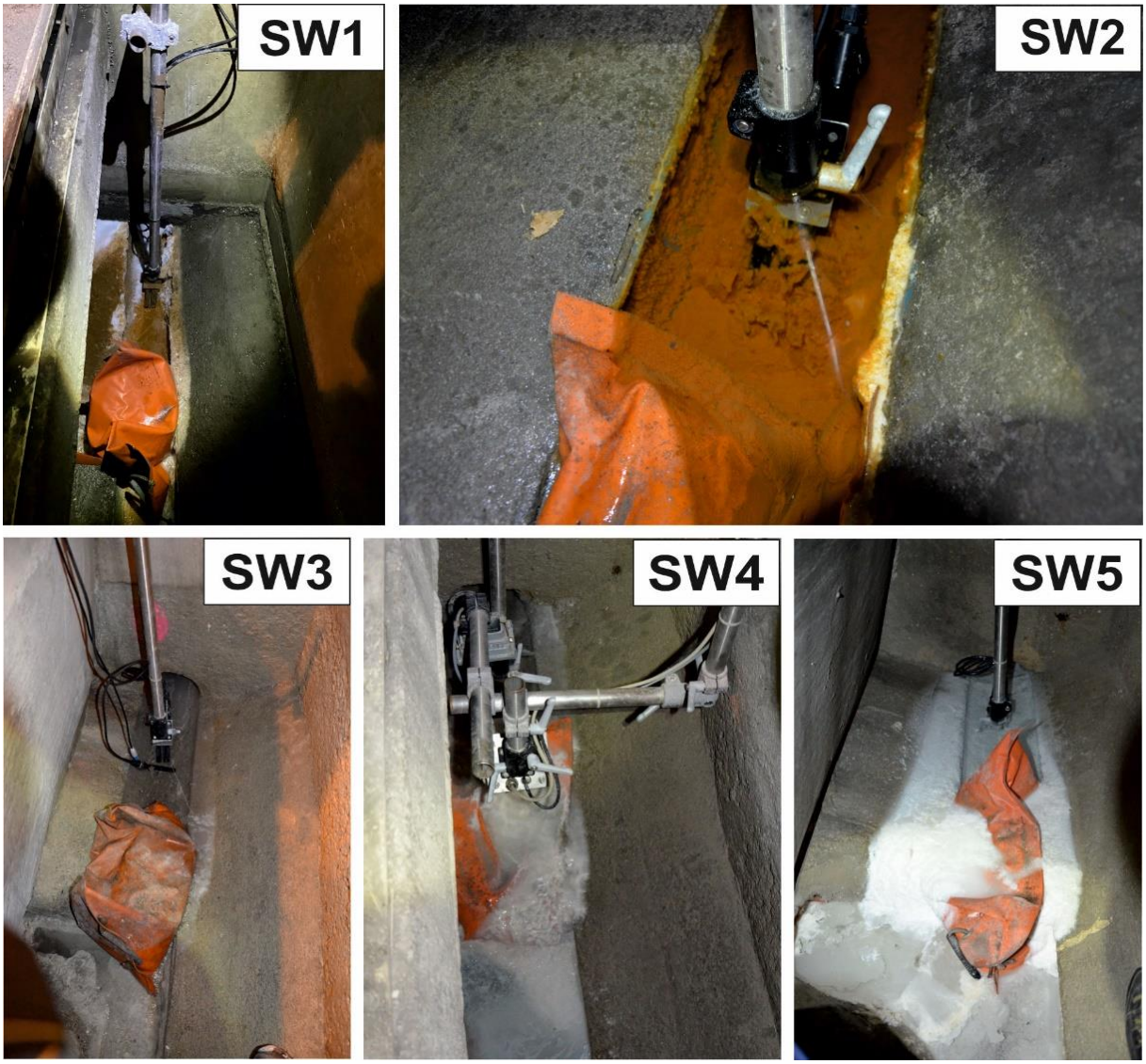

Figure A.1: *Photographs of clogged drainages from tunnel Spital (SW1-2) and tunnel Steinhaus (SW3-5) before small amounts of the inhibitor PASP were added. The leverages on the images are autonomous data loggers recording in-situ parameters such as pH, specific conductivity and water-temperature. The diameter of the lateral drainage pipes ("Ulmen") is 250 mm.*

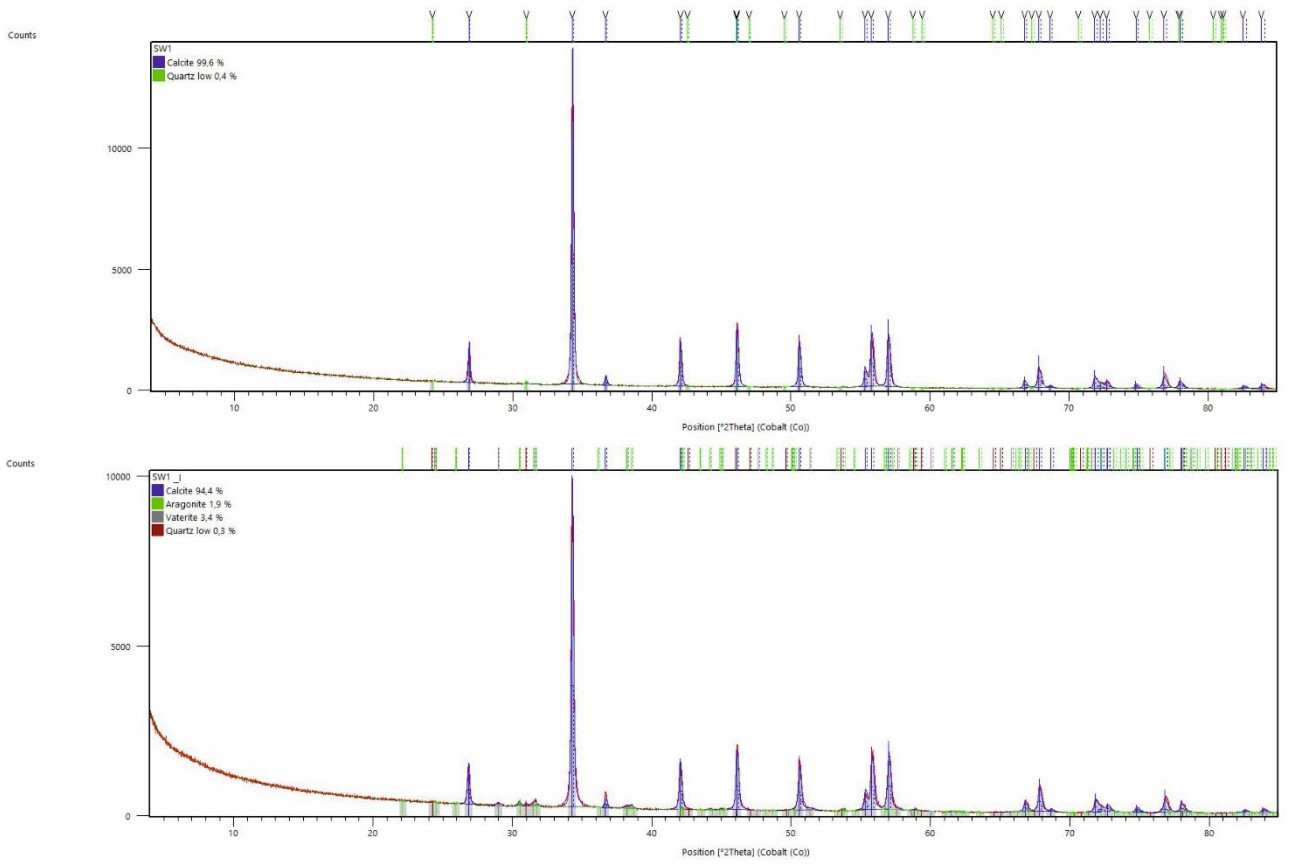

Figure B.1: *XRD-pattern of scale deposits SW1 and SW1_I. The top diffractogram shows the composition of the scale deposit SW1 (without PASP), while the lower diagram reveals the bulk composition of scale deposit SW1_I (with PASP).*

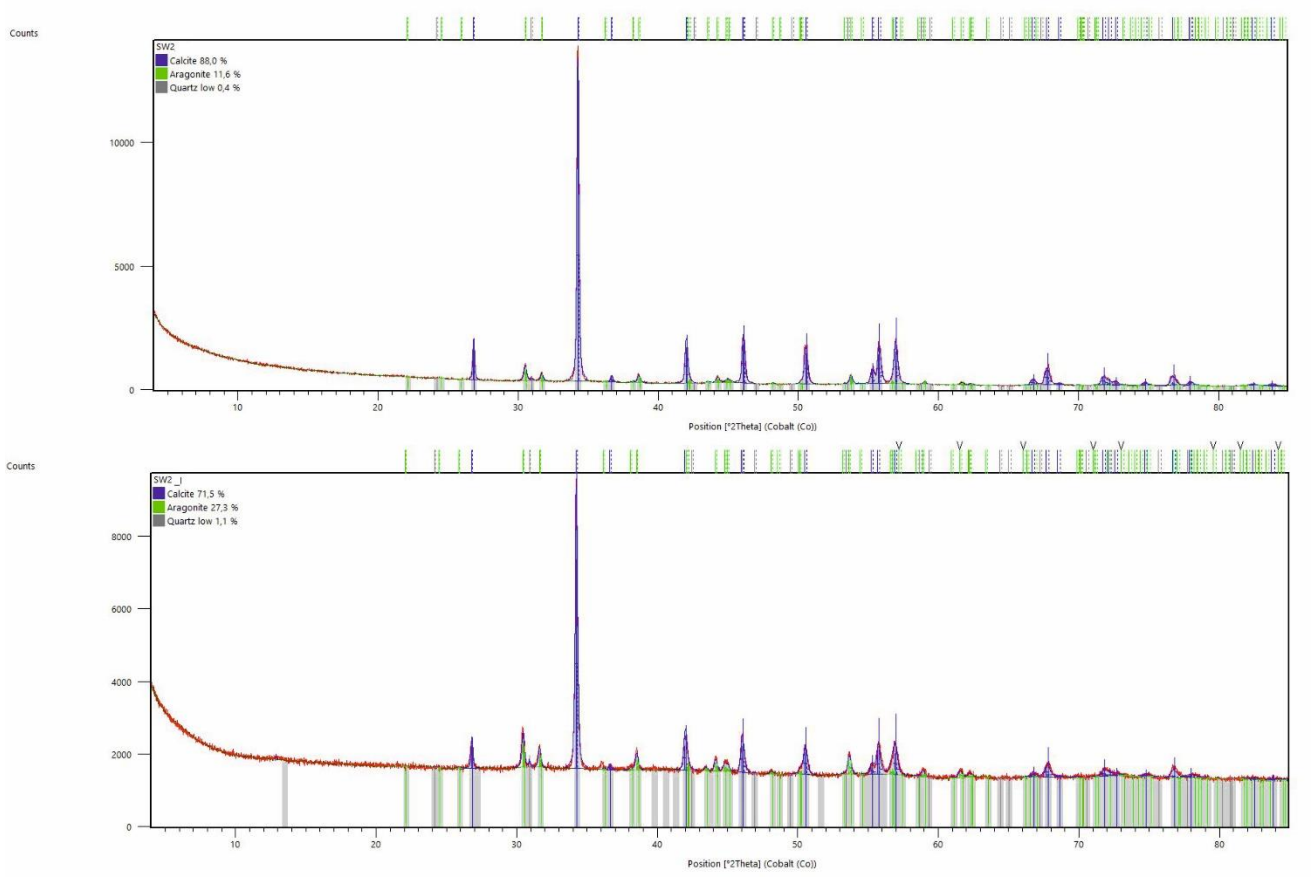

Figure B.2: *XRD-pattern of scale deposits SW2 and SW2_I. The top diffractogram shows the composition of the scale deposit SW2 (without PASP), while the lower diagram reveals the bulk composition of scale deposit SW2_I (with PASP). Note the elevated background in SW2_I suggesting the possible presence of low crystallinity Fe-(hydr)oxides.*

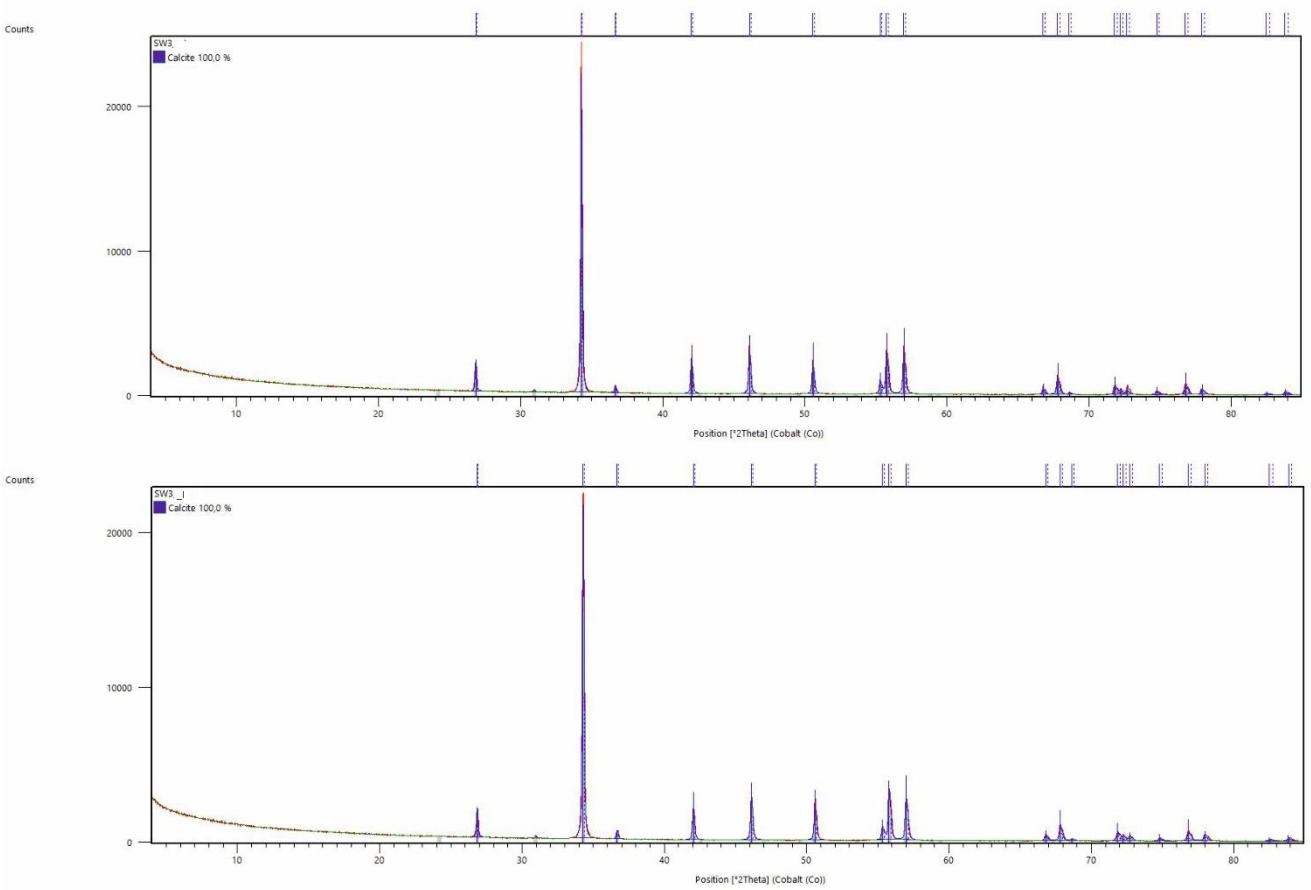

Figure B.3: *XRD-pattern of scale deposits SW3 and SW3_I. The top diffractogram shows the composition of the scale deposit SW3 (without PASP), while the lower diagram reveals the bulk composition of scale deposit SW3_I (with PASP).*

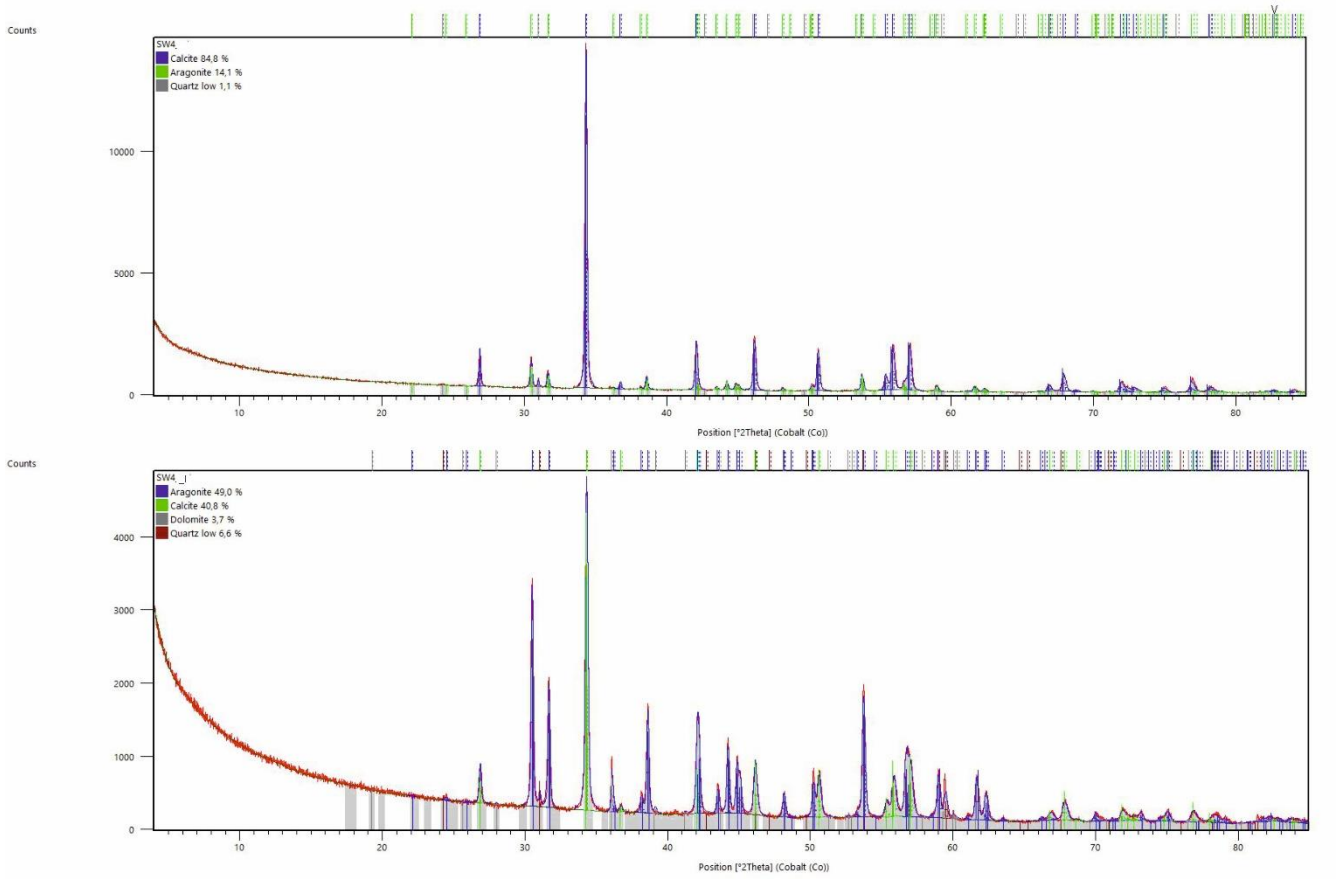

***Figure B.4**: XRD-pattern of scale deposits SW4 and SW4_I. The top diffractogram shows the composition of the scale deposit SW4 (without PASP), while the lower diagram reveals the bulk composition of scale deposit SW4_I (with PASP).*

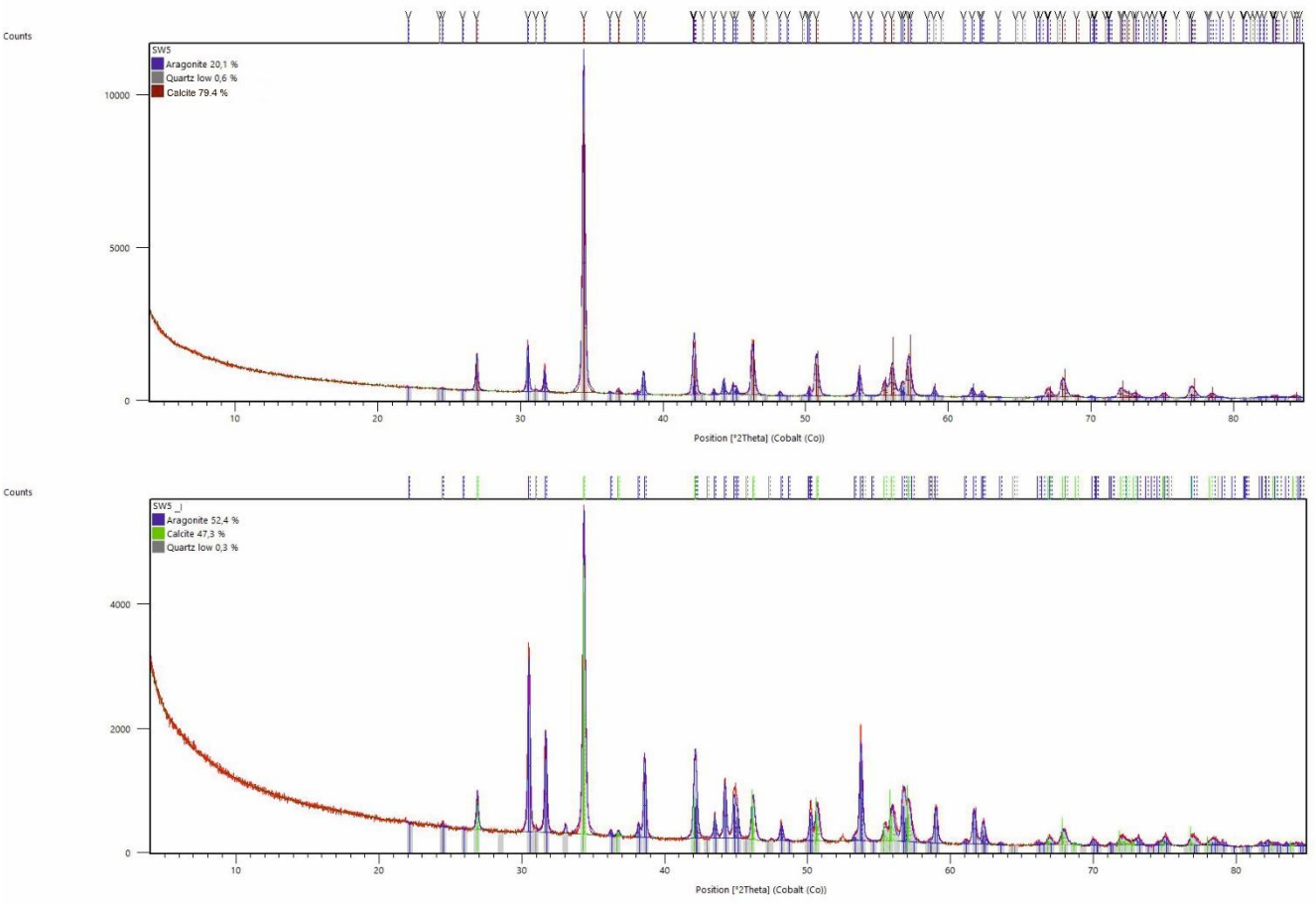

Figure B.5: *XRD-pattern of scale deposits SW5 and SW5_I. The top diffractogram shows the composition of the scale deposit SW5 (without PASP), while the lower diagram reveals the bulk composition of scale deposit SW5_I (with PASP).*

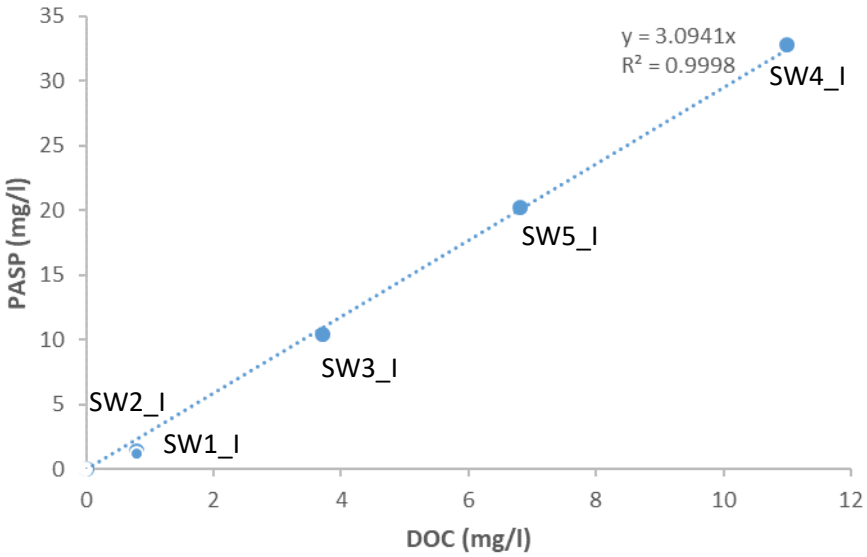

Figure C.1: *Plot of the PASP concentration (mg/l) vs. the DOC concentration (mg/l) measured in the drainage solutions showing that the two methods used are accurate.*

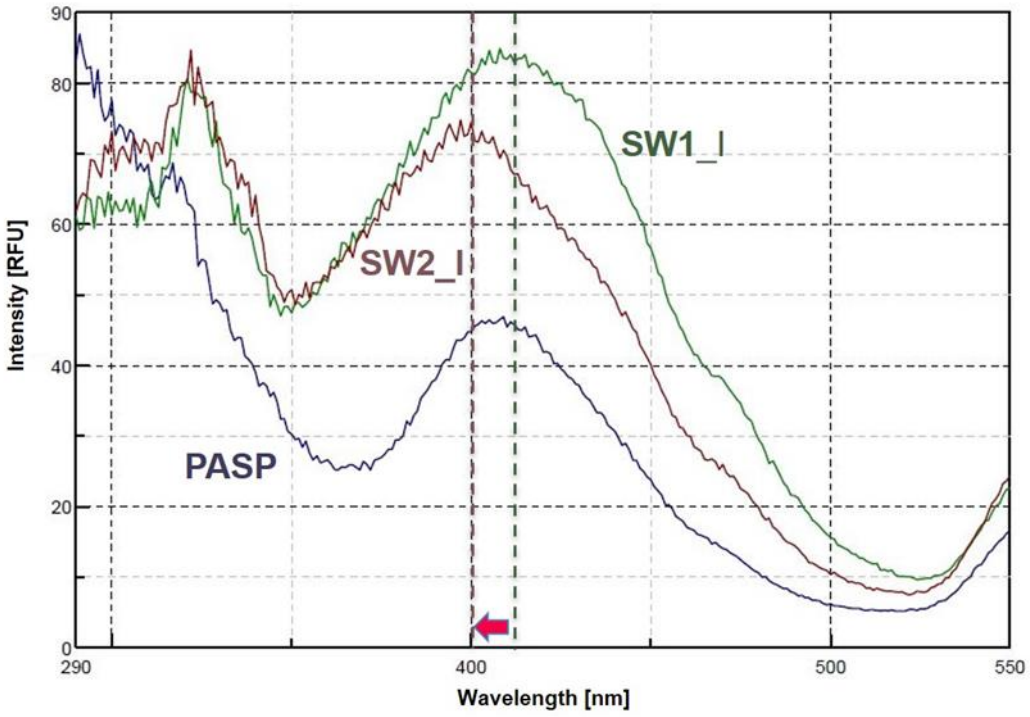

Figure D.1: *Synchronous fluorescence spectra obtained from an aqueous PASP standard solution (blue) and from the two drainage solutions SW1_I (green) and SW2_I (red). The main peak in SW2_I is shifted to a lower wavelength (red arrow), while the main peak of SW1_I corresponds to the PASP standard curve (green dotted line). This shift could indicate bacterial degradation of long-chained PASP polymers through the bacteria Leptothrix ochracea, which are predominant in SW2_I (e.g. Stedmon and Markager, 2005; Jalalvandi and Shavandi, 2018). RFU: Intensity measured in relative fluorescent units.*

References

Abdel-Aal, N., Sawada, K., 2003. Inhibition of adhesion and precipitation of $CaCO_3$ by aminopolyphosphonate. Journal of Crystal Growth, 256(1-2), 188-200.

Andreassen, J. P., 2005. Formation mechanism and morphology in precipitation of vaterite—nano-aggregation or crystal growth? Journal of Crystal Growth, 274(1-2), 256-264. https://doi.org/10.1016/j.jcrysgro.2004.09.090.

Baldermann, C., Baldermann, A., Furat, O., Krüger, M., Nachtnebel, M., Schroettner, H., Juhart, J., Schmidt, V., Tritthart, J., 2019. Mineralogical and microstructural response of hydrated cement blends to leaching. Construction and Building Materials, 229, 116902. https://doi.org/10.1016/j.conbuildmat.2019.116902.

Baldermann, A., Mittermayr, F., Bernasconi, S. M., Dietzel, M., Grengg, C., Hippler, D., Kluge, T., Leis, A., Lin, K., Wang, X., Zünterl, A., and Boch, R., 2020. Fracture dolomite as an archive of continental palaeo-environmental conditions. Communications Earth & Environment, 1(1), 1-12. https://doi.org/10.1038/s43247-020-00040-3.

Behrens, H., 1971. Untersuchungen zum quantitativen Nachweis von Fluoreszenzfarbstoffen bei ihrer Anwendung als hydrologische Markierungsstoffe. Geologica Bavarica, 64, 120-131.

Bischoff, J. L., Fitzpatrick, J. A., and Rosenbauer, R. J., 1993. The solubility and stabilization of ikaite ($CaCO_3 \cdot 6H_2O$) from 0 to 25 C: Environmental and paleoclimatic implications for thinolite tufa. The Journal of Geology, 101(1), 21-33. https://doi.org/10.1086/648194.

Boch, R., Dietzel, M., Reichl, P., Leis, A., Baldermann, A., Mittermayr, F., and Pölt, P., 2015. Rapid ikaite ($CaCO_3 \cdot 6H_2O$) crystallization in a man-made river bed: hydrogeochemical monitoring of a rarely documented mineral formation. Applied Geochemistry, 63, 366-379. http://dx.doi.org/10.1016/j.apgeochem.2015.10.003.

Boch, R., Leis, A., Haslinger, E., Goldbrunner, J.E., Mittermayr, F., Fröschl, H., Hippler, D., Dietzel, M., 2017. Scale-fragment formation impairing geothermal energy production: interacting H_2S corrosion and $CaCO_3$ crystal growth. Geothermal Energy 5 (1), 4, 1-19. https://doi.org/10.1186/s40517-017-0062-3.

Boch, R., 2019. Carbonates in natural and geotechnical settings - chemical sediments as environmental archives. Jahrbuch der Geologischen Bundesanstalt, 159, 67-130. https://www.zobodat.at/publikation_volumes.php?id=65659.

Brečević, L., Nielsen, A. E., 1989. Solubility of amorphous calcium carbonate. Journal of crystal growth, 98(3), 504-510. https://doi.org/10.1016/0022-0248(89)90168-1.

Busenberg, E., Plummer, L. N., 1985. Kinetic and thermodynamic factors controlling the distribution of SO_3^{2-} and Na^+ in calcites and selected aragonites. Geochimica et Cosmochimica Acta, 49(3), 713-725. https://doi.org/10.1016/0016-7037(85)90166-8.

Chan, C. S., Fakra, S. C., Emerson, D., Fleming, E. J., Edwards, K. J., 2011. Lithotrophic iron-oxidizing bacteria produce organic stalks to control mineral growth: implications for

biosignature formation. The ISME journal, 5(4), 717-727. https://doi.org/10.1038/ismej.2010.173.

Chan, C.S., McAllister, S.M., Leavitt, A.H., Glazer, B.T., Krepski, S.T., Emerson, D., 2016. The architecture of iron microbial mats reflects the adaptation of chemolithotrophic iron oxidation in freshwater and marine environments. Front. Microbiol. 7, 796. https://doi.org/10.3389/fmicb.2016.00796.

Chaussemier, M., Pourmohtasham, E., Gelus, D., Pécoul, N., Perrot, H., Lédion, J., Cheap-Charpentier, H., Horner, O., 2015. State of art of natural inhibitors of calcium carbonate scaling. A review article. Desalination, 356, 47-55. https://doi.org/10.1016/j.desal.2014.10.014.

Chen, Y., Cui, Y., Barrett, A.G., Chille, F., Lassalle, S., 2019. Investigation of calcite precipitation in the drainage system of railway tunnels. Tunn. Undergr. Space Technol. 84, 45–55. https://doi.org/10.1016/j.tust.2018.10.021.

Chhim, N., Haddad, E., Neveux, T., Bouteleux, C., Teychené, S., & Biscans, B., 2020. Performance of green antiscalants and their mixtures in controlled calcium carbonate precipitation conditions reproducing industrial cooling circuits. Water Research, 186, 116334.

Cornelius, H.P., 1952. Die Geologie des Mürztalgebietes – Jahrbuch der Geologischen Bundesanstalt, Sonderbände-04, 1–94.

Dissauer, J., Leitner, A., & Mittelbach, H., 2002. Tunnel Spital-Tunnelbau in schwierigen Verhältnissen/Tunnel Spital-Tunnelling in difficult conditions. Felsbau/Rock and Soil Enineering, 20(1).

Ehrenberg, C.G., 1836. Vorläufige Mitteilungen über das wirkliche Vorkommen fossiler Infusorien und ihre große Verbreitung. Poggendorff Ann 38, 213–227.

Eichinger, S., Boch, R., Leis, A., Koraimann, G., Grengg, C., Domberger, G., Nachtnebel, M., Schwab, C., Dietzel, M., 2020a. Scale deposits in tunnel drainage systems – A study on fabrics and formation mechanisms. Science of the Total Environment, 718, 137140. https://doi.org/10.1016/j.scitotenv.2020.137140.

Eichinger, S., Leis, A., Boch, R., Seywald, C., Dietzel, M., 2020b. Assessment and formation mechanisms of scale deposits in tunnels of the ÖBB-Infrastruktur AG – A subproject of the Task Force Drainage. Geomechanics and Tunnelling, 13(3), 273-285. https://doi.org/10.1002/geot.202000006.

Fairchild, I.J., Borsato, A., Tooth, A.F., Frisia, S., Hawkesworth, C.J., Huang, Y., McDermott, F., Spiro, B., 2000. Controls on trace element (Sr-Mg) compositions of carbonate cave waters: implications for speleothem climatic records. Chem. Geol. 166, 255–269. https://doi.org/10.1016/S0009-2541(99)00216-8.

Fleming, E. J., Cetinić, I., Chan, C. S., King, D. W., Emerson, D., 2014. Ecological succession among iron-oxidizing bacteria. The ISME journal, 8(4), 804-815. https://doi.org/10.1038/ismej.2013.197.

Fleming, E. J., Woyke, T., Donatello, R. A., Kuypers, M. M., Sczyrba, A., Littmann, S., Emerson, D., 2018. Insights into the fundamental physiology of the uncultured Fe-oxidizing bacterium Leptothrix ochracea. Applied and Environmental Microbiology, 84(9). https://doi.org/10.1128/AEM.02239-17.

Gao, Y., Liu, Z., Zhang, L., Wang, Y., 2010. Synthesis and performance research of biodegradable modified polyaspartic acid. In 2010 4th International Conference on Bioinformatics and Biomedical Engineering (pp. 1-4). IEEE.

Girmscheid, G., Gamisch, T., Klein, T., Meinlschmidt, A., 2003. Versinterung von Tunneldrainagen-Mechanismen der Versinterungsentstehung. Bauingenieur 292–300.

Götschl, K. E., Purgstaller, B., Dietzel, M., Mavromatis, V., 2019. Effect of sulfate on magnesium incorporation in low-magnesium calcite. Geochimica et Cosmochimica Acta, 265, 505-519. https://doi.org/10.1016/j.gca.2019.07.024.

Guo, X., Zhao, X., Xu, Y., Zhang, P., Cheng, Y., Xu, Y., 2020. The synthesis of polyaspartic acid derivative PASP-Im and investigation of its scale inhibition performance and mechanism in industrial circulating water. RSC Advances, 10(55), 33595-33601.

Hallbeck, L., Pedersen, K., 1991. Autotrophic and mixotrophic growth of Gallionella ferruginea. Microbiology, 137(11), 2657-2661. https://doi.org/10.1099/00221287-137-11-2657.

Hallberg, R., Ferris, F. G., 2004. Biomineralization by Gallionella. Geomicrobiology Journal, 21(5), 325-330. https://doi.org/10.1080/01490450490454001.

Han, Y. S., Hadiko, G., Fuji, M., Takahashi, M., 2006. Crystallization and transformation of vaterite at controlled pH. Journal of crystal growth, 289(1), 269-274. https://doi.org/10.1016/j.jcrysgro.2005.11.011.

Harer, G., 2017. Measures for the reduction of sinter formations in tunnels. In IOP Conference Series: Materials Science and Engineering (Vol. 236, p. 012071). IOP Publishing.

Hashimoto, H., Yokoyama, S., Asaoka, H., Kusano, Y., Ikeda, Y., Seno, M., Takada, J., Fujii, T., Nakanishi, M., Murakami, R., 2007. Characteristics of hollow microtubes consisting of amorphous iron oxide nanoparticles produced by iron oxidizing bacteria, Leptothrix ochracea. Journal of Magnetism and Magnetic Materials, 310(2), 2405-2407. https://doi.org/10.1016/j.jmmm.2006.10.793.

Hasson, D., Shemer, H., Sher, A., 2011. State of the art of friendly “green” scale control inhibitors: a review article. Industrial & Engineering Chemistry Research, 50(12), 7601-7607. https://doi.org/10.1021/ie200370v.

Huang, Y., Fairchild, I.J., 2001. Partitioning of Sr^{2+} and Mg^{2+} into calcite under karstanalogue experimental conditions. Geochim. Cosmochim. Acta 65 (1), 47–62. https://doi.org/10.1016/S0016-7037(00)00513-5.

Jalalvandi, E., and Shavandi, A., 2018. Polysuccinimide and its derivatives: degradable and water soluble polymers. European Polymer Journal, 109, 43-54. https://doi.org/10.1016/j.eurpolymj.2018.08.056.

Jamero, J., Zarrouk, S.J., and Mroczek, E., 2018. Mineral scaling in two-phase geothermal pipelines: Two case studies. Geothermics 72, 1-14. https://doi.org/10.1016/j.geothermics.2017.10.015.

Jia, N., Tassin, B., Calon, N., Deneele, D., Koscielny, M., Prévot, F., 2016. Scaling in railway infrastructural drainage devices: site study. Innovative Infrastructure Solutions, 1(1), 1-11. https://doi.org/10.1007/s41062-016-0042-7.

Jones, B., Renaut, R. W., Bernhart Owen, R., Torfason, H., 2005. Growth patterns and implications of complex dendrites in calcite travertines from Lýsuhóll, Snæfellsnes, Iceland. Sedimentology, 52(6), 1277-1301. https://doi.org/10.1111/j.1365-3091.2005.00742.x.

Jones, B., 2017. Review of Calcium Carbonate Polymorph Precipitation in Spring Systems. Sediment. Geol., 353, 64–75. https://doi.org/10.1016/j.sedgeo.2017.03.006.

Jung, H.-S., Han, Y.-S. Chung, S.-R., Chun, B.-S., and Lee, Y.-J., 2013. Evaluation of advanced drainage treatment for old tunnel drainage system in Korea. Tunnelling and Underground Space Technology, 38, 476-486. https://doi.org/10.1016/j.tust.2013.08.004.

Ketrane, R., Saidani, B., Gil, O., Leleyter, L., Baraud, F., 2009. Efficiency of five scale inhibitors on calcium carbonate precipitation from hard water: effect of temperature and concentration. Desalination 249 (3), 1397–1404. https://doi.org/10.1016/j.desal.2009.06.013.

Kirboga, S., Öner, M., 2012. The inhibitory effects of carboxymethyl inulin on the seeded growth of calcium carbonate. Colloids and Surfaces B: Biointerfaces, 91, 18-25. https://doi.org/10.1016/j.colsurfb.2011.10.031.

Kitamura, M., 2009. Strategy for control of crystallization of polymorphs. CrystEngComm, 11(6), 949-964.

Konopacka-Łyskawa, D., 2019. Synthesis methods and favorable conditions for spherical vaterite precipitation: a review. Crystals, 9(4), 223. https://doi.org/10.3390/cryst9040223.

Kukreja, D., Moran, P., 2004. Rehabilitation of the big walker mountain tunnel in Bristol, Virginia. In North American Tunneling 2004: Proceedings of the North American Tunneling Conference 2004, 17–22 April 2004, Atlanta, Georgia, USA (p. 381). CRC Press.

Kumar, A., 2012. Polyaspartic Acid - A Versatile Green Chemical. *Chem. Sci. Rev. Lett.*, *1* (3), 162–167.

Kumar, S., Naiya, T. K., Kumar, T., 2018. Developments in oilfield scale handling towards green technology-A review. Journal of Petroleum Science and Engineering, 169, 428-444. https://doi.org/10.1016/j.petrol.2018.05.068.

Li, H. Y., Ma, W., Wang, L., Liu, R., Wei, L. S., & Wang, Q., 2006. Inhibition of calcium and magnesium-containing scale by a new antiscalant polymer in laboratory tests and a field trial. Desalination, 196(1-3), 237-247.

Liu, Z., Sun, Y., Zhou, X., Wu, T., Tian, Y., Wang, Y., 2011. Synthesis and scale inhibitor performance of polyaspartic acid. *Journal of Environmental Sciences*, *23*, S153-S155.

Liu, D., Dong, W., Li, F., Hui, F., Lédion, J., 2012. Comparative performance of polyepoxysuccinic acid and polyaspartic acid on scaling inhibition by static and rapid controlled precipitation methods. Desalination, 304, 1-10. https://doi.org/10.1016/j.desal.2012.07.032.

Liu, S., Zhang, X., Gao, F., Wei, L., Liu, Q., Lü, H., & Wang, B., 2020. Two-dimensional flow field distribution characteristics of flocking drainage pipes in tunnel. Open Physics, 18(1), 139-148.

Lloyd, J. B. F., 1971. Synchronized excitation of fluorescence emission spectra. Nature physical science, 231(20), 64-65. https://doi.org/10.1038/physci231064a0.

Martinod, A., Neville, A., Euvrad, M., Sorbie, K., 2009. Electrodeposition of a calcareous layer: Effects of green inhibitors. Chemical Engineering Science, 64(10), 2413-2421. https://doi.org/10.1016/j.ces.2009.01.024.

Nayunigari, M. K., Gupta, S. K., Kokkarachedu, V., Kanny, K., Bux, F., 2014. Development of anti-scale poly (aspartic acid–citric acid) dual polymer systems for water treatment. Environmental technology, 35(23), 2903-2909. https://doi.org/10.1080/09593330.2014.925510.

Niedermayr, A., Köhler, S. J., Dietzel, M., 2013. Impacts of aqueous carbonate accumulation rate, magnesium and polyaspartic acid on calcium carbonate formation (6–40 °C). Chemical Geology, 340, 105-120. http://dx.doi.org/10.1016/j.chemgeo.2012.12.014.

Njegić-Džakula, B., Falini, G., Brečević, L., Skoko, Ž., Kralj, D., 2010. Effects of initial supersaturation on spontaneous precipitation of calcium carbonate in the presence of charged poly-l-amino acids. Journal of colloid and interface science, 343(2), 553-563. https://doi.org/10.1016/j.jcis.2009.12.010.

Parkhurst, D.L., Appelo, C.A.J., 2013. Description of Input and Examples for PHREEQC Version 3: A Computer Program for Speciation, Batch-reaction, One-dimensional Transport, and Inverse Geochemical Calculations (No. 6-A43). US Geological Survey. https://doi.org/10.3133/tm6A43.

Pedley, M., 2014. The morphology and function of thrombolitic calcite precipitating biofilms: A universal model derived from freshwater mesocosm experiments. Sedimentology, 61(1), 22-40. https://doi.org/10.1111/sed.12042.

Peronno, D., Cheap-Charpentier, H., Horner, O., & Perrot, H., 2015. Study of the inhibition effect of two polymers on calcium carbonate formation by fast controlled precipitation method and quartz crystal microbalance. Journal of Water Process Engineering, 7, 11-20.

Pervov, A.G., and Andrianov, A.P., 2017. Assessment of the effectiveness of new “green” scale inhibitors used in reverse-osmosis seawater desalination. Petroleum Chemistry, 57(2), 139-152. https://doi.org/10.1134/S0965544117020062.

Plummer, L. N., Busenberg, E., 1982. The solubilities of calcite, aragonite and vaterite in CO_2-H2O solutions between 0 and 90 C, and an evaluation of the aqueous model for the system $CaCO_3$-CO_2-H_2O. Geochimica et cosmochimica acta, 46(6), 1011-1040. https://doi.org/10.1016/0016-7037(82)90056-4.

Quan, Z., Chen, Y., Wang, X., Shi, C., Liu, Y., & Ma, C., 2008. Experimental study on scale inhibition performance of a green scale inhibitor polyaspartic acid. Science in China Series B: Chemistry, 51(7), 695-699.

Riechelmann, S., Schröder-Ritzrau, A., Wassenburg, J. A., Schreuer, J., Richter, D. K., Riechelmann, D. F., Terente, M., Constantin, S., Mangini, A., Immenhauser, A., 2014. Physicochemical characteristics of drip waters: influence on mineralogy and crystal morphology of recent cave carbonate precipitates. Geochimica et Cosmochimica Acta, 145, 13-29. https://doi.org/10.1016/j.gca.2014.09.019.

Rinder, T., Dietzel, M., Leis, A., 2013. Calcium carbonate scaling under alkaline conditions–case studies and hydrochemical modelling. Appl. Geochem. 35, 132–141. http://dx.doi.org/10.1016/j.apgeochem.2013.03.019.

Rodriguez-Navarro, C., Benning, L. G., 2013. Control of Crystal Nucleation and Growth by Additives. Elements, 9, 203-209. https://doi.org/10.2113/gselements.9.3.203.

Shen, Z., Zhi, X., Zhang, P., 2017. Preparation of fluorescent polyaspartic acid and evaluation of its scale inhibition for $CaCO_3$ and CaSO4. *Polymers for Advanced Technologies*, *28*(3), 367-372. https://doi.org/10.1002/pat.3897.

Shiraishi, F., Eno, Y., Nakamura, Y., Hanzawa, Y., Asada, J., Bahniuk, A. M., 2019. Relative influence of biotic and abiotic processes on travertine fabrics, Satono-yu hot spring, Japan. Sedimentology, 66(2), 459-479. https://doi.org/10.1111/sed.12482.

Spinthaki, A., Kamaratou, M., Skordalou, G., Petratos, G., Petrou, I., Tramaux, A., David, G., and Demadis, K.D, 2021. Searching for a Universal Scale Inhibitor: A Multi-Scale Approach Towards Inhibitor Efficiency. Geothermics, 89, 101954. https://doi.org/10.1016/j.geothermics.2020.101954.

Stedmon, C. A., and Markager, S., 2005. Tracing the production and degradation of autochthonous fractions of dissolved organic matter by fluorescence analysis. Limnology and Oceanography, 50(5), 1415-1426. https://doi.org/10.4319/lo.2005.50.5.1415.

Tuhela, L., Carlson, L., Tuovinen, O. H., 1997. Biogeochemical transformations of Fe and Mn in oxic groundwater and well water environments. Journal of Environmental Science & Health Part A, 32(2), 407-426. https://doi.org/10.1080/10934529709376551.

Wada, N., Kanamura, K., Umegaki, T., 2001. Effects of carboxylic acids on the crystallization of calcium carbonate. Journal of colloid and interface science, 233(1), 65-72. https://doi.org/10.1006/jcis.2000.7215.

Wedenig, M., Boch, R., Leis, A., Wagner, H., Dietzel, M., 2021. Green Inhibitor Performance against $CaCO_3$- Scaling: Rate-Modeling aided Test Procedure. Crystal Growth & Design. https://doi.org/10.1021/acs.cgd.0c01258.

Westphal, A., Eichinger, F., Eichinger, L., Würdemann, H., 2019. Change in the microbial community of saline geothermal fluids amended with a scaling inhibitor: effects of heat extraction and nitrate dosage. Extremophiles, 23, 283-304. https://doi.org/10.1007/s00792-019-01080-0.

Wierzbicki, A., Sikes, C., Madura, J., Drake, B., 1994. Atomic force microscopy and molecular modeling of protein and peptide binding to calcite. Calcified Tissue International 54, 133–141. https://doi.org/10.1007/BF00296064.

Wu, Y. T., Grant, C., 2002. Effect of chelation chemistry of sodium polyaspartate on the dissolution of calcite. Langmuir, 18(18), 6813-6820.

Xin, Z., Moon, J. H., Kim, Y. U., 2018. Reduction of adherent forces of sedimentous contaminants in tunnel drainage using vibrations from flexible and transparent organic films. KSCE Journal of Civil Engineering, 22(7), 2619-2622. https://doi.org/10.1007/s12205-017-0688-5.

Yang, Q., Liu, Y., Gu, A., Ding, J., Shen, Z., 2001. Investigation of calcium carbonate scaling inhibition and scale morphology by AFM. Journal of colloid and interface science, 240(2), 608-621. https://doi.org/10.1006/jcis.2001.7669.

Yang, M., Jin, X., Huang, Q., 2011. Facile synthesis of vaterite core-shell microspheres. Colloids and Surfaces A: Physicochemical and Engineering Aspects, 374(1-3), 102-107. https://doi.org/10.1016/j.colsurfa.2010.11.018.

Zhengshi, L., 2012. Chemical erosion under the conditions of tunnel lining concrete and drainage measures of defects prevention and treatment. Railway Construction Technology, (7), 90-93.

Chapter 6 - Use of green inhibitors for hardness stabilisation of tunnel drainage systems

Albrecht Leis[1], Hanns Wagner[2], Stefanie Eichinger[3], Gunnar Domberger[1], Michael Wedenig[3], Martin Dietzel[3], Ronny Boch[3]

[1] JR-AquaConSol GmbH, Steyrergasse 21, 8010 Graz, Austria.

[2]ÖBB-Infrastruktur AG, Streckenmanagement und Anlagenentwicklung, Fachbereich Bautechnik Tunnelbau, Europaplatz 2, 8020 Graz, Austria

[3] Institute of Applied Geosciences, Graz University of Technology & NAWI Graz GeoCenter, Rechbauerstrasse 12, 8010 Graz, Austria.

6.1 Abstract

The drainage system is a core element of tunnel construction and operation. Frequently, natural as well as technical boundary conditions lead to the deposition of scales (especially calcium carbonates) in the drainage system. As a preventive measure – in contrast to post-depositional cleaning procedures – the use of scale inhibitors to treat the drainage water (hardness stabilisation) is an option. 'Green inhibitors' are tailored green organic substances that delay or prevent scale formation when added in small concentrations. Moreover, green inhibitors can change the material consistency of scale deposits (soft sinter). An additional advantage of their use is the good environmental compatibility compared to conventional inhibitors. Suitable test procedures can be used to select a substance or product and evaluate or optimize its dosage. The application of polyaspartic acid or polysuccinimide products as ecologically harmless and readily biodegradable agents has proven advantageous in tunnel structures. The choice of liquid or depot stone conditioning essentially depends on the scaling mechanism, in addition to the technical considerations, flow rates and water chemistry. Regarding discharge to existing receiving water bodies, the inhibitor concentration in the water can be measured and controlled by DOC analysis and fluorescence spectroscopy. This article presents contemporary and tunnel-specific case studies.

6.2 Introduction

The formation of solid, mainly carbonate deposits in the drainage systems of underground construction works – known as scaling – presents a major challenge to the operation and

maintenance of tunnel systems and can lead to substantial costs for the tunnel operator [1–5]. Essentially, there are two processes involved in the formation of carbonate scale deposits:

– the interaction between the groundwater and the cement-bound building materials
– the precipitation of calcium carbonate due to the degassing of dissolved CO_2 from the drainage water to the atmosphere.

In the former process, the dissolution of alkaline materials within shotcrete, concrete drains, anchor mortar and cement grouting produces alkaline, mostly calcium-rich water. The corresponding increase in pH value and calcium concentration causes some of the dissolved calcium and carbonate to precipitate in the tunnel drainage system in the form of calcium carbonate. Very high pH levels (pH > 11) can further increase the rate of carbonate formation in the drainage system due to the additional absorption of atmospheric carbon dioxide by the calcium-rich, highly alkaline solutions, while weakly alkaline solutions can reduce it [6–8]. The second process responsible for the formation of carbonate scaling is the degassing of CO_2 from the drainage water to the tunnel atmosphere, causing an increase in the pH level and a redistribution of the dissolved carbonate species [9]. The targeted use of hardness stabilisers (inhibitors) has proved effective in reducing scaling in tunnel drainage systems [2, 7, 10, 11]. The main advantage of using these inhibitors as a preventive measure is that they can suppress scaling effectively and inexpensively even in very low doses. In addition to inhibiting the crystal growth of carbonate deposits, inhibitors can favourably alter their material consistency, often resulting in the formation of unconsolidated or even substantially softer, porous deposits [12]. These modified deposits can be removed by means of hydraulic flushing, thereby avoiding adverse mechanical wear of the drainage system.

6.3 Hardness stabilisation as a practical measure to reduce scaling

6.3.1 Green inhibitors and prevention strategies

Various options are available to the operators of tunnel construction works to minimise scaling. Some measures remove scale deposits retrospectively (post-sedimentary), while others are preventive (pre-depositional) and inhibit or reduce scaling. Hydraulic and mechanical methods are typically used to remove mineral deposits retrospectively. These are associated with high personnel costs and increased risk of damage to the drainage pipes due to the high mechanical stresses required to remove persistent deposits. Apart from optimising the design of the drainage system, hardness stabilisation is one of the most important preventive measures. The idea of

using hardness stabilisation for the targeted prevention of deposits in the drainage systems of construction works was patented in 1995 [13]. The advantage of hardness stabilisers is that they form specific bonds with seed crystals and carbonate mineral surfaces, thereby effectively inhibiting the precipitation (nucleation) of crystals and their further growth. The scale-inhibiting effect of hardness stabilisers works at very low concentrations of active ingredient in the sub-stoichiometric range to prevent calcification, unlike inorganic acids such as dilute hydrochloric acid. Water legislation requirements and increased environmental awareness in recent decades have resulted in the wider use of environmentally friendly inhibitors. Unlike conventional hardness stabilisers such as polyphosphates, phosphate esters and phosphonates, these are based on eco-toxicologically safe, biodegradable organic compounds and are thus referred to as green inhibitors [14, 15]. Most green inhibitors are synthetic organic polymers whose chemical structure is derived from naturally occurring organic compounds such as amino and fruit acids. Certain green inhibitors such as chitosan are derived directly from biopolymers. Due to their special structural characteristics and functional groups, e.g. amino and carboxyl groups, green inhibitors can inhibit the formation of seed crystals and reduce the growth of calcium carbonate deposits (Figure 1). Furthermore, as complexing agents they can keep a proportion of the calcium (Ca^{2+}) dissolved in the drainage water stably suspended in solution. Although this does not entirely prevent the precipitation process, it significantly inhibits it. Many green inhibitors are highly effective at preventing calcium carbonate scaling ($CaCO_3$) even when added in very small quantities (concentrations of 2 to 10 mg/l).

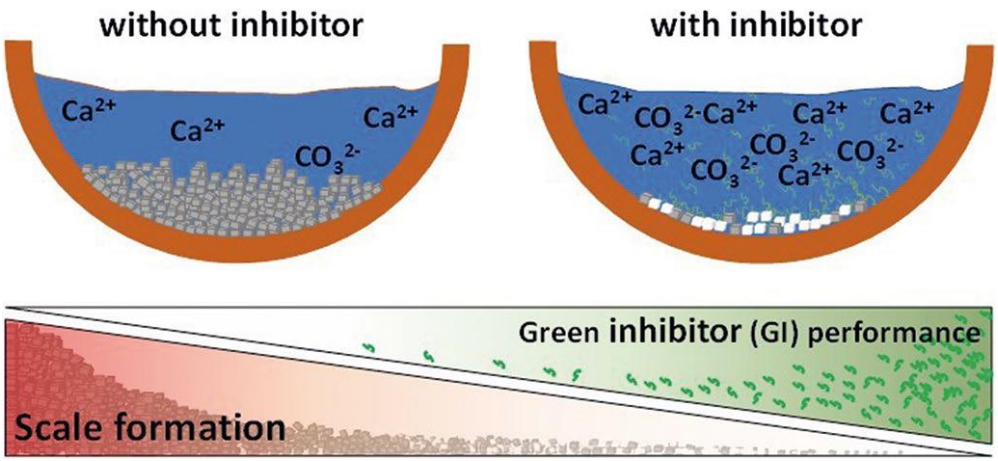

Figure 1: *Schematic view of the mode of action of green inhibitors in hardness treatment as a practical measure for reducing scaling in tunnel drainage systems. The upper left image shows the formation of strong, solidified carbonate scale (grey cubes) without inhibitor. On the right the situation in the presence of an inhibitor is visualised. The inhibitor prevents the formation of crystallisation nuclei and thus leads to a reduction of scale deposition and a beneficial change in the consistency of the scale deposits (formation of soft deposits; white cubes).*

In addition to various types of polyaspartic acid (PASP), the active ingredients currently used in green inhibitors also include polyepoxy succinic acid (PESA) and hydrolysed polymaleic anhydride (HPMA) as well as fruit acid derivatives obtained from ascetic, citric or lactic acid, and modified biopolymers such as carboxymethyl inulin (CMI) and the polysaccharide chitosan [14, 15]. Complexing agents such as tetrasodium N, N-bis(carboxylatomethyl)-L-glutamate ($GLDA\text{-}Na_4$) and tetrasodium iminodisuccinate ($IDS\text{-}Na_4$) are also used in some cases. Similar to IDS-Na4, the substance GLDA-Na4, which is derived from the amino acid glutamine, is used as a green substitute for the ecotoxic complexing agents EDTA and NTA. Polyacrylates such as polyacrylic acid (PAA), its sodium salt (PAAS) and the maleic acid-acrylic acid copolymer (MA-AA) are also widely used as substitutes for hardness stabilisers containing phosphorus, but due to the relatively poor degradability of these compounds, they are not strictly classed as green inhibitors. Current investigations using a new experimental test method in which the scale-inhibiting effect of four PASP products was compared with the performance of two other commercially available hardness stabilisers based on HPMA and MA-AA show that the PASP inhibitors are highly effective [16]. For this reason we will explore the characteristics and practical application of the polyaspartic acids and their derivates used as green inhibitors in tunnel drainage systems in more detail below.

6.3.2 Polyaspartic acid and polysuccinimide

6.3.2.1 Characteristics and use

PASPs are organic polymer compounds which are chemically derived from the amino acid aspartic acid (ASP). The manufacture of PASPs was first described by Hugo Schiff in 1897 [17]. Numerous methods of synthesizing PASP have been developed in the past few decades. As a result, it is apparent that the manufacturing process has a significant influence on the characteristics and structure of the polymers produced. This relates in particular to the molecular chain length, the degree of molecular crosslinking and the chemical purity [18]. The manufacture of PASP generally follows the same procedure. First a polysuccinimide (PSI) is produced by thermal condensation. This precursor is then converted to PASP by alkaline hydrolysis. Using the same principle, PSI can be formed into ‘solid tablets’ (PASP-release tabs) which are placed in tunnel drainage systems. These tablet-like stones release the scale-inhibiting agent PASP by hydrolysis of PSI. We will briefly explain the practical aspects of liquid and tablet conditioning agents in the next section.

6.3.2.2 Liquid versus tablet conditioning agents

Tablets stones release PASP by means of a chemical reaction (hydrolysis) in which the virtually insoluble polysuccinimide (PSI) in the stones is slowly converted to the highly water-soluble active substance PASP. The rate of PASP release depends on the conditions in the drainage system and increases as the pH value, flow rate and water temperature rise. The effectiveness of depot stones largely depends on the hydrogeological and hydrochemical boundary conditions and the technical design of the drainage system. In principle, the stones can be inserted in sections of the tunnel drainage that are at risk of scaling as a preventive measure. Although the relatively slow release of the active ingredient acts as a form of automated dosing, the amounts actually released in practice are virtually impossible to control and can occasionally increase significantly, leading to rapid depletion of the solid tablets. In addition, scale and detrital deposits can build up on the nets and netting tubes used to apply the PASP-release tabs, especially in areas where there is increased CO_2 degassing. This inhibits or prevents the continuous release of the hardness stabiliser to the extent that the unimpeded flow of ground and drainage water can no longer be assured. This process has been documented in tunnel construction works in Germany (Saukopf Tunnel) [10] and France (Marseille Tunnel, SNCF) [5]. Furthermore, tabs used in areas with increased microbiological activity are prone to biofilm development (biofouling, e.g. fungal attack). Unlike release tabs, liquid dosing systems can be precisely controlled and are therefore more versatile, especially for hardness stabilisation in longer drainage sections with medium to large volumes of water. Since PASP-release tabs are significantly more expensive than liquid PASP products in terms of the amount of active ingredients, it makes sense to use them where liquid dosing is not an option. For example, areas where small to medium volumes of slow-flowing water occur or sections of the drainage system that periodically dry up. Tabs can also be used preventively in the primary drainage system, e.g. in seepage slits, percolation packing and drainage holes, provided these are accessible and have an adequate cross-sectional area (pipe diameter).

6.3.2.3 Analytics and monitoring

To ensure efficient and cost-effective hardness stabilisation, it is important to control the PASP concentration in tunnel sections that are susceptible to scaling so as to avoid under- or overdosing. If the background organic load is known, the PASP concentration can be approximated by measuring the dissolved organic carbon (DOC) (Figure 2A). The PASP concentration can be calculated from the difference between the measured DOC concentration

(DOCA) and the background DOC concentration (DOCB) via the stoichiometric factor of the carbon fraction ($f_{C(PASP)}$ = 0.3609) in PASP $(C_4H_7NO_4)n$ using the following equation:

$$C_{PASP}(mg/l) = \frac{(DOC_A - DOC_B)}{0.3609} \quad (1)$$

This indirect calculation method is also suitable for determining the actual PASP concentration of commercially available products. Fluorescence spectroscopy is suitable for direct determination of the PASP concentration [18] as it is highly sensitive and permits the direct detection of PASP at very low concentrations. Measurement uncertainty (1σ) with this particularly sensitive synchronous scanning technology is around ±0.25 mg/l PASP [12]. The intensity of the measured fluorescence signal is proportional to the PASP concentration and can be calculated by calibration from a known concentration (Figure 2B). Due to its high level of accuracy, the measurement method can be used to optimise the dosage of liquid dosing systems or to check the actual PASP concentration of tab conditioning systems [17]. A combination of X-ray diffraction (XRD) and scanning electron microscopy (SEM) has proved an effective means of investigating the effect of green inhibitors on the composition and consistency of mineral deposits. While XRD investigations provide information about the mineralogical composition of the scale material, SEM images permit the visualisation of modified crystal growth caused by the use of green inhibitors in the micrometre range. This provides valuable additional information which improves our understanding of the mode of action of the inhibitor used [16] (Figure 2D and 2E).

6.3.2.4 Environmental compatibility

Green inhibitors are claimed to be ecologically and toxicologically safe. Unlike the conventional hardness stabilisers frequently used in geo-engineering, e.g. oil production and deep geothermics, PASP products are free from phosphorus (in the form of phosphate or phosphonate) and halogens (e.g. chlorine and bromine) and contain comparatively little nitrogen. Due to the very low dosage (usually < 20 mg/l), the use of PASP products does not cause any appreciable changes in pH, nor does it increase the organic load in the drainage water. Due to their special structure, PASP products are also highly biodegradable. Thus, it is virtually impossible for PASP to accumulate in the outfall drain as a result of hardness stabilisation within the tunnel.

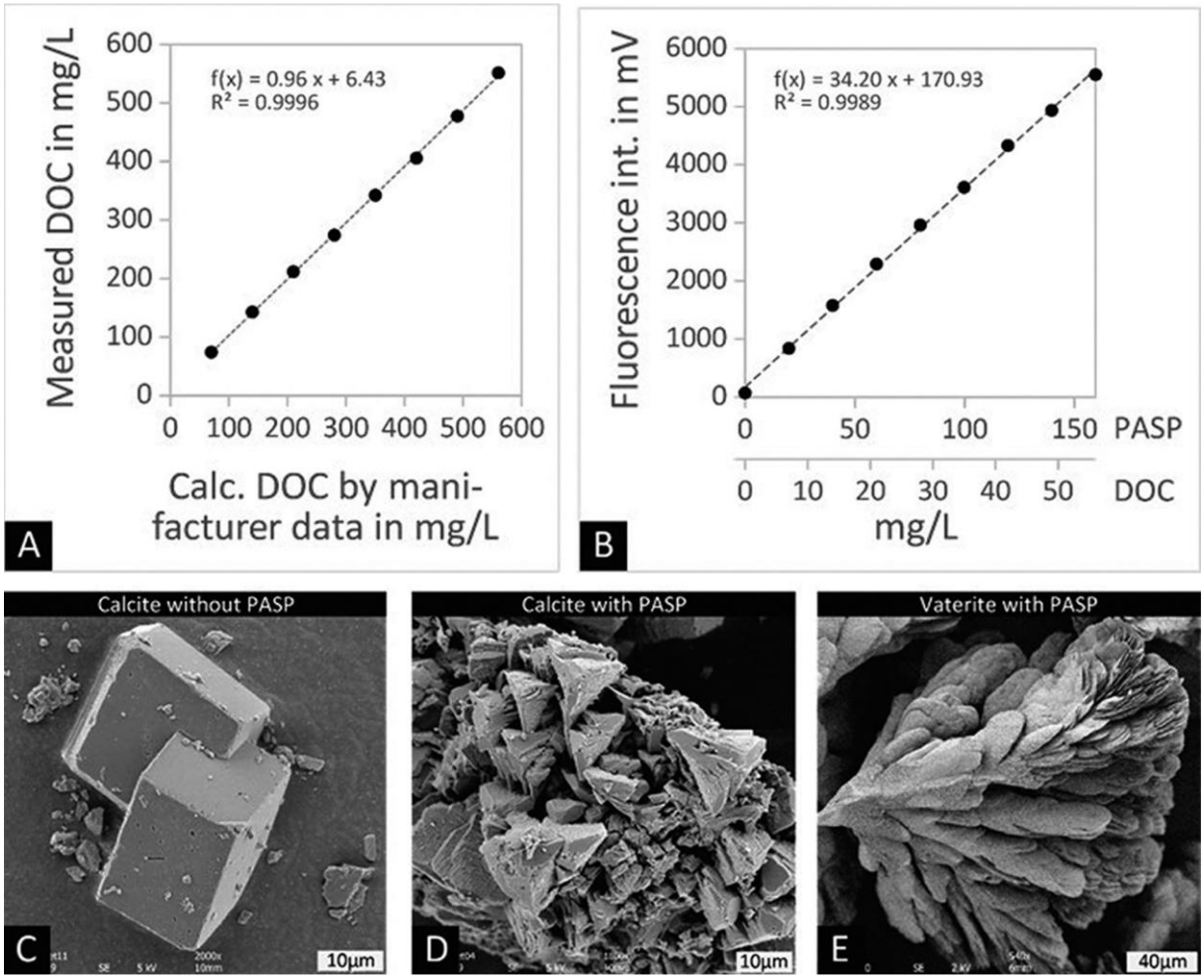

Figure 2: *A) Dilution series with the comparison of measured DOC concentration and DOC value calculated from molecular weight; B) fluorescence signal dependent on PASP/DOC concentration; C) rhombohedral calcite; D) skeletal calcite formed in the presence of PASP; E) vaterite formed in the presence of another PASP product.*

6.3.2.5 Test procedures and evaluation

A range of test protocols are available for investigating the effectiveness of hardness stabilisers. Most of these were developed to assess high-saline water in the oil and gas industry [19, 20] or for seawater desalination [21], with little consideration of the kinetic aspects of hardness stabilisation. However, kinetic reaction effects play a major role in the formation of scale deposits in tunnel drainage systems and must therefore be taken into account when assessing the effect of an inhibitor [17]. The new compact test described by Wedenig et al. [16] is one such method which was developed for the rapid, quantitative assessment of different active ingredients and products (Figure 3). In this approach, the experimental results of an in-situ

measurement (Figure 3A) are combined with results of a hydrochemical simulation calculation (Figure 3B) and jointly evaluated. This enables the chronological sequence of the precipitation reaction in the presence of a green inhibitor to be numerically modelled and the performance of the inhibitor to be assessed under variable hydrochemical boundary conditions. Using this test method, the effectiveness of different green inhibitors can be tested and then the most suitable product(s) selected on a case-by-case basis and dosed according to requirements.

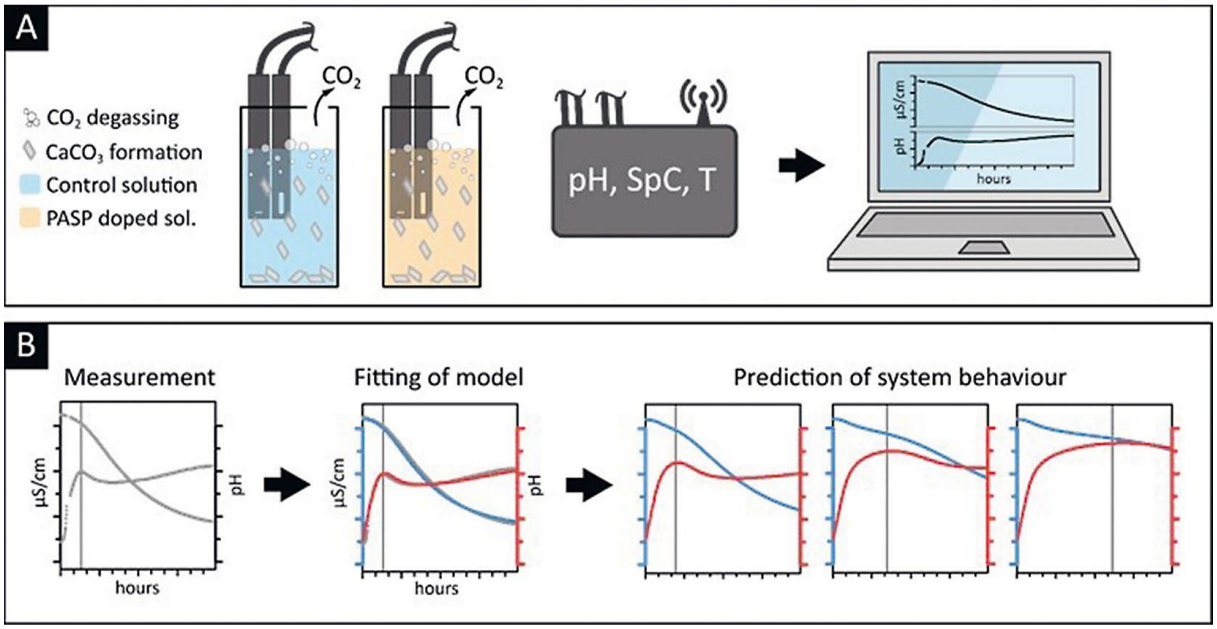

Figure 3: *A) Schematic plot of the experimental setup of the inhibitor compact test; B) Combined modelling approach where the experimental data are combined with the results of hydrochemical simulation calculations and jointly evaluated.*

6.4 Case studies for hardness stabilisation systems

6.4.1 Planned hardness stabilisation units in the drainage system of the Koralm Tunnel

The Koralm Tunnel drainage system is designed without conventional drainage pipes in the sidewalls. Instead, it relies on 40 mm thick dimpled membranes which is installed during the structural work, after which it is inaccessible. To maintain the integrity of the dimpled sheeting and to prevent scaling, the groundwater in areas with increased scaling potential is conditioned with hardness stabilisers. These inhibitors are dosed by hardness stabilisation plants installed in cross-passages that occur every 500 m. Water from the elevated tanks near the Leibenfeld and Paierdorf ventilation buildings is piped into the tunnel to supply these dosing units. Each hardness stabilisation unit treats a defined section (250 m) in one of the two tunnel tubes. The dosage mix comprising water and inhibitor is distributed within the corresponding treatment

zone by means of perforated hoses (DN32) with openings approximately every 10 m, which are laid behind the dimpled membranes (Figure 4).

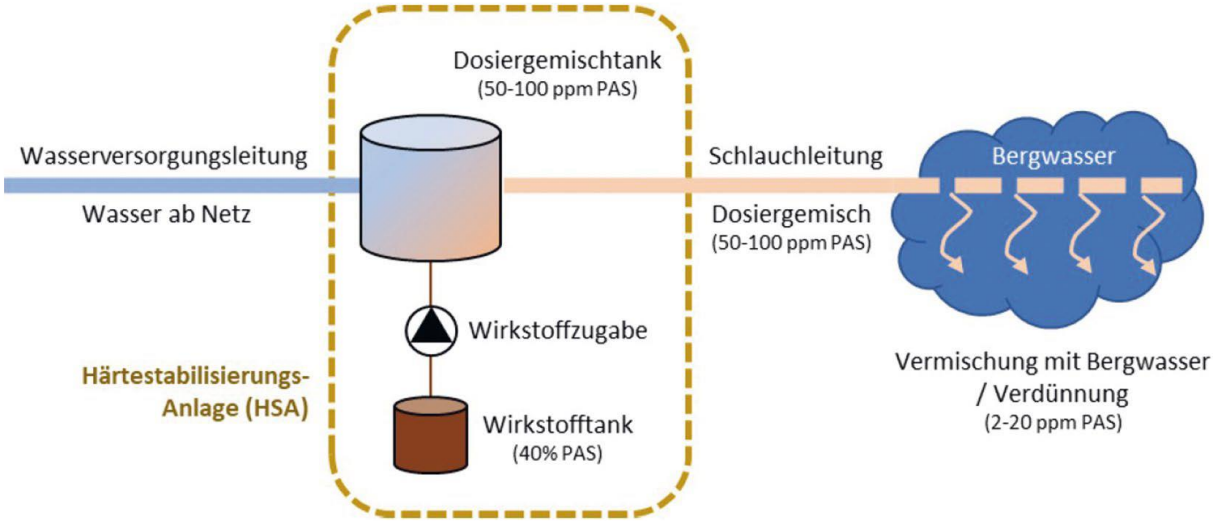

Figure 4: *Path of the inhibitor from the container to the distribution in the perforated hose.*

6.4.1.1 Decentralised hardness stabilisation plant

The decentralised hardness stabilisation units designed by the Swiss company F. Preisig AG during the planning phase and located in the cross-passages of the Koralm Tunnel consist of the following components:

– Water connection to the water supply in the tunnel

– Inhibitor storage tank and dosing pump

– Mixing tank

– Feed pump with dosing unit and hose connection.

Figure 5 shows a schematic diagram of this type of hardness stabilisation unit. The water supply line in track 1 supplies the approximately 0.2 l/s of water required by each unit. The double-walled tank has a usable volume of 250 l. The solenoid-diaphragm dosing pump mounted on the tank delivers up to 2 l of inhibitor solution per hour and is fitted with remote monitoring. Inside a mixing tank, the inhibitor solution is diluted with water to the target concentration. The mixing tank has a usable volume of 500 l. Once conditioned, the inhibitor solution is pumped into the distribution unit by a high-pressure pump at a rate of at least 1.5 l/s. The distribution

unit has a corresponding number of branches fitted with diaphragm valves, which supply the conditioned inhibitor solution to the individual hoses.

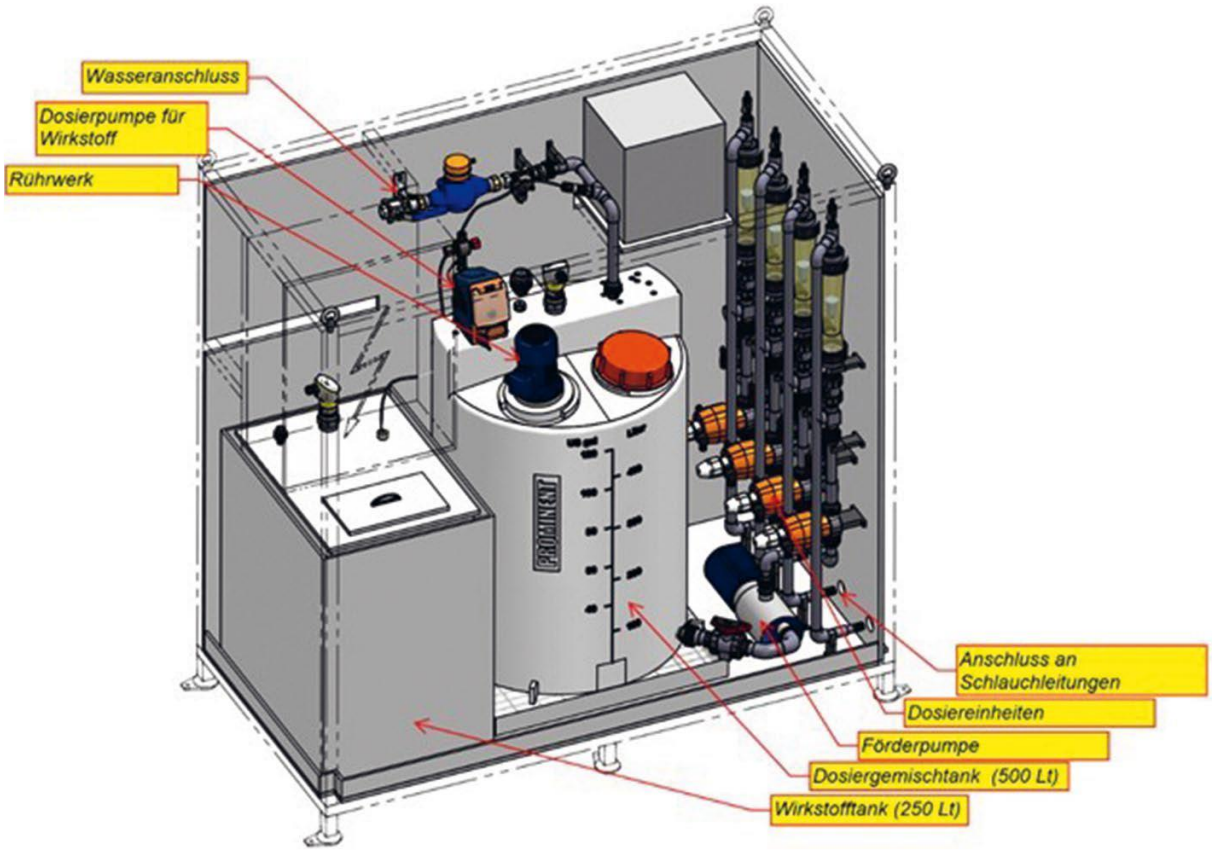

Figure 5: *Schematic drawing of the antiscalant dosing system in the Koralm Tunnel.*

6.4.1.2 Centralised hardness stabilisation plant

Subject to the necessary water supply line, it is also possible to inject the inhibitor solution centrally in the Koralm Tunnel. This is envisaged as a further adaptation, since the location of the two elevated tanks near the Leibenfeld and Paierdorf ventilation buildings enable a pre-conditioned inhibitor solution to be dosed from the surface. This option would simplify logistics (wheelbased, not dependent on the railway system) and optimise operation and maintenance. A centralised hardness stabilisation plant in the Koralm Tunnel is scheduled for construction from 2023, in parallel with the installation of a water supply line.

6.4.2 Hardness stabilisation pilot unit in the drainage system of the Semmering Tunnel Chain

Decentralised pilot plants for dosing the liquid PASP product Baypure DS 100 were installed in five recesses for maintenance work in the Spital and Steinhaus Tunnels which form part of the Semmering Tunnel Chain. The dosing units are located in areas where five monitoring stations (scale monitoring plants) have been installed to continuously monitor water temperature, electrical conductivity and pH value. Figure 6 shows a schematic diagram of the pilot plant and a photograph of the liquid dosing unit installed in a road tunnel recess. The precipitation behaviour of calcium carbonate deposits in the absence [12] and presence [11] of hardness stabilisation measures has been extensively investigated in drainage systems in recent years. These studies show that the use of PASP inhibitors can reduce precipitation by 60 to 85% [11].

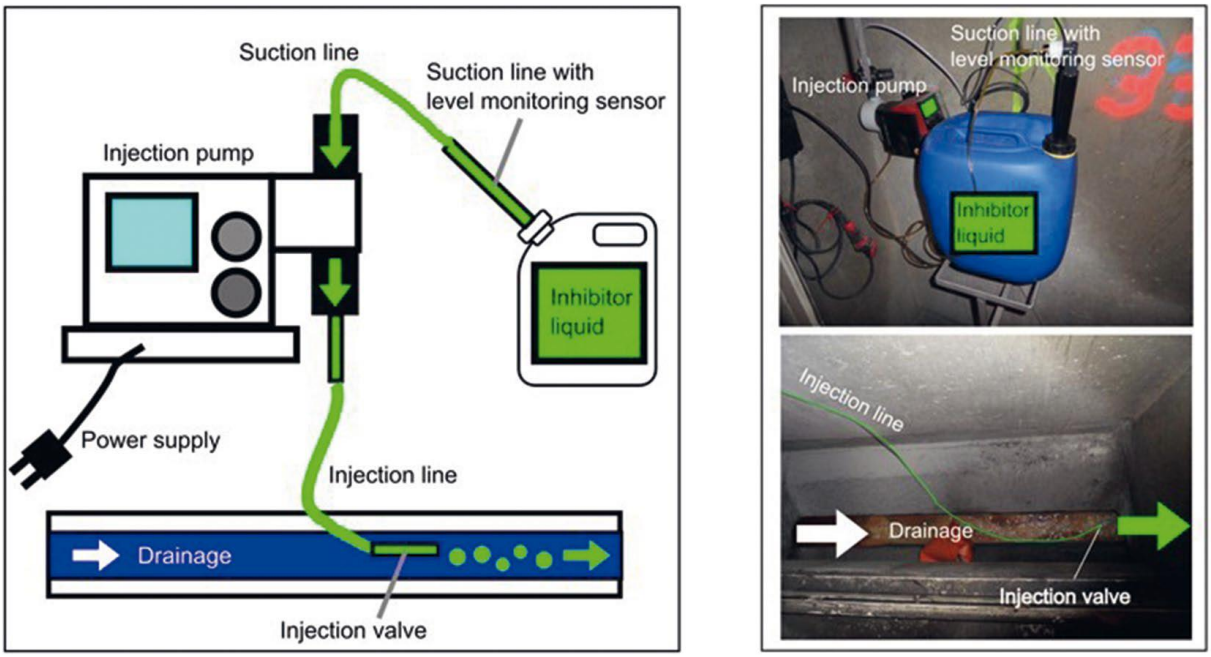

Figure 6: *Decentralised antiscalant dosing test unit in the tunnel chain Semmering: left) schematical drawing; right) installed unit.*

6.5 Conclusion and outlook

The use of green inhibitors can significantly reduce scale formation in tunnel drainage systems and have a positive effect on their material consistency (softer deposits). Among the commercially available green inhibitors, PASP-based products have proved particularly effective. They are available both in liquid form and in the form of solid tablets (PSI-release tabs). The PASP release mechanism in the tabs involves a chemical reaction in which the

polysuccinimide (PSI) contained within them is converted to PASP. All PASP products have one thing in common; as green inhibitors they biodegrade easily and completely, which makes them particularly eco-friendly. Suitable analytical methods are available to determine PASP concentrations in the drainage system and to characterize scale materials. A new compact test has been developed which is particularly suitable for determining the effectiveness of green inhibitors and current concepts and case studies on liquid conditioning from the Koralm Tunnel (rail tunnel) and in the Semmering Tunnel Chain (road tunnels) are being presented.

6.6 Acknowledgements

The authors would like to thank Roman Heissenberger and Manfred Stadlober (ÖBB-Infrastruktur AG) for their invaluable support with this paper. Thanks also go to colleagues Heimo Berghold, Walter Schaffenberger, Christian Schwab and Michel Steiner from ASFINAG (the Austrian federal agency responsible for constructing and operating motorways and expressways) for their help with the Semmering Tunnel Chain sections.

References

[1] Saxer, A.; Draschitz, C. (2006) *Versinterungsproblematik der Tunneldrainagen – Einfluss zementgebundener Tunnelbaustoffe* in Spritzbeton-Technologie 1, pp. 87–103.

[2] Gamisch, T.; Girmscheid, G. (2007) *Versinterungsprobleme in Bauwerksentwässerungen*. Berlin: Bauwerk.

[3] Dietzel, M.; Kieffer, S.; Schubert, W.; Schweiger, H. Semprich, S. (2008) (eds.) *Drainagesysteme im Tunnelbau: Design, Versinterung und Instandhaltung*. Mitteilungshefte Gruppe Geotechnik Graz 34.

[4] Harer, G. (2009) *Planerische Vorkehrungen zur Erzielung eines erhaltungsarmen Entwässerungssystems beim Koralmtunnel* in: Dietzel, Kieffer, Schubert, Schweiger, Semprich (eds.): *Drainagesysteme im Tunnelbau: Design, Versinterung und Instandhaltung.* pp. 1–14. Mitteilungshefte Gruppe Geotechnik Graz 34

[5] Chen, Y.; Cui, Y.; Barrett, A.G.; Chille, F.; Lassalle, (2019) *Investigation of calcite precipitation in the drain system of railway tunnels* in Tunnelling and Underground Space Technology 84, pp. 45–55.

[6] Dietzel, M. (1995) *13C/12C- und 18C/16O-Signaturen von Kalzit-Abscheidungen in Drainagesystemen* in Acta hydrochim. Hydrobiol, 23, no. 4, pp. 180–184.

[7] Dietzel, M.; Purgstaller, B.; Leis, A.; Reichl, P.; Stadler, H.; Niedermayr, A.; Rinder, T.; Wagner, H. (2013) *Current challenges for scaling of tunnel drainage systems–Modelling approaches, monitoring tools and prevention strategies/ Aktuelle Herausforderungen bei der*

Versinterung von Tunneldränagen–Modellierungsansätze, Monitoringwerkzeuge und Präventionsstrategien in Geomechanics and Tunnelling 6, no. 6, pp. 743–753. https://doi.org/10.1002/ geot.201310014.

[8] Rinder, T.; Dietzel, M.; Leis, A., (2013) *Calcium carbonate scaling under alkaline conditions–case studies and hydrochemical modelling* in Appl. Geochem. 35, pp. 132–141.

[9] Eichinger, S.; Leis, A.; Boch, R.; Seywald, C.; Dietzel, M. (2020) *Assessment and formation mechanisms of scale deposits in tunnels of the ÖBB-Infrastruktur AG – A subproject of the Task Force Drainage/Bewertung von Sinter und deren Bildungsbedingungen in Tunnelbauwerken der ÖBBInfrastruktur AG – Ein Teilprojekt der Task Force Drainage* in Geomechanics and Tunnelling 13, no. 3, pp. 273–285. https://doi.org/10.1002/geot.202000006.

[10] Vollmann, G. (2005) *Zur Härtestabilisierung als versinterungsreduzierende Maßnahme für Tunneldränagesysteme*. Cuvillier, Göttingen.

[11] Eichinger, S.; Boch, R.; Leis, A.; Baldermann, A.; Domberger, G.; Schwab, C.; Dietzel, M. (2022) *Green inhibitors reduce unwanted calcium carbonate precipitation: Implications for technical settings* in Water Research 208, 117850.

[12] Eichinger, S.; Boch, R.; Leis, A.; Koraimann, G.; Grengg, C.; Domberger, G.; Nachtnebel, M.; Schwab, C.; Dietzel, M. (2020) *Scale deposits in tunnel drainage systems–A study on fabrics and formation mechanisms* In Science of the total environment 718, 137140.

[13] Wegmueller, M.C., (1995) *Verfahren zur Härtestabilisation von Bergwasser in Entwässerungssystemen* Patentschrift CH 686040 A5, Switzerland.

[14] Hasson, D.K.; Shemer, H.; Sher, A., (2011) *State of the Art of Friendly "Green" Scale Control Inhibitors: A Review Arin Industrial & Engineering Chemistry Research 50,* no. 12, pp. 7601–7607.

[15] Chaussemier, M.; Pourmohtasham, E.; Gelus, D.; Pécoul, N.; Perrot, H.; Lédion, J.; Cheap-Charpentier, H.; Horner, O. (2015) State of art of natural inhibitors of calcium carbonate scaling. A review article in Desalination 356, pp. 47–55.

[16] Wedenig, M.; Boch, R.; Leis, A.; Wagner, H.; Dietzel, M. (2021) *Green Inhibitor Performance against $CaCO_3$ Scaling:* Rate-Modeling Aided Test Procedure in Crystal Growth & Design 21, no. 4, pp. 1959–1971.

[17] Schiff, H. (1897) *Ueber Polyaspartsäuren* in Berichte der deutschen chemischen Gesellschaft 30, no. 3, pp. 2449–2459.

[18] Klein, T.; Moritz, R.J.; Graupner, R. (2012) *Polyaspartates and Polysuccinimide,* Ullmann's Encyclopedia of Industrial Chemistry. Weinheim: Wiley-VCH.

[19] Wedenig, M.; Eichinger, S.; Boch, R.; Leis, A.; Wagner, H.; Dietzel, M. (2022) *Understanding of Tunnel Drainage Scale Formation by In-Situ Monitoring* (under review in Tunnelling and Underground Space Technology).

[20] NACE International (2007*) Laboratory screening tests to determine the ability of scale inhibitors to prevent the precipitation of calcium sulfate and calcium carbonate from solution (for oil and gas production systems).* National Association of Corrosion Engineers, Houston.

[21] Kumar, S.; Naiya, T.K.; Kumar, T. (2018*) Developments in oilfield scale handling towards green technology* – A review in Journal of Petroleum Science and Engineering 169, pp. 428–444.

[22] Pervov, A.G.; Andrianov, A.P.; Danilycheva, M.N. (2017*) Preliminary evaluation of new green antiscalants for reverse osmosis water desalination* in Water Supply 18, no. 1, pp. 167–174.

Chapter 7 - Research on optimized polymer-pipe materials for use in tunnel drainage systems

7.1 Optimized Polymer Pipe Materials for Efficient Drainage Systems in Tunnel Structures – PolyDrain I + II

7.1.1 Abstract

Keeping tunnel drainage systems operational requires to deploy less expensive and time-consuming maintenance procedures. Therefore, the inter-disciplinary research project "PolyDrain" was initiated. Aim of this project was to develop modified polymers which can reduce the precipitation of scale deposits in tunnel drainage pipes. Based on this issue the chosen approach is based on modifying the polymer matrix of drainage pipes by adding active fillers to obtain a final composite material. Accordingly, the durability of pipes can be increased and/or the precipitation can be reduced in the drainage, including areas of drainage slits. Thus, 7 different compounds, consisting of a polyethylene base polymer and active fillers were developed. However, before these findings can be applied in large scale reality, further long-term evaluations—also in the lab—are necessary. Thus, the developed compounds were processed into specimens and exposed to drainage-waters both in laboratory as well as field tests in actual tunnels. Subsequently, $CaCO_3$ precipitations on the materials were analysed using chemical and optical methods. Regarding the efficacy, especially the compounds with polyethyleneglycol and zeolite proved to be very promising.

7.1.2 Introduction

Drainage systems are used in pressure-relieved tunnel structures for the continuous drainage of the accumulating groundwater. Until the second half of the 20th century, brick invert channels were mostly used for water drainage. Since the 1990s, however, pipes made of thermoplastic materials have been used exclusively. In the Austrian road and railway network there are currently tunnels with a length of approximately 650km, whereby most tunnels are equipped with drainage systems. For the ÖBB alone, there are currently about 445km of drainage tunnels. In 2027, due to the current construction activity, there will be approximately 1081 km. Together with the tunnels of ASFINAG and the federal provinces, there are currently well over 1000 km of tunnel drainage systems in Austria. However, for geogenic reasons and/or due to building materials used during construction, mineral precipitations, called scale deposits, occur in the

drainage systems. To ensure the functionality of the structures, these drainages must therefore be regularly maintained and cleaned. Especially in the case of scale deposits that are difficult to remove, the effort of cleaning drainage pipes can increase exorbitantly, which not only leads to higher maintenance costs, but also to a limited availability of tunnel sections as well as possible damage to the drainage systems. The concrete aim of this work was therefore to modify plastics that could be used for future drainage pipes in tunnel structures in such a way that the tendency to form scale deposits is lower. Since the cleaning of drainage pipes by high-pressure flushing or other methods is very time-consuming and cost-intensive, the structures could be operated more efficiently overall in this way (Schachinger et al., 2018, 2019).

7.1.3 Scale deposits in tunnel drainage systems

7.1.3.1 Formation of scale deposits

The formation of carbonate scale deposits is based on the one hand on the degassing or absorption of CO_2 from or into the drainage solution, but on the other hand also on the mineralogical composition and alkaline property of the concrete in the tunnel structure, whereby here essentially the dissolution of the mineral portlandite ($Ca(OH)_2$) in the shotcrete plays an important role (Dietzel et al., 2008a, b, 2013; Rinder et al., 2013). The intensive contact of water with cementitious materials significantly changes the properties and chemism of the drainage solution, generating alkaline, mostly calcium-rich drainage solutions, which can lead to an increased sintering potential in the tunnel drainage systems (Rinder et al., 2013). Furthermore, the geology and mineralogical composition of the surrounding rocks in the aquifer also have an impact on the groundwater chemistry and thus on the possible sintering potential in the tunnel, as well as mixed water formations and flow characteristics (turbulent vs. laminar flow vs. stagnant condition, Fig. 1; Dietzel et al., 2008a; Rinder et al., 2013; Wu et al., 2019).

7.1.3.2 Cleaning procedures of drainage pipes

In order to maintain the functionality of the tunnel structure, the drainages must be cleaned regularly according to the systematics in the guideline "Tunnel drainage" of the Austrian Association for Concrete and Civil Engineering (Österreichische Vereinigung für Beton- und Bautechnik, 2010). Depending on the material consistence of the scale deposits, either hydraulic (high-pressure flushing), hydromechanical (e.g. vibrating nozzle), or mechanical (chain spinner, milling cutter, percussion drill) cleaning processes can be used. In the case of very intensive cleaning processes, the surfaces of the installed drainage pipes may be attacked or even destroyed (Fig. 2). Drainage pipes in tunnel structures cannot simply be replaced due to

their location in the tunnel, which is why, in the event of damage, parts of the entire tunnel wall including the sealing and seepage packing must be removed, as there are currently no trenchless rehabilitation methods available.

Figure 1: *Removal of scale deposits in a railway tunnel and the different visual appearance (e.g. chemical composition, coloring, consistency) of deposits in tunnel drainages.*

Figure 2: *Camera inspection after intensive cleaning processes in the Sieberg tunnel - complete destruction of the pipe wall (a), or local destruction of the drainage layer after intensive mechanical cleaning (b).*

Due to the urgency of this topic, possibilities to reduce scale deposit formation in tunnel structures have been investigated for several years (Girmscheid et al., 2003; Wagner et al., 2014; Schachinger et al., 2017, 2018; Zhou et al., 2018). Hardness stabilisers" are currently being used in various tunnels to support cleaning. These are low-dose additions of various

chemical agents in solid and liquid form to the drainage water which are intended to either reduce existing scale deposits, slow down, inhibit or prevent the precipitation of unwanted scale deposits (Galli, 2000; Girmscheid et al., 2003; Vollmann, 2005; Stur et al., 2015; Zhou et al., 2018). A disadvantage of this method, however, is that the applicable environmental regulations require a great deal of effort in terms of control and documentation of the change in water chemistry. In addition, liquid hardness stabilisers currently only work in the bottom of the pipe and not in the area of the drainage slots.

7.1.4. Project PolyDrain

Based on the experiences described above, a research project supported by ÖBB Infrastruktur AG, ASFINAG and BMVIT was launched in 2017 to concern with the material of the drainage pipes. The primary goal of this "PolyDrain" project is to further develop the plastics used for the production of drainage pipes in order to achieve a reduced tendency to scale deposit formation. Experts from the fields of tunnel construction, geology and hydrogeology, hydrochemistry and mineralogy, material sciences and polymer chemistry were brought together to work on this complex and interdisciplinary issue.

7.1.4.1 Material development

There are two ways to optimize the properties of plastics used in drainage pipes. Either active fillers are incorporated into the plastic, or the surfaces of the pipes themselves are modified. Due to the mechanical cleaning methods currently used for tunnel drainage pipes, which have been proven to attack surfaces, the way of mixing in fillers is therefore considered to be advantageous. To test the effectiveness of the fillers in a plastic matrix, they were mixed into a commercially available material (polyethylene) and formed into compounds using a kneader and plate press. Cylindrical test specimens with a diameter of 10 mm were taken from these plates for further investigations. All 7 selected und tested plastics are formulated in Table 1.

Table 1: *Material formulations investigated to test their effectiveness with regard to the tendency to form scale deposits.*

TABELLE 1
Untersuchte Materialrezepturen zur Überprüfung ihrer Wirksamkeit hinsichtlich der Versinterungsneigung

Matrix	Füll- bzw. Wirkstoff	Kennung	Wirkungsmechanismus
PE-HD Rohrmaterial (PE100)	–	PE	Benchmark
	4% Silan +0,5% Peroxid	PE + Silan & Peroxid	Oberflächenpolarität
	4% Polyethylen-Glykol Copolymer	PE + PEG	Oberflächenpolarität
	4% Natriumstearat	PE + Na-Stearat	Chem. Puffer im sauren Bereich
	4% Ammonium-polyphosphat	PE + Amm.Phosphat	Chem. Puffer im sauren und basischen Milieu
	4% Stearinsäure	PE + Stearinsäure	Chem. Puffer im basischen Bereich
	4% Zeolith [a]	PE + Zeolith	Ionen-Tauscher
	4% $Mg(OH)_2$ [b]	PE + $Mg(OH)_2$	Ionen-Tauscher

[a] Inzeo 15/5, Paltentaler Splitt- & Marmorwerke GmbH
[b] Magnifin H-10, Martinswerk GmbH

7.1.5 Experiments

In order to test the effectiveness of the developed compounds under conditions that are as real as possible, different test methods, in which scale deposits should occur on the samples, were selected and carried out in the laboratory under controlled conditions as well as in real tunnel structures.

7.1.5.1 Dynamic tests

Dynamic tests include all experiments in which a continuous flow of water flows over the exposed compounds. This includes both the laboratory test described in the following, as well as deposits in real tunnel drainage systems. Figure 3 and 4 show the experimental test setup, which was developed at the TU-Graz.

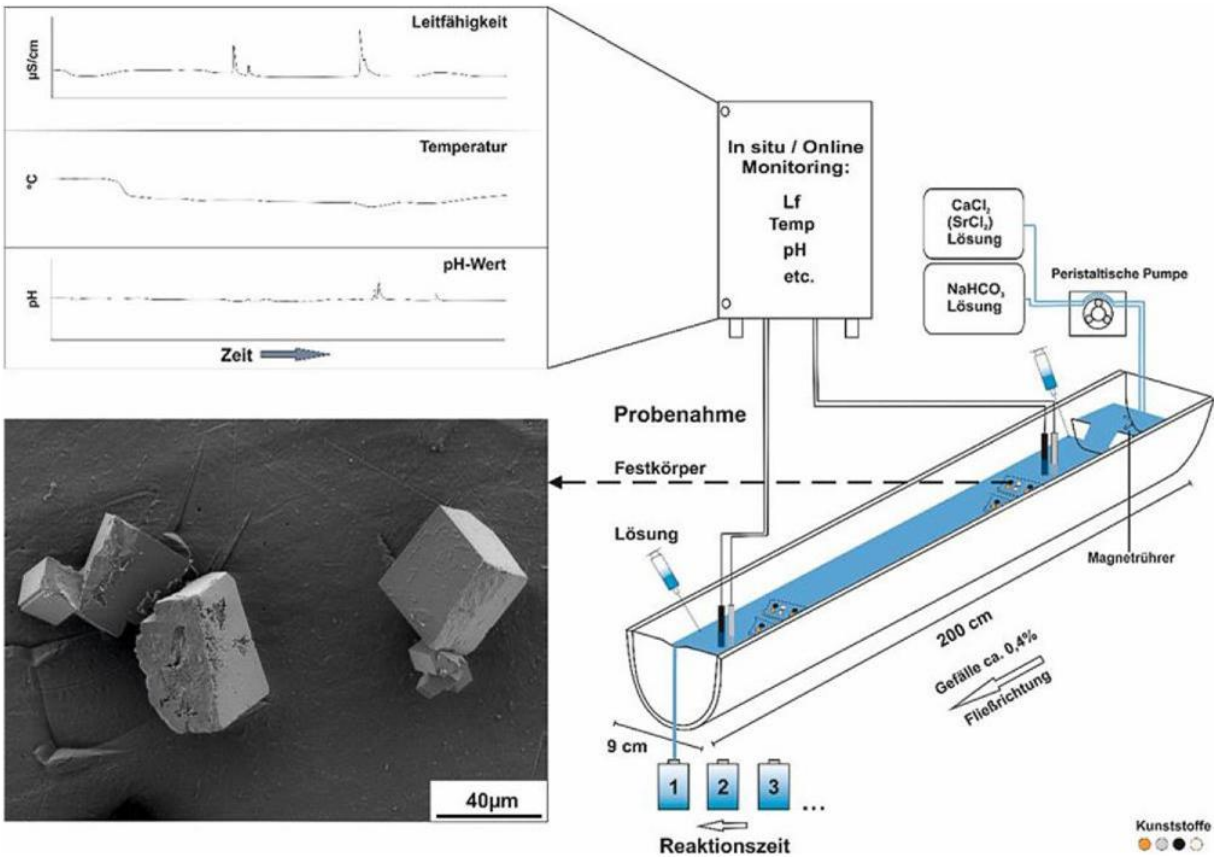

Figure 3: *Experimental setup for determining the variable sintering behaviour under dynamic conditions, including continuous measurement of electrical conductivity, temperature and pH value.*

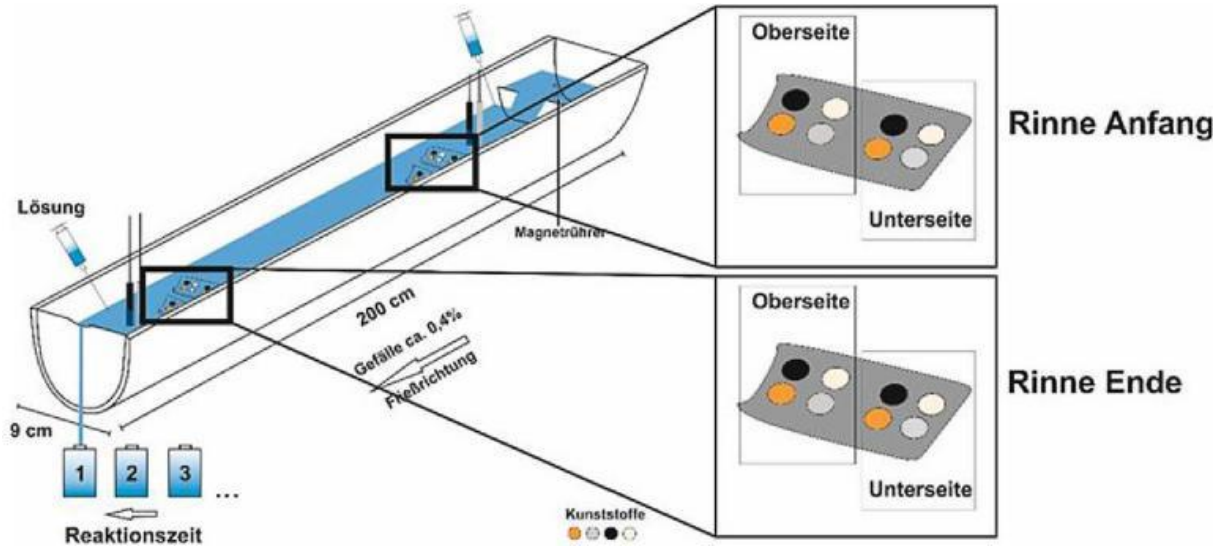

Figure 4: *Detailed image of the dynamic experimental setup including illustration of the different observation possibilities of scale deposit formation.*

The test setup simulates the precipitation of calcium carbonate minerals from a solution supersaturated with these minerals on a laboratory scale. The focus of the investigations is on the crystallization of calcium carbonate minerals on the surface of individual plastics. The chemical composition, temperature and flow rate of the test solution are selected in such a way that carbonate precipitation occurs within minutes to several days. For this purpose, a test water (reaction solution) is continuously generated by mixing, for example, a 10 millimolar (mM) $CaCl_2$ + 0.1 mM $SrCl_2$ stock solution with a 10 mM $NaHCO_3^-$containing stock solution and this mixed reaction solution is drained over a 2 m long flow section via laminar flow, whereby the flow rate is about 9 ml/min (see Fig. 3). The duration of the experiment in this approach was 10 days at a constant water temperature of 20°C and an initial pH value of 8.0± 0.1. In this laboratory-designed test setup, the practice-relevant parameters, such as pH value, solution contents and temperature, as well as the spatiotemporal development of the composition of the solution and the carbonate deposits on the plastic surfaces along the flow section are investigated in-situ and via sampling and subsequent hydro- and material-chemical analyses. The plastics to be tested were introduced into the solution at the beginning and end of two parallel flow paths in specially made sample holders (Fig. 4). The latter allow a differentiation between mineral growth and mineral growth with mineral sedimentation (heterogeneous versus homogeneous crystal nucleation). While the precipitates on the upper side of the individual plastics in the solution could also have been formed by mineral sedimentation by crystals in suspension, the precipitates formed on the lower side of the individual plastics grew exclusively on the individual plastics. All results in this paper therefore always refer to the underside of the samples examined.

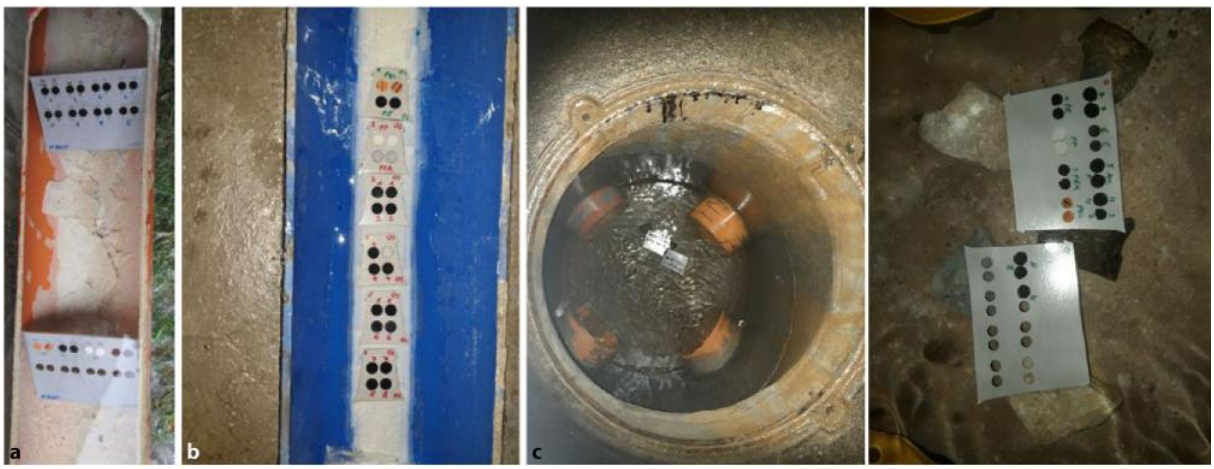

Figure 5: *Depositing the plastic samples at the drainage systems of the Steinhaus tunnel (a), Lainzer Tunnel (b) and Zentrum am Berg (c).*

In comparison to these laboratory tests under controlled conditions, additional tests were carried out in three real tunnel structures. For this purpose, the 7 plastic compounds, as shown in Fig. 5a-c, were exposed in the tunnels Steinhaus, Lainzer Tunnel and at the Zentrum am Berg and subsequently examined.

7.1.5.2 Stationary tests

In order to also investigate the influence of stagnant water and supersaturated with calcium carbonate, samples (rectangular geometry - 40 × 25 mm^2 for larger surfaces for quantitative evaluation) were also exposed in a stationary reactor in a second test setup at the TU-Graz (Fig. 6). The experimental setup was designed in the same chemical composition as in the dynamic experiments before to ensure comparability of the individual experiments. The tendency of the plastics to form scale deposits was investigated under stationary conditions (instead of dynamic conditions in the flow section). Under steady-state conditions, the rectangular plastics are fixed using Nie-Roster screws to prevent floating in the water column in a 1-litre reactor. 4 plastic samples were exposed per reactor. A magnetic stirrer with stir bars (400 rpm) ensured moderate but continuous water circulation in the reactor (Fig. 6). The duration of the experiment was 7 days.

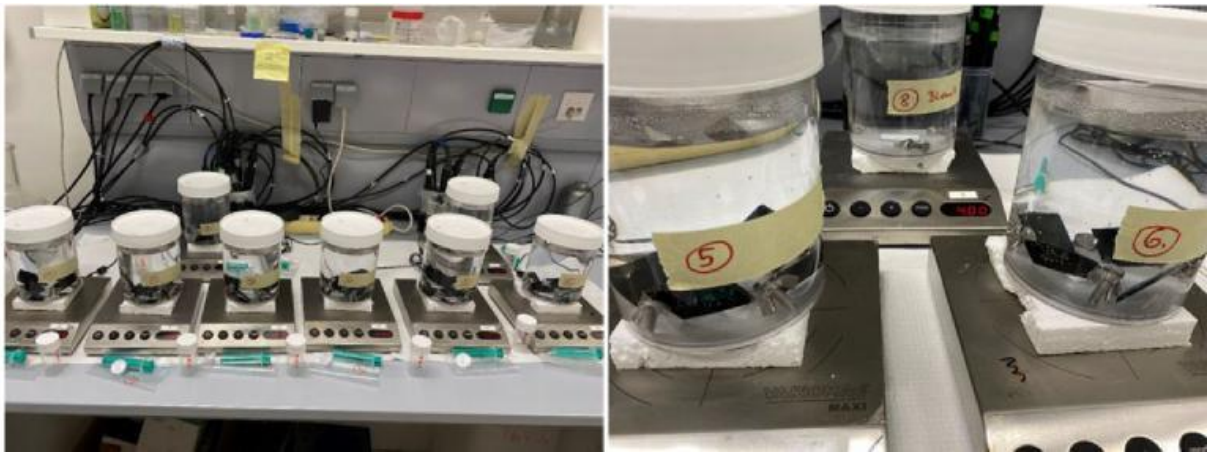

Figure 6: *Test reactors for the storage of larger test samples under stationary conditions at the TU Graz.*

7.1.5.3 Evaluation & Assessment

Two different evaluation methods were used to assess the effectiveness of the developed compounds against scale deposit formation. On the one hand, a chemical analysis by means of acid digestion and on the other hand an optical analysis of the covered surface were carried out.

Acid digestion was carried out separately for each plastic in order to determine the amount of precipitates formed on the respective plastic surface (mg/cm^2) via the calcium concentration, and to rank the plastics in terms of their efficiency against scale deposit formation. For this purpose, the calcium carbonate minerals formed during the tests were dissolved in 6% HNO_3. Subsequently, the calcium concentration was determined, converted to the absolute amount and the plastic was evaluated. In addition, microscopy-based images of the plastic surfaces were taken and examined using an adapted image analysis procedure. In the image analysis, the cumulative areas of the calcite crystal particles were set in relation to the examined image section for each plastic. For a better comparability of the two methods, the results were normalized to the results of the pure polyethylene (matrix). This means that all values below 100% indicate a reduction of the tendency to form scale deposits compared to polyethylene and values >100% indicate an increase of the tendency to form scale deposits of the respective plastic. In the result graphs, this was additionally highlighted in color, with a green coloring for a reduction and a red coloring for an increase in the sintering tendency compared to the pure matrix material.

7.1.6 Results

7.1.6.1 Dynamic Tests

When the first dynamic tests were carried out in the laboratory test setup, it became apparent that both in the optical analysis and in the acid digestion, the best results (low tendency to form scale deposits) were achieved with the compounds consisting of PE+ PEG, PE+ zeolite, PE + ammonium phosphate and PE + Na-stearate (cf. Fig. 7). Additional analyses using a scanning electron microscope (SEM) showed nicely (idiomorphically) formed calcite crystals on all samples examined (see exemplary Fig. 3).

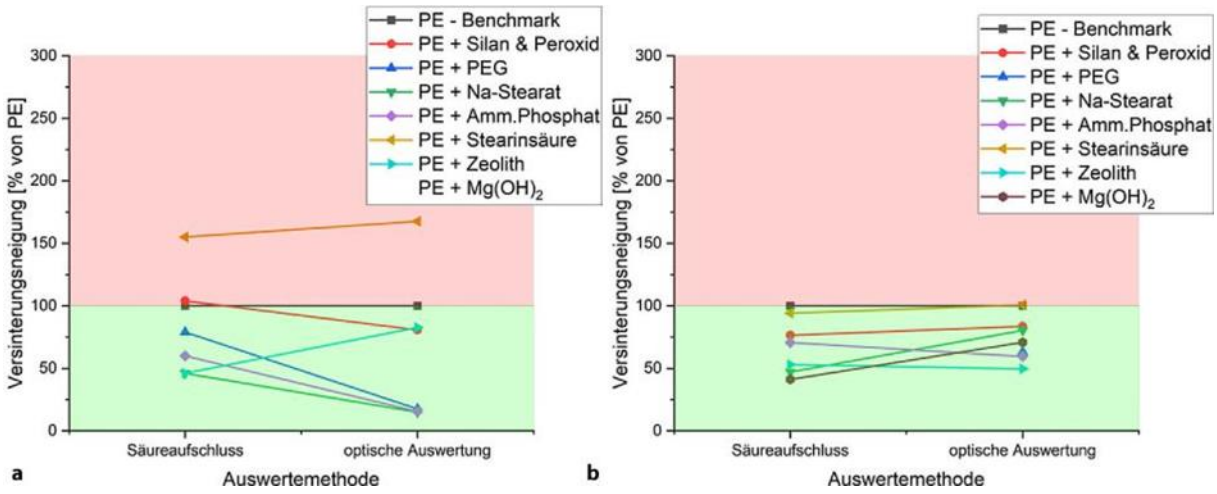

Figure 7: *Comparison of the evaluation methodology using the example of the dynamic tests at the TU Graz (a), and the exposed compounds in the Lainzer Tunnel(b).*

Further samples for dynamic tests were exposed at the Zentrum am Berg in Eisenerz. The samples were placed in shafts of the STR North road tunnel and the EBT West railway tunnel and exposed for one and three weeks respectively. Remarkable is the difference or generally the high pH-values of the waters (North; pH= 11.5 and South pH= 8.5). At a very high pH value of 11.5, severe scale deposits occurred on the exposed test compounds after only one week. Interestingly, the non-modified matrix material (PE) made it into the top 3 of the ranking (Fig. 10). This could be an indication that at such high pH values the selected modifications are not effective compared to more moderate environments. In contrast, the samples that were removed from the south junction and a moderate pH value of~8.5 primarily showed the usual order of the plastics again. In order to check whether the effects of the investigated compounds are only effective once or also several times, the same samples were exposed, evaluated and cleaned several times at the ZaB EBT West site. This process was repeated a total of five times, as shown in Fig. 8. With the exception of the second measurement, where the values are shifted upwards, all other measurements showed similar trends and especially the compounds with PEG and zeolite showed consistently good results. The analysis results of the second measurement can be explained by the introduction of mine water via additional pipelines, for which the shaft had to be drilled for pipes and a briefly increased mobilization of substances

can be assumed, which increased the tendency to form scale deposits. This can also explain the decreasing trend of the tendency to from scale deposits in deposits 2 to 4.

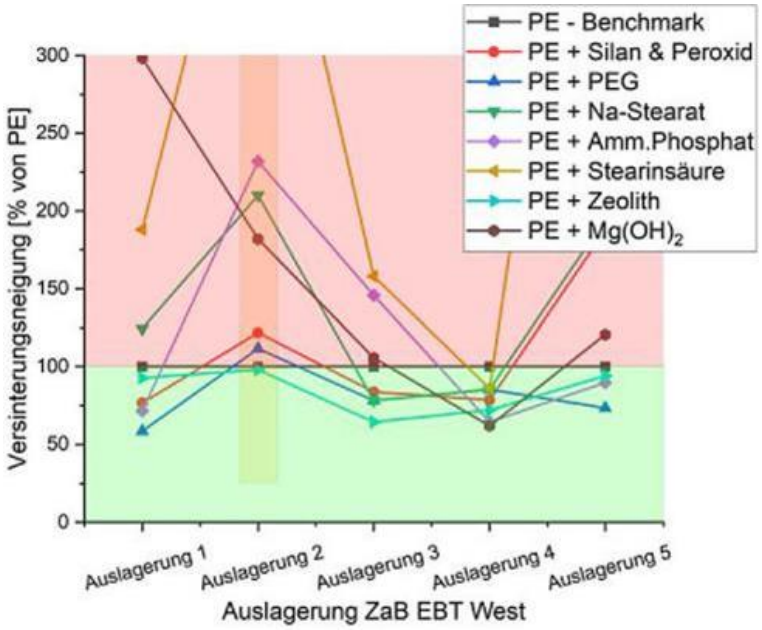

Figure 8: *Result of the repeated dynamic test at ZaB EBTWest.*

7.1.6.2 Stationary tests

As mentioned at the beginning, stationary experiments were also carried out in addition to the dynamic ones. The primary difference here is that the solutions prepared in the reactor are not exchanged (renewed) as in flowing waters. Analogous to the repeat measurements in the ZaB EBT West, the samples of these tests were also cleaned after the first tests and exposed again. The results of the stationary tests are shown below in Fig. 9. It should be noted at this point that the compounds with silane and stearic acid were not investigated further in these additional tests, based on the less promising results of the previous tests. As can be seen, PE with PEG, zeolite and polyphosphate are again the most efficient materials in the stationary test.

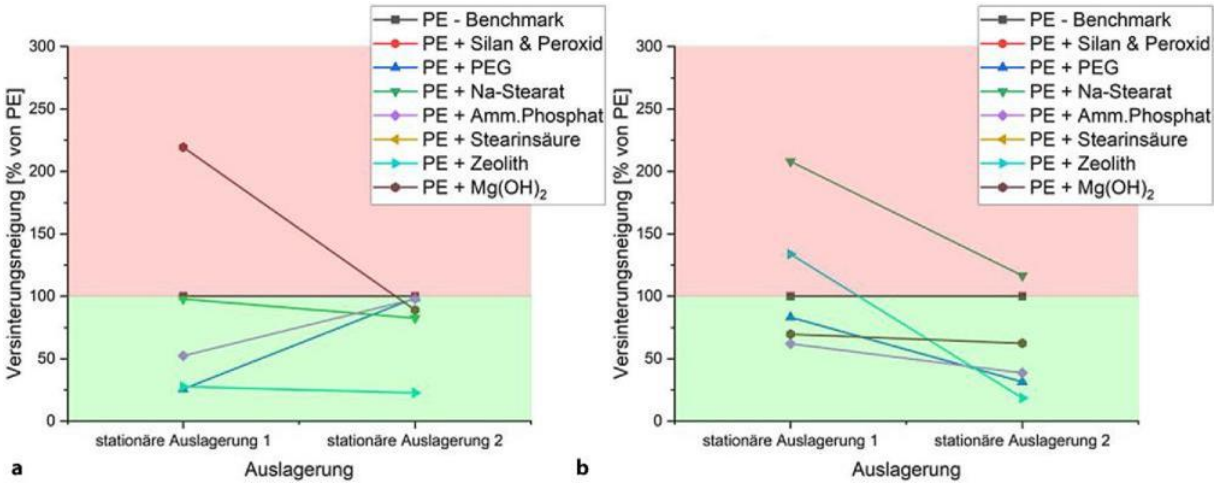

***Figure 9**: Result of repeated exposing of the plastics in the stationary test reactor at the TU-Graz - evaluation by means of acid digestion and optical analysis of the surface.*

7.1.6.3 Summary of the results

For a clear presentation, the three most promising plastic compounds of all tests in terms of reduced tendency to form scale deposits were summarized in Fig. 10. This form of presentation makes it possible to make basic statements about the general effectiveness of the compounds relatively quickly. The colors only serve to simplify the perception of the same compounds, but have no significance in terms of effectiveness. Based on this table and the rankings, the PE compound with zeolite seems to be the most effective against scale deposit formation under the given test conditions. The compounds with polyethylene glycol and ammonium polyphosphate follow in second place with approximately the same efficiency.

Bauwerk / Bezeichnung	Auswerte-methode	1. Platz	2. Platz	3. Platz	pH
dynamische Versuche					
Rinne	Optisch	PE+Amm.Phosphat	PE+Na-Stearat	PE+PEG	**7.8-8.1**
	Säureaufschluss	PE+Zeolith	PE+Na-Stearat	PE+Amm.Phosphat	
Lainzer Tunnel	Optisch	PE+Zeolith	PE+Amm.Phosphat	PE+PEG	**8.1-8.5**
	Säureaufschluss	PE+Mg(OH)2	PE+Na-Stearat	PE+Zeolith	
ZaB Süd	Optisch	PE+Zeolith	PE+PEG	PE+Silan	**8.5**
	Säureaufschluss	PE+Zeolith	PE+Amm.Phosphat	PE	
ZaB Nord	Optisch	PE+PEG	PE	PE+Silan	**11.5**
	Säureaufschluss	PE	PE+Zeolith	PE+Na-Stearat	
statische Versuche					
Statischer Versuch 1	Optisch	PE+Amm.Phosphat	PE+Mg(OH)2	PE+PEG	**7.7-8.1**
	Säureaufschluss	PE+PEG	PE+Zeolith	PE+Amm.Phosphat	
Statischer Versuch 2	Optisch	PE+Zeolith	PE+PEG	PE+Amm.Phosphat	
	Säureaufschluss	PE+Zeolith	PE+Na-Stearat	PE+Mg(OH)2	

***Figure 10:** Summary and evaluation of all investigations with regard to the tendency to form scale deposits of the PE plastics used with additives.*

7.1.7 Conclusion

Based on the results obtained in this study, the plastic compounds with zeolite, polyethylene glycol and ammonium phosphate seem to positively influence the scale deposit formation behaviour, in the sense of a lower tendency to scale deposit formation. However, at very high pH values (>>9), extremely high supersaturations of $CaCO_3$ minerals lead to very rapid scale deposit formation on the exposed plastic surfaces, which can significantly limit the efficiency of the active substances. Therefore, the results found in structures with very high pH values should be considered with caution. Nevertheless, the logical next step is to "upscale" the compounds found to real pipe geometries, with a subsequent series of tests in tunnel structures.

References

Dietzel, M.; Rinder, T.; Niedermayr, A.; Mittermayr, F.; Leis, A.; Klammer, D. et al.: Ursachen und Mechanismen der Versinterung von Tunneldrainagen. BHM Berg- und Hüttenmännische Monatshefte 153 (2008a), H. 10, S. 369–372.

Dietzel, M.; Rinder, T.; Leis, A.; Reichl, P.; Sellner, P.; Draschitz, C. et al.: Koralm Tunnel as a Case Study for Sinter Formation in Drainage Systems – Precipitation Mechanisms and Retaliatory Action. Geomechanik und Tunnelbau 1 (2008b), iss. 4, pp 271–278. https:// doi.org/10.1002/geot.200800024.

Dietzel, M.; Purgstaller, B.; Leis, A.; Reichl, P.; Stadler, H.; Niedermayr, A. et al.: Current challenges for scaling of tunnel drainage systems – Modelling approaches, monitoring tools and prevention strategies / Aktuelle Herausforderungen bei der Versinterung von Tunneldränagen – Modellierungsansätze, Monitoringwerkzeuge und Präventionsstrategien. Geomechanik und Tunnelbau 6 (2013), iss. 6, pp 743–753. https://doi.org/10.1002/geot.201310014.

Galli, M.: Härtestabilisierung in kalkführenden Entwässerungen: Verhinderung von Kalkablagerungen. Verlags-AG der akademischen technischen Vereine, Schweizer Ingenieur und Architekt, 118 (2000), H. 12, S. 249–253.

Girmscheid, G.; Gamisch, T.; Meinlschmidt, A.: Versinterung von Tunneldrainagen – Empfehlungen für die Instandhaltung von Tunneln. Bauingenieur 78 (2003), H. 12, S. 571–580.

Österreichische Vereinigung für Beton- und Bautechnik: Richtlinie Tunnelentwässerung. Wien, 2010.

Rinder, T.; Dietzel, M.; Leis, A.: Calcium carbonate scaling under alkaline conditions—Case studies and hydrochemical modelling. Applied Geochemistry 35 (2013), pp132–41. https://doi.org/10.1016/j. apgeochem.2013.03.019.

Schachinger, T.; Sperger, L.; Heissenberger, R.; Wagner, O.K.: Task Force Drainage (TFD)—The project for life after. Geomechanik und Tunnelbau 10 (2017), iss. 6, pp 779–787. https://doi.org/10.1002/geot. 201700045.

Schachinger, T.; Zagar, B.; Schwab, C.; Saliger, F.; Stur, M.: Current research by ÖBB Infrastruktur AG on scale monitoring without track closures. Geomechanik Tunnelbau 11 (2018), iss. 3, pp 277–285. https://doi.org/10.1002/geot.201800012

Schachinger, T.; Arbeiter, F.J.; Eichinger, S.; Saliger, F.: Research on pipe materials for tunnel drainage by the ÖBB Task Force Drainage. Geomechanik und Tunnelbau 12 (2019), iss. 5, pp 467–471. https:// doi.org/10.1002/geot.201900022.

Stur, M.; Ottner, F.; Schachinger, T.; Wriessnig, K.: Lokale Beseitigung von Versinterungen in Bergwasserdrainagen. Tunnel 2015, https:// www.tunnel-online.info/de/artikel/tunnel_Lokale_Beseitigung_von_Versinterungen_in_Bergwasserdrainagen_2242030.html.

Vollmann, G.: Zur Härtestabilisierung als versinterungsreduzierende Maßnahme für Tunneldränagesysteme, 1. Aufl., Göttingen: Cuvillier, 2005.

Wagner, O.K.; Koch, D.; Lemmerer, J.; Druckfeuchter, H.; Petraschek, T.: Maintenance-optimised drainage system for the New Semmering Base tunnel and Pummersdorf Tunnel / Instandhaltungsoptimiertes Entwässerungssystem für den Semmering-Basistunnel neu und Tunnel Pummersdorf. Geomechanik und Tunnelbau 7 (2014), iss. 5, pp 626–635. https://doi.org/10.1002/geot.201400032.

Wu Z, Cui Y, Barrett AG, Moreno MM, Deng Y. Role of surrounding soils and pore water in calcium carbonate precipitation in railway tunnel drainage system. Transportation Geotechnics 21 (2019): 21100257. https://doi.org/10.1016/j.trgeo.2019.100257.

Zhou, Y.; Zhang, X.; Wei, L.; Liu, S.; Zhang, B.; Zhou, C.: Experimental Study on Prevention of Calcium Carbonate Crystallizing in Drainage Pipe of Tunnel Engineering. Advances in Civil Engineering, vol. 2018, Article ID 9430517, 11 p. https://doi.org/10.1155/2018/ 9430517.

7.2 Research on pipe materials for tunnel drainage by the ÖBB Task Force Drainage

Tobias Schachinger[1], Florian Arbeiter[2], Stefanie Eichinger[3], Florian Saliger[1]

[1]Österreichische Bundesbahnen ÖBB Infrastruktur AG, Wien, Österreich
[2]Lehrstuhl für Werkstoffkunde und Prüfung der Kunststoffe, Montanuniversität Leoben, Leoben, Österreich
[3]Institut für Angewandte Geowissenschaften, Technische Universität Graz, Graz, Österreich

7.2.1 Abstract

Due to the additional tunnels that are currently under design or construction, drainage maintenance costs are expected to rise significantly over the next few years. An increased amount of maintenance will also be necessary due to older drainage pipes damaged during intensive cleaning and flushing. To counter these problems, an internal task force for drainage pipes has been installed within the ÖBB. Together with research institutions from several fields of science, projects are being carried out to find ways to decrease the overall maintenance effort. Topics include screening of possible rehabilitation methods for damaged pipes, and investigation of currently used materials with regard to their mechanical suitability. A multi-disciplinary research topic has also been initiated to investigate the potential of material modifications with the goal to decrease overall precipitation in drainage pipes and associated maintenance. First results on modified materials already show potential to decrease calcite precipitation.

7.2.2 Introduction - Drainage pipes in tunnel drainage systems

Austrian Railways ÖBB currently has to maintain about 420 km of drainage (drainage pipes and invert drainage channels) in tunnels, which are water pressure – relieved. On completion of the tunnel projects that are currently under construction (Semmering Base Tunnel, Koralm Tunnel, Brenner Base Tunnel), it is foreseeable that in 2026 a total of about 1,081 km of drainage pipes will be installed in Austrian railway tunnels, which will also have to be constantly maintained. The current costs for personnel, equipment for flushing drainage will therefore be multiplied. Since 2016 the ÖBB Task Force Drainage (TFD) has initiated projects [1] in order to reduce future maintenance measures for drainage as much as possible. One essential part of these projects was to investigate the material of tunnel drainage pipes. Since there were no uniform requirements for the material of drainage pipes in tunnels until 2003, thin-walled pipes of uPVC (unplasticized PVC) were mostly used. From 2003, the requirements

were specified in a guideline for the "detailing of tunnel drainage systems" [2], which was revised in 2010 [3]. According to this guideline, the use of drainage pipes of the materials uPVC, PE-HD and PP is possible as long as they comply with the normative requirements. Drainage pipes must however be subjected to additional testing of their resistance to high pressure jetting and to cleaning with chain scrapers [3]. Therefore, there are in principle two large groups of existing installed pipes: those installed before the issue of the guideline and those installed after.

When maintenance is carried out on uPVC pipes installed in the past, intensive or wrong cleaning work can often lead to pipe breakages or hand-sized pieces being broken out (Figure 1a), which on the one hand hinders current maintenance activity and also makes more extensive repair measures necessary. In a few cases, repairs have been attempted using "Cured in Place Pipes" (CIPP) since this can be undertaken without disturbing the inner lining and the waterproofing system. This type of repair is however very expensive in terms of time and money and remands extensive closures of the affected track or tunnel. In a few cases, "shortliner" repairs have been damaged during flushing work or even torn out completely (Figure 1b).

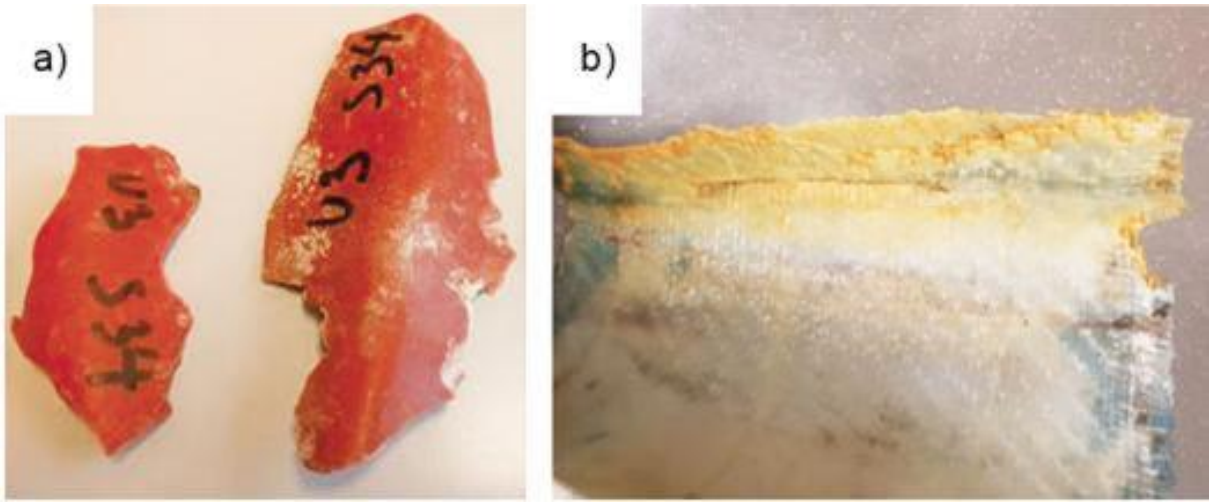

Figure 1: *Fractured pieces of a uPVC pipe (a) and a CIPP inliner (b), which were damaged during flushing of a tunnel drainage system*.

Due to this experience with uPVC pipes, drainage pipes of PP and PE-HD have been used since 2013 for the construction of more recent ÖBB tunnels instead of the much cheaper PVC pipes. This results in the following problems to be addressed by investigations and research work: – For existing drainage pipes, which could be damaged or even destroyed during cleaning work

due to lacking or inadequate technical requirements, suitable methods of repairing have to be sought. This subject is heavily dependent on the situation, has not yet been investigated in detail and is not part of this article.

– For drainage pipe materials regulated according to [2] and [3], which have already been installed or are currently being installed, it is necessary to investigate to what extent they can resist the exposure resulting from intensive cleaning in order to then be able to make estimates of the expected service life.

– In line with international developments as described in [4] [5] [6], research will also be undertaken on future materials with reduced scaling potential in order to reduce the associated flushing work. For this purpose, expertise from several professions has to be unified in order to understand the complex interaction of pipe wall, water chemistry and tunnel structure.

7.2.3 Mechanical properties of installed drainage pipes

In the current view, there are two possible explanations for damage to existing tunnel drainage. Either the pipes belong to the first group mentioned above, which were installed without a clear specification, or failure occurs due to exceptionally high loading. Damage in the first case is often due to very thin pipe walls (sometimes corrugated pipes). For the second case, two hypotheses are being considered in more detail: is the resistance of the material against impact loading (i.e. mechanical cleaning) insufficient, or has the material aged? Four materials were tested for their impact toughness: a PE-HD, a PP, a uPVC from the wall of a new pipe in accordance with [3] and uPVC from broken out pieces (cf. Figure 1a).

Due to existing drainage slits, stress concentrations can occur in the installed pipes in the slits themselves or at micro-cracks produced by the process of cutting the slits. Therefore, both the impact toughness and the notched impact toughness according to ISO 179¬1 are tested. As can be seen in Figure 2, all the materials show very high energies (>100 kJ/m2, no-break) in the impact toughness test without a notch and should therefore have no problems with impact loading. In the determination of the notched impact toughness, all the materials failed (values < 20 kJ/m2). The heaviest fall was determined for the uPVC materials. Broken pieces of the destroyed drainage pipe show nearly the same impact toughness and notched toughness as the new material. Thus it can be suspected that the uPVC material has not significantly aged. It is also clear that the notched toughness of PE and PP is better than that of uPVC under the present testing conditions. In combination with thicker walls (due to the lesser stiffness of PE and PP,

with constant specified SN class), PE and PP with drainage slits should have a higher overall resistance against impact loading than uPVC.

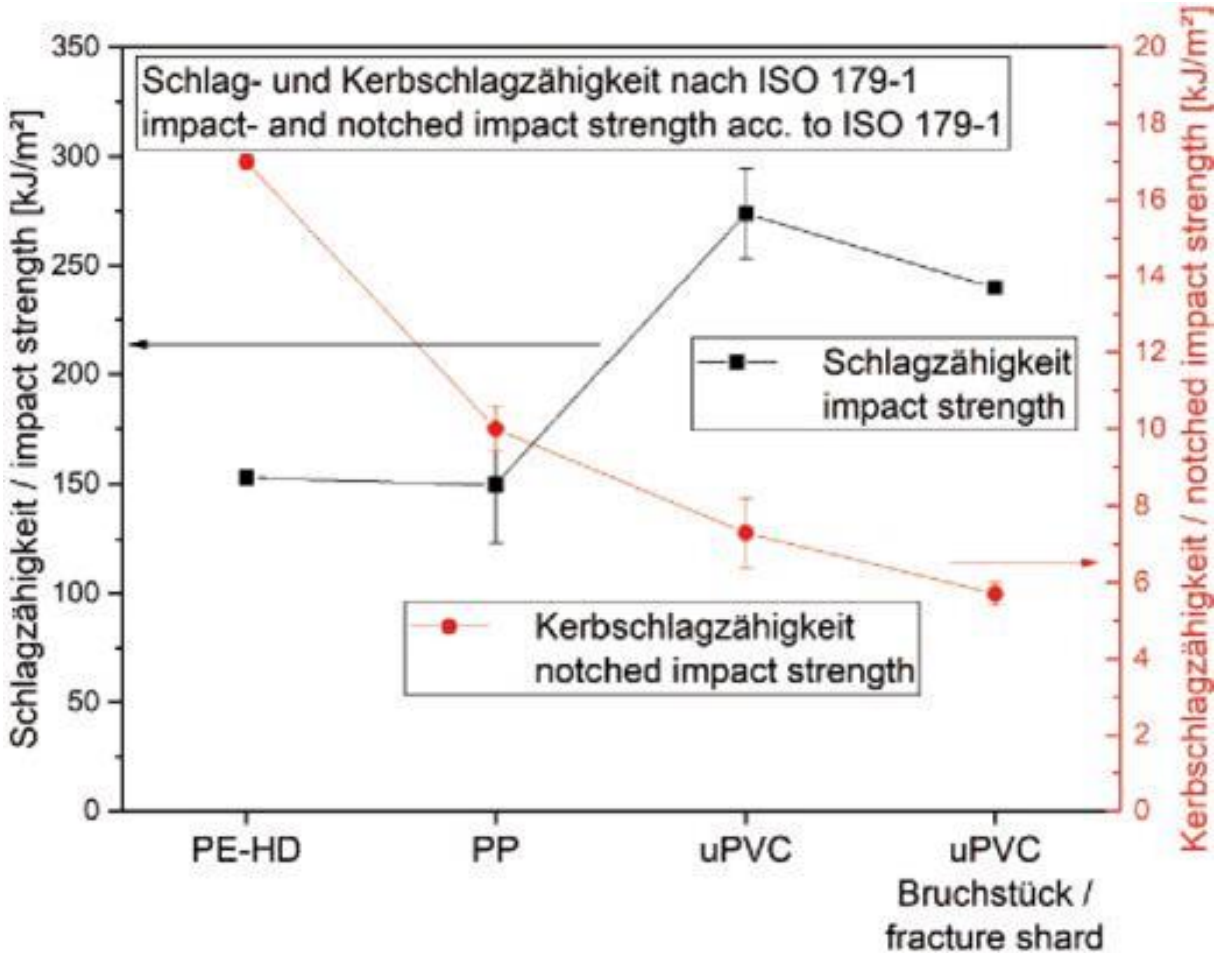

Figure 2: *Impact and notched impact strength of commercial pipe grade materials, as well as of the fractured pipe segment shown in Figure 1.*

7.2.4 Influence of pipe materials on the scaling behaviour: methodology and further development

In addition to the potential damage to tunnel drainage, any cleaning activity represents a reduction of the availability of the tunnel. Therefore, it is of great interest to reduce the required amount of cleaning. Since the precipitation of calcite is a large factor influencing the necessary cleaning activities, investigations are being carried out to determine whether it is possible to influence the precipitation behaviour through appropriate choice or modification of materials.

Since the process of scale formation is very complex, the processes have to be investigated in more detail before conclusions can be reached or material development can progress. In order to be able to understand the interaction of pipe surface, water chemistry, surrounding geology

and tunnel structure, it is necessary to clarify the problems from the viewpoint of various specialists. In the current FFG research project PolyDrain, an expert consortium consisting of geologists, mineralogists, Polymer scientists, tunnel engineers, (hydro)chemists, and tribologists is working on the further development of pipe materials. In addition to tests, a test rig has been developed (Figure 3a), with which it is possible to store plastic samples in open pipes. Using dosed dissolved compounds and the most modern sensor technology, the formation of scales can be controlled and evaluated with in-situ monitoring.

With this set-up, it is possible to investigate the effectiveness of material modifications. In first studies, tests were carried out on classic pipe materials and investigated with an electron microscope (Figure 3b), with differences being determined between the materials regarding the resulting quantity and properties of the scale, which are currently being validated in further tests.

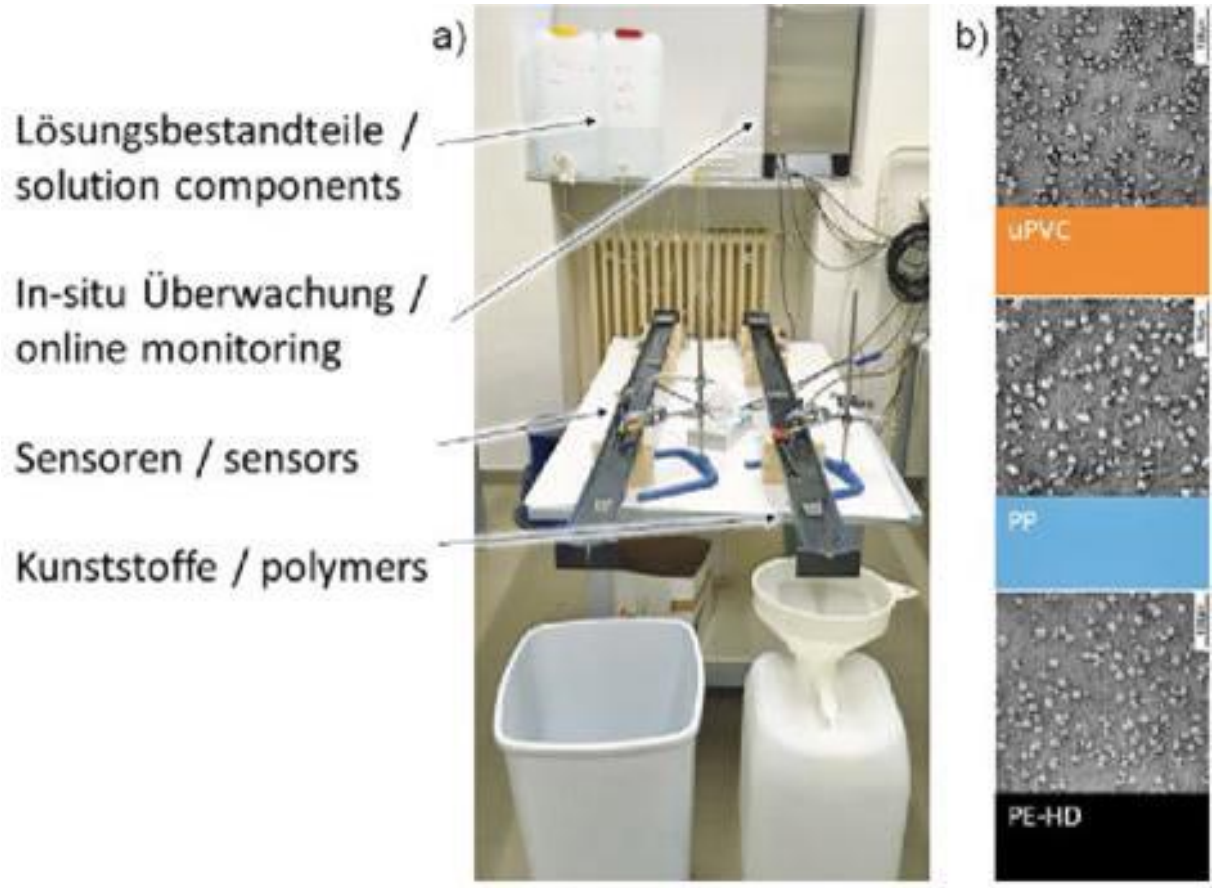

Figure 3: *Development of a test rig for controlled precipitation and analysis of calcite (a) and subsequent analysis of polymer surfaces and precipitation via scanning electron microscope (b).*

In addition to the selection of the base material, the chemistry of calcite formation can also be influenced by the intentional use of additives. Building on the work of Siegmann et. al. 2013 [6] with polyethylene glycol (PEG), various additives are currently being tested. It is important to find a suitable compromise for the application. While materials like PEG, which migrate to settle on the surface of the material, show high potential effectiveness, additives present in the entire volume of the material offer more safety in case cleaning processes remove material from the surface. It is important to note that plastics with a high content of fillers or active additives can become brittle.

7.2.5 Summary and outlook

From investigations that have been carried out, it is clear that thin-walled uPVC pipes tend to have a lower overall resistance against mechanical cleaning. Due to the survey of existing drainage pipe materials, it is therefore assumed that numerous tunnels have been built in the past – i.e. until about 2012 – in which the drainage will represent a weakness in the future. In the tunnels that are currently under construction by ÖBB, in which PP and PE drainage pipes with appropriate requirements are being used a long lifetime can be expected. Due to this, one aim for the future will be to discuss and agree suitable repair processes with requirements for pipes in ÖBB rail tunnels. The resulting findings should also be applicable for other infrastructure tunnel operators.

7.2.6 Acknowledgement

The works reported in this publication have partially been carried out in direct cooperation with the ÖBB-Infrastruk tur AG and as part of the VIF-2016 project PolyDrain (10549986) with the involvement of the ÖBB-Infrastruktur AG, the ASFINAG and the Federal Ministry for Transport, Innovation and Technology. Particular thanks are due to all the parties involved in the PolyDrain peoject: TU-Graz, BOKU Wien, Montanuniversität Leoben, Ingenieurbüro Strobl and Polymer Competence Center Leoben GmbH.

References

[1] Schachinger, T., Sperger, L., Heissenberger, R., Wagner, O.K.: Task Force Drainage (TFD) – The project for life after. Task-Force Dränagen (TFD) – Das Projekt für das Leben danach. Geomechanics and Tunnelling 10 (2017), No. 6, pp. 779–787. https://doi.org/10.1002/geot.201700045.

[2] ÖBV: Richtlinie Ausbildung von Tunnelentwässerung. Österreichische Vereinigung für Beton und Bautechnik, Wien, 2003.

[3] ÖBV: Richtlinie Tunnelentwässerung. Österreichische Vereinigung für Beton und Bautechnik, Wien, 2010.

[4] Yuanfu Zhou, Xuefu Zhang, Liangwen Wei, Shiyang Liu, Bin Zhang, Chao Zhou: Experimental Study on Prevention of Calcium Carbonate Crystallizing in Drainage Pipe of Tunnel Engineering. Advances in Civil Engineering (2018), S. 1–11.

[5] Alimia, F., Tlilia, M., Amora, M., Gabriellib, C., Maurin, G.: Influence of magnetic field on calcium carbonate precipita-tion. Desalination 206 (2007), S. 163–168.

[6] Siegmann, K., Sterchi, R., Widler, R., Hirayama, M.: Lime Repellent Polyethylene Additives. Journal of Applied Polymer.

Chapter 8 – Perspectives

The results of this PhD study clearly support a tunnel drainage to be a spatiotemporally highly variable and physicochemically complex system. Many individual (site-specific) influencing factors and environmental dependencies affect the distinct formation of scale deposits resulting in a variable macroscopic appearance, mineralogical composition and material consistency (see Chapters 2 to 7). No two tunnel drainages behave the same. Thus a tunnel drainage system has to be individually investigated and evaluated based on systematic documentation, sampling and monitoring campaigns.

For a detailed investigation of a drainage system, additionally to the conventional mineralogical, petrographic and hydrochemical analysis of aqueous solutions and precipitates, in-situ monitoring of the ongoing carbonate scaling process in different sections of the drainage system including pH, temperature, and electric conductivity, as well as the partial pressure of CO_2, humidity and air temperature are excellent compounds of a tool box and should be used as a kind of standard modules when assessing the variable formation processes in a tunnel drainage system in the future.

After a detailed investigation and assessment of a drainage system the specified dosage of green inhibitors provides a promising prevention strategy against calcareous scale deposit formation. In this doctoral thesis, polyaspartate (PASP) is mainly tested in tunnel drainage systems and measured using a fluorescence spectrophotometer in the laboratory. A so-called fluorometer is well suited for the direct determination of the PASP concentration, as it is very sensitive and allows direct PASP detection even at very low PASP concentrations (1 mg/l and less). This is important for an individual adaptation of the dosage in a tunnel drainage system, as under- or overdosing can have a negative effect on the efficient prevention of scale deposits. In future studies, the PASP concentration should therefore be analysed and measured in-situ in the drainage solution using a mobile fluorometer and consequently tunnel-specific calibration. In a tunnel drainage system, it is not easy to measure the flow rate of the incoming drainage solution. In a next step, such flow rate determinations could be measured or even monitored with the use of a fluorometer to detect possible seasonal changes in the water income. In addition, the newly developed compact test procedure for determining the effectiveness of green inhibitors on liquid conditioning could also be used in existing tunnel structures.

Four different types of calcareous scale deposits exist: (i) unconsolidated-particulate, (ii) shard-like, (iii) porous, and (iv) compact scales. For future studies, it would be very helpful and

purposeful to develop a method or even a field method to determine and classify the strength and hardness of each of these individual scale types directly in tunnel drainage systems in order to evolve straightforward strategies for maintenance and cleaning procedures of drainage systems.

Suitable building materials are also an important factor in preventing unwanted scale deposits. In the research project Polydrain, plastics containing polyethylene glycol copolymer and zeolite additives were found to be well suited materials for reducing scale deposit formation. Thus these specific plastics in the form of typical constructive compounds should be tested on a bigger scale in new and existing tunnel drainage systems.

Another approach for future investigations could also be more detailed investigations and analyses with regard to the ubiquitous microbiology and their frequent effect on scale deposits, builing materials and on applications of various green inhibitors. Microbial activity, for example, consumes PASP in liquid form as a nutrient. In future approaches it would be very interesting to investigate how microbes react when PASP is used in the form of depot stones in tunnel drainage systems (liquid vs. solid). Fe-oxidizing bacteria are very common in scales and its influence on $CaCO_3$ scale deposit formation is relatively well understood. However, it would also be interesting to figure out what possible role sulphur or sulphate bacteria play in the formation of scale deposits and wether they also influence the material consistency.

With all these and further future approaches a better process understanding of scale desposit formation and possible prevention strategies could be achieved in order to develop an improved drainage management and conservation plan and more efficient maintenance and service concepts (cleaning sequences, intervals, hydropressurized and hydromechanic procedures, etc.).

Appendix

A.1 Peer-reviewed publications

A.1.1 Publication as first author

Dietzel, M. and **Eichinger, S**.* (2022). Scale formation processes – state of knowledge and current challenges. Geomechanics and Tunnelling. https://doi.org/10.1002/geot.202200009.

Eichinger, S., Boch, R., Leis, A., Baldermann, A., Domberger, G., Schwab, C., & Dietzel, M. (2022). Green inhibitors reduce unwanted calcium carbonate precipitation: Implications for technical settings. Water Research, 208, 117850.

Eichinger, S., Leis, A., Boch, R., Seywald, C., Dietzel, M. (2020). Assessment and formation mechanisms of scale deposits in tunnels of the ÖBB-Infrastruktur AG – A subproject of the Task Force Drainage. Geomechanics and Tunnelling, 13(3), 273-285. https://doi.org/10.1002/geot.202000006.

Eichinger, S., Boch, R., Leis, A., Koraimann, G., Grengg, C., Domberger, G., Nachtnebel, M., Schwab, C., Dietzel, M. (2020). Scale deposits in tunnel drainage systems – A study on fabrics and formation mechanisms. Science of the Total Environment, 718, 137140. https://doi.org/10.1016/j.scitotenv.2020.137140.

A.1.2 Publications as co-author

Wedenig, M.; **Eichinger, S.;** Boch, R.; Leis, A.; Wagner, H.; Dietzel, M. (2022). Understanding of Tunnel Drainage Scale Formation by In-Situ Monitoring (under review in Tunnelling and Underground Space Technology).

Leis, A.; Wagner, H.; **Eichinger, S.;** Domberger, G.; Wedenig, M.; Dietzel, M.; Boch, R. (2022). Application of green inhibitors for threshold scale inhibitor treatment of tunnel drainage systems. Geomechanics and Tunnelling. https://doi.org/10.1002/geot.202200018.

Schachinger, T., Arbeiter, F. J., **Eichinger, S.,** & Saliger, F. (2019). Research on pipe materials for tunnel drainage by the ÖBB Task Force Drainage. Geomechanics and Tunnelling, 12(5), 467-471.

* equal corresponding authors

A.2 Other Journal Publications

Arbeiter, F., **Eichinger, S.,** Rieß, G., Schachinger, T., Boch, R., Wenighofer, R.; Galler, R., Hausberger, A.; Strobl, E.; Stur, M.; Saliger, F.; Steiner, M.; Dietzel, M., & Pinter, G. (2020). Optimierte Polymer-Rohrwerkstoffe für effiziente Drainagesysteme in Tunnelbauwerken—PolyDrain Teil II. BHM Berg-und Hüttenmännische Monatshefte, 165(12), 623-630.

Arbeiter, F.; **Eichinger, S.;** Rieß, G.; Schachinger, T.; Boch, R.; Wenighofer, R.; Galler, R.; Hausberger, A.; Strobl, E.; Stur, M.; Saliger, F.; Steiner, M.; Dietzel, M., Pinter; G. (2019). Optimierte Polymer-Rohrwerkstoffe für effiziente Drainagesysteme in Tunnelbauwerken – Poly-Drain. Berg- u. Hüttenmännische Monatshefte 164, H. 12, S. 545–551. https://doi.org/10.1007/s00501-019-00918-6.

A.3 Conference contributions

Eichinger S., Boch R., Leis, A., & Dietzel, M. (2022). Formation processes and prevention strategies of scale deposits in tunnel drainage systems. In *Pangeo Conference Abstracts* 2022, Leoben, Austria. (Talk)

Eichinger, S., Boch, R., Leis, A., Baldermann, A., Domberger, G., Schwab, C., & Dietzel, M. (2021). Green inhibitors against CaCO3 scale deposits–On-site assessment and tuning in tunnel drainages. In MinPet 2021. (Poster)

Eichinger, S., Arbeiter, F., Boch, R., Schachinger, T., & Dietzel, M. (2019, September). Influencing Carbonate Scaling by Tailored Drainage Materials in Tunnels-An Experimental Approach. In *MinPet2019* (p. 34). (Poster)

Eichinger, S., Boch, R., Koraimann, G., Leis, A., & Dietzel, M. (2019, August). Influence of microbial activity on carbonate dominated mineral precipitates in tunnel drainage systems. In *Goldschmidt Conference 2019*. (Poster)

Eichinger, S., Boch, R., Leis, A., & Dietzel, M. (2018, November). Calcium carbonate precipitation impairing the draining of tunnels–Stable C and O isotope fractionation and growth dynamics. In *Stable Isotope Network Austria Meeting 2018* (p. 25). (Poster)

Eichinger, S., Boch, R., Hippler, D., Egartner, I., Orieschnig, A., Leis, A., & Dietzel, M. (2018, April). Carbonate precipitates impairing drainages in an Austrian motorway tunnel-

Investigation on growth dynamics and environmental dependencies. In *EGU General Assembly Conference Abstracts* (p. 8895). (Poster)

A.4 Invited Workshop Talks

µCT – Symposium (29.06.2022)

Eichinger S., Boch R., Götschl, K., Wenighofer, R., Hoffmann, R., Grengg, C., Baldermann, A., Galler, R., Immenhauser, A., Dietzel, M. (2022): Subsurface low Mg-calcite-aragonite formation – Field based experiments and in-situ monitoring in the Erzberg mine (Austria).

Carbonate Workshop, Veszprém, Hungary (04.07.2022)

Eichinger S., Boch R., Götschl, K., Wenighofer, R., Hoffmann, R., Grengg, C., Baldermann, A., Galler, R., Immenhauser, A., Dietzel, M. (2022): Subsurface low Mg-calcite-aragonite formation – Field based experiments and in-situ monitoring in the Erzberg mine (Austria).

Versinterungsworkshop ÖBB, Graz, Austria (06.07.2022)

Eichinger, S., Dietzel, M. (2022): Typisierung von Tunnelsintern – Entstehung und Eigenschaften.